UAB

Universitat Autònoma de Barcelona

School of Engineering
Department of Chemical Engineering

AEROBIC BIOTRICKLING FILTRATION FOR BIOGAS DESULFURIZATION

PhD Thesis

Directed by
Dr. David Gabriel Buguña
Dr. María del Mar Baeza Labat

Andrea Monzón Montebello

May 2013

Title   Aerobic biotrickling filtration for biogas desulfurization

Presented by   Andrea Monzón Montebello

Directors   Dr. David Gabriel Buguña

Dr. María del Mar Baeza Labat

Doctoral Programme in Environmental Science and
Technology, Specialization in Environmental Technology.

Programa de Doctorat en Ciència i Tecnologia Ambientals,
Especialitat en Tecnologia Ambiental.
ICTA – Institut de Ciència i Tecnologia Ambientals.

Departament d'Enginyeria Química.
Escola d'Enginyeria.
Universitat Autònoma de Barcelona.

Bellaterra, May 2013.

DAVID GABRIEL BUGUÑA, professor agregat del Departament d'Enginyeria Química de la Universitat Autònoma de Barcelona i **MARÍA DEL MAR BAEZA LABAT**, professora titular del Departament de Química de la Universitat Autònoma de Barcelona,

CERTIFIQUEM:

Que l'enginyera química **ANDREA MONZÓN MONTEBELLO** ha realitzat sota la nostra direcció el treball titulat: **"AEROBIC BIOTRICKLING FILTRATION FOR BIOGAS DESULFURIZATION"**, el qual es presenta en aquesta memòria i que constitueix la seva Tesi per a optar al Grau de Doctor per la Universitat Autònoma de Barcelona.

I perquè en prengueu coneixement i consti als efectes oportuns, presentem a l'Escola d'Enginyeria de la Universitat Autònoma de Barcelona l'esmentada Tesi, signant el present certificat a

Bellaterra, 31 de Maig de 2013.

Dr. David Gabriel Buguña   Dra. María del Mar Baeza Labat

to Sávio,

music and love of my life.

Acknowledgements

Table of contents

✳

Index

※

List of Figures and Tables

2 **Introduction**

4 **General materials and methods**

꿍

5   On-line monitoring of H₂S and sulfide by a flow analyzer

꿍

6   Preliminary study on the on-line determination of sulfate

∽

7 Neutral H$_2$S biotrickling filtration and transition to acidic pH

∽

8 Simultaneous removal of methylmercaptan and H$_2$S

∽

List of Equations

※

x

List of Abbreviations

ABPP	N-4-4-(anilinocarbothioyl)-amino benzylphenyl-N-phenyl thiourea	
ABS	acrylonitrile butadiene styrene	
AD	anaerobic digestio n	
AP	acetophenone	
ATC	automatic temperature compensation	
BA	benzylacetate	
BBPA	bis(1-butylpentyl) adipate	
BDPP	4-(4-bromophenyl)-2,6-diphenylpyrilium perchlorate	
BEHP	bis(2-ethylhexyl) phthalate	
BEHS	bis(2-ethylhexyl) sebacate	
Bis-thiourea 2	α,α-bis(N-butylthio-ureylene)-m-xylene	
Bis-thiourea 3	α,α-bis(N-phenyl-thioureylene)-m-xylene	
Bis-thiourea B	1,3-bis(3-phenylthio-ureidomethyl)-benzene	
Bis-thiourea HA	α,α-bis(N-phenylthio-ureylene)-2-hexyl-adamantyl	
Bis-urea 1	α,α-bis(N-butylureylene)-m-xylene	
Bis-urea 4	α,α-bis(N-1-heptyldecyl-ureylene)-m-xylene	
BMImBF4	1-butyl-3-methyl imidazolium tetrafluoro borate	
BMImPF6	1-butyl-3-methyl imidazolium hexafluoro phosphate	
BN	1-bromonaphthalene	
BTF	biotrickling filter	
CAS	chemical abstracts service	
CFA	continuous flow analysis	
★ **CH₃SH**	methylmercaptan	
CH₄	methane	
CMCPE	chemically modified carbon paste electrode	
CN	α-chloronaphthalene	
CO₂	carbon dioxide	
★ **COS**	carbonyl sulfide	
CP	chloroparaffin	

CrL Schiff	N-N'-ethylenebis(5-hydroxy-salicyldeneiminate)-chromium(III) chloride	
CRS	cold-rolled steel	
CS	carbon steel	
CS₂	carbon disulfide	
CTAB	cetyltrimethylammonium bromide	
CuL	N-N'-bis(2-amino-1-oxo-phenelenyl)phenylenediamine copper(II)	
DBP	dibutyl phthalate	
DEA	diethanolamine	
★ **DMDS**	dimethyl disulfide	
DMFC	differential mass flow controller	
★ **DMS**	dimethyl sulfide	
★ **DMTS**	dimethyl trisulfide	
DO	dissolved oxygen	
DOP	dioctyl phthalate	
DOS	bis(2-ethylhexyl) sebacate	
DTOA	dodecyltrioctylammonium iodide	
E	electrical potential	
EBRT	empty bed residence time	
EC	elimination capacity	
EDTA	ethylenediamine tetraacetic acid	
★ **ET**	ethylmercaptan	
FIA	flow injection analysis	
FID	flame ionization detector	
FIM	fixed interference method	
FNDPE	2-fluoro-2-nitrodiphenyl ether	
FPNPE	2-fluorophenyl 2-nitrophenyl ether	
FSS	final solid sample	
GC	gas chromatography	
GD-CFA	gas diffusion-continuous flow analysis	
Guanidine-I	N-N'-dicyclohexyl-N''-octadecyl guanidine	
★ **H₂S**	hydrogen sulfide (gas)	
HCO₃⁻	bicarbonate	

HDAB hexadecylammonium bromide
HDTODAB hexadecyltrioctadecyl-ammonium bromide
HEPES 2-(4,2-hydroxyethyl-1-pipera-zinyl) ethanesulfonic acid
HPLC high-performance liquid chromatography
HRT hydraulic residence time
HTAB hexadecyltrimethylammonium bromide
HTFAB hexyl p-trifluoroacetyl benzoate
Hydroxyl-Schiff 2,2'-(2,5,8,11-tetraazadodeca-1,11-diene-1,12-diyl)bis-4-nitrophenol
IC ion chromatography
ICP-MS inductively coupled plasma - mass spectrometry
IDLH immediately dangerous to life and health
IL ionic liquid
Imidazole-P 2,6-bis(6-nitrobenzo-imidazoyl)-N-octadecyl piperidine
Ionophore-L 2,5-diphenyl-1,2,4,5-tetraazabicyclo-(2,2,1)-heptane
ISE ion-selective electrode
K(TFPB) potassium tetrakis(3,5-bis-trifluoromethylphenyl) borate
KTpClPB potassium tetrakis(4-chlorophenyl) borate
LCD liquid-crystal display
LD limit of detection
LD$_{ap}$ apparent limit of detection
LED light-emitting diode
LinR linear range
LLRL low linear-range limit
LO$_2$ load of O_2
LOV lab-on-a-valve
LR loading rate
LTCC low temperature cofired ceramics
MB methylene blue
MCFA multicommutation flow analysis
MDEA methyldiethanolamine
MEA monoethanolamine

MES 2-(N-morpholino) ethanesulfonic acid
Mg/Al-SO4 HT hydrotalcite compound ($Mg_6Al_2(OH)\cdot 16SO_4\cdot 4H_2O$)
MOImCl 1-methyl-3-octylimidazolium chloride
MPM matched potential method
MSFA multisyringe flow analysis
MTOAC methyltrioctylammonium chloride
Na-TPB sodiumtetraphenyl borate
NB nitrobenzene
N$_{cell}$ cellular nitrogen
NDIR nondispersive infrared
NDPE 2-nitrodiphenyl ether
NO$_2^-$ nitrite
NO$_3^-$ nitrate
NOB 1-nonyloxyl-2-butanol
NTA nitrilotriacetic acid
O$_2$ oxygen
OA oleic acid
o-NPOE o-nitrophenyloctyl ether
ORP oxidation-reduction potential
PACA-I polyazacycloalkane
PANI polyaniline
PBS phosphate buffer saline
PDMS poly(dimethylsiloxane)
pK$_a$ dissociation constant
PP polypropylene
ppb$_v$ part per billion (volumetric)
ppm$_m$ part per million (volumetric)
PPS polyphenylene sulfide
pS-S^0 production rate of S^0
-pS-S^0 consumption rate of S^0
pS-SO$_4^{2-}$ production rate of SO_4^{2-}
PTFE polytetrafluoroethylene
PU polyurethane
PVC polyvinylchloride
PVC-HMW polyvinylchloride high molecular weight
PVDF polyvinylidene fluoride
PVF polyvinyl fluoride
QAS-DM tris(2,3,4-dodecyloxyl)benzyl-dimethyloctylammonium chloride
QAS-MM tris(2,3,4-dodecyloxyl)benzyl-dioctylmethylammonium chloride

QAS-TM	tris(2,3,4-dodecyloxyl)benzyl trimethylammonium chloride	**TDDMA Cl**	tridodecylmethylammonium chloride
RE	removal efficiency	**TDS**	total dissolved sulfide
RSC	reduced sulfur compound	**THF**	tetrahydrofuran
S	sulfur (in general)	**THTDP Cl**	trihexyltetradecyl-phosphonium chloride
★ **S^0**	elemental sulfur		
S^{2-}	sulfide	**TIC**	total inorganic carbon
★ **$S_2O_3^{2-}$**	thiosulfate	**TLV**	tickling liquid velocity
★ **$S_2O_6^{2-}$**	dithionate	**TLV-STEL**	threshold limit value – short-term exposure limit
★ **$S_3O_6^{2-}$**	trithionate		
★ **$S_4O_6^{2-}$**	tetrathionate	**TLV-TWA**	threshold limit value – time-weighted average
SAOB	sulfide antioxidant buffer		
Schiff base-I	6-6'-diethoxy-2-2'-(2,2-dimethylpropane-1,3-diylbis-nitrilomethylidyne-diphenolato nickel (II)	**TNODA**	trinonyloctadecylammonium chloride
		TOMAC	trioctylmethylammonium chloride
SIA	sequential injection analysis	**Tripodal-2**	aminochromenone tris-(2-aminoethylamine)
SL	sensitivity of an ISE		
★ **SO_2**	sulfur dioxide	**TRIS**	tris-(hydroximethyl) aminoethylamine
★ **SO_3^{2-}**	sulfite		
★ **SO_4^{2-}**	sulfate	**TSS**	total suspended solids
SOB	sulfur-oxidizing bacteria	**VOC**	volatile organic compound
SS	stainless steel	**VOSC**	volatile organic S compound
SSM	separate solutions method	**VSS**	volatile suspended solids
TDDBTMA Cl	tris(2,3,4-dodecyloxy) benzyltrimethylammonium chloride	**ZPC**	zinc-phthalocyanine
		Zwiterrion-2	bis(guanidinium) dihydrochloride

★ *Molecular representation in **Annexes***

※

Abstract

The performance of an aerobic biotrickling filter (BTF) was assessed during a total period of 990 days on the desulfurization of a synthetic biogas containing 2,000 ppm_v of H_2S ($\approx$50 g S-$H_2S \cdot m^{-3} \cdot h^{-1}$), using a metallic random packing material (stainless steel Pall rings). After the optimization of the operation at neutral pH, the simultaneous removal of methylmercaptan (CH_3SH) and H_2S was studied. Afterwards, the uninterrupted transition from 440 days at neutral pH (6.0 – 6.5) to 550 days at acidic pH (2.50 – 2.75) was performed. In parallel, sensing tools for the on-line monitoring of H_2S, total dissolved sulfide (TDS = $H_2S_{(aq)}$ + HS^- + S^{2-}) and sulfate (SO_4^{2-}) were developed applying ion-selective electrodes (ISEs).

An ISE of crystalline membrane was used in the proposed analytical system, consisting in a flow injection analyzer (FIA) for TDS detection integrated as a detector into a continuous flow analyzer with a gas diffusion step (GD-CFA) for H_2S detection, which was proven to be reliable for on-line monitoring of the BTF. The preliminary study on the on-line determination of SO_4^{2-} was performed by an ISE of polymeric liquid membrane, prepared with a commercial ionophore. However, low selectivity to SO_4^{2-} was found in the presence of interfering anions, discouraging the application of constructed electrodes.

Operational parameters of the BTF were optimized under neutral pH, such as the aeration rate, the trickling liquid velocity (TLV) and the hydraulic residence time (HRT), achieving a minimum elemental sulfur (S^0) production. Also, the behavior of the BTF was studied as a function of the empty bed residence time (EBRT) and the H_2S loading rate (LR). A maximum elimination capacity (EC) of 135 g S-$H_2S \cdot m^{-3} \cdot h^{-1}$ was found. Removal efficiency (RE) above 99% was obtained at the reference EBRT of 131 s. The simultaneous removal of CH_3SH and H_2S was investigated at neutral pH, for concentrations commonly found in biogas (2,000 ppm_v of H_2S and 10 – 75 ppm_v of CH_3SH). Maximum ECs were 1.8 g S-$CH_3SH \cdot m^{-3} \cdot h^{-1}$ and 100 g S-$H_2S \cdot m^{-3} \cdot h^{-1}$. The natural presence of CH_3SH in biogas was considered beneficial because of the unclogging effect produced by the consumption of S^0 by chemical reaction with CH_3SH. Finally, the BTF long-term operation under acidic pH was characterized in terms of EBRT and LR, obtaining an EC_{max} of 220 g S-$H_2S \cdot m^{-3} \cdot h^{-1}$. The H_2S removal profile was assessed and the oxidation rate of S^0 accumulated inside the filter bed was evaluated by periodical H_2S starvation episodes. Results indicate that the first third of the filter bed is responsible for 70 to 80% of the total H_2S removal. Oxidation of S^0 to SO_4^{2-} was suggested as a S-clogging control strategy under acidic conditions. Despite the important amount of S^0 produced under acidic pH, overall BTF desulfurizing capacity was comparable to that obtained previously under neutral pH.

Resum

Es va gestionar l'operació d'un biofiltre percolador (BTF) durant un període total de 990 dies per a la dessulfuració d'un biogàs sintètic contenint 2,000 ppm$_v$ d'H$_2$S (≈ 50 g S-H$_2$S·m^{-3}·h^{-1}), utilitzant un material de rebliment aleatori (anelles *Pall* d'acer inoxidable). Després de l'optimització de l'operació a pH neutre, es va estudiar l'eliminació simultània de metilmercaptà (CH$_3$SH) i H$_2$S. A continuació es va executar la transició ininterrompuda des de 440 dies a pH neutre (6.0 – 6.5) a 550 dies a pH àcid (2.50 – 2.75). Paral·lelament es van desenvolupar eines per a la monitorització en línia d'H$_2$S, sulfur dissolt total (TDS = H$_2$S$_{(aq)}$ + HS$^-$ + S^{2-}) i sulfat (SO$_4^{2-}$), aplicant elèctrodes selectius d'ions (ISEs).

Es va emprar un ISE de membrana cristal·lina en el sistema analític proposat, que consisteix en un analitzador per injecció de flux (FIA) per anàlisi de TDS integrat com a detector en un analitzador de flux continu amb una etapa prèvia de difusió de gas (GD-CFA) per l'anàlisi d'H$_2$S, el qual es va mostrar idoni per a la monitorització en línia del BTF. Es va realitzar l'estudi preliminar de la determinació en línia de SO$_4^{2-}$ utilitzant un ISE de membrana líquida polimèrica, preparada amb un ionòfor comercial. No obstant això, es va obtenir baixa selectivitat per al SO$_4^{2-}$ en presència d'anions interferents, el que desaconsella l'aplicació dels elèctrodes construïts.

Es van optimitzar paràmetres operacionals del BTF a pH neutre, com ara la taxa d'aeració, la velocitat de percolació (TLV) i el temps de residència hidràulica (HRT), obtenint una mínima producció de sofre elemental (S^0). També es va estudiar la resposta del BTF enfront del temps de contacte del gas (EBRT) i de la càrrega aplicada (LR) d'H$_2$S. La capacitat d'eliminació (EC) màxima va ser de 135 g S-H$_2$S·m^{-3}·h^{-1}. Per a un EBRT de referència de 131 s, l'eficàcia d'eliminació (RE) va ser superior al 99%. Es va investigar l'eliminació simultània de CH$_3$SH i H$_2$S a pH neutre, a concentracions normalment trobades en biogàs (2,000 ppm$_v$ d'H$_2$S i 10 – 75 ppm$_v$ de CH$_3$SH). Les màximes EC trobades van ser de 1.8 g S-CH$_3$SH·m^{-3}·h^{-1} i 100 g S-H$_2$S·m^{-3}·h^{-1}. La presència natural de CH$_3$SH en el biogàs va ser considerada beneficiosa per l'efecte de descolmatació del llit produït pel consum de S^0 per reacció química amb CH$_3$SH. Finalment, es va caracteritzar l'operació a llarg termini del BTF sota condicions àcides de pH en funció del EBRT i la LR, obtenint una EC$_{max}$ de 220 g S-H$_2$S·m^{-3}·h^{-1}. Es va estudiar el perfil d'eliminació d'H$_2$S i es va avaluar la velocitat d'oxidació del S^0 acumulat dintre del llit durant episodis periòdics d'inanició. Els resultats indiquen que el primer terç del llit és responsable pel 70 – 80% del total eliminat d'H$_2$S. L'oxidació de S^0 a SO$_4^{2-}$ se suggereix com una estratègia de control contra la colmatació del llit per sofre. Tot i la important quantitat de S^0 produït a pH àcid, la capacitat de dessulfuració global del BTF va ser comparable a l'obtinguda anteriorment a pH neutre.

Resumen

Se gestionó la operación de un biofiltro percolador (BTF) durante un período total de 990 días en la desulfuración de un biogás sintético conteniendo 2,000 ppm_v de H_2S ($\approx$50 g S-$H_2S \cdot m^{-3} \cdot h^{-1}$), utilizando un material de empaque aleatorio (anillos *Pall* de acero inoxidable). Después de la optimización de la operación a pH neutro, se estudió la eliminación simultánea de metilmercaptano (CH_3SH) y H_2S. A continuación se ejecutó la transición ininterrumpida de 440 días a pH neutro (6.0 – 6.5) a 550 días a pH ácido (2.50 – 2.75). Paralelamente se desarrollaron herramientas para la monitorización en línea de H_2S, sulfuro disuelto total (TDS = $H_2S_{(aq)}$ + HS^- + S^{2-}) y sulfato (SO_4^{2-}), aplicando electrodos selectivos de iones (ISE).

Se empleó un ISE de membrana cristalina en el sistema analítico propuesto, que consiste en un analizador por inyección de flujo (FIA) para análisis de TDS integrado como detector en un analizador de flujo continuo con una etapa previa de difusión de gas (GD-CFA) para análisis de H_2S, el cual se mostró idóneo para la monitorización en línea del BTF. Se realizó el estudio preliminar de la determinación en línea de SO_4^{2-} utilizando un ISE de membrana líquida polimérica, preparada con un ionóforo comercial. Sin embargo, se obtuvo baja selectividad al SO_4^{2-} en presencia de aniones interferentes, lo que desaconseja la aplicación de los electrodos construidos.

Se optimizaron parámetros operacionales del BTF a pH neutro, tales como la tasa de aeración, la velocidad de percolación (TLV) y el tiempo de residencia hidráulica (HRT), obteniendo una mínima producción de azufre elemental (S^0). También se estudió la respuesta del BTF frente al tiempo de contacto del gas (EBRT) y a la carga aplicada (LR) de H_2S. La capacidad de eliminación (EC) máxima fue de 135 g S-$H_2S \cdot m^{-3} \cdot h^{-1}$. Para un EBRT de referencia de 131 s, la eficacia de eliminación (RE) fue superior al 99%. Se investigó la eliminación simultánea de CH_3SH y H_2S a pH neutro, a concentraciones comúnmente encontradas en biogás (2,000 ppm_v de H_2S y 10 – 75 ppm_v de CH_3SH). Las ECs máximas halladas fueron de 1.8 g S-$CH_3SH \cdot m^{-3} \cdot h^{-1}$ y 100 g S-$H_2S \cdot m^{-3} \cdot h^{-1}$. La presencia natural de CH_3SH en el biogás fue considerada beneficial debido al efecto de descolmatación del lecho producido por el consumo de S^0 por reacción química con CH_3SH. Finalmente, se caracterizó la operación a largo plazo del BTF bajo condiciones ácidas de pH en función del EBRT y la LR, obteniendo una EC_{max} de 220 g S-$H_2S \cdot m^{-3} \cdot h^{-1}$. Se estudió el perfil de eliminación de H_2S y se evaluó la velocidad de oxidación del S^0 acumulado en el lecho durante episodios periódicos de inanición. Los resultados indican que el primer tercio del lecho es responsable por el 70 – 80% del total eliminado de H_2S. La oxidación de S^0 a SO_4^{2-} se sugiere como una estrategia de control contra la colmatación del lecho por azufre. A pesar de la importante cantidad de S^0 producido a pH ácido, la capacidad de desulfuración global del BTF fue comparable a la obtenida anteriormente a pH neutro.

※

1

research motivation and
thesis overview

"There is no subject so old that
something new cannot be said about it."

Fyodor M. Dostoyevsky
(Moscow, 1821 – Saint Petersburg, 1881)

1 Research motivation and thesis overview

1.1 Research motivation

Renewable energy sources are becoming more important over the last decades as a result of both increasing global energy demand and the restriction caused by the scarcity of fossil energy sources. Environmental legislation evolves alongside scientific and technical development, aiming for the protection and preservation of natural resources and also to ensure the ideal standards of health, social welfare and quality of life for us and for our future generations. The exploitation of biogas as a renewable energy source is one of the promoted technologies in the European Union and particularly in Spain, in order to achieve the goal of 20% of energy coming from renewable sources until 2020. Before entering any energy conversion system, the quality of the biogas must be carefully monitored and hydrogen sulfide (H_2S) must be removed, jointly with other reduced sulfur compounds (RSCs), attending to technical restrictions and for environmental and health protection. In addition to these irrefutable motivations, the economical advantage of applying a biological process for biogas desulfurization, instead of a physicochemical one, should be considered as a really attractive subject in the sphere of the energy business.

This research has been done at the Department of Chemical Engineering of the UAB, within the Gas Treatment Group. Construction of electrodes and other analytical procedures were performed in collaboration with the Sensors and Biosensors Group of the Chemical Department at UAB. A previous study was developed by others in order to design and build a lab-scale biotrickling filter (BTF) system to treat highly H_2S-loaded gas streams (Fortuny *et al.*, 2010; 2011). In this way, a comprehensive study of biogas mimics sweetening was done, characterizing the operation of the reactor under neutral pH conditions applying a structured, organized packing material.

This thesis intended to deepen the study on the desulfurization of highly H_2S-loaded synthetic biogas by aerobic biotrickling filtration under different conditions and, concomitantly, to develop analytical tools for the on-line monitoring of the reactor. The performance of the system was assessed under neutral and acidic pH conditions, applying a random packing material, for a total period of 990 consecutive days.

1.2 Thesis overview

Research motivation is exposed in this first Chapter. A general overview of the thesis is herein presented to facilitate the consulting and understanding of the structure of the document. A general introduction is provided in **Chapter 2**, by briefly defining the principal concepts that are used in this study. Main topics treated are related to the characterization of H_2S and methylmercaptan (CH_3SH), including available technologies for detection and removal of sulfur compounds. Special attention is paid to biological technologies for H_2S elimination from biogas, specifically biotrickling filtration. The biological sulfide oxidation is also briefly described. In **Chapter 3**, main objectives of the research are stated, dividing the actions into two principal categories: Monitoring and Performance.

General materials and methods applied during this research are described in **Chapter 4**. A comprehensive description of the BTF experimental setup is provided, as well as the explanation of the construction of used electrodes, the exposition of parameters used in analytical systems characterization and the specification of common analytical techniques. Specific experimental conditions and reagents are detailed in each result Chapter.

Results obtained during the experimental period are presented and discussed from **Chapter 5** to **Chapter 9**. The optimization of an analytical flow-based system for the integrated detection and quantification of $H_2S_{(g)}$ and total dissolved sulfide (TDS = $H_2S_{(aq)}$ + HS^- + S^{2-}) is presented in

Chapter 5. Moreover, the analytical system was implemented in the studied BTF, allowing the on-line determination of the targeted species. A preliminary study on the on-line determination of sulfate (SO_4^{2-}) is outlined in **Chapter 6**. Based on a commercially available selective ionophore, a liquid membrane is optimized for the construction of an ion-selective electrode (ISE), aiming the on-line determination of SO_4^{2-}. After evaluating the drawbacks faced during this study, technical alternatives are suggested.

In **Chapter 7**, the uninterrupted transition from neutral to acidic pH conditions is described and overall results in terms of desulfurization performance are presented up to day 600 of operation. The start-up at neutral pH, the optimization of the operation aiming at the minimization of biologically produced elemental sulfur and the steady-state operation at neutral pH for 440 days are presented in detail. In **Chapter 8**, the simultaneous removal of H_2S and CH_3SH is studied under neutral pH conditions, for concentrations of both pollutants normally found in biogas. Furthermore, the effect of the gas contact time reduction and the pollutants load increase are evaluated. The operation at acidic pH was carried out for 550 days, after the uninterrupted pH transition described in **Chapter 7**, totalizing 990-uninterrupted operation days. Results obtained during the acidic pH operation until the end of operation are presented in **Chapter 9**. The response of the reactor to H_2S starvation episodes is also investigated, as well as the H_2S removal profile along the filter bed height.

Finally, in **Chapter 10**, general conclusions are presented and future research recommendations are proposed.

※

2

introduction

"Only fools and charlatans know everything
and understand nothing."

Anton P. Chekhov
(Taganrog, 1860 – Badenweiler, 1904)

2 Introduction

2.1 Atmospheric sulfur pollution

Sulfur is involved in a wide variety of biogeochemical reactions that affect the global carbon and oxygen cycles. Sulfur is found abundantly in pyrite and gypsum sediments and in oceanic sulfate salts. It is also essential for life. The sulfur cycle is fundamental to understand the geochemical evolution of the Earth and other planets, like recently discussed about the bulk sulfur composition on Mars (King and McLennan, 2010). Sulfur can be found in 25 isotopic forms, from which 4 are stable: ^{32}S, ^{33}S, ^{34}S and ^{36}S, with relative abundance values of 94.93%, 0.76%, 4.29% and 0.02%, respectively (Johnston, 2011). As can be deduced, ^{32}S is the most significant occurring isotope, and engineering calculations are made over this assumption. The study of sulfur isotope composition of seawater sulfate reflects the balance of fluxes of sulfur into and out the ocean and can be considered as a powerful tool to explain global biogeochemical changes.

Sulfur occurs in a variety of valence states, from -2 (S^{2-}), 0 (elemental sulfur, S^0) and +6 (SO_4^{2-}). Volcanoes are responsible for natural release of sulfur compounds, primarily sulfur dioxide (SO_2), but also other sulfur compounds are found in biological processes, like H_2S and other RSCs, namely volatile organic sulfur compounds (VOSCs) such as CH_3SH, dimethyl sulfide (DMS), dimethyl disulfide (DMDS) and carbonyl sulfide (COS). H_2S release to the atmosphere causes the phenomenon known as acid rain, since H_2S reacts with ozone to form sulfuric acid. Also SO_2 is considered as extremely dangerous to the atmosphere because it is an acid rain precursor. SO_2 emissions from anthropogenic sources are considered as the major issue related to the environmental management. SO_2 is formed by the combustion of sulfur-containing fuels, thus desulfurization processes must be applied before fuels burning. It is also the case of biogas, which H_2S content can be significantly high, as later discussed.

Besides the environmental implications of sulfur compounds, also they are considered extremely toxic for human health, and special protection measures must be taken when the risk of exposure is present.

2.2 Hydrogen sulfide

2.2.1 Physicochemical properties of H_2S

H_2S is a colorless gas and has a strong offensive odor of rotten eggs at low concentrations. At higher concentrations, it has a sweetish odor, but at concentrations higher than 100 ppm$_v$ of H_2S, paralysis of the olfactory nerve occurs an odor may not be detected. The primary uses of H_2S include the production of elemental sulfur and sulfuric acid, the manufacture of heavy water and other chemicals, in metallurgy and as an analytical reagent (HSDB, 2012). In agriculture, it is used as a disinfectant. Occupational exposure to H_2S occurs primarily from its presence in petroleum, natural gas, soil, sewer gas and as a byproduct of chemical reactions. H_2S is produced from numerous environmental sources including bacterial decomposition of vegetable and animal proteinaceous material.

H_2S is soluble in certain polar organic solvents, notably methanol, acetone, propylene carbonate, sulfolane, tributyl phosphate, various glycols, and glycol ethers. It is also soluble in glycerol, gasoline, kerosene, carbon disulfide, and crude oil.

However, aqueous solutions of H_2S are not stable. H_2S is a weak diprotic acid and the level of deprotonation depends on the pH of the solution, according to **Equation 1** and **Equation 2** (Steudel, 2004).

$$H_2S + H_2O \leftrightarrow HS^- + H_3O^+ \qquad\qquad [1]$$

$$HS^- + H_2O \leftrightarrow S^{2-} + H_3O^+ \qquad\qquad [2]$$

Relevant information and physicochemical characteristics of H_2S are summarized in **Table 2.1**. (ATSDR, 2006; HSDB, 2012).

Table 2.1 Physicochemical properties of H_2S

Common name	Hydrogen sulfide
Synonyms	Hydrosulfuric acid, sulfur hydride, sulfurated hydrogen, dihydrogen monosulfide, sewer gas, swamp gas
CAS register number	7783-06-4
Chemical formula	H_2S
Spatial molecular representation	
Molecular weight (ºC)	34.08
Melting point (ºC)	-85.49
Boiling point (ºC)	-60.33
Flash point (ºC)	26.00
Auto ignition temperature (ºC)	260.00
Lower explosive limit (%)	4.30 (in air)
Upper explosive limit (%)	45.50 (in air)
Density ($g \cdot L^{-1}$)	1.5392 (0 ºC; 760 mmHg)
Relative density in air	1.192
Solubility in water ($g \cdot L^{-1}$)	5.3 (10 ºC); 4.1 (20 ºC); 3.2 (30 ºC)
Vapor pressure (mmHg)	15,600 (25 ºC)

The scientific community has systematically discussed the second dissociation constant of H_2S; reported values can differ up to eight orders of magnitude (Migdisov *et al.*, 2002; Sun *et al.*, 2008). In **Table 2.2**, the most frequently adopted values for H_2S dissociation constants are given. Despite the high uncertainty level in the reported values of the second dissociation constant ($pK_{a,2}$), it is assumed that sulfide ions (S^{2-}) are only present in extremely alkaline solutions (pH>12).

Table 2.2 Dissociation constants of H_2S

$pK_{a,1}$	$pK_{a,2}$	Reference
7.05	17.4 ± 0.3	Migdisov *et al.*, 2002 (25 ºC)
7.00	17.097	Steudel, 2004 (20 ºC)
7.02	12.912	Sun *et al.*, 2008 (20 – 30 ºC)
7.04	11.96	HSDB, 2012 (20 ºC)

The chemical auto-oxidation of sulfide to thiosulfate occurs preferentially in alkaline environments with excess of oxygen, according to **Equation 3** (van den Bosch *et al.*, 2008):

$$HS^- + O_2 \rightarrow 0.5\ S_2O_3^{2-} + 0.5\ H_2O \qquad\qquad [3]$$

In addition, H_2S is found in crude petroleum, natural gas, volcanic gases, and sulfur springs. It is released into the environment from petroleum refineries, natural gas plants, sulfur production, coke-oven plants, iron smelters, paper mills, viscose rayon manufacture, tanneries, food-processing plants, dairies, and wool-scrubbing plants. The induced concrete corrosion produced by H_2S is a major concern in sewer networks. The concrete corrosion takes place when H_2S is released from the wastewater to the sewer atmosphere, being absorbed into the concrete surface above the wastewater line. H_2S is oxidized both chemically and biologically to sulfuric acid on the concrete surface, then reacting with the alkaline components of the concrete to form gypsum, which weakens the structure of the concrete pipes (Jensen *et al.*, 2011).

2.2.2 Toxicology, hazards and therapeutic potential of H_2S

Toxicity studies suggest that H_2S gas is absorbed rapidly through the lungs. Toxicological effects in human health of the exposure to H_2S are summarized in **Figure 2.1** (US-EPA, 2003; ATSDR, 2006; HSDB, 2012).
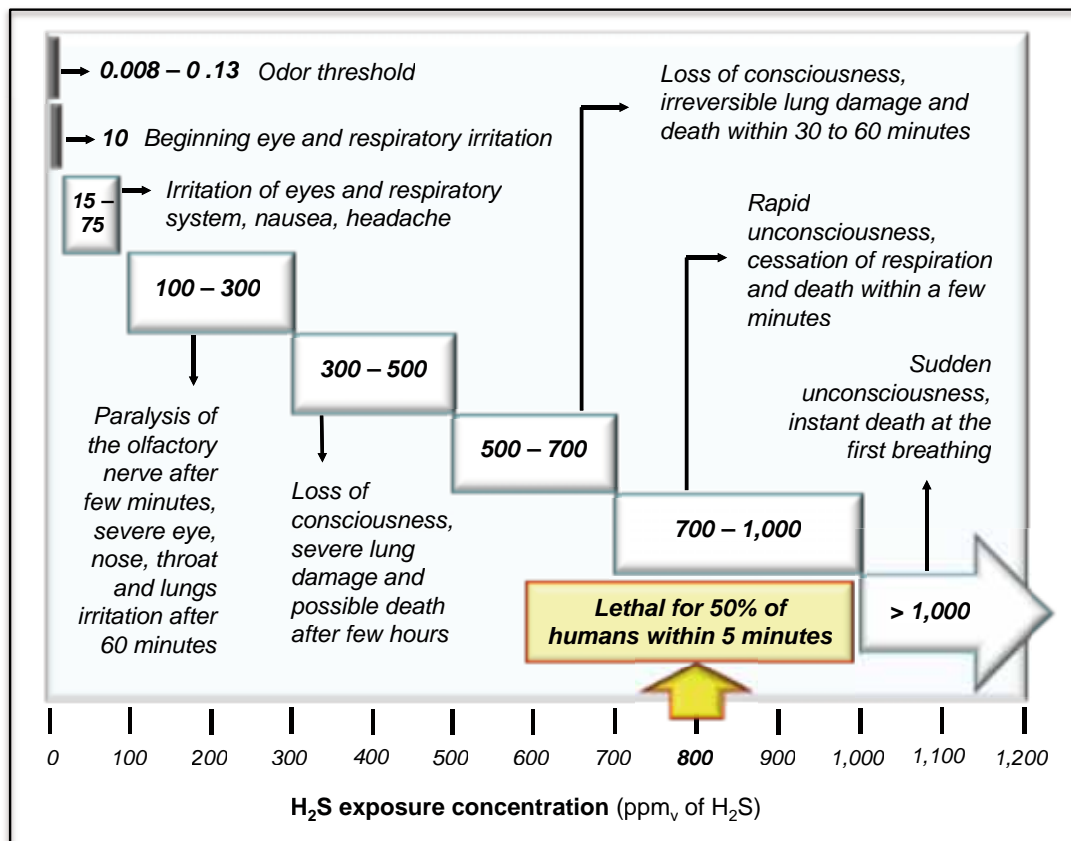
Figure 2.1 Toxicological effects in human health by exposure to H_2S

H_2S is an extremely toxic and irritating gas. In sufficiently high concentrations, it can cause instant death by blocking the oxidative processes of tissue cells and by reducing the O_2-carrying capacity of the blood. Free H_2S in blood depresses the nervous system and larger amounts can paralyze the nervous system. In acute poisoning, death is due to respiratory failure and asphyxiation. Although absorption through the skin is minimal, contact with liquid H_2S causes frostbite. In animals and humans, it distributes to the blood, brain, lung, heart, liver, spleen, and kidney.

Moreover, the exposure to H_2S is a major concern in occupational health management and strict limits are imposed. Common exposure accidents with fatal victims are due to the accumulation of H_2S in close environments, like pits or sumps, since the gas is heavier than air. The loss of the sense of smell at concentrations relatively low for the industrial emission parameters ($\approx$100 ppm$_v$ of H_2S) is the major concern for health protection actions, and proper detection and protection equipment must be used when working in

potential H_2S risk areas. For this reason, the immediately dangerous to life and health concentration (IDLH) is defined at 100 ppm_v of H_2S (NIOSH, 2011a). At this concentration, adverse health effects are irreversible and the ability to escape from the contaminated environment is already impaired.

Exposure limits to H_2S are defined as follows (ACGIH, 1996):
- TLV-TWA (Threshold Limit Value – time-weighted average): is the time-weighted average concentration for a normal 8-hours workday and a 40-hours workweek to which nearly all workers may be repeatedly exposed, day after day, without adverse effect.
- TLV-STEL (Threshold Limit Value – short-term exposure limit): is the short-term exposure limit for a 15-minutes exposure.

In Spain, H_2S was included in 2012 in the index of controlled substances for occupational exposure (INSHT, 2012), adopting the values recommended in USA and the EU. Exposure limits are as follows:

TLV-TWA = 5 ppm_v of H_2S
TLV-STEL = 10 ppm_v of H_2S

Despite its intrinsic toxicity, H_2S has been the focus of intensive medicine research in the past few years, with special attention to its therapeutic potentialities. Recently recognized as a gasotransmitter, H_2S is, jointly with nitric oxide and carbon monoxide, one of the gaseous signaling molecules that modulate many cellular functions (Epelman and Tang, 2012; Predmore *et al*, 2012).

Promising results are been obtained in the pharmaceutical investigation on the beneficial effects of several H_2S-releasing drugs. Many therapeutic targets have been successfully proved for H_2S therapy, including cancer, heart failure, organ transplant, peripheral artery disease, inflammatory bowel disease, Alzheimer's disease, acute myocardial infarction, stroke, atherosclerosis, hypertension, erectile dysfunction, metabolic syndrome, diabetes and thrombosis (Martelli *et al.*, 2012; Vandiver and Snyder, 2012).

2.3 Methylmercaptan

2.3.1 Physicochemical properties of CH₃SH

CH_3SH is a colorless gas with an extremely unpleasant characteristic odor of rotten cabbage and an odor threshold as low as 1.5 ppb_v of CH_3SH (ATSDR, 1992; Roberts, 2000). Like H_2S, CH_3SH is heavier than air and accumulates in lower closed environments, representing a high risk for human health, specially for workers at underground labors in petrochemical industry and in wastewater treatment facilities. CH_3SH is soluble in alcohol, ether, petroleum and naphta. Commercially produced by the reaction of H_2S with methanol, CH_3SH is extensively used in the synthesis of the amino acid methionine. It is also used as an intermediate in the manufacture of jet fuels, pesticides, fungicides, and plastics. CH_3SH occurs naturally in sour gases during drilling operations, in coal tar and petroleum distillates. Because of its distinctive strong odor, trace of CH_3SH is used as an odorant in gas natural networks, ensuring its early detection in potential dangerous situations. CH_3SH is also employed in pharmaceutical formulations and as a flavor and fragrance additive of a large number of products; it can be found also in cheese, milk, coffee and oysters (Roberts, 2000).

CH_3SH is a weak monoprotic acid that deprotonates in aqueous solutions according to **Equation 4**, with a dissociation constant (pK_a) value of approximately 9.7 (Smet *et al.*, 1998). Under aerobic conditions, CH_3SH chemically auto-oxidizes to form mainly DMDS, according to **Equation 5** (Jocelyn, 1972):

$$CH_3SH + H_2O \leftrightarrow CH_3S^- + H_3O^+ \qquad\qquad [4]$$

$$2\ CH_3SH + 0.5\ O_2 \rightarrow CH_3SSCH_3 + H_2O \qquad\qquad [5]$$
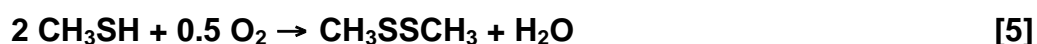
Relevant information and physicochemical characteristics of CH_3SH are summarized in **Table 2.3** (ATSDR, 1992; HSDB, 2003).

Table 2.3 Physicochemical properties of CH_3SH

Common name	Methylmercaptan
Synonyms	Methanethiol, thiomethyl alcohol, methyl sulfhydrate, mercaptomethane, thiomethanol
CAS register number	74-93-1
Chemical formula	CH_3SH
Spatial molecular representation	
Molecular weight (°C)	48.11
Melting point (°C)	-123.10
Boiling point (°C)	6.20
Flash point (°C)	-17.78
Lower explosive limit (%)	3.90 (in air)
Upper explosive limit (%)	21.80 (in air)
Density (g·L⁻¹)	0.8665 (0°C; 760 mmHg)
Relative density in air	1.66
Solubility in water (g·L⁻¹)	23.30 (20 °C); 15.39 (25 °C)
Vapor pressure (mmHg)	1,515 (26.1 °C)

2.3.2 Toxicology and occupational hazards of CH_3SH

The toxicology of CH_3SH has been less investigated than in the case of H_2S, probably because of its less occurrence. However, the intense noxious odor of CH_3SH and the variety of health effects reported indicates than CH_3SH is more toxic than other higher thiols, even when the metabolic path in humans has not been yet fully described (HSDB, 2003). CH_3SH is primary absorbed by the lungs and exposure occurs by inhalation. Nevertheless, no agreement has been established regarding to the relation between the extension of the exposure and the severity of the symptoms (ATSDR, 1992).

Potential symptoms of the exposure to CH_3SH include irritation of eyes, skin and respiratory tract, cough, sore throat, headache, nausea, shortness of breath, dizziness, unconsciousness, pulmonary edema and respiratory failure. Dermic contact with CH_3SH liquid can produces frostbite, despite it is the less frequent exposure via (ATSDR, 1992). The IDLH concentration for CH_3SH is defined as 150 ppm_v of CH_3SH (NIOSH, 2011b). Occupational exposure limits established in Spain are as follows (INSHT, 2012):

TLV-TWA = 0.5 ppm_v of CH_3SH

TLV-STEL = 10 ppm_v of CH_3SH

2.4 Sulfur compounds detection

The determination of sulfur compounds like H_2S, CH_3SH, DMS and DMDS has been traditionally performed by gas chromatography (GC) (NIOSH, 1994). However, accurate analytical methodology is scarce in different matrices (Vitenberg *et al*, 2007; Tangerman, 2009).

2.4.1 Hydrogen sulfide detection

Gas-phase H_2S can be measured indirectly, as in the case of GC, especially for low H_2S concentrations, commonly found in biological, food and pharmaceutical samples (Catalan *et al*., 2006; Vitenberg *et al*., 2007). However, this off-line methodology presents a series of drawbacks, mainly in relation with the loss of the analyte during the sampling procedure (NIOSH, 2006). Direct, real-time methodologies are also available. However, commercially available sensors for direct determination of H_2S normally operate in a range up to 1,000 ppm_v of H_2S, which represents an operational limitation for high H_2S-cointaining gases, as biogas. Most representative sensors for direct detection of H_2S are shown in **Table 2.4**, (Pandey *et al*., 2012) and their principal characteristics, regarding to the sensing principle, common fabrication materials and performance characterization are summarized.

Table 2.4   Sensors for direct detection of H_2S

Sensor type	Semiconducting oxide	Electro-chemical	Optical	Conducting polymer	Surface acoustic wave
Sensing principle	Conductivity impedance	Ampero-metry, Potentio-metry	Absorption, Fluorescence, Colorimetry	Conductivity impedance	Oscilla-tion frequen-cy
Common materials	SnO_2, Fe_2O_3, WO_3, $BaTiO_3$, ZnO, In_2O_3, CuO-SnO_2	Pt-electrode, Au-Nafion, Ceramic, doped-SnO_2	Fused silica, photoacoustic cells, quartz crystal, colorimetric dyes	Polyaniline-gold, polyaniline-metal salts	WO_3, Au, $LiNbO_3$, Poly-aniline
Response time (s)	3 – 120	4 – 10	≈0.2	66 – 120	100 – 240
Recovery time (s)	9 – 240	12 – 30	-	180 – 300	360
Range (ppm_v H_2S)	0.005 – 1,200	0.1 – 100	0.02 – 100	0.0001 – 100	$5x10^{-4}$ – 500
Limit of detection (ppb_v H_2S)	4 – 3,000	100 – sub-ppm	1 – sub-ppm	0.1	< 10

Semiconducting metal-oxide sensors are considered a simple, small and low cost technology and have been successfully applied for H_2S sensing, mostly with SnO_2 or doped-SnO_2 thin film. These sensors work by identifying the electronic changes in the surface of the metal-oxide film produced by the reaction of the targeted gas with the sensor metal-oxide component (Fine *et al.*, 2010). Electrochemical sensors may be of liquid or solid electrolytes, but for H_2S determination, mostly solid-electrolyte sensors are applied (Pandey *et al.*, 2012). Sensing principle is either amperometric or potentiometric. In amperometry, changes in the current signal are related to the concentration of the analyte; in potentiometry, changes in the voltage are measured (Vlasov *et al.*, 2010). In optical sensors, the analyte interacts with the light emitted by the optical fiber and the attenuation of the light

waves can be detected by absorption, luminescence or by the optical response of an intermediate agent (Sarma and Tao, 2007). Different types of carbon nanotubes are used as the conducting material in conducting-polymer sensors, while the polymer offers the selectivity to the targeted gas (Hernandez *et al.*, 2012; Mohammadzadeh *et al.*, 2012). Also polyaniline-based nanofibers are used for H_2S and VOSCs sensing (Liu *et al.*, 2012).

2.4.2 Sulfide detection

Once dissociated in aqueous solutions, H_2S is found as TDS, commonly referred to as simply sulfide. Many sulfide detection systems are available, as the traditional methods of methylene blue (MB), the iodimetric and the ion-selective methods (APHA, 2006a). In the MB method, sulfide, ferric chloride and dimethyl-p-phenylenediamine react to form MB, quantified by a colorimetric method. The iodimetric method consists in the titrimetric quantification of oxidated S^{2-} with iodine. ISEs based on silver sulfide electrodes are commercially available for reliable determination of S^{2-}.

However, the use of flow-based methods for sulfide determination has gain importance in the last few years, for both direct and indirect approach (Ferrer *et al.*, 2007). In the direct mode, the analyte can be directly detected by a wide number of techniques, like spectrophotometry, fluorescence, chemiluminescence, polarography, voltammetry, amperometry or potentiometry. In the indirect approach, sulfide is separated from the liquid matrix and detected as H_2S. Diverse flow-based techniques are available, namely flow injection analysis (FIA), continuous flow analysis (CFA), sequential injection analysis (SIA), multicommutation flow analysis (MCFA), multisyringe flow analysis (MSFA) and the latest developed lab-on-a-valve platforms (LOV) (Cerda *et al.*, 1999; Miro and Hansen, 2012). In despite of the wide range of flow techniques existent and the large analytical applicability of such systems, only the FIA technique will be summarized in this thesis.

The FIA technique was first described by Ruzicka and Hansen (1975) and since then it has promoted a huge develop in modern analytical procedures in diverse fields like environmental, pharmaceutical, biological and food applications, among others (Ruzicka, 1994; Hansen, 1996; Evgenev *et al.*, 2001; Trojanowicz, 2009; Felix and Angnes, 2010; Dilgin *et al.*, 2012; Ertek *et al.*, 2012; Melchert *et al.*, 2012). A simplified schematic of a FIA manifold is shown in **Figure 2.2**. The sample to be analyzed is injected and dispersed into a continuous carrier solution flow that is directed to the detection system, in which a transitory signal peak is obtained. The detector identifies a baseline when no sample is present and a peak when the sample is detected. The analytical response is the difference between peak heights and the baseline.
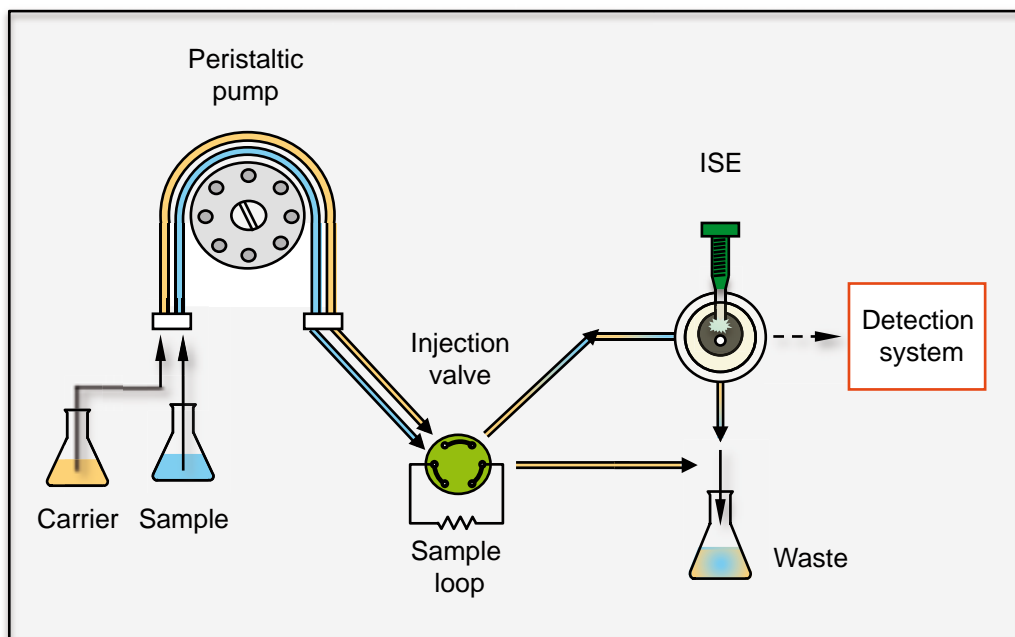
Figure 2.2 Schematic of a typical FIA manifold

FIA, as well as others flow-based techniques, offers several advantages when compared to off-line systems, such as the automatic preparation of samples, the continued calibration of sensors and the simultaneous detection of multiple analytes, besides the well-known advantages related to the high reproducibility, stability, fast response, low reagents consumption and low cost.

2.4.3 Sulfate detection

SO_4^{2-} is one of the most abundant anions in marine environment and it is the predominant S-species in soil. SO_4^{2-} determination is of special importance for environmental atmospheric management, remarkably when referred to the acid rain precipitation. It is also a relevant compound in various chemical and pharmaceutical processes. In water analysis, SO_4^{2-} is analyzed by a turbidimetric method (APHA, 1980). However, different methods have been developed for other applications in which SO_4^{2-} is present at low concentrations, such as ion chromatography (IC), capillary electrophoresis and ISEs.

Polymeric-based membrane ISEs have been developed for more than 60 analytes, being the most frequently applied chemical sensor type. Among others chemical sensors, ISEs present many advantages, such as analysis speed, portability, no sample destruction and a wide range of measuring, besides their essential property of selectivity (de Marco *et al.*, 2007). However, selectivity in ISEs depends on a large extend on the presence of neutral or electrically charged lipophilic complexing agents known as ionophores, that interact selectively with the targeted analyte (Bakker *et al.*, 1999; Buhlmann *et al.*, 2000). Besides the ionophore, other components of a polymeric membrane are the polymeric matrix, a plasticizer and lipophilic ionic additives (Faridbod *et al.*, 2008). Lipophilic additives enhance the diffusion of the analyte inside the membrane and are of capital significance in highly hydrophilic anions, like SO_4^{2-}, which is at the end of the Hofmeister selectivity sequence (organic anions > ClO_4^- > SCN^- > I^- > NO_3^- > Br^- > Cl^- > HCO_3^- > SO_4^{2-}, HPO_4^{2-}), a widely accepted and used lipophilicity expression (Wojciechowski *et al.*, 2010). Ionophores based on urea compounds have been successfully applied for SO_4^{2-} sensing, due to their high binding affinity and selectivity (Nishizawa *et al.*, 1998; Phillips *et al.*, 2005; Jia *et al.*, 2010; Young and Jolliffe, 2012). A comprehensive review on nowadays-published literature regarding polymeric matrix ISEs for SO_4^{2-} sensing is presented later on **Chapter 6**.

2.5 Energy from biogas

The European Union has a target from its energy and climate change policy known as the 20/20/20 goal that establish 20% of renewable energy in the final energy demand, 20% of reduction of greenhouse gases emissions and 20% of increase of energy efficiency. Global actions are been already taken at a long term perspective, envisioning the reduction of global emissions by about 40% by 2050 and decreasing greenhouse gases emissions by 80-95% by 2050 (European Commission, 2011; Duic *et al.*, 2013). In Spain, about 25% of the electric power comes currently from renewable energy sources, mainly wind and solar thermoelectric and photovoltaic technologies (Ruiz-Romero *et al.*, 2012). Promotion policies for the development of renewable energy technologies, such as biogas, are priority in global sustainable energy actions (San Miguel *et al.*, 2010). However, besides the inherent technical challenge, social resistance showed by the unwillingness to pay extra costs of renewable energy (Gracia *et al.*, 2012), is another difficulty to overcome.

Biogas is a versatile renewable fuel that, because of its high energetic content, can be used as an energy source for power and heat or cool production. Biogas consists mainly of methane (CH_4) and carbon dioxide (CO_2), but also contains some trace compounds such as H_2S, thiols, siloxanes, ammonia and other volatile organic compounds (VOCs), as detailed in **Table 2.5**. Yet, the composition of biogas depends intimately on the origin and characteristics of the substrate.

A content in CH_4 higher than 45% makes the biogas a flammable mixture, whit 4.4 to 15% of CH_4 in air. Thus, the conversion of its chemical energy into heat, electricity or fuel is possible by combustion. Also, the interest in the exploitation of biogas energy potential has been encouraged by the increasing global concern about climate change, specially related to the greenhouse gases emissions, and as an alternative option to facing the fossil fuels depletion (Abatzoglou and Boivin, 2009; Hennig and Gawor, 2012; Yamasaki *et al.*, 2013).

Table 2.5 Main components in biogas and related effects

Component	Content	Effect
CH_4 (% v·v^{-1})	50 – 75 [a] 35 – 75 [b] 60 – 68 [c] 62 – 65 [d]	Energy source
CO_2 (% v·v^{-1})	25 – 50 [a] 25 – 65 [b] 32 – 40 [c] 35 – 38 [d]	Lost of calorific value; corrosion in wet gas
H_2S (% v·v^{-1})	0 – 0.5 [a] 0.0001 – 1.0 [b] 0.1 – 2.0 [c] < 0.001 [d]	Stress corrosion in equipment and piping; SO_2 emissions after burning
NH_3 (% v·v^{-1})	0 – 0.05 [a] < 0.0005 [d]	NO_x emissions after burning
Water vapour (% v·v^{-1})	1.0 – 5.0 [a]	Corrosion / freezing of equipment and piping; condensates are harmful for instruments
Dust (μm)	> 5.0 [a]	Blocks of nozzles
N_2 (% v·v^{-1})	0.0 – 5.0 [a]	Lost of calorific value
Siloxanes (mg·m^{-3})	0.0 – 50.0 [a] 200 – 700 [d]	Abrasion of engines

[a] Deublein and Steinhauser, 2008   [b] Abatzoglou and Boivin, 2009
[c] Lastella *et al.*, 2002   [d] Kymalainen *et al.*, 2012

Formation of CH_4 is the natural biological process of organic matter degradation in the absence of O_2 by anaerobic digestion (AD). In nature, CH_4 is formed as swamp gas and in the digestive tract of ruminants. Anthropogenic sources of biogas such as landfill, composting, wastewater and industrial sludge anaerobic treatment normally yield high CH_4 concentrations (Abatzoglou and Boivin, 2009).

AD is widely applied for wastewater sludge and municipal solid waste treatment, agricultural and livestock wastes and diverse industrial effluents (Khalid *et al.*, 2011). AD can be understood as a succession of four main reactions: hydrolysis, acidogenesis, acetogenesis and methanogenesis. During hydrolysis, organic molecules are de-polymerised by extra-cellular enzymes; obtained monomers are then converted into short- and long-chain organic acid, alcohols, hydrogen and CO_2. Then, bacteria known as acetogens degrade the products from acidogenesis phase to produce acetic acid, hydrogen and CO_2. Acetic acid is finally degraded by methanogenic bacteria, producing CH_4 (Deublein and Steinhauser, 2008). The CH_4 content in the biogas depends on the control of several operational parameters during AD, such as H_2 partial pressure, concentration of microorganisms, type of substrate, pH, temperature and nutrients C/N ratio.

Biogas impurities, remarkably H_2S and other RSCs, must be removed before energy production, avoiding equipment corrosion and because of the risk of releasing sulfur oxides. Allowable H_2S amount in biogas for energy recovery purposes varies from 1 to 10 ppm_v of H_2S in the case of fuel cells applications and through 130 to 500 ppm_v of H_2S for gas motor and burning engines, respectively (Deublein and Steinhauser, 2008; Ciccoli *et al.*, 2010).

2.6 Desulfurization technologies

2.6.1 Physicochemical technologies

Technologies for the desulfurization of gas streams could be divided according to the quantity of H_2S to be removed. In this way, for large quantities of H_2S removed (> 20 t S·day^{-1}), we must refer to the classical Claus process, schematized in **Figure 2.3** (de Angelis, 2012), applied largely at the petrochemical and related industries (Tyurina *et al.*, 2011). Normally used for the recovery of sulfur after a previous concentration step by amine absorption, the Claus process consists in a step of combustion followed by a cascade configuration of catalytic reactors. When CO_2 and

H$_2$S are present, the selection of the amine is related to the ratio of these components. Commonly used amine solutions are monoethanolamine (MEA), diethanolamine (DEA) and methyldiethanolamine (MDEA) (Busca and Pistarino, 2003).
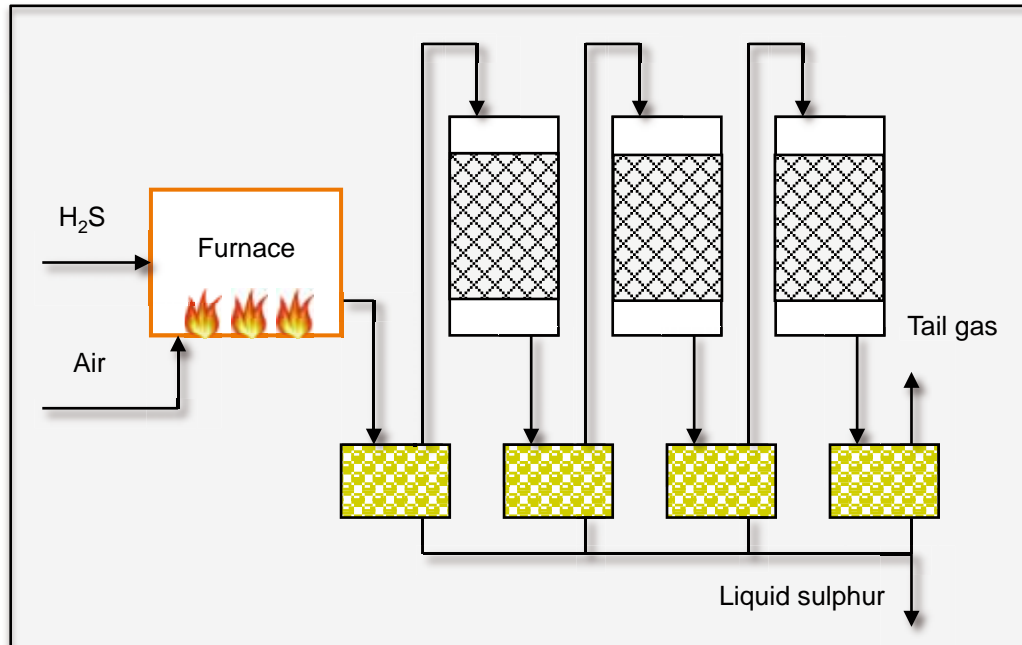
Figure 2.3 Schematic of the Claus process

Most of S^0 is currently produced by the Claus process and commercially valorized for the production of sulfur compounds, mainly sulfuric acid (Busca and Pistarino, 2003). However, the gaseous out stream of the last catalytic reactor of the Claus process (tail gas) contain a mixture of sulfur compounds (H$_2$S, SO$_2$, COS, CS$_2$ and S^0) and need further hydrogenation before being recycled to the first reactor (de Angelis, 2012).

For the removal of moderate to low H$_2$S quantities (< 20 t S·day^{-1}), most frequently applied physicochemical technologies are based in absorption, adsorption and direct conversion of sulfur compounds. The dissolution of a gas stream directly into a solvent liquid is known as chemical absorption (**Figure 2.4**) (Busca and Pistarino, 2003). The selection of the liquid absorbent is done accordingly with the nature and properties of the contaminant and the operational conditions (Rene *et al.*, 2012).
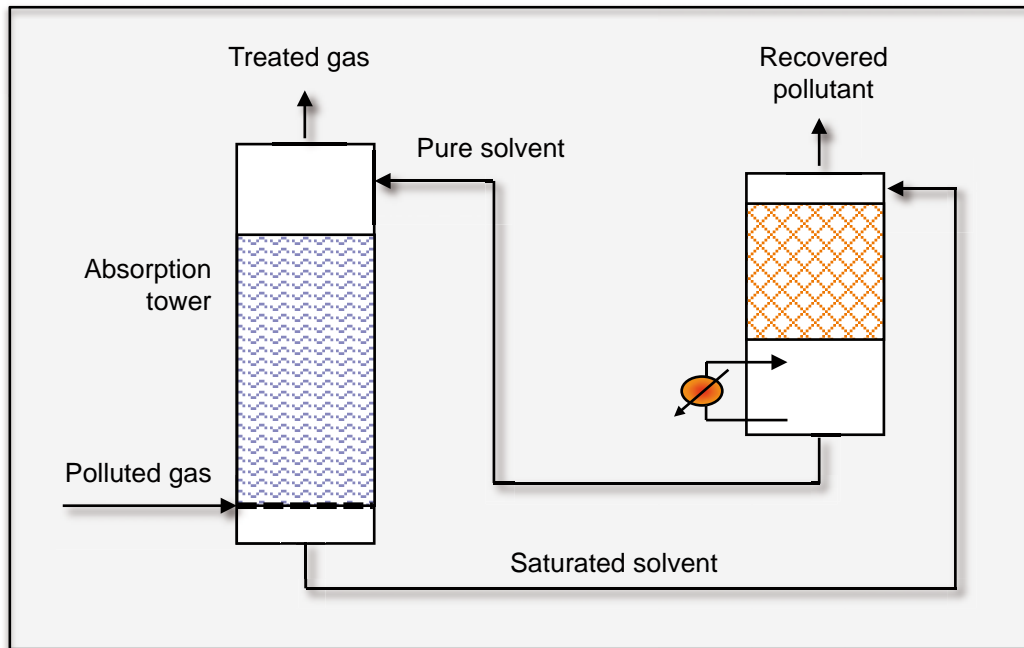
Figure 2.4 Schematic of a chemical absorption process

Chemical absorption processes for the conversion of H_2S to sulfur are well known in industrial applications and are based on the affinity of H_2S for metallic cations (Abatzoglou and Boivin, 2009). LO-CAT® (US Filter) is the most widely used commercial desulfurizing process, followed by the SulFerox® (Shell/Dow) process (de Angelis, 2012). In these processes the H_2S is absorbed in an alkaline ferric solution; H_2S is oxidized to sulfur by the ferric ions, which are then reduced to ferrous ions. A chelant compound is used as a catalyst, usually ethylenediaminetetraacetic acid (EDTA) and nitrilotriacetic acid (NTA), in order to keep the iron in solution, preventing the precipitation of iron hydroxide or iron sulfide (Horikawa *et al.*, 2004). After S^0 separation, the ferrous solution must be re-oxidized by air. The recovered S^0 is frequently contaminated by organic compounds and traces of iron sulfides, thus requiring post treatment.

Chemical scrubbing is also an absorption process in which the most commonly used chemicals are oxidative compounds, like ozone, hydrogen peroxide and sodium hypochlorite. This kind of technology is not commonly applied in biogas purification process, keeping the field of application to the large-scale industrial operations (Abatzoglou and Boivin, 2009). Also water

scrubbing is suitable for air pollution control, normally in countercurrent type packed scrubbers, but the elevated consumption of water and the need of multiple units are economical and technical limitations for its application in environmental desulfurization (Rene *et al.*, 2012). Conversion of H_2S to low solubility metallic sulfides is done by the diffusion of the H_2S-containing gas into sulfate aqueous solutions, such as $CuSO_4$ or $ZnSO_4$, but also a ferric solution is needed to form S^0 via a redox reaction. The application of this technology implies high costs and complexity, being not suitable for low scale desulfurization (Abatzoglou and Boivin, 2009).

Physical or physicochemical adsorption is based in the selective adsorption of the pollutant into a solid adsorbent. Most commonly applied adsorbents are activated carbons, activated alumina, silica gels and zeolites (Schlegelmilch *et al.*, 2005; Estrada *et al.*, 2012). Wood chips impregnated with iron oxides, also known as iron sponge, is the most frequently used iron-oxide technology for biogas desulfurization, normally operated in batch mode with a separate regeneration step (Abatzoglou and Boivin, 2009). In thermal treatment, both catalytic and non-catalytic techniques can be used. Catalytic processes allow the application of lower temperatures, hence reducing energy costs. However the cost of catalysts remain an important issue to be taken into account.

2.6.2 Biological technologies

Based on naturally occurring bioprocesses, biological technologies for the desulfurization of gas streams are widely applied, mainly for biogas purification and odor control operations, but also for highly-loaded gas streams treatment. Biological reactors are considered to be effective, reliable, environmentally friendly, robust and economical. Some attractive features of biological processes are the low chemical consumption and the relatively low energy requirements, since bioprocesses normally are conducted at atmospheric pressure and ambient temperature. Also, biological systems do not transfer pollutants to other media, like scrubbing

liquids or adsorbents. The advantages of biological desulfurization when compared with physicochemical technologies are evident from both technical and economical point of views (Devinny *et al.*, 1999; Burgess *et al.*, 2001; Schlegelmilch *et al.*, 2005). Biological technologies are believed to present an operating cost up to six times lower than physicochemical ones, with the additional advantages to be less sensitive than those (Estrada *et al.*, 2012).

Microorganisms associated with sulfur compounds removal are normally present as a biofilm layer that grows attached to a carrier material, but also systems with suspended biomass are available. Pollutants in the gas phase must be transferred to the biofilm or absorbed into the liquid phase to be biologically degraded. Moisture or liquid content is thus a vital parameter, frequently controlled together with others such as temperature, pH and nutrients content (Devinny *et al.*, 1999). Biofilters and BTFs are the most commonly used reactor configurations for desulfurization of waste gases (Estrada *et al.*, 2012; Rene *et al.*, 2012). Also bioscrubbers have been applied for H_2S and VOCs removal and other biotechnologies such as membrane bioreactors, two-phase bioreactors and activated sludge diffusion (Iranpour *et al.*, 2005; Kennes *et al.*, 2009). Moreover, the combination of physicochemical and biological technologies or the use of two-stage biological reactors is recommended to overcome some specific operational restrictions (Rene *et al.*, 2012). BTF operation will be presented in more details in order to define and characterize the reactor configuration used in this research.

Bioscrubbers

Bioscrubbers (**Figure 2.5**) are a combination of an absorption unit followed by a separated biological unit. In the absorption step, commonly a packed tower configuration, the contaminant is absorbed into the liquid phase and then, once absorbed, is directed to a separated agitated bioreactor, usually a conventional activated sludge reactor. Once the

degradation is completed in the bioreactor, the liquid phase could be recycled to the absorption unit.
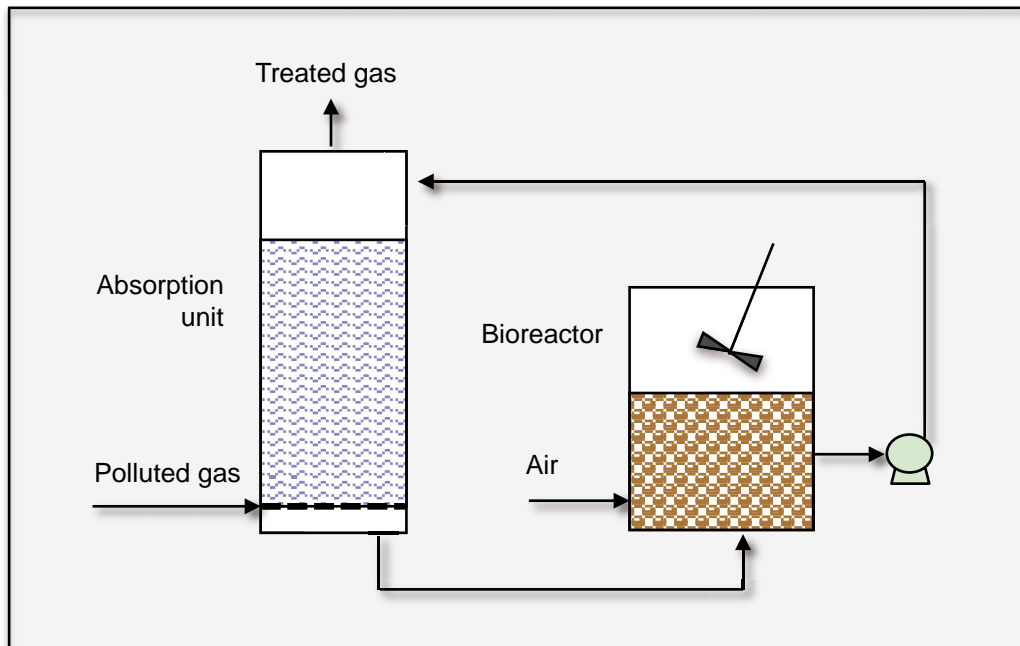
Figure 2.5 Schematic of a bioscrubber

Bioscrubbing presents some benefits when compared to other packed media bioprocesses, mainly because the control of the process, in terms of pH and temperature control and the regulation of the nutrient balance, can be performed directly in the biological reactor (Smet and van Langenhove, 1998). Also, the removal of metabolic products is done by washouts, avoiding the possible inhibition of the biomass. However, the efficiency of the bioscrubbing system relies on the dissolution of the pollutant into the water scrubbing phase and also on the control of biomass accumulation inside the bioreactor, to reduce the solid waste output and to increase the gas treatment capacity (Janssen *et al.*, 1995; Burgess *et al.*, 2001). Gas pollutants, such as H_2S and SO_2 and highly water-soluble compounds, such as alcohols and aldehydes have been successfully removed in bioscrubbers (Rene *et al.*, 2012). The most used bioscrubbing system for large-scale industrial biogas desulfurization is the THIOPAQ® (Paques) process (Abatzoglou and Boivin, 2009), originally developed for biogas treatment, but currently adapted also for high-pressure natural gas and other refinery

gases desulfurization (van den Bosch *et al.*, 2007; Janssen *et al.*, 2008). The system consists in a scrubbing unit with sodium carbonate followed by a bioreactor, in which microorganisms of the genus *Thiobacillus* are responsible for the oxidation of sulfide to elemental sulfur. THIOPAQ® technology is also frequently applied in the petrochemical industry, with the advantage of substituting the traditional amine absorption plus Claus process plus Tail gas treatment (Benschop *et al.*, 2004).

Biofilters

Traditionally designed as open soil beds, biofilters (**Figure 2.6**) have been extensively used for waste gas and odor control in industrial and municipal facilities (Iranpour *et al.*, 2005). The improvement on the design and operation of this kind of reactor lead to more complex features with closed system configurations and automated control (Rene *et al.*, 2012; Shareefdeen, 2012). When potentially toxic pollutants are treated by biofiltration, a closed reactor configuration is required because of the associated environmental and health restrictions.
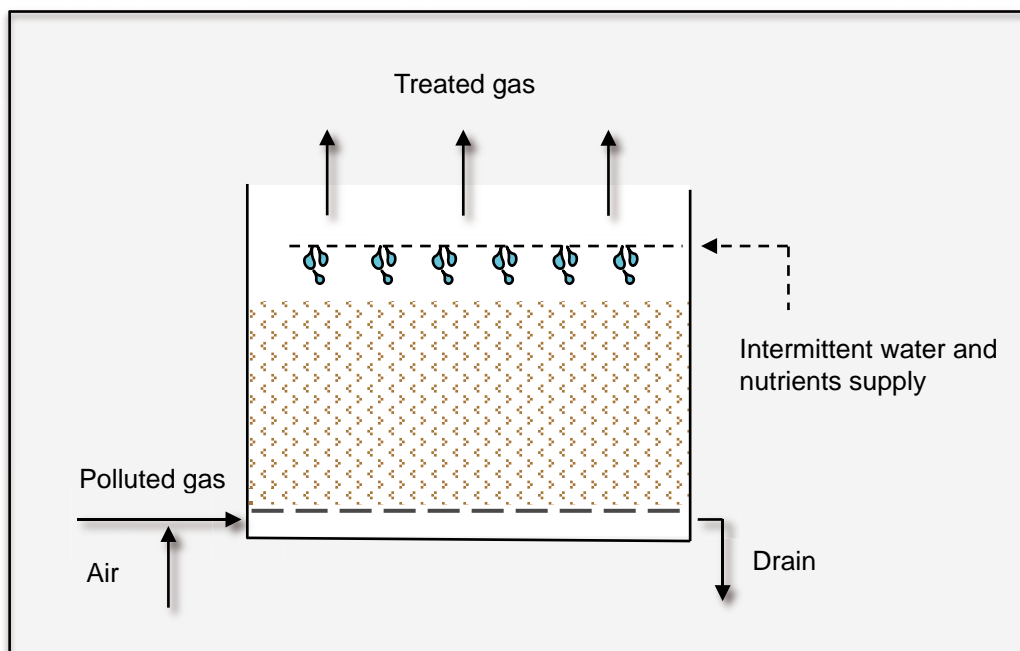
Figure 2.6 Schematic of an open-bed biofilter

Characteristically an aerobic process, biofiltration consists in the pass of the contaminated gas stream through a porous bed that supports immobilized microorganisms; the contaminant in the gas phase is first absorbed into the water interphase of the biofilm and then biologically degraded. Biofilters are normally packed with organic materials, like compost, wood, pine bark, peat, granulated sludge and other materials (Dumont and Andres, 2009; Pantoja-Filho *et al.*, 2010; Dumont *et al.*, 2012a). This feature provides a nutrient source for the microorganisms, minimizing the needs of extra nutrients supply. However, the moisture of the filter bed must be ensured and periodical watering of the biofilter must be provided in order to keep the water content of the filter bed (Devinny *et al*, 1999; Dorado *et al.*, 2010).

Major drawbacks in biofiltration refers, jointly with the humidity control of the filter bed, to the need of large quantities of packing material, to the deterioration of the packing at the long-term operation, leading to a loss of performance, and to the accumulation of metabolites from the biological degradation process. Also, major cost of the biofilters operation is related to the packing material replacement (Prado *et al.*, 2009; Rojo *et al.*, 2012). The effectiveness of the biofiltration process depends on the nature of the pollutant and its water solubility as well as on the activity of the biofilm. To ensure an effective operation, also other parameters must be controlled, such as the media pH, temperature, bed moisture, nutrients supply, O_2 availability and pressure drop inside the filter bed (Burgess *et al.*, 2001; Devinny and Ramesh, 2005; Andreasen *et al.*, 2012).

Various organic and inorganic compounds have been successfully treated in biofilters, like alcohols, aldehydes, ketones, hydrocarbons, carboxylic acids, H_2S and NH_3 (Iranpour *et al.*, 2005; Rene *et al.*, 2012; Detchanamurthy and Gostomski, 2012). The biofiltration of H_2S have been extensively reported, especially for odor control, where low concentrations of H_2S are present and high flow rates are applied (Hirai *et al.*, 1990; Wani *et al.*, 1999; Cho *et al.*, 2000; Elias *et al.*, 2002; Malhautier *et al.*, 2003; Schieder *et al*, 2003). Fungal biofilters have been successfully applied on

the removal of hydrophobic VOCs, due to the capability to perform under extreme acidic pH conditions with low humidity content (van Groenestijn *et al.*, 2001; Kennes and Veiga, 2004; Vergara-Fernandez *et al.*, 2012).

Biotrickling filters

BTFs (**Figure 2.7**) work quite similarly to biofilters, except that the packed bed is continuously trickled over with a nutrient solution. Packing material is usually of inert nature (Devinny *et al.*, 1999; Kennes *et al.*, 2009). Plastic, metallic or ceramic rings, saddles and spherical elements and polyurethane (PU) foam are commonly used. Also, perlite, celite, lava rock and activated carbon (Ramirez *et al.*, 2009) are applied.
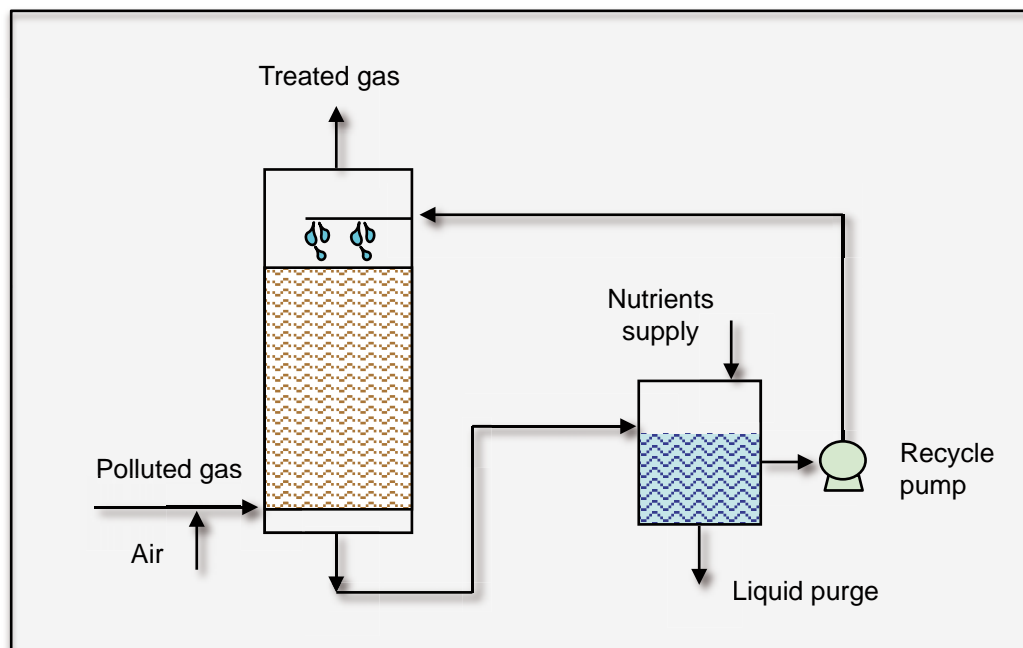
Figure 2.7 Schematic of a counter-current biotrickling filter

Mass transfer from gaseous to liquid phase of packed towers has been comprehensively studied and the effect of fluid dynamics has been established for a large number of commonly applied random packing materials (Mackowiak, 2011). However, in BTFs, mass transfer is profoundly affected by the development of the biofilm layer, even if it can be maximized with increasing the gas velocity (Kim and Deshusses, 2008a).

Microorganisms attached to packing material develop in a complex biofilm, where the pollutant absorption and diffusion take place. The polluted gas is forced to pass through the packed bed in either down or upflow mode, while the liquid phase is collected in a sump and continuously recycled over the packing. Reactor inoculation is required because of the inert nature of the packing material. Specific inoculation with selected microbial strains or non-specific inoculation, with a mixture of microorganisms can be used (Aroca *et al.*, 2007; Sercu *et al.*, 2007). Biomass growth control is an important operational parameter to prevent clogging of the filter bed. Also, the thicker the biofilm, the worse the pollutant and oxygen transfer through the deeper portion or the biofilm, thus reducing the treatment efficiency and raising the pressure drop (Devinny and Ramesh, 2005; Mannucci *et al.*, 2012). To overcome the biomass accumulation problem, several actions are possible, from the restriction on nutrients supply, the addition of growth-limiting concentrations of NaCl, to the use of predating higher organism and the development of mechanical processes for biomass removal, like backwashing and air sparging (Devinny *et al.*, 1999; van Groenestijn and Kraakman, 2005; Kennes *et al.*, 2009).

Besides maintaining the humidity and nutrients content, the recirculating liquid phase allows an accurate control of the system pH and the biological by-products removal by periodical purges, preventing possible inhibitory effects (Cox and Deshusses, 1998). The superficial trickling liquid velocity (TLV) may affect the reactor performance when exceeding a critical value up to which no sloughing of the biomass is achieved. In BTFs, normal TLV values are below 10 m·h^{-1} (Kim and Deshusses, 2008b). The performance of the system is closely related to the pollutant solubility in the liquid phase and a dimensionless air-water partitioning coefficient below 1 is recommended (van Groenestijn and Hesselink, 1993; Devinny *et al*, 1999). Treatment of compounds with air-water partitioning coefficients considerably lower than 1, such as H_2S, CH_3SH, DMS and DMDS (Smet *et al.*, 1998; Liu *et al.*, 2013) is, consequently, highly feasible in BTFs, even if the treatment of VOCs is preferentially done in biofilters (Iranpour *et al.*, 2005). BTFs have been successfully applied in the removal of H_2S and

other RSC mixtures, for low and high pollutant concentrations (Ruokojarvi *et al.*, 2000; Gabriel and Deshusses, 2004; Kim and Deshusses, 2005; Sercu *et al.*, 2005; Jin *et al.*, 2007; Fortuny *et al.*, 2008; Arellano-Garcia *et al.* 2009; Ramirez *et al.*, 2009; Tomas *et al.*, 2009; Fortuny *et al.*, 2011; Lafita *et al.*, 2012; Montebello *et al.*, 2012).

Other biological technologies

Other biological technologies are also applied in the desulphurization of air and gas streams, like membrane bioreactors, two-phase bioreactors and activated sludge diffusion. In membrane bioreactors, pollutants in the gas phase are diffused to the liquid phase, through a membrane. Biological degradation is achieved by the biofilm attached to the membrane, with high mass transfer capacities. (Reij *et al.*, 1998; Burgess *et al.*, 2001). Selection of the membrane type must be done taking into account pollutant properties and hydraulic characteristics of the system. Major drawbacks of this technique are related to the cost of the membrane. Also, excessive growth of the biofilm can lead to fouling episodes that produces, in extreme cases, the breakdown of the system (de Bo *et al.*, 2002; Kumar *et al.*, 2008).

The treatment of hydrophobic VOCs and other compounds scarcely soluble in water can be done in two-phase bioreactors. The previous addition of a non-aqueous liquid phase, such as organic solvents or polymers, improves the mass transfer of the pollutant. Solvents, known as the transfer vector, are immiscible in water and slowly releases the pollutant into the aqueous phase, where are biologically degraded; the increase in the mass transfer is larger the greater the solubility of the compound in the solvent (Cesario *et al.*, 1997; Muñoz *et al.*, 2012). Commonly used transfer vectors are silicone oils (polydimethylsiloxanes), hexadecane and perfluorocarbons. Recent research reports reveal promising possibility for the application of two-phase bioreactors at industrial scale (Rocha-Rios *et al.*, 2011; Dumont *et al.*, 2012b; Muñoz *et al.*, 2012), in contrast with the traditional laboratory-scale application of such technology.

Activated sludge diffusion represents an alternative, cost-effective technology to other biological media-based bioreactors. The polluted gas stream is sprinkled directly into the aeration tank, thus being diffused together with the oxygen into the mixed liquor of the activated sludge unit, making possible the biological degradation by the existent microorganisms (Burgess *et al.*, 2001; Barbosa *et al.*, 2006). This technology offers the possibility of overcoming most of the limitations encountered in biotrickling filters and biofilters, such as the deterioration of packing materials or the accumulation of metabolites. Nevertheless, despite the demonstrated efficiency in the removal of H_2S, the lack of reliable data has limited the application of this technique (Lebrero *et al.*, 2011).

2.7 The biological sulfur cycle

Sulfur can be present in a variety of oxidation states in the biological sulfur cycle, being -2 (S^{2-}), 0 (S^0) and +6 (SO_4^{2-}) the most significant in nature, as briefly shown in **Figure 2.8** (adapted from Robertson and Kuenen, 2006).
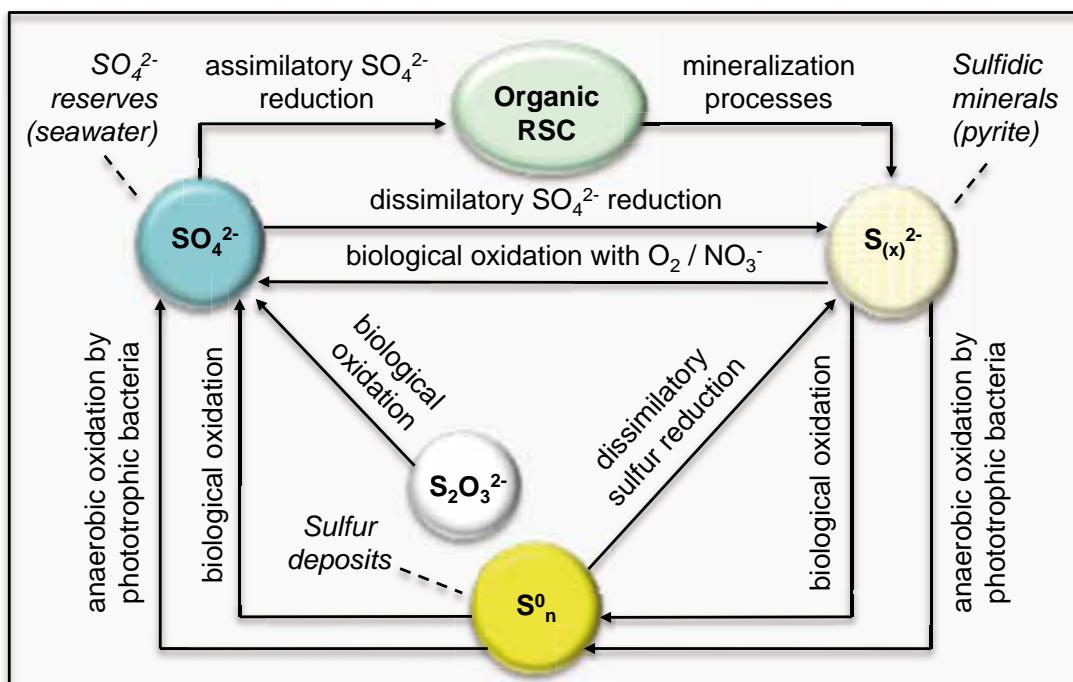
Figure 2.8 Simplified representation of the biological sulfur cycle

Inorganic sulfur plays an important role in biological metabolism, being used either as a sulfur source in assimilatory metabolism or as electron donor/acceptor in the dissimilatory metabolism, allowing very important biological energy processes (Bruser *et al.*, 2004). Many oxidation-reduction reactions occur in both sides of the sulfur cycle. SO_4^{2-}, on the reductive side, acts as an electron acceptor and is converted to S^{2-} by numerous microorganisms. On the oxidative side, RSCs act as electron donors to be converted to S^0 and SO_4^{2-} by phototrophic or chemolithotrophic bacteria (Robertson and Kuenen, 2006; Tang *et al.*, 2009). The oxidative side of the sulfur cycle is more relevant for the understanding of the concepts focused in this thesis.

The biological removal of H_2S can be overall described according to the **Equation 6** (Syed *et al.* 2006), considering the simplified metabolism of chemotrophs organisms.

$$H_2S + CO_2 + nutrients + O_2 \rightarrow cells + S^0 / SO_4^{2-} + H_2O \qquad [6]$$

When the oxidation is partially achieved, high values of SO_3^{2-} and S^{2-} are found. The complete pathway of sulfide oxidation has been proposed as the intermediates sequence oxidation according to **Equation 7** (Duan *et al.*, 2005), being S^0 and SO_4^{2-} the final products with the formation of intermediary products such as thiosulfate, dithionate, trithionate, tetrathionate and sulfite.

$$H_2S \rightarrow S^0 \rightarrow S_2O_3^{2-} \rightarrow S_2O_6^{2-} \rightarrow S_3O_6^{2-} \rightarrow S_4O_6^{2-} \rightarrow SO_3^{2-} \rightarrow SO_4^{2-} \quad [7]$$

However, biological degradation depends strongly on the type of bacteria present. Chemotrophic bacteria are able to oxidize H_2S using O_2 as an electron acceptor. The electron donors could be S^0, H_2S, or $S_2O_3^{2-}$ (Tang *et al.*, 2009). Aerobic biological sulfide oxidation can be described according to **Equation 8** and **Equation 9** (Kelly, 1999).

$$HS^- + 0.5\ O_2 \rightarrow S^0 + OH^-\ \{\Delta G^0 = -145.2\ kJ\ (mol\ S\text{-substrate})^{-1}\} \qquad [8]$$

HS⁻ + 2 O₂ → SO₄²⁻ + H⁺ {ΔG⁰ = -732.6 kJ (mol S-substrate)⁻¹}   **[9]**
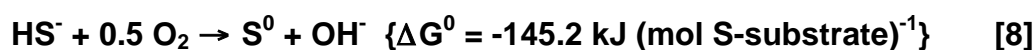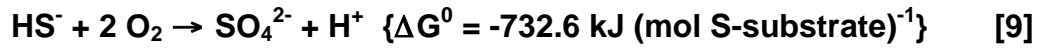
In the presence of sulfur-oxidizing bacteria (SOB), it is thought that the S^0 produced is first bound into the cell, to be further oxidized to sulfate at a much lower rate, according to **Equation 10**. Also, the biological thiosulfate oxidation happens as described in **Equation 11** (Kelly, 1999).

S⁰ + 1.5 O₂ + H₂O → SO₄²⁻ + 2 H⁺   **[10]**

S₂O₃²⁻ + 2 O₂ + H₂O → 2 SO₄²⁻ + 2 H⁺   **[11]**
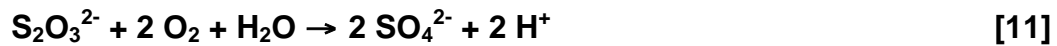
Anoxic biological sulfide oxidation can be described according to **Equation 12** and **Equation 13** (Soreanu *et al.*, 2008). However, anoxic sulfide oxidation will not be discussed further in this document because is not the main focus of this research.

3 H₂S + NO₃⁻ → 3 S⁰ + 0.5 N₂ + 3 H₂O   **[12]**

3 H₂S + 4 NO₃⁻ → 3 SO₄²⁻ + 2 N₂ + 6 H⁺   **[13]**
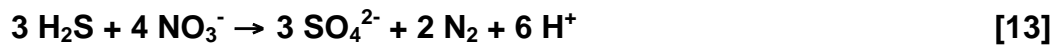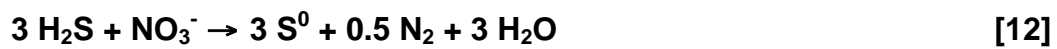
2.7.1 Sulfur-oxidizing bacteria

Carbon, energy, and electron sources are required for microorganisms' growth. Autotrophic microorganisms obtain carbon mainly from CO_2 while heterotrophs get it from reduced compounds or other organic molecules. Microorganisms that acquire energy from light are phototrophs, while those that obtain energy from the oxidation of organic or inorganic compounds are chemotrophs. The electron source for organotrophs are organic molecules, while reduced inorganic molecules in the case of lithotrophs. Most bacteria used in H_2S removal, both heterotrophics and autotrophics, are chemolithotrophs, as they obtain energy from the oxidation of H_2S, an inorganic compound. Reactors with phototrophic SOB are not frequently applied for desulfurization processes in industrial applications, since highly

clean and transparent reactors are required. In **Table 2.6**, representative chemotrophic SOB that have been described to growth lithotrophically by the oxidation of RSCs are presented (Bruser *et al.*, 2004; Robertson and Kuenen, 2006; Syed *et al.*, 2006).

Table 2.6   Representative chemotrophic SOB

	Bacteria	*Trophy*	*Substrate*	*Optimum pH growth*
α-Proteo-bacteria	*Rhodobacter*	F	HS^-, $S_2O_3^{2-}$, S^0	6.5 – 7.5
	Paracoccus versutus	F	HS^-, $S_2O_3^{2-}$, S^0	6.0 – 8.0
	Thiobacillus novellus	F	$S_2O_3^{2-}$	6.0 – 8.0
β-Proteobacteria	*Thiobacillus thioparus*	O	HS^-, $S_2O_3^{2-}$, S^0	6.0 – 8.0
	Thiobacillus denitrificans	O	HS^-, $S_2O_3^{2-}$, S^0	6.8 – 7.4
	Thiomonas thermosulfatus	F	$S_2O_3^{2-}$, S^0	5.2 – 5.6
	Thiomonas cuprinus	F	S^0	3.0 – 4.0
	Thiomonas intermedia	F	HS^-, $S_2O_3^{2-}$, S^0	5.5 – 6.0
γ-Proteobacteria	*Beggiaota*	F	HS^-, $S_2O_3^{2-}$	6.0 – 8.0
	Acidithiobacillus ferrooxidans	O	HS^-, $S_2O_3^{2-}$, S^0	2.0 – 4.0
	Acidithiobacillus thiooxidans	O	HS^-, $S_2O_3^{2-}$, S^0	2.0 – 3.5
	Halothiobacillus halophillus	O	$S_2O_3^{2-}$	7.0
	Halothiobacillus neapolitanus	O	HS^-, $S_2O_3^{2-}$, S^0	6.0 – 8.0
	Thiomicrospira	O	HS^-, $S_2O_3^{2-}$	6.0 – 8.0
	Thiotrix nivea	F	HS^-, $S_2O_3^{2-}$, S^0	6.0 – 8.5
ε-Proteo-bacteria	*Thiovulum*	O	HS^-, S^0	6.0 – 8.0
	Sulfurimonas denitrificans	O	HS^-, $S_2O_3^{2-}$, S^0	6.0 – 8.0

F: facultative autotroph
O: obligate autotroph

Several studies in H_2S biofiltration and biotrickling filtration indicate that obligate chemoautotrophs *Thiobacillus* sp. and *Acidithiobacillus* sp. are the most frequently applied SOB (Robertson and Kuenen 2006). In **Table 2.7**, main growth conditions and other information for most representative *Acidithiobacillus* sp. and *Thiobacillus* sp. are given (Robertson and Kuenen, 2006; Syed *et al.*, 2006).

Table 2.7   Main characteristics of *Acidithiobacillus* sp. and *Thiobacillus* sp.

	Acidithiobacillus ferrooxidans	*Acidithiobacillus thiooxidans*	*Thiobacillus thioparus*	*Thiobacillus denitrificans*
Optimal pH growth	2.0 – 4.0	2.0 – 3.5	6.0 – 8.0	6.8 – 7.4
Optimal temperature growth *(ºC)*	30 – 35	28 – 30	28	30
Energy source	Fe^{2+}, RSCs	H_2S, S^0, poli-thionates	$S_2O_3^{2-}$, S^{2-}	$S_2O_3^{2-}$, $S_4O_5^{2-}$, SCN^-, S^{2-}, S^0
Oxygen requirement	Facultative anaerobe	Strictly aerobe	Strictly aerobe	Facultative anaerobe

❋

3

objectives

"I want to understand you;
I study your obscure language."

Alexander S. Pushkin
(Moscow, 1799 – Saint Petersburg, 1837)

3 Objectives

The general objective of this research was to improve the existing knowledge in the aerobic biotrickling filtration of biogas mimics aiming at the desulfurization of high loads of H_2S in a lab-scale counter-current BTF, using a random packing material. To accomplish this main purpose, specific objectives are outlined into two main categories: Monitoring and Performance.

Monitoring

*   To optimize the operational conditions of an integrated continuous gas/liquid flow analytical system for the determination of $H_2S_{(g)}$ and total dissolved sulfide (TDS = $H_2S_{(aq)}$ + HS^- + S^{2-}). To achieve this objective, a tubular ISE of a crystalline membrane of Ag_2S was constructed and characterized (**Chapter 5**).

*   To incorporate the optimized H_2S/TDS analyzer based on flow injection analysis technique into the BTF, for the on-line monitoring of its performance during real operation episodes (**Chapter 5**).

*   To validate the response of the constructed Ag_2S electrodes with a commercial available ISE for TDS measurement (**Chapter 5**).

*   To study the application of a commercial bis-thiourea ionophore and to optimize the composition of the sensing cocktail for the construction of an ISE for direct determination of SO_4^{2-} (**Chapter 6**).

*   To construct conventional and tubular ISE of liquid membrane for SO_4^{2-} determination and to characterize the behavior of the electrodes as a function of the operational conditions (**Chapter 6**).

*   To study the selectivity of constructed SO_4^{2-} electrodes in the presence of interfering anions at concentrations found in real BTF samples (**Chapter 6**).

Performance

- To operate the studied aerobic BTF under neutral pH conditions, comprising the start-up of the system and the optimization of the operation. The minimization of biologically produced elemental sulfur (biosulfur) was the initial target for neutral pH operation (**Chapter 7**).

- To optimize the main operational parameters for the steady-state operation at neutral pH operation, accomplishing the minimization of biosulfur production (**Chapter 7**).

- To evaluate the influence of the simultaneous removal of CH_3SH and H_2S on the overall desulfurization capacity of the reactor under neutral pH operation (**Chapter 8**).

- To study the effect of the gas contact time and the pollutants load on the simultaneous removal of H_2S and CH_3SH (**Chapter 8**).

- To perform the uninterrupted transition from neutral to acidic pH operation, without re-inoculation of the reactor (**Chapter 7**).

- To determine the maximum elimination capacity and to investigate the effect of the gas contact time and the H_2S load over the desulfurization performance of the reactor under acidic pH operation (**Chapter 9**).

- To assess the removal efficiency and the elimination capacity along the filter bed depth, determining the desulfurization profile of the reactor under acidic pH operation (**Chapter 9**).

- To study the behavior of the system under repeated H_2S starvation periods and to evaluate the oxidation of the produced biosulfur as a clogging control strategy under acidic pH operation (**Chapter 9**).

<div align="center">※</div>

4

general materials and methods

"The strongest of all warriors
are these two – Time and Patience."

Lev N. Tolstoy
(Yasnaya Polyana, 1828 – Astapovo, 1910)

4 General materials and methods

General materials and methods are exposed in this Chapter. A detailed technical specification and operational description of the BTF system studied in **Chapter 7**, **Chapter 8** and **Chapter 9** are presented and performance calculations are explained. Also, the construction procedure of tubular and conventional electrodes investigated in **Chapter 5** and **Chapter 6** is described and definitions regarding the characterization of analytical systems are provided. Finally, analytical methods are detailed. Specific techniques and experimental conditions are presented later in each Chapter of results.

4.1 Biotrickling filter setup

The studied reactor is a conventional counter-current BTF operated at room temperature, acclimatized at 20 – 30 ºC, in gas up-flow mode. A schematic and a picture of the experimental setup are shown in **Figure 4.1** and **Figure 4.2**. Main design features, equipment information, manufacturer indication and reference conditions are detailed in **Table 4.1**. Synthetic biogas, consisting of metered amounts of H_2S and N_2 (Carburos Metálicos, Spain), was fed to the BTF by differential mass flow controllers (DMFC) (Bronkhorst, The Netherlands). Dry air was injected into the bottom of the aeration unit by a DMFC, using a fine bubble diffuser. Exceeding air from the aeration unit was directed to the bottom of the main reactor, producing under reference conditions a maximum dilution factor of the synthetic biogas inside the reactor of 27%. In the case of real biogas, and taking into account that the explosive limits for biogas are from 4.4 to 15.0% of CH_4 in air, no risk of explosion of the gas mixture is expected since the maximum dilution ratios of biogas with air are generally below 10%. In this thesis, biogas is always reported as prepared, with no dilution at all, simulating a real situation. However, as the dilution inside the BTF directly affects its performance, other parameters such as loading rate (LR), empty bed residence time (EBRT), removal efficiency (RE) and elimination capacity

(EC), are reported considering this dilution term. This methodology reflects the variation of the aeration rate, which is crucial for the calculation of the $O_2/H_2S_{\text{supplied}}$ ratio ($v \cdot v^{-1}$), an indication of the O_2 availability in gas phase.
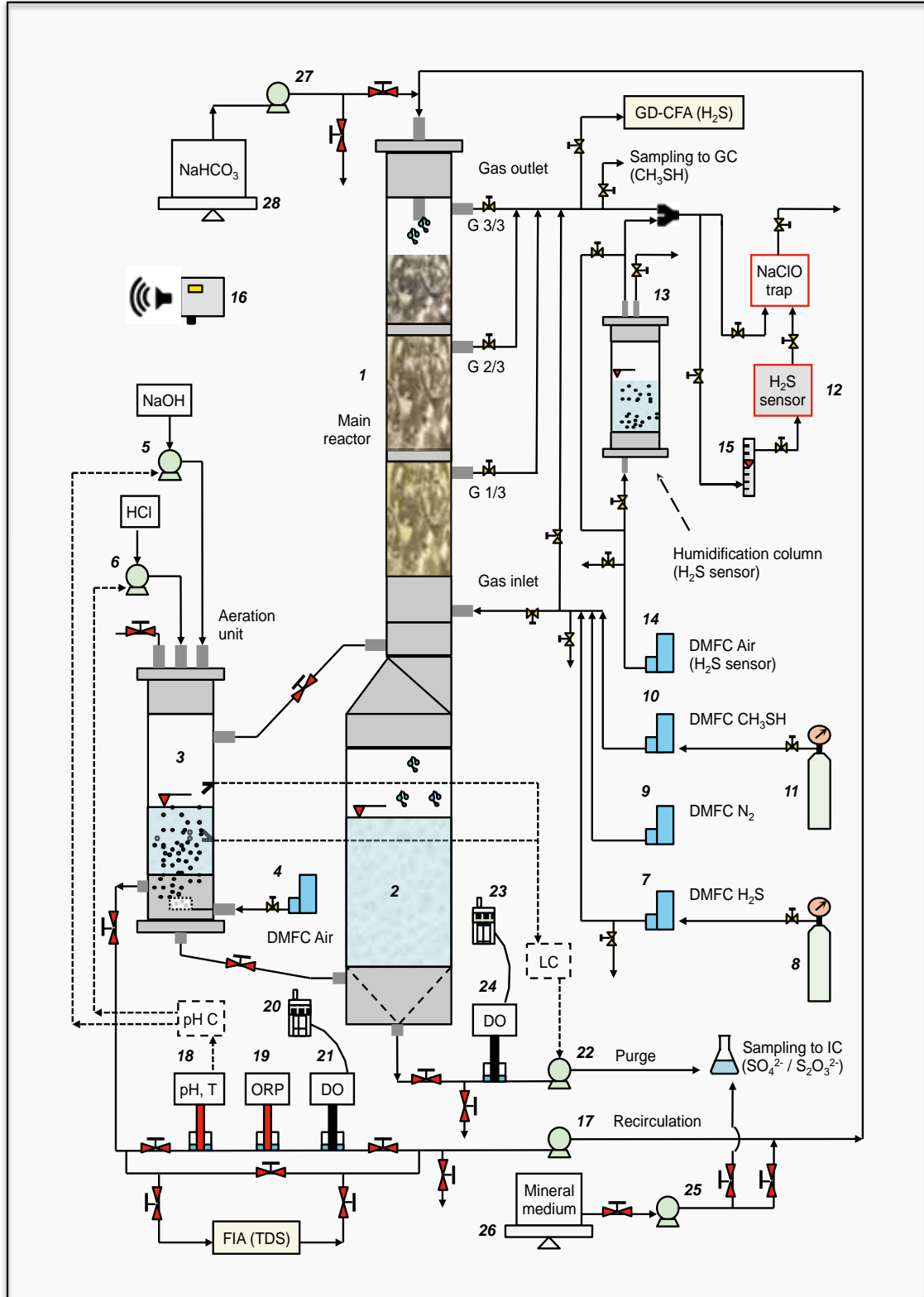
Figure 4.1 BTF system schematic. Equipment number as in **Table 4.1**
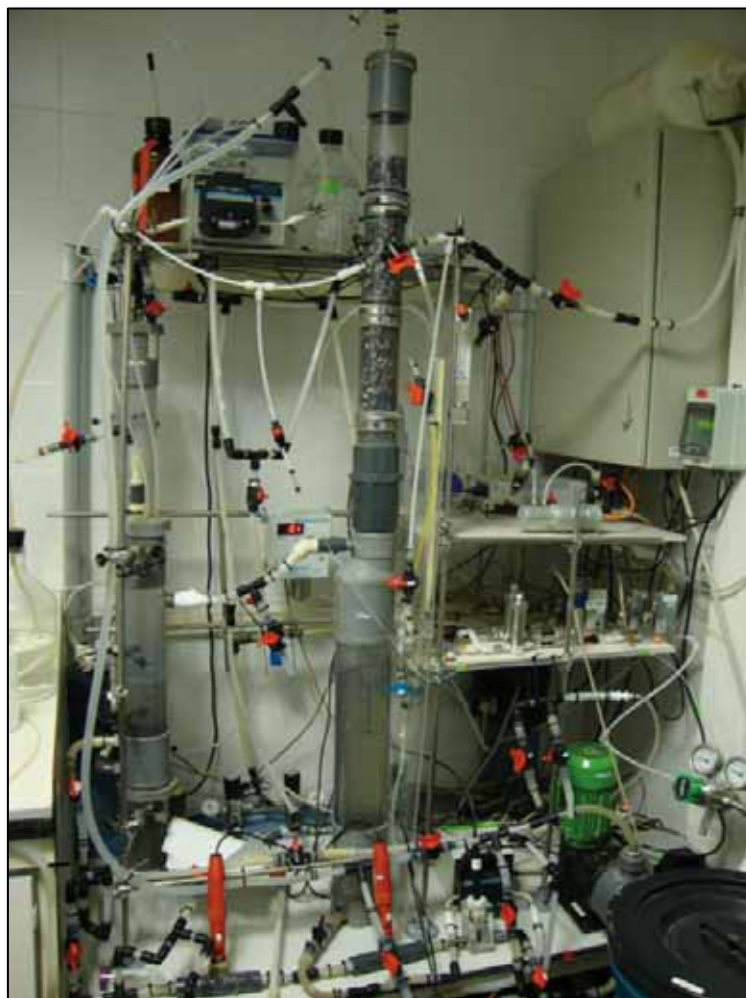
Figure 4.2 Image of the BTF experimental setup

Outlet gas phase is suited with online monitoring of H_2S (EuroGas Management, UK), as detailed further in **Section 4.7.1**. Manual valve manipulation allows H_2S detection at different gas ports. Experimental setup is prepared for the coupling of the FIA/GD-CFA system described in **Chapter 5**, for the on-line detection of H_2S and TDS. Moreover, laboratory premises are equipped with atmospheric H_2S sensor and alarm system.

The recirculation pump continuously trickles the liquid phase over the packed bed. Automated pumping of mineral medium and purge, which are interconnected to a level control system installed inside the aeration unit, warrant the renovation of the liquid phase. An on/off pH control system based on the addition of NaOH (1 mol·L^{-1}) (Panreac, Spain) or HCl (1 mol·L^{-1}) (Panreac, Spain) was used to keep the pH at the desired value.

Table 4.1 Technical specification – BTF system *(continued in next page)*

	Main reactor	Aeration unit	Gas phase inlet	Gas phase outlet	Liquid phase recirculation	Liquid phase renovation
Equipment	1 = Main reactor 2 = Liquid sump	3 = Air supply reactor 4 = Air inlet DMFC 5 = NaOH pump 6 = HCl pump	7 = H2S DMFC 8 = H2S cylinder 9 = N2 DMFC 10 = CH3SH DMFC 11 = CH3SH cylinder	12 = H2S sensor 13 = Humidification column 14 = Air DMFC 15 = Rotameter 16 = H2S alarm system	17 = Recirculation pump 18 = pH / T electrode 19 = ORP electrode 20 = DO meter 21 = DO electrode	22 = Purge pump 23 = DO meter 24 = DO electrode 25 = Mineral medium pump 26 = Mineral medium scale 27 = Bicarbonate pump 28 = Bicarbonate scale
Type / Model	1: vertical, cylindrical 2: vertical, cylindrical (excentrical union)	3: vertical, cylindrical tank 4: EL-Flow Select / F-201CV 5: peristaltic / OEM 400/M1 6: peristaltic / OEM 400/M1	7: Low ΔP-Flow / F-200DV 8: Gas cylinder / 9: EL-Flow Select / F-201AC 10: Low DP-Flow / F-200DV 11: Gas cylinder / X10A	12: electrochemical / SureCell 13: vertical, cylindrical tank 14: EL-Flow Select / F-201AC 15: variable area, float / 2150 16: atmospheric / TOCSIN610	17: diaphragm / Primus221 18: glass membrane / 5334 19: platinum wire / 5350 20: LCD display / Oxi 340i 21: galvanic / CellOx325	22: peristaltic / Masterflex L/S motor: L/S 7542-20 23: LCD display / Oxi 3310 24: galvanic / CellOx325 25: peristaltic / Masterflex L/S motor: L/S 77200-12 26: industrial / CPW Plus 35 27: peristaltic / Masterflex L/S motor 7554-95 28: precision / 572-57
Manufacturer	1: home-made reactor 2: home-made reactor	3: home-made reactor 4: Bronkhorst (Netherlands) 5: Watson Marlow (Sweden) 6: Watson Marlow (Sweden)	7: Bronkhorst (Netherlands) 8: Carburos Metálicos (Spain) 9: Bronkhorst (Netherlands) 10: Bronkhorst (Netherlands) 11: Carburos Metálicos (Spain)	12: EuroGas (UK) 13: home-made reactor 14: Bronkhorst (Netherlands) 15: Tecfluid (Spain) 16: Oliver-IGD (UK)	17: Alldos (Germany) 18: Crison (Spain) 19: Crison (Spain) 20: WTW (Germany) 21: WTW (Germany)	22: Cole Parmer (USA) 23: WTW (Germany) 24: WTW (Germany) 25: Cole Parmer (USA) 26: Adam (USA) 27: Cole Parmer (USA) 28: Kern (Germany)
Main construction materials	1: PVC 2: PVC	3: PVC 4: SS 316L, viton 5: acetal, SS, PVDF 6: acetal, SS, PVDF	7: SS 316L, viton 8: 9: SS 316L, viton 10: SS 316L, viton 11:	12: porous ceramic membrane 13: PVC 14: SS 316L, viton 15: SS 316L, glass, PTFE 16: CS panel, protection IP54	17: PVC, PP, ABS, CS 18: glass, porous PTFE 19: glass, porous PTFE 20: ABS 21: electrode Au/Pb, Viton	22: PPS, CRS, SS 23: ABS 24: electrode Au/Pb, Viton 25: PPS, CRS, SS 26: platform SS, aluminium 27: PPS, CRS, SS 28: platform SS
Main dimensions	1: D: 71 mm H: 855 mm V useful: 2 - 2.4 L 2: D: 110 mm H: 64 mm V useful: 2 - 5 L	3: D: 88 mm H: 550 mm V usefu: 1.5 - 2 L 4: 77 x 111 x 25 mm 5: 50 x 60 x 38 mm 6: 50 x 60 x 38 mm	7: 77 x 111 x 25 mm 8: D: mm, H: mm 9: 77 x 111 x 25 mm 10: 77 x 111 x 25 mm 11: D: mm, H: mm	12: D: 40 mm H: 55 mm 13: D: 88 mm H: 850 mm V useful: 3 - 4 L 14: 77 x 111 x 25 mm 15: flow tube H: 150 mm 16: 149 x 148 x 64 mm	17: 323 x 123 x 319 mm 18: D: 12 mm, H: 140 mm 19: D: 12 mm, H: 140 mm 20: 172 x 80 x 37 mm 21: D: 15 mm, H: 187 mm	22: 102 x 121 x 70 mm 23: 172 x 80 x 37 mm 24: D: 15 mm, H: 187 mm 25: 102 x 121 x 70 mm 26: 300 x 300 x 50 mm 27: 102 x 121 x 70 mm 28: 180 x 310 x 130 mm

* Monitored parameters: M = manually / A = automated

(continuation)

Table 4.1 Technical specification – BTF system

	Main reactor	*Aeration unit*	*Gas phase inlet*	*Gas phase outlet*	*Liquid phase recirculation*	*Liquid phase renovation*
Other specifications and additional information	1: gas port H: 20 cm 2: manual solid purge	3: fine diffuser (ceramic) 4: Q_{max}: 1 n L·min⁻¹, in/out pressure: 4 / 0 bar 5: on-off control Q_{max}·: 7 ml·min⁻¹, 240 VAC, 20 rpm, 50 Hz $V_{deposit\ NaOH}$: 2 L 6: on-off control Q_{max}·: 7 ml·min⁻¹, 240 VAC, 20 rpm, 50 Hz $V_{deposit\ HCl}$: 2 L	7: Q_{max}·: 15 n ml·min⁻¹, in/out pressure: 1 / 0 bar 8: V: m³, P: bar 9: Q_{max}·: 4 n L·min⁻¹, in/out pressure: 2.4 / 0 bar 10: Q_{max}·: 15 n ml·min⁻¹, in/out pressure: 1 / 0 bar 11: V: 0.8 m³, P: 85 bar	12: range 0 - 200 ppm$_v$ H$_2$S, output signal: 4 -20 mA 13: air humidification (to H$_2$S sensor) 14: Q_{max}·: 40 n L·min⁻¹, in/out pressure: 4 / 0 bar 15: floating sphere in glass 16: 4 digit LED, 2 Alarm level, 60 dB	17: Q_{max}·: 75 L·h⁻¹, 240 V, 50 Hz 18: range 0 - 14 pH, 0 - 100 ºC, electrolyte gel 19: range +- 2000 mV, electrolyte gel 20: data output RS232 21: range 0 - 50 mg O$_2$·L⁻¹	22: Q_{max}·: L·h⁻¹, 240 V, 50 Hz, 17 rpm 23: data output RS232 24: range 0 - 50 mg O$_2$·L⁻¹ 25: Q_{max} = L·h⁻¹ 240 V, 50 Hz, 2 - 200 rpm $V_{deposit\ mineral\ medium}$·: 35 L 26: range 0.10 - 35 kg 27: Q_{max}·: L·h⁻¹, 240 V, 50 Hz, 6 - 600 rpm $V_{deposit\ bicarbonate}$· : 5 L 28: range 100 - 24,000 mg
***Monitored parameters ***	1: Pressure drop (M) 2: Liquid level (A)	3: Liquid level (A) 4: Q Air $_{IN}$ (A) 5: t Base (A) (actuation time) 6: t Acid (A) (actuation time)	7: SP and Q H$_2$S (A) 8: Pressure (M) 9: SP and Q N$_2$ (A) 10: SP and Q CH$_3$SH (A) (*Chapter 7*) 11: Pressure (M) [H$_2$S]: GD-CFA (*Chapter 4*)	12: [H$_2$S] (A) GD-CFA (*Chapter 4*) 13: Liquid level (M) 14: SP and Q Air $_{to\ sensor}$ (A) 15: Q $_{to\ sensor}$ (M) 16: [H$_2$S] (A) [H$_2$S]: GD-CFA (*Chapter 4*)	17: Q $_{recirculation}$ (M) 18: pH, T (A) 19: ORP (A) 20: DO (A) 21: DO (A) TDS: FIA (*Chapter 4*)	22: Q $_{purge}$ (M) 23: DO (A) 24: DO (M) 25: Q $_{mineral\ medium}$ (M) 26: W $_{deposit\ mineral\ medium}$ (M) 27: Q $_{bicarbonate}$ (M) 28: W $_{deposit\ bicarbonate}$ (M)
Reference operation	LR = 51.48 g S-H$_2$S·m⁻³·h⁻¹ EBRT = 131 s V_{liquid} = 4 L	Q Air $_{IN}$ = 250 ml·min⁻¹ O$_2$/H$_2$S = 39.49 v·v⁻¹	[H$_2$S] $_{biogas}$ = 2,000 ppm$_v$ H$_2$S Q H$_2$S $_{IN}$ = 1.59 ml·min⁻¹ Q N$_2$ $_{IN}$ = 795 ml·min⁻¹ Q CH$_3$SH $_{IN}$ (*Chapter 7*)	[H$_2$S] $_{out}$ = 0 ppm$_v$ H$_2$S Q Air $_{to\ sensor}$ = 5,000 ml·min⁻¹ Q $_{to\ sensor}$ = 1 N L·min⁻¹	Q $_{recirculation}$ = 255 ml·min⁻¹ TLV = 3.8 m·h⁻¹ 6.0 < pH < 6.5 2.50 < pH < 2.75	Q $_{purge}$ = 2.7 ml·min⁻¹ Q $_{mineral\ medium}$ = 2.5 ml·min⁻¹ Q $_{bicarbonate}$ = 0.4 ml·min⁻¹ HRT = 33 - 34 h

ABS acrylonitrile butadiene styrene
CRS cold-rolled steel
CS carbon steel
D diameter
DMFC diferential mass flow controller
DO dissolved oxygen
EBRT empty bed residence time
H height
HRT hydraulic residence time
LCD liquid-cristal display
LED light-emitting diode
LR loading rate
ORP oxidation-reduction potential
PP polypropylene
PPS polyphenylene sulfide
PTFE polytetrafluoroethylene
PVC polyvinyl chloride
PVDF polyvinylidene fluoride
Q flow (volumetric)
SS stainless steel
T temperature
TLV trickling liquid velocity
V volume

* Monitored parameters: M = manually / A = automated

Pipe and junction accessories of H_2S and CH_3SH lines were in polyvinylidene fluoride (PVDF). Pipe of air and N_2 lines were in polyamide. Liquid pipe material was silicone rubber and polyamide. Plastic valves were used in liquid lines and safety PVDF gas valves were used in H_2S and CH_3SH lines.

Liquid phase is equipped with the on-line monitoring of dissolved oxygen (DO) (WTW, Germany), oxidation-reduction potential (ORP) (Crison Instruments, Spain) and pH/Temperature (Crison Instruments, Spain). Inorganic carbon source was continuously supplied as $NaHCO_3$ (3 g C·L^{-1}) (Panreac, Spain). Mineral medium composition and reagent's supplier are detailed in **Table 4.2**. All reagents were off analytical grade. Trace elements, added in a proportion of 1 mL of trace elements per liter of mineral medium, were prepared according to Pfenning *et al.* (1981).

Table 4.2 Mineral medium composition

Reagent	Concentration	Supplier
NH_4Cl	1.00 g·L^{-1}	Panreac, Spain
KH_2PO_4	0.12 g·L^{-1}	Sigma Aldrich, Germany
K_2HPO_4	0.15 g·L^{-1}	Panreac, Spain
$MgSO_4·7H_2O$	0.20 g·L^{-1}	Panreac, Spain
$CaCl_2$	0.02 g·L^{-1}	Panreac, Spain
Trace elements	1.00 mL·L^{-1}	
$FeCl_2·4H_2O$	1.50 mg·L^{-1}	Panreac, Spain
H_3BO_3	0.06 mg·L^{-1}	Sigma Aldrich, Germany
$MnCl_2·4H_2O$	0.10 mg·L^{-1}	Panreac, Spain
$CoCl_2·6H_2O$	0.12 mg·L^{-1}	Panreac, Spain
$ZnCl_2$	0.07 mg·L^{-1}	Panreac, Spain
$NiCl_2·6H_2O$	0.025 mg·L^{-1}	Panreac, Spain
$CuCl_2·2H_2O$	0.015 mg·L^{-1}	Panreac, Spain
$NaMoO_4·2H_2O$	0.025 mg·L^{-1}	Panreac, Spain
$EDTA·Na_2O_8·2H_2O$	4.28 mg·L^{-1}	Sigma Aldrich, Germany
HCl	6.76 mL·L^{-1}	Panreac, Spain

Trace elements: Milli-Q water (18 MΩ·cm^{-1}) up to 5 L / pH adjusted to 4.2 with NaOH

Pictures of packing material used during the complete 990-days operation are shown in **Figure 4.3**. Packing elements were the smallest commercially available at the time of the operation herein reported, with a specific surface area of 515 $m^2 \cdot m^{-3}$ and a packing density of 520 $kg \cdot m^{-3}$.

Figure 4.3 Images of packing material before and after BTF packing

Results previously obtained at our research group recommended the use of random packing material for improving the biomass sampling process. It was previously stated that the structure of the HD-QPack as packing material, as used by Fortuny *et al.* (2008; 2011) and Montebello *et al.* (2010), lead to a lost in the preservation of biomass samples. Metallic material was suggested in order to improve the integrity of the sample during its detachment from the support. The identification of the microbial consortium of the BTF and the bacterial ecology assessment are performed by others (Maestre *et al.*, 2010; Rovira *et al.*, 2010; Bezerra *et al.*, 2013). In this sense, aiming to identify possible differences in the microbial consortium along the filter bed, three ports for biomass and solids sampling were mechanized in the main reactor, corresponding gas outlet sampling ports: at the bottom section (G 1/3), at the middle section (G 2/3) and at the top section (G 3/3) of the filter bed column height, as shown in **Figure 4.1**. Also, biomass and solids were sampled from the gas inlet section, totalizing four different biomass and solids sampling points.

4.2 BTF sampling procedures

4.2.1 Gas sampling

Gas sampling of the BTF, for off-line H_2S and CH_3SH quantification, was performed using Tedlar® bags of 1 L (SKF, USA), as commonly adopted for gas sampling. Main composition of Tedlar® bags is a polyvinyl fluoride (PVF) polymer resin. Bags are suited with a PP valve and a replaceable septum of 4 mm diameter, in PTFE faced silicone. If no syringe injection is required for sample extraction, the content of the bag is extracted using the 3/16" PTFE tubing stem connection in bag's valve. Gas sampling points were located at the gas inlet port of the main reactor and at the gas outlet ports of each section of the main reactor (G 1/3, G 2/3 and G 3/3), as shown in **Figure 4.1**. Furthermore, sampling points located after H_2S and CH_3SH gas cylinders, but yet before the gas inlet port of the main reactor, allowed the preparation of standards, as required for the calibration of the respective analyzers, as well as the determination of the inlet biogas pollutant content.

Before gas sample collection, Tedlar® bags were cleaned with dry air three times, inside a gas fume hood with respiratory protection. Bags were filled up to 80% of the capacity, as normally assumed for safety reasons. Gas samples were analyzed within the first 24 hours after sample collection (Coyne *et al.*, 2011). Gas standards of H_2S and CH_3SH were prepared using unique Tedlar® bags for each standard, avoiding contamination. The same previous cleaning procedure as for sample collection was applied for standards preparation. Additionally, bags were conditioned by replenishing with the desired standard concentration before its preparation. Under reference operation, continuous on-line sampling at outlet gas port (G 3/3) was performed for H_2S monitoring by the installed dedicated electrochemical H_2S sensor, as described later on **Section 4.7.1**. During experiments, different sampling frequencies were adopted, as further detailed in the corresponding Chapters of results.

4.2.2 Liquid sampling

Liquid samples of the BTF for off-line determinations were taken primarily at the purge and at the recirculation lines. Samples of the mineral medium solution were taken at working-day frequency for ionic composition analysis by IC, under the conditions specified later on **Section 4.7.2**. Samples of bicarbonate solution were also taken for total inorganic carbon (TIC) determination. Frequency under reference operation, volume and analytical procedure applied to liquid samples are detailed in **Table 4.3**.

Table 4.3 Liquid sampling during reference operation

Sampling point *	Sampling frequency	Sample volume (mL)	Performed analysis
Purge	1 / day (labour)	1.5	SO_4^{2-}, $S_2O_3^{2-}$, NO_2^-, NO_3^-, Cl^-, PO_4^{3-} (by IC)
Mineral medium	1 / deposit preparation	1.5	SO_4^{2-}, $S_2O_3^{2-}$, NO_2^-, NO_3^-, Cl^-, PO_4^{3-} (by IC)
Bicarbonate	1 / deposit preparation	2.0	TIC

* after respective pumping system

For ionic composition and TIC analysis, liquid samples were filtered with disposable 0.22 µm syringe filter driven units from Millipore®, provided with a high-density polyethylene housing and membrane of hydrophilic Durapore®. Samples were preserved under refrigeration at 4 ⁰C for use until 24 h after sample collection and under freezer at -20 ⁰C for longer storage periods. Samples were diluted with Milli-Q water (18 MΩ·cm^{-1}), in a 1:10 proportion for IC analysis and in a 1:5 proportion for TIC determination. Additionally, a liquid sampling point was located in the recirculation line for TDS determination applying the flow analyzer described in **Chapter 5**, with a two-stage filtration system, comprising a first step of tangential filtration (3 µm) followed by a direct filtration element (0.22 µm), as later detailed in **Section 5.3.2**.

4.2.3 Solid sampling
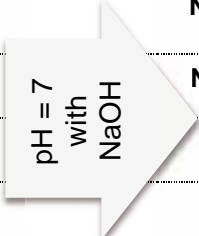
The content of the filter bed was fully withdrawn immediately after the shutdown of the system to obtain viable samples of biomass and solids from each section of the BTF (top, middle, bottom and gas inlet sections). The final sample of solids (FSS) was prepared as shown in **Figure 4.4**, obtaining one separated FSS for each filter bed section.
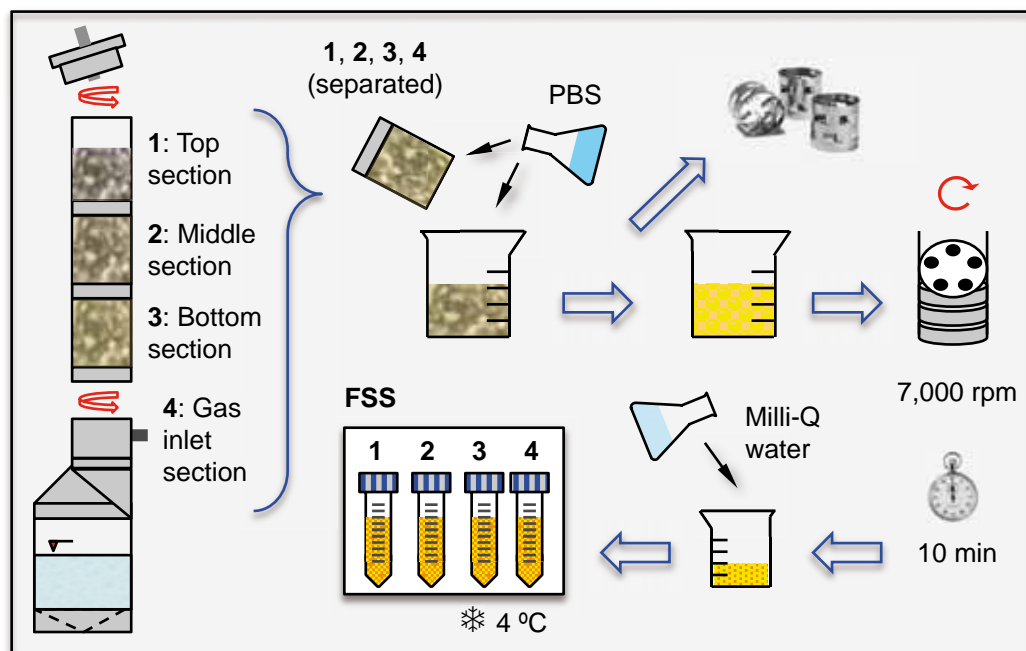
Figure 4.4 Preparation of the final solid sample (FSS)

Biomass and solids detachment from packing material elements was done by washing out with a phosphate buffer saline (PBS) solution, with the composition detailed in **Table 4.4**. After PBS washing, the solid was centrifuged at 7,000 rpm during 10 minutes and then it was re-suspended in a known volume of Milli-Q water (18 M$\Omega\cdot$cm^{-1}), to rinse out PBS traces and to recover the cleaned suspended solids. Samples were preserved under refrigeration at 4 °C. Biomass samples were taken by others for further biological identification. After an ultrasonication step, a portion of the cleaned FSS solution was used to quantify cellular nitrogen (N_{cell}). Other portion of FSS was used to determine total suspended solids (TSS) and volatile suspended solids (VSS), as detailed later on **Section 4.7.3**.

Table 4.4 PBS solution composition

Reagent	Concentration $(g \cdot L^{-1})$	Supplier
$Na_3PO_4 \cdot 12H_2O$	0.328	Sigma Aldrich, Germany
$NaH_2PO_4 \cdot H_2O$	0.552	Panreac, Spain
NaCl	0.526	Panreac, Spain
KCl	0.0746	Panreac, Spain

pH = 7 with NaOH

Another portion of the cleaned FSS solution was treated to obtain the dry-FSS, as shown in **Figure 4.5**, for further analysis of sulfur and metals. Dry-FSS was prepared from the FSS, applying centrifugation at 7,000 rpm during 10 minutes, washing out with Milli-Q water (18 MΩ·cm^{-1}) and additional centrifugation during 10 minutes, followed by drying at 105 °C in a closed Falcon tube of 50 mL. Once dry, the solid was homogenized first with spatula and then with ceramic mortar; storage was performed by refrigeration at 4 ºC. Dry-FSS was first combusted at 1,000 ºC for S analysis by high-performance liquid chromatography (HPLC). For metal trace analysis by inductively coupled plasma optical emission spectroscopy (ICP-OES), dry-FSS was first microwave-digested.
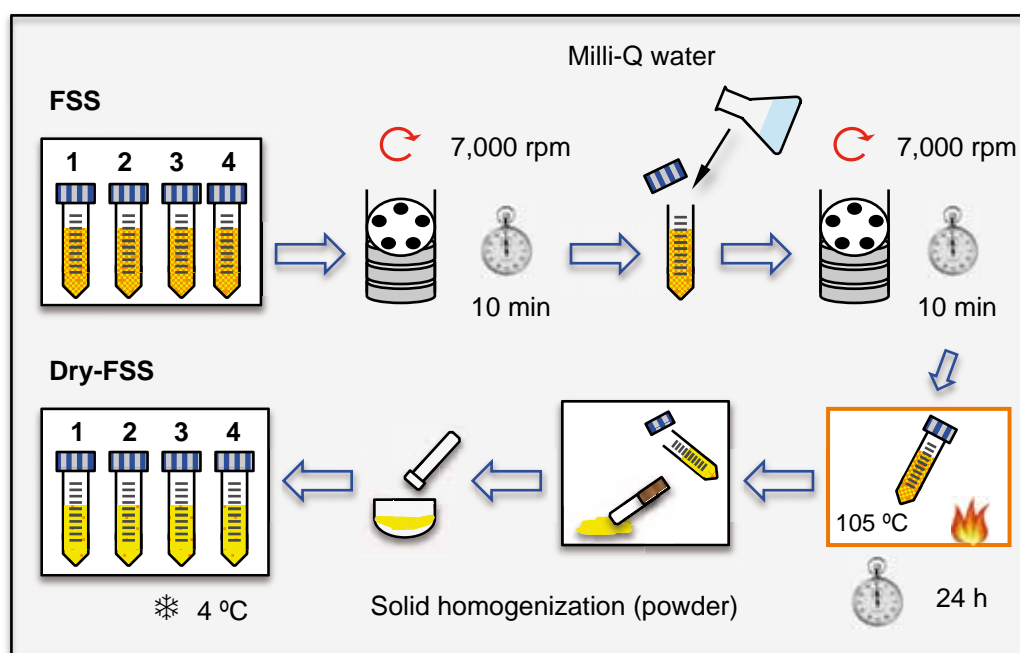
Figure 4.5 Preparation of the dry-final solid sample (dry-FSS)

4.3 Biotrickling filter performance calculations

Operation of BTFs is normally characterized by the expression of the LR and the EBRT, according to **Equation 14** and **Equation 15**. Reactor's performance can be described by the RE and the EC, according to **Equation 16** and **Equation 17** (Devinny *et al.*, 1999). The LR represents the mass of contaminant (H_2S or CH_3SH) per volume and time.

$$LR = [(Q_{biogas} + Q\ Air_{IN}) \times C_{in}] / V \qquad\qquad [14]$$

Where:

$$LR = \text{Loading rate } (g_{pollutant} \cdot m^{-3} \cdot h^{-1})$$
$$Q_{biogas} + Q\ Air_{IN} = \text{Total gas flow rate } (m^3 \cdot h^{-1})$$
$$C_{in} = \text{Pollutant inlet concentration } (g_{pollutant} \cdot m^{-3})$$
$$V = \text{Reactor's bed volume } (m^3)$$

$$EBRT = V / (Q_{biogas} + Q\ Air_{IN}) \qquad\qquad [15]$$

Where:

$$EBRT = \text{Empty bed residence time (s)}$$
$$V = \text{Reactor's bed volume } (m^3)$$
$$Q_{biogas} + Q\ Air_{IN} = \text{Total gas flow rate } (m^3 \cdot h^{-1})$$

The EBRT represents the time that the gas is in contact with the packed bed. Once the packed bed is totally colonized by the microorganisms, the real gas contact time inside the reactor is shorter than the EBRT. The true residence time is calculated multiplying the EBRT by the bed porosity.

$$RE = [(C_{in} - C_{out}) / C_{in}] \times 100 \qquad\qquad [16]$$

Where:

$$RE = \text{Removal efficiency (\%)}$$
$$C_{in} = \text{Pollutant inlet concentration } (g_{pollutant} \cdot m^{-3})$$
$$C_{out} = \text{Pollutant outlet concentration } (g_{pollutant} \cdot m^{-3})$$

The RE represents the fraction (%) of the contaminant removed and is characteristic of each reactor, since it varies with the concentration of the pollutant and is not referred to the reactor size or to the bed volume. Thus, the expression of the elimination capacity is required.

$$EC = [(Q_{biogas} + Q\ Air_{IN}) \times (C_{in} - C_{out})] / V \qquad [17]$$

Where:

$EC =$ Elimination capacity ($g_{pollutant} \cdot m^{-3} \cdot h^{-1}$)

$Q_{biogas} + Q\ Air_{IN} =$ Total gas flow rate ($m^3 \cdot h^{-1}$)

$C_{in} =$ Pollutant inlet concentration ($g_{pollutant} \cdot m^{-3}$)

$C_{out} =$ Pollutant outlet concentration ($g_{pollutant} \cdot m^{-3}$)

$V =$ Reactor's bed volume (m^3)

The EC represents the mass of the contaminant eliminated per unit volume of the reactor and time. When the reactor performs with 100% RE, the EC is equal to LR. When EC begins to be lower than LR, the critical EC is reached. If the LR is still increased, eventually an overall maximum EC is achieved (EC_{max}).

Another parameter used to characterize the BTF operation was the $O_2/H_2S_{supplied}$ ratio, which expresses the volumetric relation between the supplied O_2 and H_2S, according to **Equation 18**.

$$O_2/H_2S_{supplied} = (0.21 \times Q\ Air_{IN}) / Q\ H_2S_{IN} \qquad [18]$$

Where:

$O_2/H_2S_{supplied} =$ Ratio O_2/H_2S supplied ($v \cdot v^{-1}$)

$Q\ Air_{IN} =$ Air inlet flow – fed into aeration unit ($mL\ air \cdot min^{-1}$)

$Q\ H_2S_{IN} =$ H_2S inlet flow – fed into main reactor ($mL\ H_2S \cdot min^{-1}$)

This parameter indicates the O_2 fed (gas phase) into the reactor, considering the volume of air bubbled into the aeration unit. Noteworthy, only the O_2 dissolved into the liquid phase (measured as DO) is biologically

available for microorganisms' metabolism, and the degree of the oxygenation depends on the gas/liquid transference device type and effectiveness. In this sense, the calculation of the O_2/H_2S supplied ratio is intended to report the operational setup of O_2 (air) and H_2S, aiming the reproducibility of exposed experiments. However, the DO measurement at the recirculation line (**Figure 4.1**) disregards the effective amount of O_2 that can be transferred to the liquid as consequence of the air by-pass between the aeration unit and the main reactor. Further research recommendations on this topic are given later in **Chapter 10**.

The product of the recirculation flow rate (Q recirculation) and the DO concentration in the recirculation line, which is directly linked to the ratio O_2/H_2S supplied ratio, corresponds to the O_2 load (LO_2) effectively present into the liquid phase, calculated according to **Equation 19**. This parameter expresses the biologically available O_2 (dissolved), at the top of the reactor.

LO_2 = DO × Q recirculation [19]

Where:

LO_2 = O_2 load (mg $O_2 \cdot min^{-1}$)

DO = DO at the recirculation line (mg $O_2 \cdot L^{-1}$)

Q recirculation = Recirculation flow rate (L·min^{-1})

Also, the availability of O_2, dissolved in liquid phase, in relation with the quantity of TDS produced during sulfide accumulation episodes is the DO/S^{2-} ratio [mg $O_2 \cdot$(mg S^{2-})$^{-1}$]. The DO/S^{2-} ratio was calculated according to **Equation 20**. TDS was measured as described in **Chapter 5**.

DO/S^{2-} = DO / TDS [20]

Where:

DO/S^{2-} = DO/S^{2-} ratio (mg $O_2 \cdot$(mg S^{2-})$^{-1}$)

DO = DO at the recirculation line (mg $O_2 \cdot L^{-1}$)

TDS = TDS at the recirculation line (mg $S^{2-} \cdot L^{-1}$)

The DO/S^{2-} ratio could be related to the capability of the system to produce either SO_4^{2-} or S^0, according to the stoichiometric relation obtained from **Equation 8** and **Equation 9** (Kelly, 1999). Theoretically, a DO/S^{2-} ratio lower than 0.5 indicates that S^0 is the main product while a value higher than 2 indicates that the main product is SO_4^{2-}.

The quantity of biologically produced S^0 (also referred to as biosulfur) was estimated by the difference between total S-H_2S removed and the total (SO_4^{2-} + $S_2O_3^{2-}$ + S^{2-}) produced, according to Janssen *et al.* (1997). Calculation was performed according to **Equation 21**, where the sub-indexes $_{IN-OUT}$ and $_{P-MM}$ represent the sampling point for gas (in and out ports) and liquid (purge and mineral medium) samples, respectively. SO_4^{2-} and $S_2O_3^{2-}$ were quantified by IC, as described in **Section 4.7.2**. S^{2-} was quantified as TDS, measured as described in **Chapter 5**.

(S-S^0) $_{produced}$ = [S-H_2S] $_{IN-OUT}$ − [(S-SO_4^{2-})+(S-$S_2O_3^{2-}$)+(S-S^{2-})] $_{P-MM}$ [21]

Where:

(S-S^0) $_{produced}$ =	Amount of S^0 produced (g S-S^0)
[S-H_2S] $_{IN-OUT}$ =	Amount of H_2S removed (g S-H_2S)
[(S-SO_4^{2-})] $_{P-MM}$ =	Amount of SO_4^{2-} produced (g S-SO_4^{2-})
[(S-$S_2O_3^{2-}$)] $_{P-MM}$ =	Amount of $S_2O_3^{2-}$ produced (g S-$S_2O_3^{2-}$)
[(S-S^{2-})] $_{P-MM}$ =	Amount of S^{2-} produced (g S-S^{2-})

It is worth noticing that the calculation expressed in **Equation 21** can result in a negative figure in either the case of interruption of the H_2S feeding to the system (starvation periods) or when the S^0 accumulated inside the filter bed is consumed concomitantly with the direct H_2S oxidation, increasing the total quantity of produced sulfate. Moreover, the production rate and the selectivity of S^0 and SO_4^{2-} are defined from the results of the sulfur mass balance. The production (p$S-S^0$) and the consumption (-p$S-S^0$) rate of S^0 were calculated according to **Equation 22** and **Equation 23**, considering the expression of the velocity of each process related to the reactor's volume.

$$pS\text{-}S^0 = [(S\text{-}S^0)_{produced} / (V \times t)] \qquad\qquad [22]$$

Where:

$pS\text{-}S^0$ = Production rate of S^0 (g $S\text{-}S^0 \cdot m^{-3} \cdot h^{-1}$)

$(S\text{-}S^0)_{produced}$ = Amount of S^0 produced (g $S\text{-}S^0$)

V = Reactor's bed volume (m^3)

t = Time period of reported rate (h)

$$-pS\text{-}S^0 = [(S\text{-}S^0)_{consumed} / (V \times t)] \qquad\qquad [23]$$

Where:

$-pS\text{-}S^0$ = Consumption rate of S^0 (g $S\text{-}S^0 \cdot m^{-3} \cdot h^{-1}$)

$(S\text{-}S^0)_{consumed}$ = Amount of S^0 consumed (g $S\text{-}S^0$)

V = Reactor's bed volume (m^3)

t = Time period of reported rate (h)

The production rate of SO_4^{2-} ($pS\text{-}SO_4^{2-}$) was calculated according to **Equation 24**, also considering the velocity of production of SO_4^{2-} related to the reactor's volume.

$$pS\text{-}SO_4^{2-} = [(S\text{-}SO_4^{2-})_{produced} / (V \times t)] \qquad\qquad [24]$$

Where:

$pS\text{-}SO_4^{2-}$ = Consumption rate of SO_4^{2-} (g $S\text{-}SO_4^{2-} \cdot m^{-3} \cdot h^{-1}$)

$(S\text{-}SO_4^{2-})_{produced}$ = Amount of SO_4^{2-} produced (g $S\text{-}SO_4^{2-}$)

V = Reactor's bed volume (m^3)

t = Time period of reported rate (h)

The sulfate selectivity is defined as the quantity of produced sulfate referred to the total H_2S removed ($S\text{-}SO_4^{2-}/S\text{-}H_2S_{removed}$), expressed as a percentage (Fortuny *et al.*, 2008; Montebello *et al.*, 2010). This parameter represents the SO_4^{2-} production capacity of the system, which is complementary to the S^0 production capacity, also calculated and defined as the sulfur selectivity ($S\text{-}S^0/S\text{-}H_2S_{removed}$). Sulfate and sulfur selectivity were calculated according to **Equation 25** and **Equation 26**, respectively.

$$\text{S-SO}_4{}^{2-}/\text{S-H}_2\text{S }_{\text{removed}} = (\text{S-SO}_4{}^{2-})_{\text{produced}} / (\text{S-H}_2\text{S})_{\text{removed}} \qquad [25]$$

Where:

$\text{S-SO}_4{}^{2-}/\text{S-H}_2\text{S }_{\text{removed}}$ =   Sulfate selectivity (%)

$(\text{S-SO}_4{}^{2-})_{\text{produced}}$ =   Amount of $\text{SO}_4{}^{2-}$ produced (g $\text{S-SO}_4{}^{2-}$)

$(\text{S-H}_2\text{S})_{\text{removed}}$ =   Amount of H_2S removed (g $\text{S-H}_2\text{S}$)

$$\text{S-S}^0/\text{S-H}_2\text{S}_{\text{removed}} = (\text{S-S}^0)_{\text{produced}} / (\text{S-H}_2\text{S})_{\text{removed}} \qquad [26]$$

Where:

$\text{S-S}^0/\text{S-H}_2\text{S }_{\text{removed}}$ =   Sulfur selectivity (%)

$(\text{S-S}^0)_{\text{produced}}$ =   Amount of S^0 produced (g S-S^0)

$(\text{S-H}_2\text{S})_{\text{removed}}$ =   Amount of H_2S removed (g $\text{S-H}_2\text{S}$)

4.4 Construction of tubular electrodes

Two different kind of tubular electrodes were constructed: of crystalline membrane for H_2S/TDS determination (**Chapter 5**) and of polymeric liquid membrane for $\text{SO}_4{}^{2-}$ determination (**Chapter 6**). Electrodes were integrated like detectors in two different analyzers based on FIA technique.

4.4.1 Tubular electrodes of crystalline membrane

Tubular electrodes of homogeneous crystalline membrane were constructed as previously described (Ruzicka and Lamm, 1971; Barquero, 2001; Baeza, 2004). The membrane was shaped in tablets of 5 mm diameter and 0.6 mm thickness. Tablets were obtained by agglutination of precisely weighted powdered Ag_2S (0.09 g) applying a constant pressure of 4 ton·cm^{-2} for 2 minutes. The manual tablet press machine was used by courtesy of Adasa Sistemas S.A. Ag_2S was prepared by precipitation of AgNO_3 (0.1 mol·L^{-1}) (Panreac, Spain) with Na_2S (0.1 mol·L^{-1}) (Sigma Aldrich, Germany) and further separation. The procedure for construction of tubular electrodes of crystalline membrane is schematized in **Figure 4.6**.
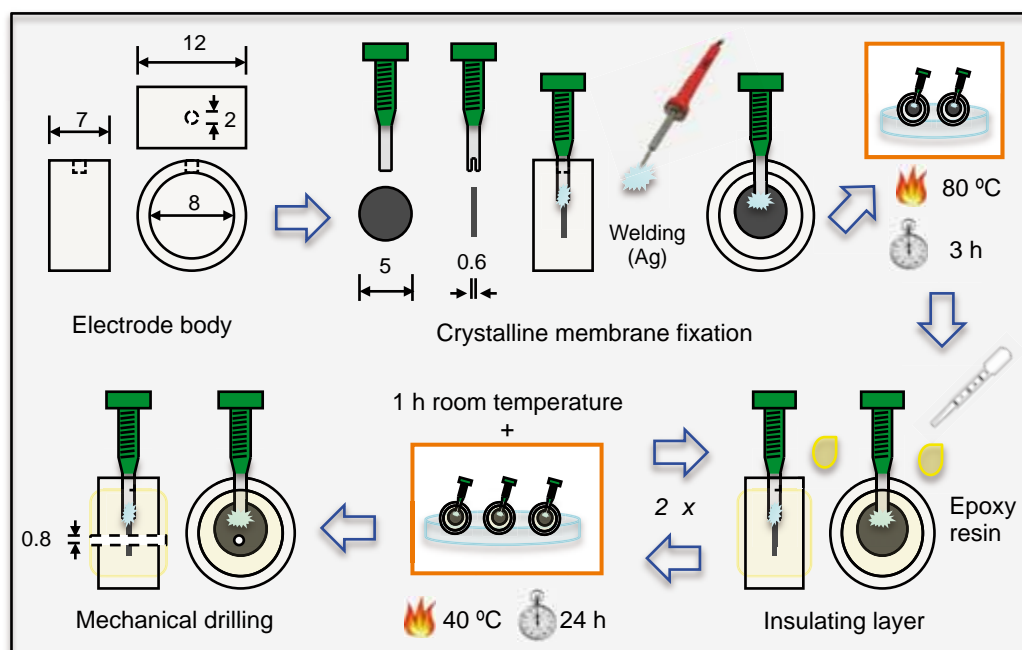
Figure 4.6 Construction of tubular electrodes of crystalline membrane (Ag$_2$S) for S^{2-} analysis (dimensions in millimeters)

Electrode body consisted in a cylindrical element of methacrylate of 7 mm width, 12 mm external diameter and 8 mm internal diameter, with an orifice of 2 mm in which the electrical connector was inserted through. Once positioned, the membrane tablet was securely fixed to the electrical connector metallic extremity by welding with an electrically conductive silver-epoxy resin (EPO-TEK® H20E-PFC – Epoxy Technology, Inc., USA). Silver welding was carefully performed avoiding the paste to spread over the membrane. Silver-epoxy resin was cured at 80 ºC during 3 h. After that, both sides of the electrode body were replenished with an insulating non-conductive solvent-free modified bisphenol-A epoxy resin (Araldite® RenlamM/REN HY5162 – Huntsman Advanced Materials, Switzerland). Epoxy resin was cured during 1 h at room temperature and afterwards during 24 h at 40 ºC after each side application. Finally, electrodes were perforated perpendicularly to the membrane, opening an orifice of 0.8 mm diameter across the electrode body, which allows the contact of the analyte with the sensing membrane when electrodes are installed in analytical systems based on FIA technique. Pictures of constructed crystalline-membrane tubular electrodes are shown in **Figure 4.7**.
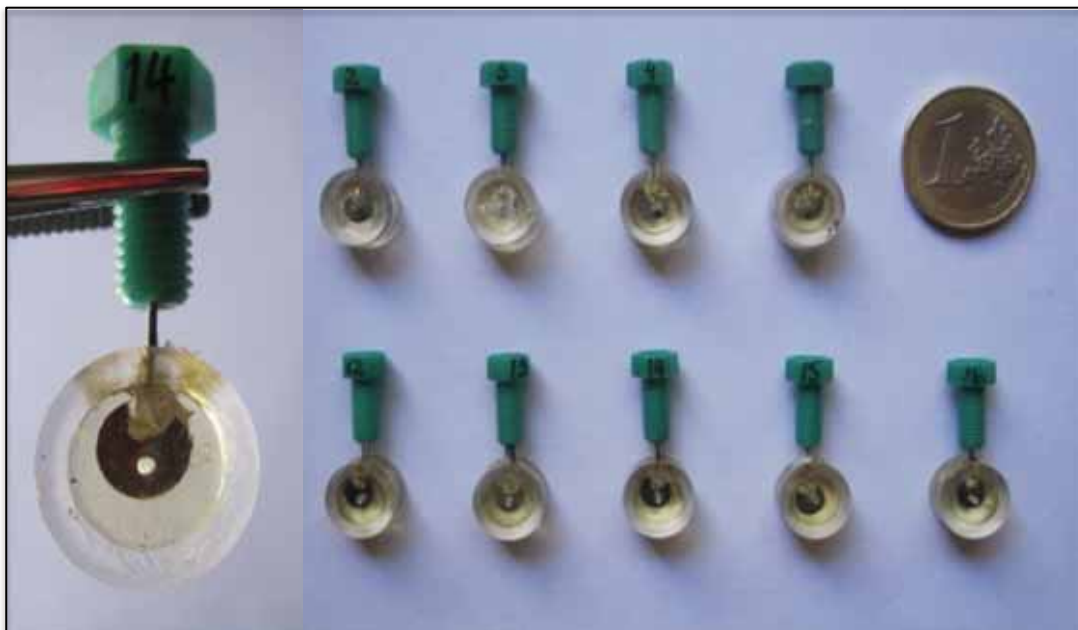
Figure 4.7 Images of constructed tubular electrodes of crystalline membrane (Ag$_2$S) for S^{2-} analysis

Mechanical drilling was carefully done to completely positioning the orifice over the membrane tablet, without reaching the silver epoxy resin welding point. Perforation of electrodes was executed by courtesy of the Institute of Textile Research and Industrial Cooperation of Terrassa, at the *Universitat Politècnica de Catalunya*, UPC. After perforation, each electrode was wet polished by inserting an ultra-fine abrasive paper inside the membrane orifice, to clean out any trace of particles from the mechanical drilling; then, the orifice surface was thoroughly smoothed with a wet alumina-polishing strip. Before use, electrodes were conditioned during 12 hours in a S^{2-} solution (0.001 M S^{2-}), prepared according specified in **Section 5.3.1**. For storage, electrodes were cleaned with distilled water and kept dried, covered with an aluminum sheet, to protect them from the light.

4.4.2 Tubular electrodes of polymeric liquid membrane

Tubular electrodes of polymeric liquid membrane were constructed according to previously described (Barquero, 2001), as schematized in **Figure 4.8**. The liquid sensing cocktail (**Section 6.3.2**) is deposited by dropping it over an epoxy-graphite conducting composite surface.
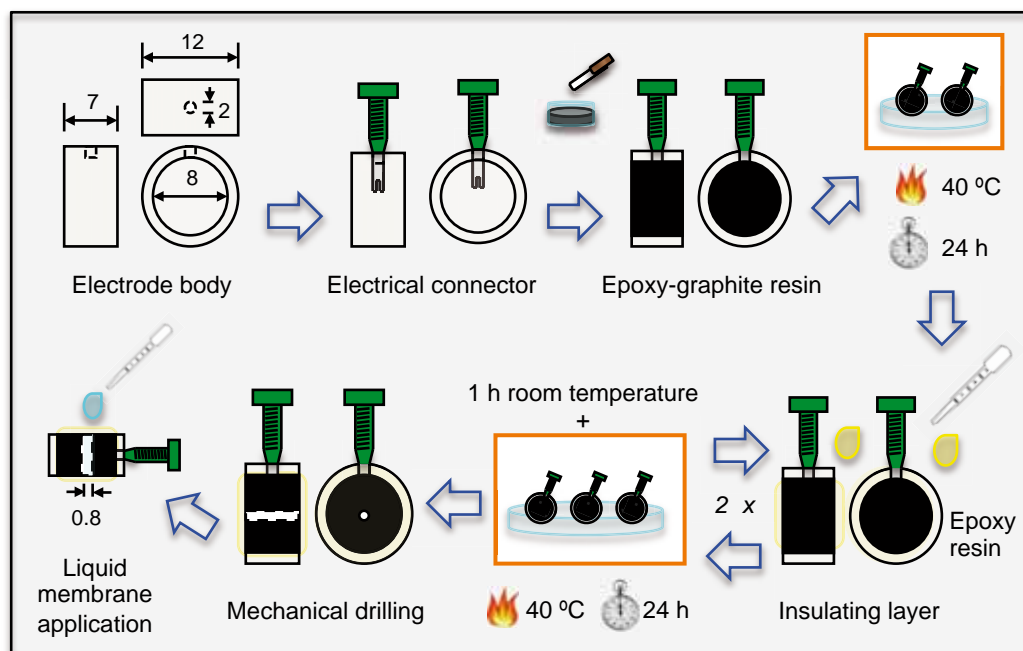
Figure 4.8 Construction of tubular electrodes of polymeric liquid membrane for SO$_4^{2-}$ analysis (dimensions in millimeters)

Similarly to crystalline membrane tubular electrodes, for polymeric liquid membrane, electrode body also consisted in a cylindrical element of methacrylate with 7 mm width, 12 mm external diameter and 8 mm internal diameter with an orifice of 2 mm in which the electrical connector will be inserted through. The electrode body was completely replenished with the epoxy-graphite conducting composite freshly prepared. The epoxy-graphite composite was prepared in a proportion of 1:1 epoxy:graphite while the epoxy resin was prepared in a proportion of 1:0.4 Araldit® M/5490:HR hardener resin (Huntsman Advanced Materials, Switzerland). This composite paste was thoroughly mixed and air bubbles were eliminated. Epoxy-graphite composite was cured at 40 ºC during 24 h. After that, an insulating layer of a non-conductive epoxy resin was applied for both sides of the electrode. Epoxy resin was prepared as described for tubular electrodes of crystalline membrane. After each side application, the resin was cured during 1 hour at room temperature and then during 24 h at 40 ºC. Excess of resin was cleaned off from the edges of the electrode body. Pictures of constructed liquid-membrane tubular electrodes of polymeric liquid membrane are shown in **Figure 4.9**.

Figure 4.9 Images of constructed tubular electrodes of polymeric liquid membrane for SO_4^{2-} analysis

Finally, constructed electrodes were perforated, opening an orifice of 0.8 mm diameter across the electrode body in which the liquid sensing cocktail was deposited. The internal orifice surface was wet polished by inserting an ultra-fine abrasive paper inside the orifice. The membrane cocktail was applied, in a gas fume hood, by gently depositing 1 drop of the freshly prepared cocktail right inside the orifice of the electrode each 60 to 90 minutes, up to approximately 5 drops, allowing the membrane to dry. In this type of electrodes, the internal solid reference is the potential generated when epoxy-graphite is in contact with O_2/H_2O spread across the membrane, due to the permeability of the PVC to O_2 and water. Before use, electrodes were dried at room temperature for 48 h and conditioned in Na_2SO_4 solution (1.0×10^{-3} mol S-$SO_4^{2-} \cdot L^{-1}$) (Panreac, Spain) during 15 h.

4.5 Construction of conventional electrodes

Conventional electrodes were constructed according to previously described (Barquero, 2001), for batch measurement of SO_4^{2-}, as presented in **Chapter 6**. The procedure adopted for construction of conventional electrodes is schematized in **Figure 4.10**.
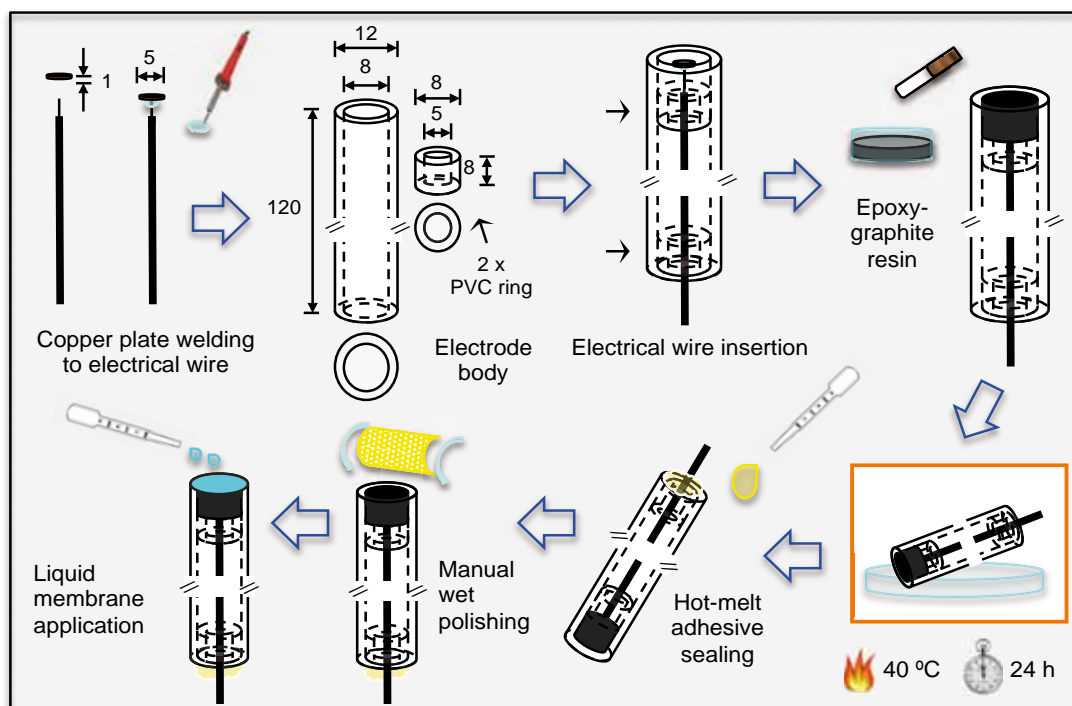
Figure 4.10 Construction of conventional electrodes of polymeric liquid membrane for batch measure of SO_4^{2-} (dimensions in millimeters)

Firstly, a plastic-covered electrical wire was gently pilled off in one of its extremities, leaving an exposed portion of the internal copper wire of approximately 5 mm. Then, the electrical wire was welded to a circular copper plate of 5 mm diameter and 1 mm thickness. The copper plate was previously immersed in a 5% HNO_3 (Panreac, Spain) solution for 2 min and then rinsed with water, for oxide cleaning. Finished electrical connection was then inserted inside a methacrylate cylindrical body of 8 mm internal diameter, 12 mm external diameter and 120 mm length. Also, two PVC rings were tightly fixed in the internal wall of the electrode body applying a general purpose cyanoacrylate instant adhesive. One PVC ring was fixed at approximately 5 mm from the top of the electrode body and served to support the copper plate previously prepared. The other PVC ring was used to secure the electrical wire at the end of the electrode body. Then, the empty space between the upper PVC ring and the top of the electrode was replenished with the epoxy-graphite conducting composite freshly prepared, as described in **Section 4.4.2**. Pictures of constructed conventional electrodes of liquid membrane are shown in **Figure 4.11**.

Figure 4.11 Images of constructed conventional electrodes of polymeric liquid membrane for SO_4^{2-} batch measure

The epoxy-graphite composite was cured at 40 ºC during 24 h. Excess of resin was immediately wiped of the electrode edges. The electrical wire was securely fixed to the electrode body extremity using a holt-melt adhesive based on ethylene vinyl acetate (3764Q-Clear – 3M, USA). Then, manual wet polishing with fine sand paper was carried out until obtaining a maximum cavity of 0.3 mm in the epoxy-graphite composite surface, where the liquid sensing cocktail will be dropped in. After cleaning the polished surface with neutral soap and water, polishing with a wet alumina-polishing strip was done until obtaining a smoothed and regular surface. The liquid membrane cocktail, freshly prepared as described in **Section 6.3.2**, was applied over the epoxy-graphite polished surface by gently depositing 1 drop each 30 – 45 minutes, up to 8 – 10 drops. The membrane application was performed inside a gas fume hood. Subsequently, electrodes with fresh applied membrane were completely dried at room temperature during 48 h. Some electrodes were recycled when the liquid membrane was deteriorated by eliminating liquid membrane residues and, after cleaning and polishing procedures, applying new layers of a new freshly prepared membrane cocktail. Pictures of the polymeric liquid membrane during and after application on conventional electrodes are shown in **Figure 4.12**.
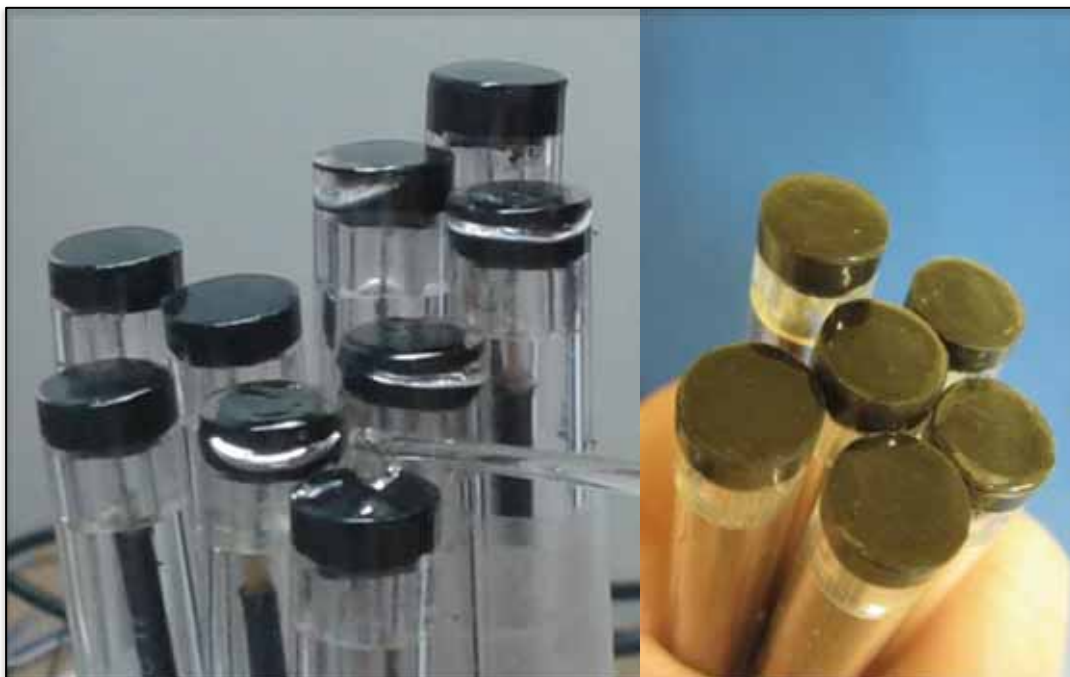
Figure 4.12 Images during and after application of the polymeric liquid membrane on constructed conventional electrodes

Before use, electrodes were conditioned in a diluted solution of Na_2SO_4 (1.0×10^{-3} mol $S\text{-}SO_4^{2-} \cdot L^{-1}$) (Panreac, Spain) during 15 h with magnetic stirring. Electrodes were cleaned with distilled water after each calibration and were kept dry and covered for long-periods storage.

4.6 Characterization of analytical systems

Analytical systems developed during this research for H_2S/TDS and SO_4^{2-} determination, as presented in **Chapter 5** and **Chapter 6**, were based in direct potentiometry, which is a widely used method for environmental monitoring because the instrumentation required for electrical potential (E) measurement is simple and inexpensive (de Marco *et al.*, 2007). In this work, the potentiometric analytical systems studied were characterized by evaluating typical calibration parameters, such as the sensitivity (SL), the linear range (LinR), the low linear-range limit (LLRL), the limit of detection (LD) and the response time. Also, the selectivity for SO_4^{2-} of polymeric liquid membrane electrodes was studied in the presence of the interfering anions found in the BTF liquid phase.

ISEs are electrochemical sensors in which the E depends on the concentration and nature of the chemical species in solution. The determination of the activity of the analyte or the determination of its concentration, when the ionic force of the medium is adjusted, is achieved by the measurement of the E gradient established between the ISE and a reference electrode. The calibration curve of an ISE in discontinuous mode is obtained by plotting the measured E *versus* the logarithm of the activity (a_i) of the main ion, as schematized in **Figure 4.13**, in which graphical definition of LD and LLRL can be found. Two different zones can be defined: the sub-Nernstian zone and the Nernstian zone. Electrodes that operate in the LinR of the calibration curve present a Nernstian behavior.
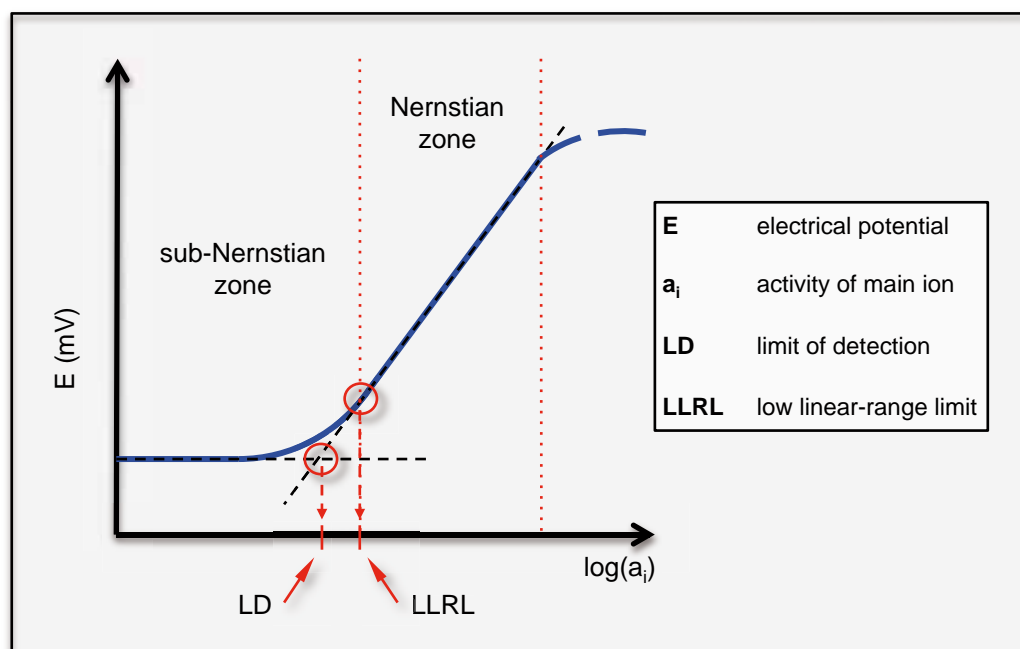
Figure 4.13 Typical ISE calibration curve

Data obtained from the calibration of the different electrodes used in this research were treated as herein presented, applying the software Microsoft Excel 2007 and Microsoft Excel 2011 for Mac (Microsoft, USA) for linear regressions and statistical analysis. The software Sigma Plot 10.0 (Systat Software Inc., USA) was used for non-linear regressions, applying a Marquardt-Levenberg algorithm. The behavior of an ISE can be described by the Nernst-Nikolsky expression, according to **Equation 27**.

E = K + [SL$_1$ × log(a$_i$)] [27]

Where:

E = Electrical potential (mV)

K = Electrode calibration constant (mV)

SL$_1$ = Sensitivity in the Nernstian zone (mV·dec^{-1})

a$_i$ = Activity of the main ion

The coefficients of the Nernst-Nikolsky equation are obtained by linear regression fitting. The slope (SL$_1$) of the linear regression is positive when the electrode is sensible to a cation and negative when it is sensible to an anion. Also, non-linear regressions were applied to characterize the response of the electrodes in the complete calibration curve range, including linear and non-linear zones. Non-linear regression calculations were performed based on the Nikolsky-Eisenman expression, an extension to the Nernst equation, according to **Equation 28** and **Equation 29**.

E = K + [SL$_2$ × log(a$_i$ + Σ((Kpot $_{i,j}$ × aj$^{zi/zj}$) + LD$_{ap}$)] [28]

E = K + [SL$_2$ × log(a$_i$ + C)] [29]

Where:

E = Electrical potential (mV)

K = Electrode calibration constant (mV)

SL$_2$ = Sensitivity in the entire calibration range (mV·dec^{-1})

a$_i$ = Activity of the main ion

z$_i$ = Ionic charge of the main ion (z = 2 for S^{2-} and SO$_4^{2-}$)

Kpot $_{i,j}$ = Potentiometric selectivity coefficient of the main ion (i) in the presence of the interfering ion (j)

LD$_{ap}$ = Apparent limit of detection (mol·L^{-1})

a$_j$ = Activity of the interfering ion

z$_j$ = Ionic charge of the interfering ion

The term "*C*" in the **Equation 29** is defined as the sum of an apparent limit of detection (LD$_{ap}$) and the Kpot. LD$_{ap}$ is an empirical constant obtained

during the regression fittings. In the presence of an ionic background, the value of the Kpot is considered to be sufficiently higher than the value of the LD_{ap}, so the LD_{ap} was not consider in the calculation expressed by the **Equation 28**, applied when interfering ions are present in the solution.

The characterization of tubular electrodes integrated to flow-based analytical systems was done, similarly to the case of conventional electrodes in batch systems, by performing serial calibrations with standards of exact known concentration. Standards were injected into the flow system in ascending concentration order, avoiding the saturation of the sensing membranes. The typical analytical response of an ISE in a potentiometric FIA system is a transitory signal like a peak, obtained by the difference between the electrode response signal and the base line. The base line is the electrode response in the presence of a low concentration of the analyte, normally lower than the LD (S^{2-} or SO_4^{2-} background).

The calibration curve of flow-based systems was obtained by plotting the peak height (H) *versus* the $\log(a_i)$, where $a_i = \gamma\ c_i$, analogously to the calculation described by the **Equation 27**. However, a high-ionic strength solution is used in flow systems, allowing considering that activity coefficient (γ) is constant. Then, consistently $\log(\gamma)$ is also constant and can be comprised by the calibration curve constant (K'). This assumption lead to a modification of the Nernst-Nikolsky expression, according to **Equation 30**, where the potentiometric response variation depends on the logarithm of the concentration of the main ion (c_i). Calibration curves resulted thus in the representation of the H *versus* the $\log(c_i)$.

H = K' + [SL$_1$ × log(c$_i$)]   **[30]**

Where:

H = Peak height (mV)

K' = Electrode calibration constant, including the activity coefficient (mV)

SL_1 = Sensitivity in the Nernstian zone ($mV·dec^{-1}$)

c_i = Concentration of the main ion ($mol·L^{-1}$)

Finally, when the response of the electrodes was investigated in the non-linear zone of the calibration curve. Calculations were performed according to **Equation 31**.

$$H = K' + [SL_2 \times \log(c_i + C)] \qquad\qquad [31]$$

Where:

H =   Peak height (mV)

K' =   Electrode calibration constant, including the activity coefficient (mV)

SL_2 =   Sensitivity in the non-linear zone (mV·dec^{-1})

c_i =   Concentration of the main ion (mol·L^{-1})

C =   Term related to the LD$_{ap}$ (mol·L^{-1})

4.6.1   Definition of performance parameters of ISEs

The performance of the electrodes constructed during this research was evaluated by the calculation and analysis of the SL, the LLRL and the LD for TDS and SO$_4^{2-}$ electrodes (**Chapter 5** and **Chapter 6**). The characterization of the constructed ISEs for SO$_4^{2-}$ determination also comprised the study of the lifetime and the response time of the electrodes. Furthermore, the selectivity to SO$_4^{2-}$ of the constructed electrodes was studied for the anions commonly present in the liquid phase of the BTF, applying the matched potential method (MPM), a widely used method for the calculation of interferences for ISEs (Umezawa *et al.*, 1995).

The FIA/GD-CFA system developed for TDS/H$_2$S analysis (**Chapter 5**) has been already characterized (Redondo *et al.*, 2008) and no further studies in this sense were performed during this research. Nevertheless, the system previously developed for on-line biogas analysis and non-continuous S^{2-} analysis was modified and optimized in order to perform the on-line monitoring of TDS at the BTF liquid phase. Other than that, it was not necessary to study the effect of interferences for TDS determination due to the lack of interfering ions in the solution. However, the lifetime of the constructed ISEs for TDS was assessed during this work.

Sensitivity

The sensitivity (SL) of an ISE is a parameter commonly applied to easily compare the behavior of different electrodes and it gives an indication of the performance of the electrode. The IUPAC defines the SL of an ISE as the slope of the calibration curve. The SL of an electrode is an important parameter and its study allows assessing the lifetime of the sensor, applying a discriminatory criterion based on the SL.

The theoretical or ideal value of SL for monovalent ions in the linear zone of the calibration curve is 59.16 mV·dec^{-1} for cations and -59.16 mV·dec^{-1} for anions. For divalent ions, the ideal value of SL in the linear zone is 29.58 mV·dec^{-1} for cations and -29.58 mV·dec^{-1} for anions, as is the case of S^{2-} and SO_4^{2-}. When the slope of the linear regression fitting resulted in a value lower than -29.58 mV·dec^{-1}, the SL of the electrodes was considered to exhibit a sub-Nernstian response. Analogously, when the linear slope resulted in a value higher than -29.58 mV·dec^{-1}, it was considered that the electrodes presented a super-Nernstian response.

Low linear-range limit

The low linear-range limit (LLRL) is defined as the minimum value of the activity of the main ion, from which the electrode presents a Nernstian behavior. This parameter was calculated as previously described (Hara *et al.*, 1994), applying a statistical procedure based on the determination of the Pearson's correlation coefficient.

The calculation of the LLRL for calibrations performed on analytical flow systems consisted on a least-squares fitting approach, using the complete data set of the linear regression results, until obtaining a regression coefficient as close to 1 as possible (> 0.99). The LLRL is widely applied for comparing electrodes performance and, jointly with the LinR, defines the applicability of the electrodes in terms of a reliable response interval.

Limit of detection

A wide variety of criteria can be adopted to define the limit of detection (LD) in potentiometric analyses. By analogy to other fields, the LD can be defined as the concentration of the analyte from which the E suffers a deviation of an arbitrary multiple from the standard error of the average E that corresponds to the operational region of low concentrations (sub-Nernstian zone). The IUPAC defines the LD for potentiometric determinations as the activity (or the concentration) of the main ion corresponding to the intersection point between the extrapolation of the line with Nernstian behavior and the initial segment of low concentrations, usually horizontal, as showed in **Figure 4.13**. In this work, another accepted definition of the LD was considered, which is derived from the application of non-linear fitting methods to the complete experimental data set, including those values below the LLRL. Calculations were performed according to **Equation 29**, in which the term "C" comprises two factors, the LD_{ap} and the effect of interfering ions, as described by **Equation 32**, in the case of SO_4^{2-} as the main ion (**Chapter 6**).

$$C = LD_{ap} + \Sigma \ (Kpot_{SO4^{2-},j} \times aj^{2/zj}) \qquad\qquad [32]$$

Where:

$C =$ Term related to the LD (mV)

$LD_{ap} =$ Apparent LD (mol·L^{-1})

$Kpot_{SO4^{2-},j} =$ Kpot of SO_4^{2-} in the presence of the interfering ion (j)

$a_j =$ Activity of the interfering ion

$z_j =$ Ionic charge of the interfering ion

In the case of TDS determination (**Chapter 5**), the calculation of the LD corresponded directly to the value of the term "C" ($LD_{ap} = C$), since the system operated in absence of interferences (Martinez-Barrachina *et al.*, 1999). This definition was assumed because the only interfering ion for a homogeneous crystalline membrane electrode of Ag_2S is Hg^{2+} (Olenic *et al.*, 1997), which was not present in the BTF liquid phase.

Potentiometric selectivity coefficient (Kpot)

ISEs are selective but not specific to the analyte. In this sense, the E response depends not only on the main ion activity, but also on the Kpot of all the interfering ions present in the solution, according to the Nikolsky-Eisenman expression (**Equation 28**). Selectivity is one of the most important characteristics of an ISE. The applicability of an electrode in any analytical system depends in a great extend on the selectivity of its sensing element. The Kpot is defined as the capacity of an ISE of distinguishing an ionic species from others present in the solution (Umezawa *et al.*, 2000). The lower the value of Kpot, the higher the preference of the ISE for the main ion. The determination of the Kpot for SO_4^{2-} was performed in both FIA and batch modes, as specified in **Section 6.3.3**. The method applied was the MPM (Alegret *et al.*, 1985), which presents the advantage of being applicable for ions of different ionic charge, because it is independent of the Nernst equation (Gadzekpo and Christian, 1984). This methodology consisted in the measurement of the E variation between the ISE and the reference electrode produced by the progressive addition of increasing concentration of SO_4^{2-} while the concentration of the interfering ion was kept constant at a known value. Since interference studies considered the presence of a single interfering ion, for overcoming crossed effects, the calculation of the Kpot was performed according to the **Equation 33**, derived from the Nikolsky-Eisenman expression, taking into account that the value of the LD_{ap} is sufficiently lower than the Kpot in the presence of interferences. Normally, resulting LD_{ap} in the presence of the interfering ion is higher than when no interfering ions are present in the sample.

$$\textbf{Kpot}_{\textbf{SO4}^{2-}, j} = \textbf{\textit{C}} / \textbf{cj}^{2/zj} \qquad\qquad \textbf{[33]}$$

Where:

$\text{Kpot}_{SO4^{2-}, j}$ =   Kpot of SO_4^{2-} in the presence of the interfering ion (j)

C =   LD (mV)

c_j =   Concentration of the interfering ion (mol·L^{-1})

z_i =   Ionic charge of the interfering ion

Lifetime and response time

The lifetime of the constructed ISEs was evaluated by performing successive calibrations over the time, covering the LinR of the electrode. The slope and the parameters of the linear regression fitting were calculated and the stability of the obtained E of each ISE was assessed. Lifetime of ISEs is lower for polymeric liquid membrane than for crystalline membrane electrodes, because of the potential lost of active ionophore from the polymeric matrix, beside other related factors, such as ionophore leaching (Buhlmann and Umezawa, 2000) or the irreversibility of the interaction between the ionophore and the analyte. Electrodes were considered non-operative when the obtained response was irreversibly affected, even after recovering procedures, which was verified by either the lost of SL (> -29.58 mV·dec^{-1}) or the increment of the LLRL. Also, the stability of the obtained E acted as an indication of the proper operation of the electrodes; the response was classified as unstable when the E variation was above 2 mV. When the first signs of performance impairment were noticed, the electrodes were subjected to a recovering procedure in order to improve their response and to extending their lifetime. Electrodes of crystalline membrane were recovered by polishing and cleaning their membrane orifice. In the case of ISEs of polymeric liquid membrane, electrodes recovering consisted in a recycling procedure including first the removal of the deteriorated membrane and then, after fine wet polishing and cleaning, in the application of a new sensing cocktail.

The response time of an ISE is as a critical factor for the application of the electrode, in both FIA and batch mode analytical systems. It was investigated by measuring the speed of the response obtained at the detection system after producing a variation in the activity of the main ion. The response time (t_{95}) was considered as the time required by the system to reach 95% of the total variation of the signal after the injection of a standard. The response time of the ISEs characterized during this research was evaluated considering both low and high concentrations of the main ion, covering the complete LinR of the electrode.

4.7 Analytical methods

Analytical methods applied during this research are specified in this Section. When indicated, equipment number according to **Table 4.1**.

4.7.1 Gas analysis

H$_2$S

H$_2$S was on-line analyzed by an electrochemical sensor (SureCell – EuroGas Management, UK) (Equipment **#12**), whit the technical specification given in **Table 4.5**. Commercially available H$_2$S sensors operate in a range significantly lower than the concentration found in biogas. Dilution with humidified air was performed by bubbling dry air into the humidification column (Equipment **#13**), before joining the H$_2$S gas line. Additionally, an impinger was used as a droplet separator, because non-condensing conditions are required. The flow of gas fed into the sensor (1 NL·min^{-1}) was manually monitored by a rotameter (Equipment **#15**). Periodical calibrations in the complete range of operation of the sensor were performed to assure the accuracy of the BTF performance calculations. Moreover, H$_2$S was analyzed by the flow analyzer, based on a CFA system with a previous gas diffusion step (FIA/GD-CFA), as described in **Chapter 5**.

Table 4.5 Technical specification – H$_2$S sensor (SureCell)

Principle	Electrochemical
Measuring range *(ppm$_v$ of H$_2$S)*	0 – 200
Maximum overload *(ppm$_v$ of H$_2$S)*	400
Output signal *(mA)*	4 – 20
Output response *(μA·ppm$_v$ of H$_2$S^{-1})*	0.35 ± 0.1
Temperature range *(ºC)*	-20 to +40
Humidity range *(%)*	15 – 90
Response time t$_{90}$ (s)	< 10

CH$_3$SH

CH$_3$SH was off-line analyzed using a gas chromatograph (6890N – Hewlett Packard, USA), equipped with a fused silica capillary column (Supel-Q PLOT – Supelco, USA) of 30 m length, 0.53 mm inner diameter and 40 μm film thickness. GC is a separation technique in which the analytes contained in a mobile gas phase are dispersed and separated through a stationary phase and then directed to a detector by a carrier gas, where an electrical signal is generated proportionally to the quantity of each analyte eluted. The chromatogram is the graphical record of the obtained signal *versus* the time; each separated compound appears as a separated peak. Areas under the peaks are proportional to the concentration of the analyte, allowing its quantification. The chromatograph was equipped with a flame ionization detector (FID). Main chromatographic conditions adopted for CH$_3$SH analysis are summarized in **Table 4.6**.

Table 4.6   Chromatographic conditions for CH$_3$SH analysis

Mode	Constant flow
Carrier gas flow (mL·min^{-1})	3 (He)
Make-up gas flow (mL·min^{-1})	25 (N$_2$)
Injector temperature (°C)	230
Oven temperature (°C)	80 (isotermic)
Detector temperature (°C)	260
Split ratio	1:2
Run time (min)	15
Retention time (min)	≈8.1

Standards and samples were manually injected (1 mL) using a glass precision-syringe (Hamilton, USA). Standards were prepared by a DMFC dedicated to CH$_3$SH (Equipment **#10**) and covered the concentration range studied in **Chapter 8**. Calibrations with 6 points were daily performed, assuring the reliability of the obtained results. Samples taken during experiments were analyzed within 12 h after collection, which warranted the integrity of the sample, as verified during analytical method adjustment.

4.7.2 Liquid analysis

pH

On-line pH measurement at the recirculation line of the BTF was performed using a sensitive glass-membrane combined electrode with temperature sensor and electrolyte gel (5334 – Crison Instruments, Spain) (Equipment **#18**). Technical specification of this sensor is presented in **Table 4.7**. Periodical calibrations were performed with pH buffers of 4.01 and 7.00 pH units (Crison Instruments, Spain), assuring the proper operation of the probe. This sensor was connected to a pH controller (PH28 – Crison Instruments, Spain), allowing the actuation on the NaOH pump (Equipment **#5**) or the HCl pump (Equipment **#6**), depending on the operational pH setpoint. The electrode was installed into a PVC insertion housing (Crison Instruments, Spain), connected to the recirculation pipe through fast-type connections, which easily allowed executing cleaning and calibration procedures.

Table 4.7 Technical specification – pH sensor (5334)

Measuring range (pH)	0 – 14
Temperature range (ºC)	0 – 100
Maximum pressure (bar)	5
Reference element	Sleeved Ag wire coated with AgCl
Diaphragm	Ring of porous PTFE
Temperature sensor	Pt 1000, with automatic temperature compensation (ATC)
Response time (pH 4 – 7) (s)	< 20

Moreover, the measurement of pH during the SO_4^{2-} determination studies (**Chapter 6**) was performed using a pH bench meter (EL20 – Mettler Toledo, Switzerland) equipped with an electrode arm and a pH glass-membrane combined electrode (U405 – Mettler Toledo, Switzerland), according to the technical specification presented in **Table 4.8**.

Table 4.8   Technical specification – pH sensor (U405)

Measuring range (pH)	0 – 12
Temperature range (ºC)	0 – 100
Reference system	ARGENTHAL™ (AgCl granulate-filled cartridge with Ag^+ trap)
Diaphragm	Triple ceramic
Reference electrolyte	FRISCOLYT-B® (glycerol / KCl)
Temperature compensation	ATC

Potential measurement and control of FIA/GD-CFA system

The measurement of the E in the flow system described in **Chapter 5** for the on-line monitoring of H_2S and TDS was performed with a potentiometer-voltmeter specially designed for this application (UAB-IQ-11003 – TMI S.L., Spain). This instrument presented 2 potentiometric sensor inputs with their respective references and proportional E signal output (0 – 10 V). Measuring range was -1,999 to +1,999 mV, with a resolution of 0.5 mV. Additionally, this instrument controlled the 6-way injection valve (EASI1215/342 – Easi Technologies, Spain) installed in the flow system. E measurement executed during the determination of SO_4^{2-}, as described in **Chapter 6**, was performed with a potentiometer (micropH2002 – Crison Instruments, Spain) connected to a digital commutator (TMI-6017CONM16 – TMI S.L., Spain), which allowed the measurement of E for 16 electrodes simultaneously. For practical reason, calibrations were performed for a maximum of 6 simultaneous electrodes. This instrument is a pHmeter controller operated in E continuous mode. Measuring range was -1,999 to +1,999 mV, with a resolution of 1 mV. Both potentiometric analytical systems operated with a double-junction reference electrode (ORION 900200 – Thermo Fisher Scientific, USA), a sleeve-type refillable Ag/AgCl electrode. A solution of KNO_3 saturated in AgCl, provided by the same manufacturer, was used as internal reference electrolyte. External reference electrolyte consisted in a solution of KNO_3 (10%) (Panreac, Spain).

Total dissolved sulfide

TDS was analyzed by the FIA/GD-CFA system described in **Chapter 5**. Moreover, the proposed analytical system was validated using a benchtop pHmeter/potenciometer (SB90M5 – VWR International, Germany) operating in the continuous ISE-measuring mode. TDS concentration was directly quantified in mol $S^{2-} \cdot L^{1-}$ or ppm S^{2-} (mg $S^{2-} \cdot L^{1-}$), with 5% of relative accuracy. The sensing device consisted in a silver/sulfide ISE combination electrode (Symphony 14002-790 – VWR International, Germany), with the technical specification presented in **Table 4.9**.

Table 4.9 Technical specification – TDS sensor (SympHony)

Principle	Crystalline membrane of Ag^+/S^{2-}
Measuring range (mg $S^{2-} \cdot L^{-1}$)	0.003 – 32,000
Linear range (mg $S^{2-} \cdot L^{-1}$)	0.32 – 32,000
Temperature range (ºC)	0 – 80
pH range	10 – 12
Reproducibility	± 4%
Reference electrode	Internal, Ag/AgCl

Sulfate, thiosulfate, nitrite, nitrate, chloride and phosphate

The determination of SO_4^{2-}, $S_2O_3^{2-}$, NO_2^-, NO_3^-, Cl^- and PO_4^{3-} was off-line performed using an ionic chromatograph (ICS-2000 – Dionex, USA), equipped with an integrated reagent-free system with eluent generation and coupled to an electrolytic suppression device, suited with a dedicated management software (Chromeleon – Dionex, USA). IC is a simple and robust technique widely applied for the separation of ions, based on the use of columns filled with ion-exchange resins. A carbonate eluent anion-exchange analytical column was used (IonPac® AS9-HC – Thermo Fisher Scientific, USA) in combination with a guard column. Chromatographic conditions for anionic analysis are described in **Table 4.10**.

Table 4.10 Chromatographic conditions for anionic analysis

Column	IonPac® AS9-HC (analytical + guard)
Column length *(mm)*	Analytical: maximum 250 Guard: maximum 50
Column temperature *(ºC)*	30
Eluent	KOH
Eluent gradient	18 – 50 mM KOH from 0 – 10 min 50 – 18 mM KOH from 10 – 15 min
Eluent flow rate *(mL·min^{-1})*	1.6
Auto-sampler	AS40
Injection volume *(μL)*	25.00
Suppressor	Self-regenerating SRS® 300 (H_2CO_3)

Periodical calibrations, according to the manufacturer recommendation, were performed by the preparation of 5 standards by serial dilution from standard stock solutions of each compound (Merck, Germany).

Total inorganic carbon

TIC was off-line analyzed using an automated system for carbon analysis (TOC 1020A – OI Analytical, USA). The detector consisted in a nondispersive infrared (NDIR) cell, which allows the efficient selective detection of carbon in a wide range of matrices. When carbon compounds are combusted in an O_2-rich environment, the complete conversion of carbon to CO_2 is obtained. TIC is determined by measuring the CO_2 released following sample acidification.

Samples of 25 mL were automatically injected by duplicate by a vial auto-sampler of 53 positions for 40-mL vials. The high-efficiency combustion of the injected samples was made with Pt-catalyst at 680 ºC, with an O_2 flow rate of 550 mL·min^{-1}. Also N_2 was consumed at a flow rate of 70 mL·min^{-1}. The measuring range for TIC was 5 – 1,000 mg C·L^{-1}, with a precision of 2%. The instrument was suited with a dedicated management software (WinTOC™, OI Analytical, USA).

4.7.3 Solid analysis

Total suspended solids and volatile suspended solids

TSS and VSS analysis were performed according to the Standard Methods (APHA, 2006b). TSS calculation allowed the quantification of the amount of organic and inorganic matter in suspension in the sample. Basically, for the determination of TSS, a homogeneous sample was filtered through a weighed standard glass microfiber filter of 0.7 μm (GF/F grade – Whatman, USA). The residue left on the filter after filtration was dried to a constant weight at a temperature between 103 – 105 ºC. The increase in weight of the filter represents the TSS of the sample. VSS calculation allowed the quantification of the amount of volatile matter in the sample, which can be related to the quantity of biomass. Basically, the filter used for TSS analysis was ignited at 550 ± 50 ºC for 30 minutes. The weight lost on ignition of the solids represents the VSS of the sample. Both TSS and VSS analysis were performed by triplicate.

Cellular nitrogen

N_{cell} analysis was performed using commercial kits for total nitrogen (LCK238 – Hach Lange, UK), based on a colorimetric detection on a portable split beam spectrophotometer (DR2800 – Hach Lange, UK), after the digestion of the sample. Inorganically and organically bonded nitrogen is oxidized to NO_3^- by digestion with peroxodisulfate. NO_3^- ions react with 2,6-dimethylphenol in a solution of H_2SO_4 and H_3PO_4 to form nitrophenol. The measurement range was 5 – 40 mg N·L^{-1}. Kits are commercialized with all necessary reagents. The spectrophotometer was suited with a tungsten lamp and operated within a wavelength range of 340 to 900 nm. Kits were measured at 345 nm, after aeration. The photometric measuring range was ± 3 of Abs and the photometric accuracy was 5.5×10^{-3} of Abs. Operational temperature range of the spectrophotometer was 10 – 40 ºC.

Elemental analysis (C, N, H, P and S)

Elemental analysis was performed by combustion at 1,000 °C under pure O_2 atmosphere in a bomb calorimeter (CPH330 – IKA, Germany) with an aliquot of 20 mg of dry solid sample and subsequent IC analysis (Alliance HPLC – Waters, USA). The calorimeter maximum measurement range was 40,000 J with a measuring time of approximately 8 minutes. The reproducibility was 0.1% and the temperature measurement resolution was 1.0×10^{-5} K. The decomposition vessel of the calorimeter was filled with a weighed sample and with pure O_2 at an operating pressure of 30 bar, to optimize the combustion process. The cooling medium used was tap water.

Metal trace analysis

Metal trace analysis (Fe, Zn, Cu, Cr, Ni, Pb, Mo, Na and K) was performed by ICP-OES (Optima8000, Perkin Elmer, USA). Dry homogenous powdered sample, prepared as shown in **Figure 4.5** (Dry-FSS), was first microwave digested (StartD – Milestone, USA). Microwave digestion is used to mineralize solid samples, so they became into liquid ones. The sample containing biomass and solids (0.500 g) was heated inside the microwave vessels with a mixture of $HCl:HNO_3$ 9:3 ($v \cdot v^{-1}$) at a working temperature of 180 – 220 ºC. At this temperature, degradation of the sample is produced. After digestion, an acid solution was obtained, which was analyzed by ICP-OES, with a flat plate system. The spectral range was 165 – 900 nm, with a resolution < 9.0×10^{-3} nm. Sample was sprayed into flowing Ar (20 $L \cdot min^{-1}$) and passed into a torch, which was inductively heated to ≈10,000 ºC. At this temperature, gas is atomized and ionized, forming a plasma. Detection of almost the entire periodic table with LD < 0.1 $mg \cdot L^{-1}$ can be obtained by the identification of the mass spectrum of the plasma.

※

5

on-line monitoring of H₂S

and sulfide by a flow analyzer

"A writer should have the precision of a poet
and the imagination of a scientist."

Vladimir V. Nabokov
(Saint Petersburg, 1899 – Montreux, 1977)

5 On-line monitoring of H$_2$S and sulfide by a flow analyzer

5.1 Summary and scope

Results obtained during the on-line monitoring of the BTF with the developed H$_2$S/TDS flow analyzer are presented in this Chapter. The analyzer consisted in a flow injection analysis (FIA) system for TDS determination and a continuous flow analysis with a previous gas diffusion (GD-CFA) system for H$_2$S determination. The conceptual definition of this analytical system has been already reported by others (Delgado *et al.*, 2006; Redondo *et al.*, 2008). Nevertheless, operational conditions were optimized during this research in order to incorporate a two-stage filtration system and an in-line system for pH adjustment, conditions required for the utilization of the analyzer in on-line monitoring tasks. Moreover, tubular ISEs of homogeneous crystalline membrane of Ag$_2$S were constructed and characterized by potentiometric detection. The analytical system was suited with a homemade program, which allowed the execution of unattended analysis during uninterrupted 24-hours monitoring episodes. Analyses were validated *versus* commercial sensors during the real-time operation of the BTF, under aerobic and anoxic conditions.

The BTF experimental setup was slightly different to that described in **Section 4.1**, mainly because of the packing material consisted in structured plastic elements, as published by Fortuny *et al.* (2008, 2011). It is worth observing that the long-term operation of the BTF with random packing material, as described in details in **Chapter 7**, **Chapter 8** and **Chapter 9**, was initiated right after the execution of the experiments reported in this Chapter. However, analytical results were considered completely comparable, since the analytical response of the H$_2$S/TDS determination system is independent of the type of packing material installed in the BTF. During the aerobic experiments herein reported, the inlet H$_2$S concentration was stepwise increased from 2,000 ppm$_v$ of H$_2$S (51.08 g S-H$_2$S·m^{-3}·h^{-1}) up

to 8,000 ppm_v of H_2S (215.30 g $S-H_2S \cdot m^{-3} \cdot h^{-1}$). Sulfur mass balance results indicated that S^0 production proportionally increased with the O_2/H_2S volumetric ratio decrease, as expected from the stoichiometric ratio. Maximum TDS detected in the liquid phase was 3.08 mg $S-S^{2-} \cdot L^{-1}$ while the EC_{max} was 201 g $S-H_2S \cdot m^{-3} \cdot h^{-1}$. Furthermore, the proposed analyzer was consistently applied during experiments reported in **Chapter 7**, **Chapter 8** and **Chapter 9**, allowing the investigation of the analytical stability of the system under different operational conditions over the time. Moreover, different samples from other experimental desulfurizing BTF setup (Hernandez, 2012) were analyzed as well with the presented analytical system, for TDS quantification.

The objectives of the work presented in this Chapter were to integrate the FIA/GD-CFA system to the BTF for on-line monitoring of TDS and H_2S and to validate the equipment under continuous operation, as a tool for describing the BTF performance. To this aim, tubular electrodes of crystalline membrane of Ag_2S were constructed and characterized. Then, controlled experiments were performed in the BTF by increasing the inlet H_2S concentration, in order to force TDS accumulation in the liquid phase. On-line values obtained by the FIA/GD-CFA analyzer were validated with conventional commercial sensors in both liquid (S^{2-} analysis) and gas (H_2S analysis) phases. Overall results demonstrated that the proposed analytical system is reliable for on-line monitoring applications and can serve as a valuable tool to understand the complex mechanism of biological desulfurization in BTFs.

5.2 Introduction

Flow injection systems are based in the automation of standard, conventional analytical process. Advantages of automated flow injection systems with respect to off-line processes are the speed, robustness and versatility, in addition to the low samples and reagents consumption and the low cost per analysis (Ferrer *et al.*, 2007). Flow injection systems are widely used for on-line process monitoring in water and waste water treatment, as well as in fermentation process, pharmaceutical, food industry and clinical analysis, among other applications (Gabriel *et al.*, 1998; Yuan and Kuriyama, 2000; Baeza, 2004; Santos and Korn, 2006; Zayed and Issa, 2010; Piano *et al.*, 2010). In general, the outstanding improvement of the LD and the selectivity enhancement of ISEs analytical systems have promoted a huge increment on potentiometric analysis investigation in different application fields. Over the last decade, a spectacular improvement on the overall ISEs capabilities has been reported, with an improvement factor of up to 1 million for LD determination of a wide variety of analytes and up to 1 billion for interferences coefficient discrimination (Egorov *et al.*, 2004; Pretsch, 2007; Zuliani and Diamond, 2012), resulting in more selective electrodes with lower detection limits.

The determination of sulfur species by FIA systems have been intensively used, resulting in the development of reliable systems for the direct determination of SO_4^{2-}, SO_3^{2-} and S^{2-} (Miro *et al.*, 2004; Santos and Korn, 2006). However, water containing dissolved sulfides readily loses H$_2$S, especially at acidic pH, as assumed from the value of the second dissociation constant of H$_2$S, as presented in **Table 2.2**. Consequently, the on-line determination of S^{2-} in real monitoring tasks requires the pH adjustment of the sample to values higher than pH = 12 before entering the analytical system, which allows the representative quantification of the TDS content of the studied sample.

Moreover, particularly for the application studied in this research, a complementary on-line filtration of the sample was required to ensure the proper analytical system response under continuous operation with real samples, avoiding the contamination of the analytical system internals by biomass colonization.

The utilization of gas diffusion cells in continuous flow analyzers is done for the separation of volatile compounds from the sample solution, or donor stream, through a gas-permeable microporous membrane into a receiver liquid solution, or acceptor stream (Miro and Frenzel, 2004). A typical gas diffusion cell in counter-current flow configuration is shown in **Figure 5.1**. Gas diffusion takes place in the PVDF membrane inside the diffusion cell, in which the acceptor solution flows in counter-current with the gas flow.
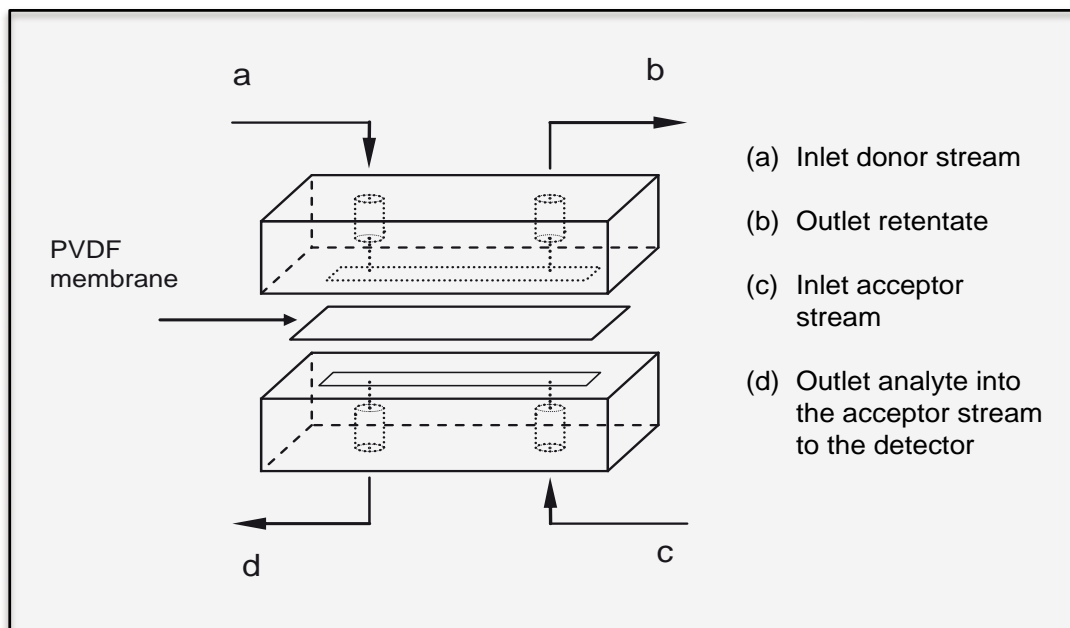
Figure 5.1 Typical gas diffusion cell with a PVDF membrane

Mass transfer is based on the diffusion of the analyte (in gaseous form) across the gas layer separating the two phases. The acceptor solution, also called carrier solution, flows counter-currently with gas stream for maximizing the diffusion phenomena and convert the H_2S into detectable species (TDS).

5.3 Materials and methods

5.3.1 Standards and reagents

All aqueous solutions were prepared with deionized Milli-Q water (18 MΩ·cm^{-1}). Reagents employed were of analytical grade. A sulfide antioxidant buffer solution (SAOB, pH = 14) was used as pH-adjustment solution, converting all dissolved H_2S and HS^- to S^{2-} (Card, 2001). The SAOB solution was daily prepared with 40 g·L^{-1} of NaOH (Panreac, Spain) and 10.1 g·L^{-1} of L-(+)ascorbic acid (Panreac, Spain), for avoiding S^{2-} oxidation (Garcia-Calzada *et al.*, 1999). The stock solution of S^{2-}, with approximate concentration of around 1 mol S-S^{2-}·L^{-1}, was prepared with 60.05 g of $Na_2S\cdot9H_2O$ (Sigma Aldrich, Germany) dissolved in 250 mL of NaOH 1×10^{-2} mol·L^{-1} (Panreac, Spain). Carrier was prepared by doping SAOB solution with background concentration of S^{2-} (2×10^{-5} mol S-S^{2-}·L^{-1}). The analyte background is added to the SAOB solution in order to stabilize the baseline and to contribute to the fast recovery of the base line signal after sample analysis (Baeza, 2004).

The determination of the real concentration of the stock solution of sulfide was performed applying an iodometric method, according to the Standard Methods (APHA, 2006a). Briefly, the method is based on the reaction of S^{2-} with excess of iodide (Panreac, Spain) in acid solution; the produced iodine is then determined by titration with standardized $Na_2S_2O_3\cdot5H_2O$ (Panreac, Spain) using soluble starch (Sigma Aldrich, Germany) as indicator, which forms an intense blue-black complex with iodine, present as I_3^- (Kolthoff *et al.*, 1969). S^{2-} is then calculated from the difference between the volume of $S_2O_3^{2-}$ required for the titration of the blank and the volume used for the sample. The standardization of the $S_2O_3^{2-}$ solution was performed by triplicated titration with KIO_3 (Panreac, Spain) as primary standard. Standard solutions of S^{2-} were daily prepared as previously described (Sekerka and Lechner, 1977), by serial dilution of the concentrated stock solution with SAOB, in order to avoid S^{2-} oxidation to

other forms of sulfur. S^{2-} standards covered a concentration range from 10^{-5} to 10^{-1} mol $S-S^{2-}\cdot L^{-1}$ (0.32 to 3,206 mg $S-S^{2-}\cdot L^{-1}$), and at least 7 different standards were used for calibration of the analytical system. Gaseous standards of H_2S were prepared as described in **Section 4.2.1**, covering a concentration range from 100 to 10,000 ppm$_v$ of H_2S. Gas standards were considered valid until 8 h after preparation, a more restrictive limitation than normally applied (Coyne *et al.*, 2011), in order to warrant standard's quality.

5.3.2 Experimental set-up

The FIA/GD-CFA experimental setup is shown in **Figure 5.2**.
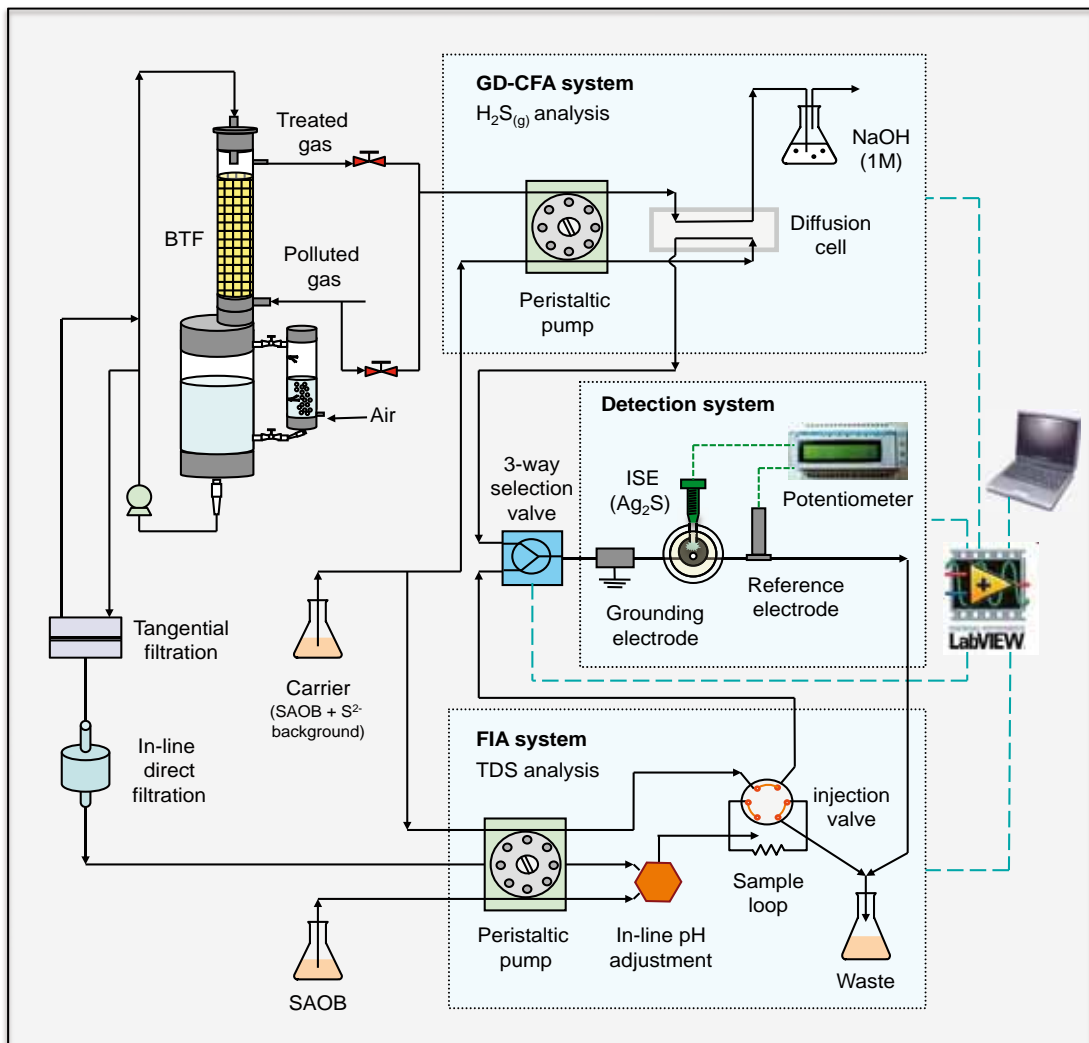
Figure 5.2 Schematic of the FIA/GD-CFA analytical system for on-line monitoring of the BTF

Liquid samples were processed by the FIA system, while gas samples were processed by the CFA system, suited with a gas diffusion cell for selective H_2S-absorption. Both systems are connected to a single detection unit based on an ISE of crystalline membrane (Ag_2S), constructed as described in **Section 4.4**, for TDS detection (Redondo *et al.*, 2008). However, since the analyzer described by Redondo *et al.* (2008) was not prepared for on-line sampling, an in-line sampling filtration system and a continuous sample pH adjustment step were developed during this work.

Connection of all system units was done with PTFE tubing of 0.8 mm internal diameter and 1.6 mm external diameter. The entire system was controlled and supervised by a tailor-made application previously developed by others (Redondo *et al.*, 2008), adapted during the work presented in this Chapter to on-line monitoring applications, using the software Labview 10.1 (National Instruments, USA). The data transfer was automatically done by a data acquisition module NI-USB-6008 (National Instrument, USA). The selection between FIA or GD/CFA operation mode was performed by the operator prior to the analyzer operation, using a friendly interface in the control software; physically it is made by a three-way electrovalve (NResearch 161T031; NResearch Inc., USA), installed right before the detection system. The custom-made program for data acquisition and for controlling the selection valve was adapted for any gas or liquid phase sampling frequency configuration including continuous, full-time gas phase or liquid phase on-line monitoring.

For the FIA system operation under continuous mode, liquid samples from the recirculation line of the BTF were pumped to the detection system by a peristaltic pump (Minipuls – Wilson, France). Samples were previously in-line filtered using a combination of tangential and direct flow filtration devices. Filtration is required for prevent any solid particle to enter the analytical system; filtration until 0.22 µm grade also avoid any undesirable biomass microfilm formation in electrode surface or any other place of the system internals. A combination of a primary filtration unit of a tangential flow type filter (Mini-Ultrasette™; Pall Corporation, USA) with 3 µm pore

size, followed by a secondary filtration unit of a disposable direct flow type filter (DIF-MN-40; Headline Filters, UK) with 0.22 μm pore size was installed before the liquid sampling peristaltic pump. Permeate from tangential flow type filter was returned to the BTF recirculation line (**Figure 5.2**). Injection cycles were executed by a six-way valve (EASI 1215/342; EASI Technologies, Spain). Each injection volume tested was measured with a specific sample loop. FIA system sampling time was 90 seconds, with the injection pulse being initiated after 60 seconds of each analytical cycle.

The proposed analytical system was equipped with an in-line pH adjustment step for liquid samples, to provide robustness to the FIA system because desulfurizing bioreactors may operate in a wide range of pH (van Langenhove and De Heyder, 2001; Abatzoglou and Boivin, 2009) and experiment important pH changes during operation if pH is not controlled (Sublette *et al.*, 1998; Gonzalez-Sanchez *et al.*, 2008). Since the optimal pH for the ISE is 14 (Redondo *et al.*, 2008), the sample stream was mixed with a metered flow of SAOB before the injection valve, previously to injection and detection steps. The optimal flow rate, and consequently the dilution ratio, was selected based on the lowest pH value allowed by the biotrickling filter pH control system (pH = 6). Different tubing combinations were tested, resulting in a minimum SAOB/sample flow rate ratio of 0.13, which corresponded to a pH adjusting solution flow rate of 0.26 mL·min^{-1}. The sample pH adjustment unit comprised a mixture T-shaped connection device (Omnifit, UK), in which the sample flow was mixed with the fixed SAOB solution flow. The pH adjustment unit was installed after the sample peristaltic pump, right before the injection valve (**Figure 5.2**).

For the CFA system operation coupled to on-line monitoring tasks, samples taken from the outlet gas line of BTF were automatically pumped by a peristaltic pump (Perimax 12; Spetec, Germany) to the gas diffusion cell, which was made of two Perspex pieces that support the diffusion membrane, a PVDF membrane (Millipore GVHP 142 50) with pore diameter of 0.22 μm and 7.2×0.25 cm^2 exchange area. Diffusion cell can be easily opened and the membrane replaced. For safety reasons, a trap deposit with

NaOH solution (1 mol·L^{-1}) was installed after the gas cell diffusion. For the operation of the CFA system in off-line mode, or during calibration procedures, samples (or standards) were conditioned 1 L Tedlar® bags (SKC, USA), as described in **Section 4.2.1**, and then were inserted into the analytical system applying the same above-mentioned peristaltic pump.

Finally, the detection system consisted of a stainless steel grounding electrode (33 mm × 0.8 mm internal diameter), an ISE of homogeneous crystalline Ag$_2$S membrane used as an indicator electrode and a reference electrode of a double liquid junction of Ag/AgCl (Thermo Orion 900200; Orion, USA). The indicator electrode construction was made according to the procedure developed by the Sensors and Biosensors Group (UAB), previously presented in **Figure 4.6**.

5.3.3 Experimental conditions and bioreactor monitoring

Reference operation of the BTF was adopted as detailed in **Table 4.1**. Basically, an inlet H$_2$S concentration of 2,000 ppm$_v$ of H$_2$S (51.08 g S-H$_2$S·m^{-3}·h^{-1}) was fed to the BTF under neutral pH conditions (6.0 – 6.5). The aeration flow was fixed at 150 mL·min^{-1} during the reference operation and was kept unaltered during the experiments, thus reducing the O$_2$/H$_2$S $_{supplied}$ ratio. The EBRT was 180 s and an average HRT of 51 ± 6 h were maintained during reference operation.

Under such reference conditions, no TDS accumulation in the liquid phase was noticed. Thus, different experiments under anoxic and aerobic conditions were performed in which the synthetic biogas inlet H$_2$S concentration was increased and the HRT reduced, in order to force the accumulation of significant amounts of TDS in the liquid phase. Experimental conditions applied during the aerobic experiments reported in this Chapter are shown in **Table 5.1**. Each transient condition was kept for 120 minutes, before resuming reference conditions at the end of the experiment. Overall, experiments allowed measuring H$_2$S concentrations in

the outlet gas phase up to 6,500 ppm$_v$ of H$_2$S and TDS concentrations up to 37 mg S-S^{2-}·L^{-1} in the liquid phase, thus covering the range of concentrations of the FIA/GD-CFA analyzer. In the experiments under aerobic conditions reported herein, the HRT was reduced to 9 h.

Table 5.1 Experimental conditions for TDS accumulation

[H$_2$S]$_{biogas}$ (ppm$_v$ of H$_2$S)	[H$_2$S] LR (g S-H$_2$S·m^{-3}·h^{-1})	O$_2$/H$_2$S $_{supplied}$ (v·v^{-1})
1,999.79	51.08	23.60
4,001.78	107.65	11.20
6,001.33	161.48	7.47
8,000.00	215.30	5.60

The FIA system was validated by a commercially available sulfide ISE combined with an Ag/AgCl electrode as reference (SympHony 14002-790; VWR International, Germany), installed in the waste line right after the constructed ISE electrode. The GD-CFA was validated by an electrochemical commercial H$_2$S$_{(g)}$ sensor (Sure-cell; Euro-Gas Management Services LTD, UK) installed in the BTF outlet gas line. Technical specification of employed sensors is presented in **Section 4.7**. In addition to the FIA/GD-CFA analyses, liquid samples were taken every 20 minutes from the liquid phase during the experiments, for off-line SO$_4^{2-}$ and S$_2$O$_3^{2-}$ analyses by IC.

5.4 Results and discussion

5.4.1 On-line monitoring with FIA/GD-CFA system

Monitoring data of the complete experimental period under aerobic conditions as acquired by the FIA/GD-CFA system are shown in **Figure 5.3.** The electrode baseline presented a gradual increase along the monitored period, as normally observed in flow injection analyzers when operating in

continuous mode (Baeza, 2004). Similar results were obtained also under anoxic conditions (results not shown). Thus, the total peak (FIA configuration) and plateau (GD-CFA configuration) heights were calculated considering the correspondent baseline for each analytical cycle.
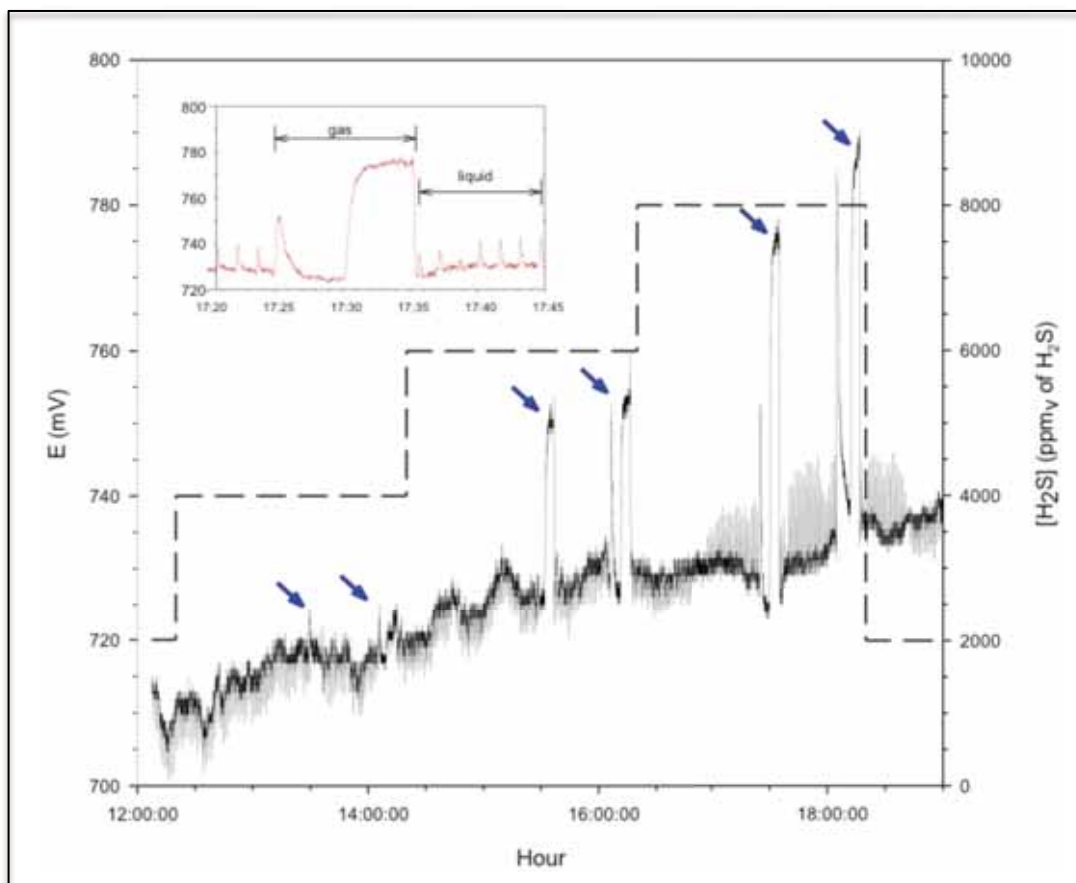
Figure 5.3 Experimental on-line monitoring data. Dotted line indicates inlet H₂S concentration. Arrows show gas phase determinations.
Inset shows a detailed 25-minutes period data

During the experiment, the analytical system was programmed for continuous on-line determination of TDS in the liquid phase and to sample the gas phase twice per each inlet concentration step (at minute 70 and 110 of each interval of 120 minutes). The selection valve of the analytical system was used for automatically switching from the FIA to the GD-CFA configuration. As shown in **Figure 5.3** inset, the selection valve change produced a sharp increase in the system response, probably as a consequence of a signal noise instant disturbance. Thus, an extended time

for the baseline stabilization is needed during gas samples analysis, consequently leading to a decrease in the gas analysis frequency. Under alternating operating conditions, the gas analysis time was 8 minutes on average (4 minutes for baseline stabilization and 4 minutes for maximum signal *plateau* stabilization), while only 90 seconds were required for liquid samples analysis. The total analysis time for each system can be easily configured using the control program.

The analyser was validated by comparing its results for gas and liquid samples from the biotrickling filter with those obtained with commercial sensors. **Figure 5.4a** for the FIA configuration and **Figure 5.4b** for the GD-CFA configuration demonstrate, by the linear regression test, that no significant differences were observed at 95% confidence level. In the linear regression test for the FIA, a slope of 1.0 ± 0.0 and intercept of 0.0 ± 0.2 were obtained. For the GD-CFA, a slope of 1.0 ± 0.0 and intercept of 16.8 ± 36.4 were obtained. Thus, analytical results can be considered acceptable for both liquid and gas phase measurements for the concentration range studied. Calibrations performed in this study resulted in a detection limit of $1.5 \times 10^{-5} \pm 0.9 \times 10^{-5}$ mol $S\text{-}S^{2-} \cdot L^{-1}$ for the FIA system and 159 ± 57 ppm$_v$ of H_2S for the GD-CFA system. Moreover, electrodes presented a good stability behavior over 3 years of discontinued use, requiring minimum maintenance procedures, a clear evidence of the system robustness. It is worth mentioning that the filtration step, with a first tangential filtration unit plus a direct flow filter element was used for more than 80 h without significant signs of clogging. Such configuration revealed enough in the present case, for the filtration of 0.12 $L \cdot h^{-1}$ with a concentration of total suspended solids < 2 $mg \cdot L^{-1}$. According to this and because liquid sample pH was adjusted on-line to 14, the second filtration step (0.22 μm) could have been avoided. However, SOB are known to grow in a wide range of pH, from 1 to 11 (Islander *et al.*, 1991, Devinny and Deshusses, 1999), thus the second step filtration might be necessary in the long-run operation, to protect the FIA/GD-CFA system against any contamination by biomass colonization and to avoid undesirable episodes of system channels obstruction, by the deposition of any solid particle coming from the BTF.
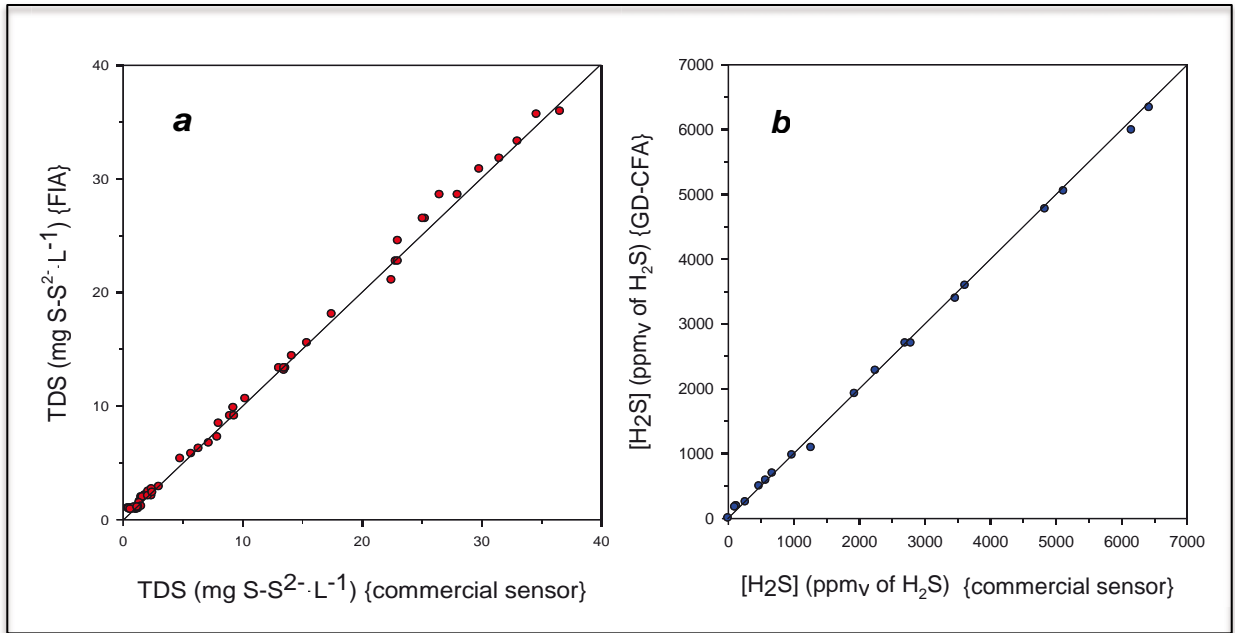
Figure 5.4 Linear regression test for (**a**) FIA system for TDS analysis and (**b**) GD-CFA system for H₂S analysis

According to the HRT in the present reactor during the experiment (9 h), FIA data averages in periods of approximately 7.5 min (i.e. 5 analysis data) were considered throughout the experiment as shown in **Figure 5.5**.
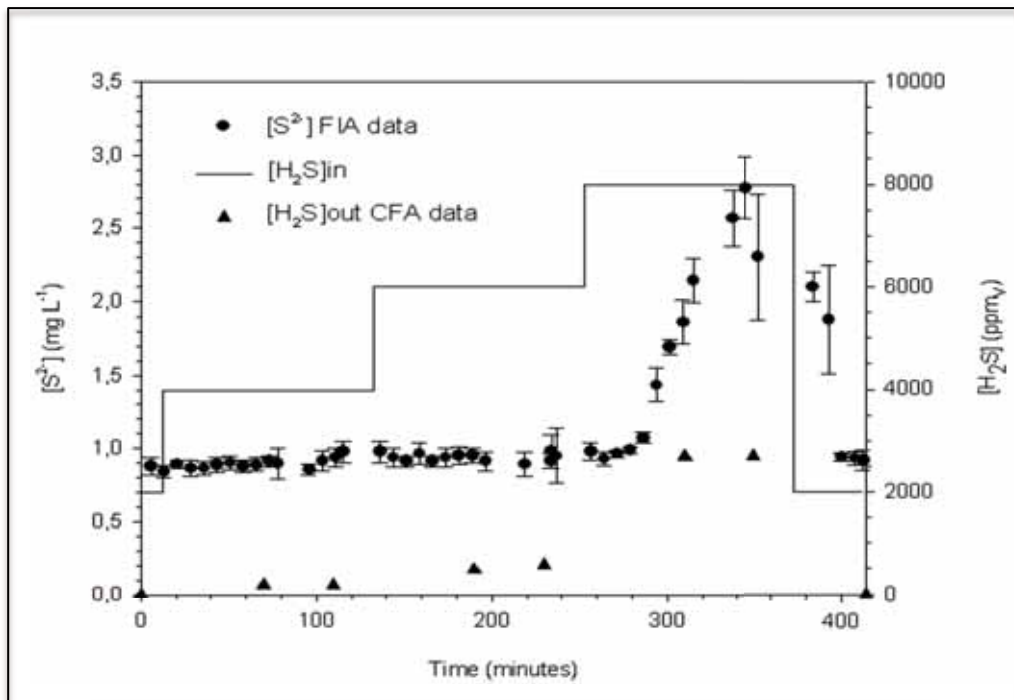
Figure 5.5 TDS and H₂S profiles. Error bars of 95% confidence interval for n=3 analysis

Until minute 280, the TDS concentration was close to the FIA detection limit. Major TDS accumulation was only detected during the 8,000 ppm$_v$ of H$_2$S step, in which TDS concentration experienced a significant gradual increase until reaching a maximum average value of 2.8 mg S-S^{2-}·L^{-1}. Once the inlet concentration of 2,000 ppm$_v$ of H$_2$S was restored, TDS concentration immediately decreased, reaching values below the FIA detection limit after one hour of operation back at reference conditions.

Also, no significant response of the H$_2$S outlet concentration was obtained in the GD-CFA system during the 4,000 ppm$_v$ of H$_2$S step, with outlet H$_2$S concentrations close to the GD-CFA detection limit ([H$_2$S]$_{out}$ < 154 ppm$_v$ of H$_2$S). Later, the outlet gas concentration gradually raised to a maximum value of 3,074 ppm$_v$ of H$_2$S. Similarly to TDS, H$_2$S outlet concentration sharply decreased once the reference operating conditions were restored, reaching values close to zero after one hour.

5.4.2 Overall biotrickling filter performance

Results of the BTF performance assessment are shown in **Figure 5.6a and 5.6b** for the BTF under study, in terms of the study of the EC and the RE. LR ranged from 51.08 to 215.30 g S-H$_2$S·m^{-3}·h^{-1}, generally considered a high load. Since the FIA/GD-CFA system was programmed to mainly analyze the liquid phase in the experiment presented herein, monitoring results of the commercial sensor allow seeing the dynamics of EC and RE during the experimental period.

Except for the step of 4,000 ppm$_v$ of H$_2$S, each step lead to a decrease in the RE, which was more significant once the reactor had reached the step of 8,000 ppm$_v$ of H$_2$S. Oppositely, the EC exhibited a marked increase right after each inlet concentration increase. However, a progressive decrease of the EC was found along the 6,000 ppm$_v$ of H$_2$S step, and a sharp decrease was found along the 8,000 ppm$_v$ of H$_2$S step, the latter due to the quick saturation of the sorption capacity of the liquid phase.
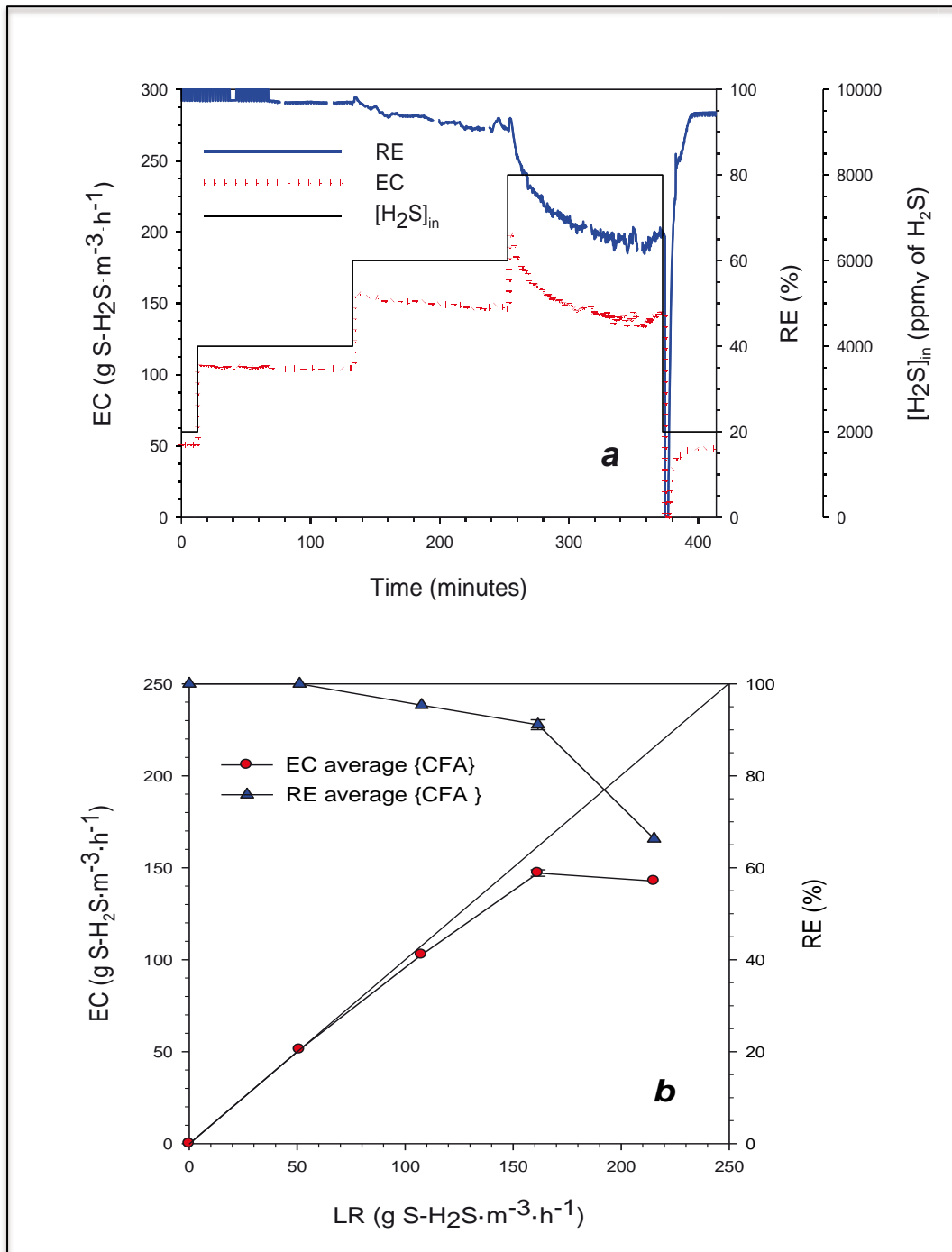
Figure 5.6 (**a**) Evolution of H$_2$S EC and RE with data from commercial sensor. (**b**) Average H$_2$S EC and RE *versus* LR with data from GD-CFA analyzer

When reference operational conditions resumed, the EC and RE suddenly dropped to zero for a period of around 3 minutes, which corresponds to the gas residence time of the reactor. Still, since some TDS had accumulated in the liquid phase, 18 minutes were required to achieve EC and RE values equivalent to the previous inlet concentration step. The

maximum instant EC registered was 201 g S-H_2S·m^{-3}·h^{-1} (**Figure 5.6a**), while the maximum averaged EC was 150 g S-H_2S·m^{-3}·h^{-1} (**Figure 5.6b**). The RE was initially 100% and kept close to 98% during the 4,000 ppm_v of H_2S step. During the 6,000 ppm_v of H_2S step, the RE was approximately 92% and dropped to a minimum average value of 68% during the highest LR period. However, the RE quickly recovered to close to 95% as soon as the 2,000 ppm_v of H_2S step resumed, indicating a fast recovery of the biotrickling filter capacity, as already reported for this kind of reactors (Fortuny *et al.*, 2010) when submitted to transient operating conditions.

Overall, results indicate that such BTF configuration under the operating conditions tested herein is able to handle high, transient H_2S loads with effective desulfurization of a wide range of concentrations. In terms of monitoring, the FIA/GD-CFA system proved sufficient for assessing the overall performance of the reactor during the performed experiments, even if continuous monitoring of the gas phase is recommended for assessing short transient periods dynamics.

5.4.3 Sulfur fate

Although desulfurization efficiencies and the reactor capacity can be assessed with the FIA/GD-CFA analyzing system, the information provided by the analyzer needs complementary data to understand the complex behavior of the biotrickling filter in terms of sulfur fate.

On-line monitoring data of pH, DO and ORP during the experimental period are shown in **Figure 5.7**. The DO profile, obtained from the DO probe located at the recirculation line of the BTF, after the aeration unit shown that the maximum oxygen consumption took place during the highest H_2S inlet concentration, as expected from the stoichiometric relations described by **Equation 8**, **Equation 9** and **Equation 10**.
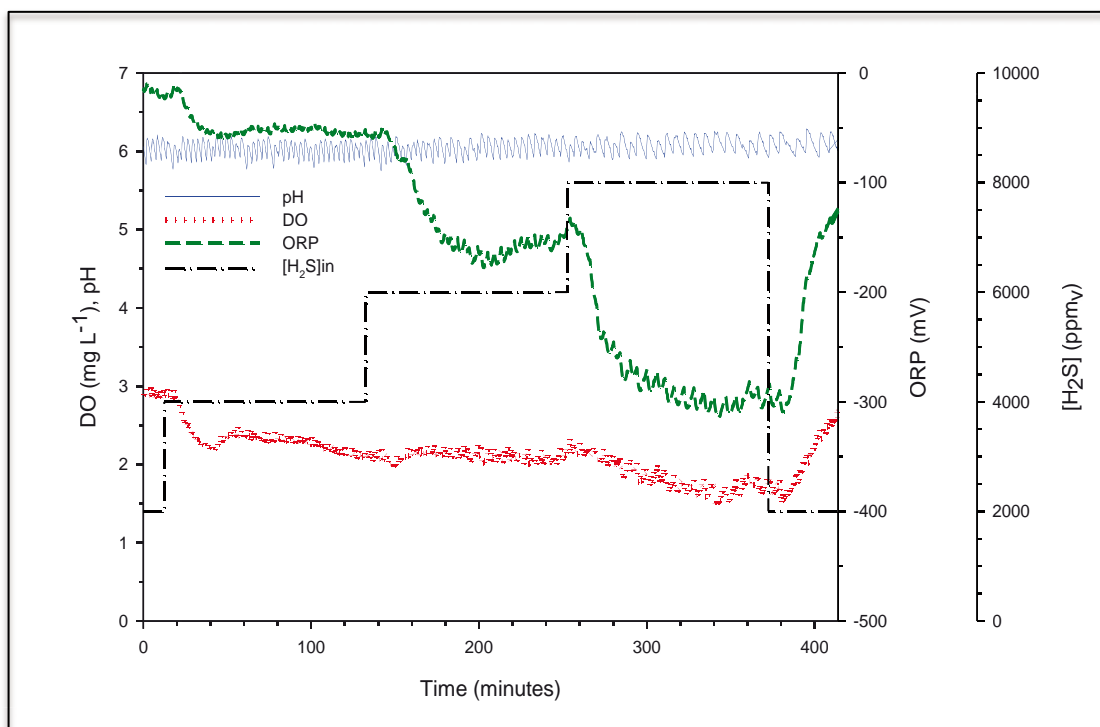
Figure 5.7 On-line monitoring of pH, DO, ORP and [H$_2$S]$_{in}$
during experimental period

After reference conditions were restored, DO rapidly recovered the initial value. It is worth mentioning that a DO sensor located in the sump of the reactor showed a value of 0 mg O$_2$·L^{-1} throughout the experimental period, indicating that oxygen availability was limited at some point along the depth of the reactor. Regarding the ORP profile, a gradual decrease for each concentration step was encountered, from the initial value of -40 mV to -50 mV, -150 mV and -300 mV for inlet H$_2$S concentrations of 4,000; 6,000 and 8,000 ppm$_v$ of H$_2$S, respectively. The initial value of -40 mV is consistent with the presence of SO$_4^{2-}$ as main product of the H$_2$S oxidation. ORP values between -250 and -400 mV indicate TDS accumulation and are in the range usually reported for the incomplete S^{2-} oxidation to S^0 (Fortuny *et al.*, 2008). At this point, one can speculate if the limitation in the performance was due to mass transfer or to biological activity. Although profiles in **Figure 5.6** appeared to indicate a mass transfer limitation during the steps of 4,000 and 6,000 ppm$_v$ of H$_2$S, the ORP profile and the average TDS concentrations of 0.90 ± 0.02 and 0.94 ± 0.02 mg S-S^{2-}·L^{-1} along the

steps of 4,000 and 6,000 ppm$_v$ of H$_2$S, respectively, indicated that the reactor was also biologically limited.

Ionic sulfur species profiles measured in the recycle liquid are shown in **Figure 5.8**. The SO$_4^{2-}$ concentration profile shows a slight tendency to decrease from around 340 mg S-SO$_4^{2-}$·L^{-1} to around 270 mg S-SO$_4^{2-}$·L^{-1} at the end of the step of 8,000 ppm$_v$ of H$_2$S, indicating that the high load applied lead to a decrease in the biological SO$_4^{2-}$ production. According to Fortuny *et al.* (2008), the O$_2$/H$_2$S $_{supplied}$ ratio (5.60 v·v^{-1}) under this condition lead to a S^0 production due to O$_2$ limitation. Interestingly, still after resumption of reference conditions, the SO$_4^{2-}$ concentration kept decreasing down to around 245 mg S-SO$_4^{2-}$·L^{-1}, even if the biological oxidation limitation due to the O$_2$/H$_2$S $_{supplied}$ ratio applied had recovered to values corresponding to complete SO$_4^{2-}$ production (23.60 v·v^{-1}) (Fortuny *et al.*, 2008). Such delay may be explained by the hydraulic conditions of the liquid phase coupled to a delay in the reactivation of the biological mechanisms that lead to SO$_4^{2-}$ production.
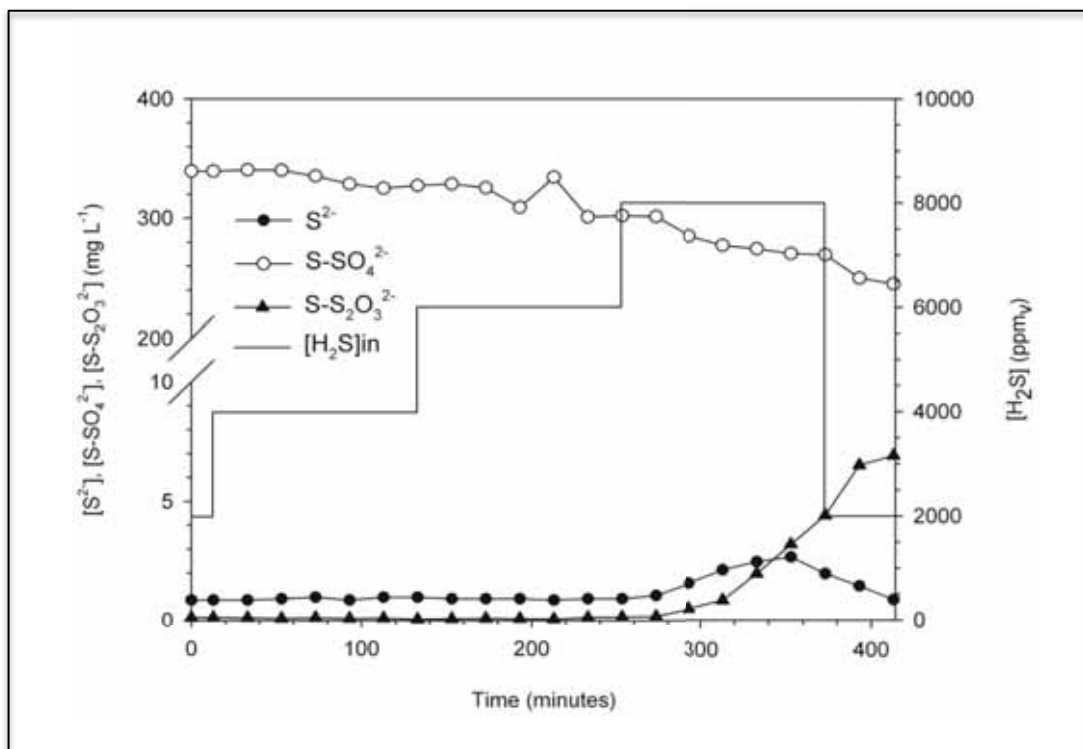
Figure 5.8 TDS, SO$_4^{2-}$ and S$_2$O$_3^{2-}$ concentration monitoring

The $S_2O_3^{2-}$ concentration kept close to zero until minute 260 of the experiment and then started to increase until 4 mg $S-S_2O_3^{2-} \cdot L^{-1}$ at the end of the step of 8,000 ppm_v of H_2S (215.30 g $S-H_2S \cdot m^{-3} \cdot h^{-1}$), showing a maximum value of 6.8 mg $S-S_2O_3^{2-} \cdot L^{-1}$ at the end of the monitoring period. Thiosulfate formation by chemical oxidation was driven by TDS accumulation (Fortuny *et al.*, 2010), not only during the maximum LR period but also after resumption of the reference LR value (51.08 g $S-H_2S \cdot m^{-3} \cdot h^{-1}$).

A sulfur mass balance was performed to calculate the S^0 concentration by subtraction, as previously described (Janssen *et al.*, 1997). The amount of sulfur as $S-S^0$ and $S-SO_4^{2-}$ produced, as well as the total sulfur removed by biological activity ($S-H_2S$) are shown in **Figure 5.9**. The DO/S^{2-} ratio in the liquid phase was calculated, representing the DO available at the top of the reactor, which could be related to the capability of the system to produce either SO_4^{2-} or S^0, according to the stoichiometric relation obtained from **Equation 8** and **Equation 9**.
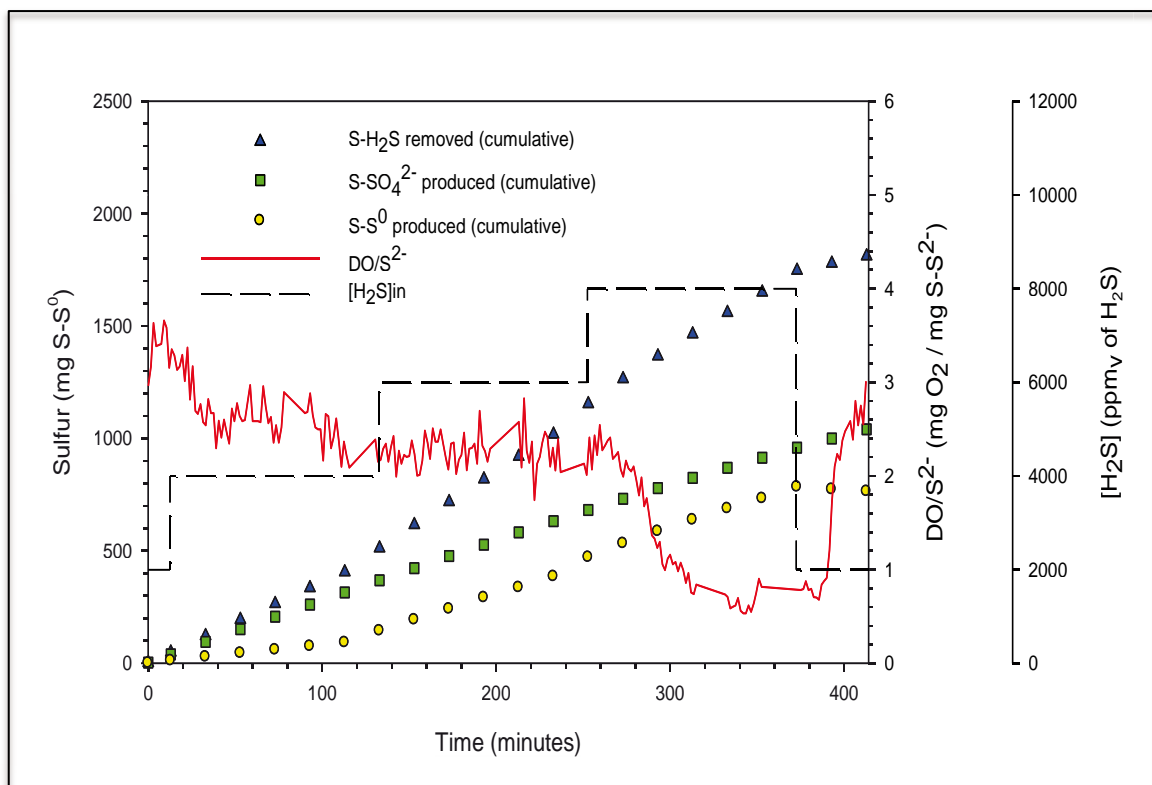
Figure 5.9 Sulfur mass balance and DO/S^{2-} ratio during experiments

Theoretically, a DO/S^{2-} ratio lower than 0.5 indicates that S^0 is the main product while a value higher than 2 indicates that the main product is SO_4^{2-}. Interestingly, even when the calculated DO/S^{2-} ratio reached values higher than 2 mg $O_2 \cdot (mg\ S^{2-})^{-1}$, sulfur mass balance results suggested a concomitant production of SO_4^{2-} and S^0. These results confirm the existence of an important DO gradient inside the filter bed, and perhaps in the biofilm, leading to O_2 depletion at the bottom of the reactor where, probably, only S^0 was being produced. Although not studied, gas circulation in counter-current to the liquid phase circulation may increase the potential of S^0 production in the reactor compared to a co-current operation. In the latter scenario, the oxygen availability would be larger at the entrance of the reactor where the H_2S concentration reaches its maximum value.

Sulfur mass balance results indicate that S^0 production started from the beginning of the step of 4,000 ppm_v of H_2S (107.65 g S-$H_2S \cdot m^{-3} \cdot h^{-1}$), when the O_2/H_2S supply ratio was 11.2. However, S^0 accumulation suffered a notable increase during steps of 6,000 and 8,000 ppm_v of H_2S (161.48 and 215.30 g S-$H_2S \cdot m^{-3} \cdot h^{-1}$ respectively), when O_2/H_2S $_{supplied}$ ratio was 7.5 and 5.6, respectively, which is considered as a limiting value for aerobic biological desulfurization (Fortuny *et al.*, 2010). At the end of the highest LR period, a total amount of 783 mg S-S^0 was produced from 1,747 mg S-H_2S removed. It is worth mentioning that as soon as reference operating condition was resumed (2,000 ppm_v of H_2S inlet concentration, O_2/H_2S supply ratio of 23.6), the S^0 production ratio instantly decreased while SO_4^{2-} production noticeable increased, confirming that during highest LR period, the O_2/H_2S $_{supplied}$ ratio limited the complete biological S^{2-} oxidation to sulfate (Kelly, 1999).

Sulfate and elemental sulfur production can be expressed as a ratio to the removed H_2S, as shown in **Table 5.2**, resulting in the expression of the SO_4^{2-} selectivity (S-SO_4^{2-} $_{produced}$/S-$H_2S_{removed}$) or S^0 selectivity (S-$S^0_{produced}$ / S-$H_2S_{removed}$), calculated according to **Equation 25** and **Equation 26**, respectively. S^0 production is clearly enhanced by oxygen limitation, as verified from obtained results.

Table 5.2 SO$_4^{2-}$ and S^0 production as a function of the O$_2$/H$_2$S $_{supplied}$ ratio and DO/S^{2-} ratio

H$_2$S $_{biogas}$ (ppm$_v$)	LR (g S-H$_2$S·m^{-3}·h^{-1})	O$_2$/H$_2$S (v·v^{-1})	S-SO$_4^{2-}$/S-H$_2$S$_{removed}$ (%)	S-S^0/S-H$_2$S$_{removed}$ (%)	DO/S^{2-} (mg O$_2$/mg S^{2-})
1,999.79	51.08	23.6	100	0	2.96 – 3.66
4,001.78	107.65	11.2	78 – 80	20 – 22	2.09 – 3.37
6,001.33	161.48	7.5	62 – 72	28 – 38	1.74 – 2.83
8,000.00	215.30	5.6	55 – 59	41 – 45	0.53 – 2.54
1999.79	51.08	23.6	56 – 57	43 – 44	0.68 – 3.01

Differently to the results obtained by Fortuny *et al.* (2008), SO$_4^{2-}$ selectivity is higher than S^0 selectivity for a equivalent LR, since the O$_2$ supply system was improved from gas-phase air injection to an aeration column previous to the BTF, enhancing the O$_2$/H$_2$S $_{supplied}$ ratio (Bailon, 2007). Also, the use of a random packing material was appointed as a possible reason for the improvement of the oxygen spread to the internal layers of the biofilm, which was probably compromised when the structured packing material was applied, because of the impairment produced on the liquid circulation through the packed bed.

As noticed in **Figure 5.9**, minimum and maximum values of the DO/S^{2-} ratio, as also shown in **Table 5.2**, confirmed that even when the calculated O$_2$ supplied in the top part of the reactor was higher than the stoichiometric requirements for the production of SO$_4^{2-}$, S^0 was being produced in the intermediate and bottom parts of the reactor. Results shown that the optimization of the O$_2$ supply in such kind of bioreactors configuration is warranted for improving the desulfurization capacity of the system.

5.5 Conclusions

The proposed analytical system, based on a flow injection analysis technique, was proven to be suitable for the on-line monitoring of the studied desulfurizing BTF, treating high loads of biogas mimics. The analyzer consisted on a FIA configuration for TDS analysis and a GD-CFA configuration for $H_2S_{(g)}$ analysis with a single ISE for S^{2-} determination. The constructed tubular electrodes of a homogeneous crystalline membrane of Ag_2S were characterized by direct potentiometry and the operational characteristics of the flow system were optimized for the proposed application. Moreover, electrodes were successfully validated by comparing the obtained analytical response obtained during different operational episodes to the response obtained with commercial sensors. Also, the particularly high upper detection limit encountered for the GD-CFA sub-system (up to 10,000 ppm_v of H_2S) offered a significantly important application field for the on-line monitoring of high concentrations of H_2S, as in the case of biogas desulfurizing treatment plants.

The proposed filtration system showed sufficient to meet de required needs for the continuous analytical system integrated to the BTF. Also, the pH adjustment system was found to be effective for the studied conditions. Nonetheless, the improvement of both pre-treatment steps is suggested in order to expand the scope of application of the proposed analytical system for the monitoring of diverse desulfurizing BTF systems.

In general, the BTF under study presented a fast recovery of their treatment capacity after load increase perturbations. Although sulfur mass balances results indicated that under oxygen limiting conditions the formation of S^0 is favored over SO_4^{2-}, results demonstrated that direct supply of oxygen into the liquid phase of the BTF system is an useful way to improve the desulfurization capacity of the reactor.

❀

6

preliminary study on the on-line
determination of sulfate

"Realists do not fear the results of their study."

Fyodor M. Dostoyevsky

(Moscow, 1821 – Saint Petersburg, 1881)

6 Preliminary study on the on-line determination of sulfate

6.1 Summary and scope

Results obtained during the preliminary study on the on-line determination of SO_4^{2-} are presented in this Chapter. The accurate monitoring of SO_4^{2-} is crucial to assess the performance of sulfate-producing systems, such as the desulfurizing BTF investigated during this research. In this sense, the use of an ion-selective electrode (ISE) based on liquid polymeric membrane sensible to SO_4^{2-} was proposed as the initial effort to develop an analytical system suitable to on-line monitoring of SO_4^{2-} under the operational conditions of the studied BTF.

The selection of the membrane active ionophore applied in this research was made based on the commercial availability of the ionophore. Electrodes response was characterized for both strategies batch mode (conventional electrodes) and FIA system (tubular electrodes). Different membrane compositions were tested aiming to investigate the effect of the presence of the active ionophore, the effect of the lipophilic additive and the effect of diverse plasticizer compounds over the response of the constructed electrodes. Also, the effect of operating pH, the effect of the concentration of the buffer solution and the effect of the analyte background concentration in the buffer solution were studied. Additionally, the stability of prepared membranes was tested in front of different operational conditions, such as washing procedures and variable conditioning time between electrodes utilization.

Overall results indicated that constructed electrodes were applicable for synthetic samples free of interferences. The best response was obtained with a sensitivity of -22.8 ± 3.5 mV·dec^{-1}, limit of detection of 5.4×10^{-5} ± 0.6×10^{-5} mol S-SO_4^{2-}·L^{-1} (5.2 ± 0.6 mg S-SO_4^{2-}·L^{-1}) and a LinR between 7.0×10^{-6} to 2.0×10^{-2} mol S-SO_4^{2-}·L^{-1} (0.7 to 1,920.0 mg S-SO_4^{2-}·L^{-1}). The

presence of active ionophore and lipophilic additives was found crucial for the electrode response. Operational pH between 4.5 and 7.5 resulted in stable response of constructed electrodes. However, the investigation of the electrodes behavior when interfering anions were present in the sample, at concentrations normally found in real samples from the studied BTF, suggested that the studied membrane composition and specially the applied ionophore were not suitable for the monitoring of sulfate with the proposed ISE during the operation of this kind of reactors, for both conventional batch measures as well as detectors into automatic flow analyzers for continuous determination.

The main objective of the work presented in this Chapter was to develop a preliminary ISE implemented as a detector in an analyzer based on the FIA technique for the on-line determination of SO_4^{2-}, aiming the application of this analytical system on the studied BTF. For this purpose, conventional and tubular ISEs of polymeric liquid membrane were constructed, characterized and their response was investigated in front of relevant operational conditions.

✍

Experiments herein reported were partially performed with the collaboration of:

Carrion R (**2013**) *Desarrollo de un analizador de ión sulfato para la monitorización de procesos medioambientales. Proyecto Final de Carrera*. Co-directed by Baeza M, Arasa E and Montebello AM. UAB, School of Engineering.

6.2 Introduction

The assessment of SO_4^{2-} production in desulfurizing BTFs is one of the crucial analytical procedures for the monitoring of the system performance. Several analytical methods are applied for SO_4^{2-} determination, such as gravimetry, nephelometry, capillary electrophoresis and the turbidimetric method recommended in water analysis (APHA, 1980). However, major drawbacks of these techniques are related to the extended analytical time, system complexity and elevated investment and operating costs. Besides offering the opportunity of obtaining real-time information, the implementation of an on-line analytical system based on an ISE for sulfate detection implies in several advantages related to the analysis speed, low sampling volumes and general low cost (Miro *et al.*, 2004; Vlasov *et al.*, 2010; Zuliani *et al.*, 2012; Firouzabadi *et al.*, 2013). ISEs of polymeric liquid membrane have been intensively used for the detection of a wide quantity of analytes (Pretsch, 2007). One of the normally studied characteristics of this kind of electrodes is the composition and stability of the sensing liquid cocktail, which includes the investigation of the ionophore origin and quantity, as well as the lipophilic additive, which promotes the formation of active ionic sites in the polymeric membrane, to facilitate the transference and extraction of the analyte from the liquid (Buhlmann *et al.*, 2000; Egorov *et al.*, 2004).

A comprehensive literature review of available reported studies on the direct detection of sulfate with ISEs is provided in **Table 6.1**. Other membrane components such as the polymeric matrix, plasticizer, ionophore and lipophilic additives are reported for each study. Finally, operational characterization of electrodes in terms of sensitivity (SL), linear range (LinR) and limit of detection (LD) are shown, as well as the response time and stability, the interference study method, the selectivity coefficient for nitrate (NO_3^-), nitrite (NO_2^-) and chloride (Cl^-), and the operational reported pH range. It is worth noticing that the selection of the studied interfering anions was made upon the typical composition of the BTF liquid samples.

Table 6.1 Literature review on ISEs for sulfate analysis *(continued in next pages)*

Reference	Polymeric matrix	Plasticizer	Ionophore	Lipophilic additives	SL^c (mV·dec^{-1}) / $LinR^d$ (M SO_4^{2-}) / LD^e (M SO_4^{2-})	Response time / Stability	Interferences / (method HCO_3^- / Cl^- / NO_3^- / NO_2^-)	pH range
Firouzabadi et al., 2013	PVC THF	o-NPOE DOP, DBP, CN	ABPP	CTAB	SL: -29.1 +- 0.4 LinR: 3E-7 - 1E-1 LD: 1.9E-7	15 s / 2 months	MPM NA / 2.9E-3 / 8.3E-3 / 1.5E-4	3.0 - 9.0
Mazloum-Ardakani et al., 2012	PVC THF	DOP	Schiff base-I	MTOAC	SL: -28.9 +- 0.1 LinR: 1E-6 - 3E-1 LD: 6.3E-7	< 15 s / NA	FIM NA / 2.8E-3 / 1.99E-3 / 3.53E-3	4.0 - 9.0
Sathyapalan et al., 2009	PVC THF	DOP	Hydroxyl-Schiff IL: BMImPF6	CTAB	SL: -28.7 LinR: NA LD: NA	NA / NA	SSM -2.18E-3 / -5.42E-4 -5.79E-4 / NA	3.0 - 9.0
Shishkanova et al., 2009	PVC THF	o-NPOE	PANI	TDDMACl	SL: -22.4 +- 1.6 LinR: 4E-6 - 2E-2 LD: NA	NA / 35 days	MPM NA / 3E-1 / 2,3 / NA	NA
Peng et al., 2008	PVC THF	o-NPOE, DOS	Bis-thiourea-B ILs: MOImCl, BMImBF4, BMImPF6, THTDPCl	TDDMACl	SL: -28.3 +- 0.9 LinR: 1E-6 - 1E-1 LD: NA	10 s / NA	SSM NA / 2.01+-0.3 / NA / NA	3.0 - 10.0
Koseoglu et al., 2008	PVC THF	o-NPOE	Guanidine-I	TDDMACl KTpClPB	SL: -29.0 LinR: 10E-5 - 10E-2 LD:10E-6	NA / NA	NA	3.0 - 10.0
Egorov et al., 2006	PVC THF	BBPA,CN, CP, DBP, BEHS, o-NPOE, BEHP	QAS-TM QAS-DM QAS-MM TNODA	HTFAB	SL: -26.0 +- 2.0 LinR: 9E-6 - 2E-2 LD: 5E-6	NA / 6 months	SSM NA / -7.3E-1 / 2.42 / NA	2.0 - 5.0
Soleymanpour et al., 2006	CMCPE	CP	CrL-Schiff	NA	SL: -28.9 +- 0.4 LinR: 1E-6 - 4E-2 LD: 9E-7	15 s / 2 months	SSM NA / -3.1 / -3.1 / -2.8	4.0 - 9.0
Lomako et al., 2006	PVC THF	BEHS, CN, BN DBP, DOP o-NPOE, BBPA	QAS-TM	HTFAB TDDBTMA Cl NOB	SL: -28.6 LinR: 2E-5 - 2E-2 LD: 6E-6	15 s / > 6 months	SSM NA / -1E-1 / 1.8 / NA	1.5 - 5.0
Mazloum-Ardakani et al., 2006	PVC THF	DBP	CuL	TOMAC HTFAB	SL: -29.5 LinR: 1E-6 - 1E-1 LD: 1E-5	10 s / 3 months	FIM < 1E-2 / < 1E-2 / < 1E-2 / < 1E-2	3.5 - 8.0

(continuation)

Table 6.1   Literature review on ISEs for sulfate analysis *(continued in next page)*

Reference	Polymeric matrix	Plasticizer	Ionophore	Lipophilic additives	SL^{c} (mV·dec^{-1}) / LinR^{d} (M SO$_4^{2-}$) / LD^{e} (M SO$_4^{2-}$)	Response time / Stability	Interferences (method HCO$_3^-$ / Cl$^-$ / NO$_3^-$ / NO$_2^-$)	pH range
Coll et al., 2005	PVC THF	o-NPOE	PACA-I IL: BMImPF6	NA	SL: -30.0 LinR: 4E-5 - 1E-1 LD: 1E-4	8 s / 1 month	FIM NA / 6.9E-2 / NA / NA	5.0 - 10.0
Phillips et al., 2005	PVC THF	CP, o-NPOE, FPNPE, BEHP	Bis-thiourea-2 Bis-thiourea-HA	TDDMACl	SL: -26.7 LinR: NA LD: NA	NA / NA	NA	3.0 - 11.0
Ganjali et al., 2003	PVC THF	DBP, BA	ZPC ^{a}	HTAB	SL: -29.2 +- 0.3 LinR: 1E-6 - 1E-2 LD: 8E-7	10 s / 2 months	MPM NA / 9.9E-4 / 2.4E-4 / 5.3E-5	2.0 - 7.0
Shamsipur et al., 2002	PVC THF	DBP, AP, o-NPOE, NB	Ionophore-L	HDAB OA	SL: -28.8 +- 0.2 LinR: 9E-6 - 1E-1 LD: 7E-6	10 - 45 s / NA	MPM NA / 4.9E-3 / 5E-3 / 9.9E-4	4.0
Ganjali et al., 2002	PVC THF	DBP, BA, AP o-NPOE, NB	BDPP	HTAB	SL: -28.9 +- 0.5 LinR: 1E-6 - 1E-2 LD: 8E-7	10 s / NA	MPM NA / 5.1E-3 / 3.4E-3 / 3.4E-3	4.0 - 9.0
Morigi et al., 2001	PVC PDMS THF	o-NPOE, DBP	Mg/Al-SO4 HT	NA	SL: NA LinR: 4E-5 - 4E-2 LD: NA	< 1 min / NA	MPM < -1.4 / < -3 / < -3 / NA	4.0 - 7.0
Fibbioli et al., 2000	PVC THF	o-NPOE	Zwitterion-2	K(TFPB) HDTODAB	SL: NA LinR: NA LD: 0.10	NA / 1 month	NA	NA
Berrocal et al., 2000	PVC THF	DOS, o-NPOE FPNPE	Tripodal-2	TDDMA Cl MES TRIS	SL: -28.9 LinR: 9E-6 - 1E-1 LD: 3E-6	< 4 min / 1 week	MPM NA / -1.4 / 4E-1 / NA	NA
Li et al., 1999	PVC	o-NPOE, DOP	Imidazole-P	Na-TPB DTOA	SL: -28.5 LinR: 4E-5 - 4E-1 LD: 1E-5	2 s / 2 months	MPM 7.5E-4 / 1.1E-1 / 126 / 2.04	3.06 - 4.02
Nishizawa et al., 1998	PVC THF	CP, o-NPOE, FNDPE, DOS, DOP	Bis-urea-1 Bis-thiourea-2 Bis-thiourea-3 ^{b} Bis-urea-4	TDDMA Cl	SL: -28.1 +- 1.8 LinR: 9E-6 - 1E-2 LD: 1E-6	3 min / 28 days	MPM -9E-1 / -1E-1 / 1.6 / 6E-1	6.8 - 7.0

[a] Commercial ionophore: Selectophore II (Sigma Aldrich). Discontinued product (2010 - 2012)

[b] Commercial ionophore: Selectophore I (Sigma Aldrich). €24.30/50 mg (Price in Spain - April, 2013)

[c] SL = Sensibility

[d] LinR = Lineal range

[e] LD = Limit of detection

NA = not available information

(continuation)

Table 6.1 Literature review on ISEs for sulfate analysis

Acronism	Compound
ABPP	N-4-4-(anilinocarbothioyl)amino benzyl phenyl-N-phenylthiourea
AP	acetophenone
BA	benzylacetate
BN	1-bromonaphtalene
BBPA	bis(1-butylpentyl) adipate
BDPP	4-(4-bromophenyl)-2,6-diphenyl pyrilium perchlorate
BEHP	bis(2-ethylhexyl) phthalate
BEHS	bis(2-ethylhexyl) sebacate
Bis-thiourea-2	α,α-bis(N-butylthioureylene)-m-xylene
Bis-thiourea-3	α,α-bis(N-phenylthioureylene)-m-xylene
Bis-thiourea-B	1,3-bis(3-phenylthioureidomethyl) benzene
Bis-thiourea-HA	α,α-bis(N-phenylthioureylene)-2-hexyl-adamantyl
Bis-urea 1	α,α-bis(N-butylureylene)-m-xylene
Bis-urea 4	α,α-bis(N-1-heptyldecylureylene)-m-xylene
BMImBF4	1-butyl-3-methyl imidazolium tetrafluoroborate
BMImPF6	1-butyl-3-methyl imidazolium hexafluorophosphate
BN	1-bromonaphthalene
CMCPE	chemically modified carbon paste electrode
CN	α-Cl-naphthalene
CP	Cl-paraffin
CrL-Schiff	n-n'-ethylenebis(5-hydroxysalicyl deneiminate) chromium(III) chloride
CTAB	cetyltrimethylammonium bromide
CuL	n,n'-bis(2-amino-1-oxo-phenelenyl)phenylenediamine copper(II)
DBP	dibutylphthalate
DOP	dioctyl phthalate
DOS	bis(2-ethylhexyl) sebacate
DTOA	dodecyltrioctylammonium iodide
FIM	fixed interference method
FNDPE	2-fluoro-2-nitrodiphenyl ether
FPNPE	2-fluorophenyl 2-nitrophenyl ether
Guanidine-I	N,N'-dicyclohexyl-N''-octadecyl-guanidine
HDAB	hexadecylammonium bromide
HDTODAB	hexadecyltrioctadecyl ammonium bromide
HTAB	hexadecyltrimethylammonium bromide
HTFAB	hexyl p-trifluoroacetylbenzoate
Hydroxyl-Schiff	2,2'-(2,5,8,11-tetraazadodeca-1,11-diene-1,12-diyl)bis (4-nitrophenol)

Acronism	Compound
IL	ionic liquid
Imidazole-P	2,6-bis(6-nitrobenzimidazoyl)-N-octadecyl piperidine
Ionophore-L	2,5-diphenyl-1,2,4,5-tetraazabicyclo heptane
K(TFPB)	potassium tetrakis[3,5-bis(trifluoromethyl)phenyl]borate
KTpClPB	potassium tetrakis(4-clorophenyl)borate
MES	2-(N-morpholino)ethanesulfonic acid
Mg/Al-SO4 HT	hydrotalcite compound (Mg6Al2(OH)16-SO4.4H2O)
MOImCl	1-methyl-3-octylimidazolium chloride
MPM	matched potential method (interference)
MTOAC	methyl trioctyl ammonium chloride
Na-TPB	sodium tetraphenylborate
NB	nitrobenzene
NDPE	2-nitrodiphenyl ether
NOB	1-nonyloxy-2-butanol
OA	oleic acid
NPOE	o-nitrophenyl octyl ether
PACA-I	polyazacycloalkane
PANI	polyaniline
PDMS	poly(dimethylsiloxane)
PVC	polyvinylchloride
QAS-DM	tris(2,3,4-dodecyloxy)benzyldimethyloctylammonium chloride
QAS-MM	tris (2,3,4-dodecyloxy)benzyldioctylmethylammonium chloride
QAS-TM	tris(2,3,4-dodecyloxy)benzyltrimethylammonium chloride
Schiff base-I	6,6'-diethoxy-2,2'-(2,2-dimethylpropane-1,3-diylbis-(nitrilomethylidyne))-diphenolato nickel II
SSM	separate solutions method (interference)
TDDBTMA CI	(2,3,4-tris-dodecyloxy) benzyltrimethylammonium chloride
TDDMA CI	tridodecylmethylammonium chloride
THF	tetrahydrofuran
THTDP CI	trihexyl tetradecyl phosphonium chloride
TNODA	trinonyloctadecylammonium chloride
TOMAC	trioctylmethyl ammonium chloride
Tripodal-2	aminochromenone tris-(2-aminoethylamine)
TRIS	tris-(hydroximethyl)aminomethane
ZPC	zinc-phthalocyanine
Zwitterion-2	bis(guanidinium) dihydrochloride

6.3 Materials and methods
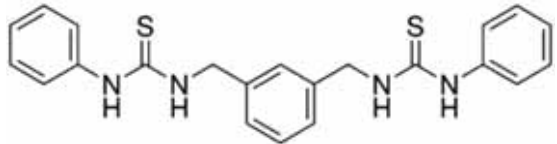
6.3.1 Reagents and standards

Reagents employed were of analytical grade and were used without further purification. Epoxy-graphite conducting composite was prepared with powdered graphite 50 μm of particle size (Merck, Germany), epoxy resin Araldite® M/5490 (Ciba Geigy, Germany) and hardener resin HR (Ciba Geigy, Germany). Plasticizer compounds studied, which act as mediating solvents, were o-nitrophenyl octyl ether (o-NPOE), bis(2-ethylhexyl) sebacate (DOS), dioctylphthalate (DOP) and 2-nitrodiphenyl ether (NDPE); all plasticizers were from Fluka brand (Sigma Aldrich, Spain). The polymeric matrix was prepared with polyvinylchloride of high molecular weight (PVC-HMW) (Sigma Aldrich, Spain) and homogenized with tetrahydrofuran (THF) (Sigma Aldrich, Spain). The lipophilic additive employed was tridodecylmethylammonium chloride (TDDMA Cl) (Sigma Aldrich, Spain). The ionophore used was the Sulfate-Ionophore I – Selectophore™ (Sigma Aldrich, Germany). Main ionophore properties are specified in **Table 6.2**. By the time of this study, the selected ionophore was the only commercially available product, synthetized as described by Buhlmann *et al.* (1997). The preparation of other ionophore formulation would require the synthesis of a different active compound, which was not the aim of this investigation.

All aqueous solutions were prepared with deionized Milli-Q water (18 MΩ·cm^{-1}). Sulfate standards were daily prepared from a stock standard Na$_2$SO$_4$ solution (Panreac, Spain) of 1×10^{-1} mol S-SO$_4^{2-}$·L^{-1} (9,606.3 mg S-SO$_4^{2-}$·L^{-1}) and covered a concentration range from 5×10^{-6} to 1×10^{-1} mol S-SO$_4^{2-}$·L^{-1} (0.5 to 9,606.3 mg S-SO$_4^{2-}$·L^{-1}). An organic buffering solution was prepared from 2-(4,2-hydroxyethyl-1-piperazinyl) ethanesulfonic acid (HEPES) (Sigma Aldrich, Spain). Adjustment of pH was done with NaOH 1 mol·L^{-1} (Panreac, Spain) and CH$_3$COOH glacial (Sigma Aldrich, Germany), as needed. Standards of interfering anions were prepared by covering the concentration range of each compound found in the real liquid samples

from the BTF. Reagents employed for interfering anions standards preparation were: $NaNO_3$ (Panreac, Spain), $NaNO_2$ (Panreac, Spain) and NaCl (Quimivita, Spain).

Table 6.2   Properties of Sulfate-Ionophore I – Selectophore™

Product name	*Sulfate-Ionophore I – Selectophore™*
Product number	17892
Brand / Manufacturer	Fluka / Sigma Aldrich (Germany)
CAS number	37042-63-0
Active compound	α,α-bis(N-phenylthioureylene)-m-xylene
Appearance	White powder
Formula	$C_{22}H_{22}N_4S_2$
Molecular weight $(g \cdot mol^{-1})$	406.57
Molecular representation	
Technical application *	Assay of SO_4^{2-} activity with solvent polymeric membrane electrode
Recommended membrane composition (% wt) *	Ionophore: 1.0 / TDDMA Cl: 0.7 / o-NPOE: 65.5 / PVC: 32.8

*   Technical application and membrane composition recommended by manufacturer are in agreement with best results reported by Nishizawa *et al*. (1998).

6.3.2 Sensing membrane cocktail composition

Liquid membrane composition was investigated and optimized, starting from the best membrane reported by Nishizawa *et al*. (1998), by the preparation of eight different sensing cocktail compositions, as detailed in **Table 6.3**. All membranes were prepared with Sulfate-Ionophore I – Selectophore™ as ionophore (**Table 6.2**). The polymeric matrix composite was prepared in all cases with PVC-HMW (60 mg) and all components were dissolved with THF (3 mL).

Table 6.3   Sensing membrane cocktail composition

Membrane	Plasticizer (% w)	Ionophore [a] (% w)	Lipophilic additive [b] (% mol)
M1			50
M2		1.0	100
M3	o-NPOE, 66	1.0 [c]	100
M4		0	100 [d]
M5			0
M6	NDPE, 66		
M7	DOS, 66	1.0	100
M8	DOP, 66		

[a]   Sulfate-Ionophore I – Selectophore™ (Sigma Aldrich, Germany)

[b]   Lipophilic additive: tridodecylmethylammonium chloride (TDDMA Cl). Quantity calculated in respect to the ionophore, in molar percentual units.

[c]   Same composition for **M2** and **M3**, but **M3** was prepared with ionophore from a new industrial batch. Membranes **M3** to **M8** were prepared with the same industrial batch.

[d]   Lipophilic additive quantity is kept unaltered, referred to an hypothetic 1.0% of ionophore composition in the membrane.

6.3.3 Sensor response characterization

Electrodes calibration in batch mode was performed by measuring the response of electrical potential (E) obtained for each sensor when put into contact with sulfate solutions of increasing concentration. The time between standards addition varied between 1 and 2 minutes, depending on the quantity of simultaneously calibrated electrodes. Calibrations with decreasing concentration standards were also performed in order to verify the stability of the electrode and the recovery of the analytical signal under the possible effect of the membrane saturation. Electrodes calibration in flow mode, applying a FIA system, was performed by the temporized injection of each standard in triplicate, with a sample throughput of 40 h^{-1}. Calibrations were executed with freshly prepared 24 standard-points of precisely calculated SO_4^{2-} concentration. The characterization of the

analytical response of the constructed electrodes was performed by direct potentiometry, as described in **Section 4.6**. Instruments specification is presented in **Section 4.7**. Electrodes were constructed according the procedure described in **Figure 4.8** (tubular electrodes for FIA system) and **Figure 4.9** (conventional electrodes for batch mode operation).

Moreover, the effect of different operational conditions over the electrodes response was investigated. Electrodes response in front of the operating pH was studied in a pH range from 3.5 to 9.5, by the addition of controlled amounts of saturated NaOH solution (Panreac, Spain) to a sample solution with initial pH value of 3.5, previously adjusted by the addition of acetic acid glacial (Panreac, Spain). Also, the concentration of the buffer solution (HEPES + NaOH) was tested, as well as the concentration of SO_4^{2-} background in the buffer solution. Finally, the effect of the cleaning procedure of the electrodes between calibrations was studied by testing distilled water and $BaCl_2$ (1×10^{-3} $mol\cdot L^{-1}$) (Panreac, Spain) as cleaning solutions.

6.3.4 Study of interferences

Real liquid samples from the studied BTF were taken during neutral and acidic pH operation (**Chapter 7, Chapter 8** and **Chapter 9**) at the purge line of the system and SO_4^{2-} and $S_2O_3^{2-}$ were analyzed by IC, under the conditions specified in **Section 4.7.2**. Main interfering anions, according to the selectivity potentiometric coefficients (Kpot) reported by Nishizawa *et al.* (1998) and, correspondingly, with the anionic species found in the liquid phase of the BTF were: nitrate (NO_3^-), nitrite (NO_2^-), chloride (Cl^-) and dihydrogen-phosphate ($H_2PO_4^-$). The calculation of Kpot for each interfering anion was performed applying the matched potential method (MPM), as defined in **Section 4.6**. This methodology was considered as the most appropriate, because represents the actual dynamic encountered in the liquid phase of the BTF, in which interfering anions are normally present at a pseudo-constant value, while SO_4^{2-} concentration is markedly variable,

depending on the operational conditions of the system. Also, for the investigation of the effect of interfering ions whit different electrical charge, the MPM method is widely accepted since first presented by Gadzekpo and Christian (1984) and recommended by Umezawa *et al.* (1995). Moreover, a preliminary investigation on the potential interfering effect of the anions present in the studied BTF was performed applying a FIA system, for the ionic composition normally found under neutral pH. For this purpose, a FIA system with potentiometric detection was optimized. Also, the interference study in batch mode was conducted for the ionic composition normally found in the BTF liquid phase, but in this case under acidic pH operation.

6.4 Results and discussion

6.4.1 Membrane composition optimization

The obtained effects of the membrane composition formulation (according to **Table 6.3**) over electrodes response are shown in **Table 6.4**. A qualitative evaluation of electrodes response was performed, in terms of SL and LD, after a series of systematic calibration procedures.

Table 6.4   Sensing membrane optimization results

Membrane	Studied condition	Effect over electrode response
M1	Initial composition	Reference formulation *
M2	> Lipophilic additive	✔
M3	Ionophore industrial batch	⊘
M4	Absence of ionophore	✗
M5	Absence of lipophilic additive	✗
M6	Plasticizer: NDPE	✗
M7	Plasticizer: DOS	✗
M8	Plasticizer: DOP	✗

*   According to Nishizawa *et al.*, 1998

✔: Positive effect / ⊘: Irrelevant effect / ✗: Negative effect

The best membrane composition corresponded to the formulation of membrane **M2**, which represented an increment on the quantity of the lipophilic additive applied up to 100% molar referred to the ionophore. Obtained SL and LD evolution over the time for consecutive calibration of 6 electrodes of **M1** and 6 electrodes of **M2** are shown in **Figure 6.1**.
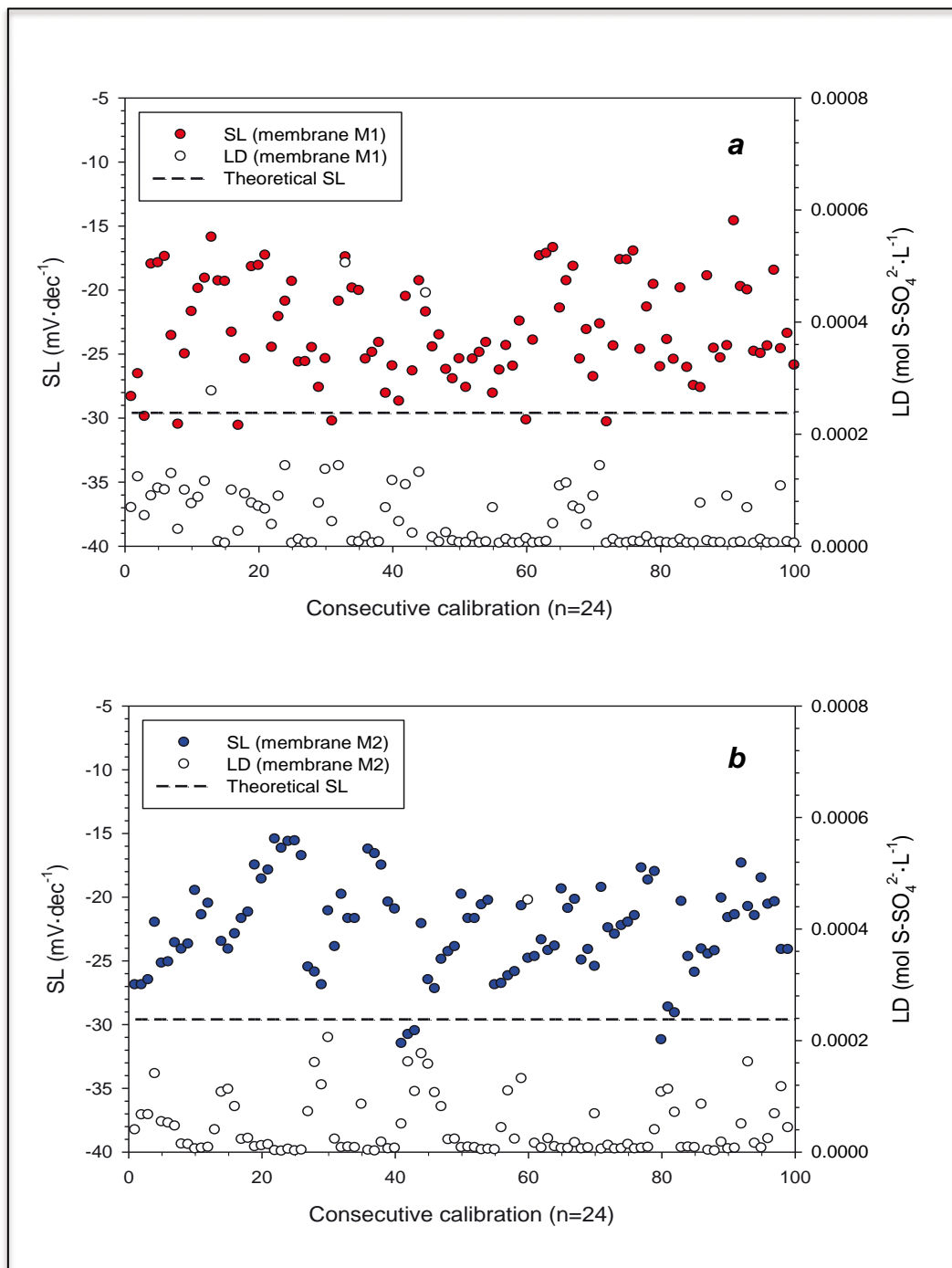
Figure 6.1 SL and LD evolution for (**a**) membrane **M1** and (**b**) membrane **M2**, with n=24 points for each electrode calibration curve. Dashed line indicates theoretical sensitivity for divalent anions (SL = -29.6 mV·dec^{-1})

Calibrations in batch mode were performed with buffer HEPES, with pH adjusted to 6.99 with NaOH (1.0 mol·L^{-1}). Time between standards injection was 1 minute. Before the first use and after each cleaning procedure, electrodes were conditioned in a HEPES solution (1×10^{-1} mol·L^{-1}) doped with SO_4^{2-} background concentration of 1.0×10^{-6} mol S-SO_4^{2-}·L^{-1} (1×10^{-1} mg S-SO_4^{2-}·L^{-1}). Electrodes were cleaned by washing with distilled water for 15 minutes with magnetic stirring after each calibration, in order to minimize the memory effect between successive calibration processes. Results obtained after consecutive calibrations (n>100) of six different electrodes prepared with membrane **M2**, with 24 points each calibration, indicated that electrodes presented a sub-Nernstian behavior, with an SL average value for **M2** of -22.8 ± 3.5 mV·dec^{-1} and LD average of 5.4×10^{-5} ± 0.6×10^{-5} mol S-SO_4^{2-}·L^{-1} (5.2 ± 0.6 mg S-SO_4^{2-}·L^{-1}). Experimental data were adjusted according to **Equation 30** to obtain the calibration curve and the analytical response parameters. A cyclic-type behavior can be delineated, more clearly for **M2**, in correspondence with cleaning and conditioning procedures; it appeared to represent a lost in sensitivity, resulting in decreasing values up to the next cleaning and conditioning procedure (approximately each 12 to 16 consecutive calibration), after which SL recovered initial values closer to the theoretical sensitivity (-29.6 mV·dec^{-1}).

Interestingly, the behavior of the LD presented the opposite tendency, rising after cleaning and conditioning procedures. However, results were not conclusive and no direct relations can be stated regarding to this particular behavior. The response time of the electrodes was found at 20-30 s for calibrations of increasing SO_4^{2-} concentration. For decreasing SO_4^{2-} concentration calibrations, the response time was found at 50-60 s, a higher value, as expected for the memory effect of higher analyte concentrations (Vlasov *et al.*, 2010), but still lower than the reported response time by Nishizawa *et al.* (1998) (3 minutes). The lifetime of prepared membranes was around 1 – 2 months. Both response time and lifetime were found at normal range for this kind of electrodes, as verified in **Table 6.1**. Moreover, the markedly negative effect obtained by the absence of lipophilic additive (**M5**) corroborated the necessity of this kind of compound for hydrophilic

anions such as SO_4^{2-}, positioned at the end of the Hofmeister's affinity series (Wojciechowski *et al.*, 2010), as commented in **Section 2.4.3**. The effect of the nature of the plasticizer was found of a less extent, even when the best results were clearly obtained for o-NPOE, in accordance with most of the reported ISEs for SO_4^{2-} sensing (**Table 6.1**).

6.4.2 Effect of operational conditions

The effect of the operational pH was tested for the best membrane composition (**M2**) over a range from 3.50 < pH < 9.50, in both ascending and descending modes. In this range, the response of the electrodes, in terms of electrical potential, was constant for a fixed SO_4^{2-} concentration in front of the pH variation. The pH was adjusted with CH_3COOH or NaOH solutions, as required, by the controlled addition directly on the buffer solution, with SO_4^{2-} concentration of 1.0×10^{-4} to 1.0×10^{-2} mol $S-SO_4^{2-} \cdot L^{-1}$ (9.6 to 960.6 mg $S-SO_4^{2-} \cdot L^{-1}$), in which electrodes were submersed. The study of the electrodes response was performed for n=16 to n=42 points, with 1 minute between acid or base solutions addition. Overall results indicated that the optimum pH range was 4.50 < pH < 7.50. Contrary to the behavior described by Nishizawa *et al.* (1998) for the same active ionophore, electrodes presented a slight loss in sensitivity when operating at pH close to neutrality, and a discreet improvement when acidic pH was investigated, with the optimal value around pH = 5.00.

The effect of the buffer solution (HEPES) concentration was tested for 1.0×10^{-1} mol$\cdot L^{-1}$ (as recommended by Nishizawa *et al.*, 1998) and 1.0×10^{-2} mol$\cdot L^{-1}$. However, no significant differences were obtained over the electrodes performance in terms of SL and LD. Also, the effect of SO_4^{2-} background concentration in the buffer solution was investigated at 1×10^{-6} and 2.5×10^{-6} mol $S-SO_4^{2-} \cdot L^{-1}$ (0.1 and 0.24 mg $S-SO_4^{2-} \cdot L^{-1}$). As expected, results indicated that the analyte background concentration in the buffer solution helped obtaining a lower response time. For further experiments, the background concentration was kept at 1×10^{-6} mol $S-SO_4^{2-} \cdot L^{-1}$ (0.1 mg

S-SO$_4^{2-}$·L^{-1}), which allowed obtaining lower values of LD. Finally, the effect of the cleaning procedure was tested by comparing the sensitivity obtained by the electrodes after a series of cleaning events conducted with distilled water and with BaCl$_2$ (1.0×10^{-3} mol·L^{-1}). The cleaning time was kept unaltered in 15 minutes, with continuous magnetic stirring. Calibrations for cleaning procedure evaluation were performed with n=16 points. Overall sensitivity results were not conclusive regarding the cleaning solution applied; however, electrodes submitted to BaCl$_2$-washing presented earlier signs of membrane deterioration, which represents an important drawback when facing real analytical applications, because of the reduction of the electrodes lifetime.

6.4.3   Sensor response to interferences

The effect of interfering anions over the electrodes response was preliminarily studied applying a FIA system. This configuration was selected in order to facilitate the experiments execution and to obtain an initial selectivity indication in a reliable, fast procedure. Previously to the interferences study, the proposed FIA system was optimized for this application. The carrier composition used was HEPES (1×10^{-2} mol·L^{-1}) with background concentration of 1.0×10^{-6} mol S-SO$_4^{2-}$·L^{-1} (0.1 mg S-SO$_4^{2-}$·L^{-1}). The sample injection volume was evaluated between 50 to 250 μL and the carrier flow rate within a range of 0.5 to 2.5 ml·min^{-1}.

Results of the optimization of injection volume and carrier flow rate are presented in **Figure 6.2**. The increase on the injection volume produced an rise on the analytical signal until reaching a maximum value. The increase of the carrier flow rate resulted in an improvement of the analytical signal and the frequency of analysis, while the decrease of the flow rate caused a reduction of the analytical signal, due to the greater dispersion. Optimal values obtained were 100 μL for the sample injection volume and 1.0 mL·min^{-1} for the carrier flow rate, respectively. These conditions ensured both an adequate analytical signal and an optimal analytical frequency.
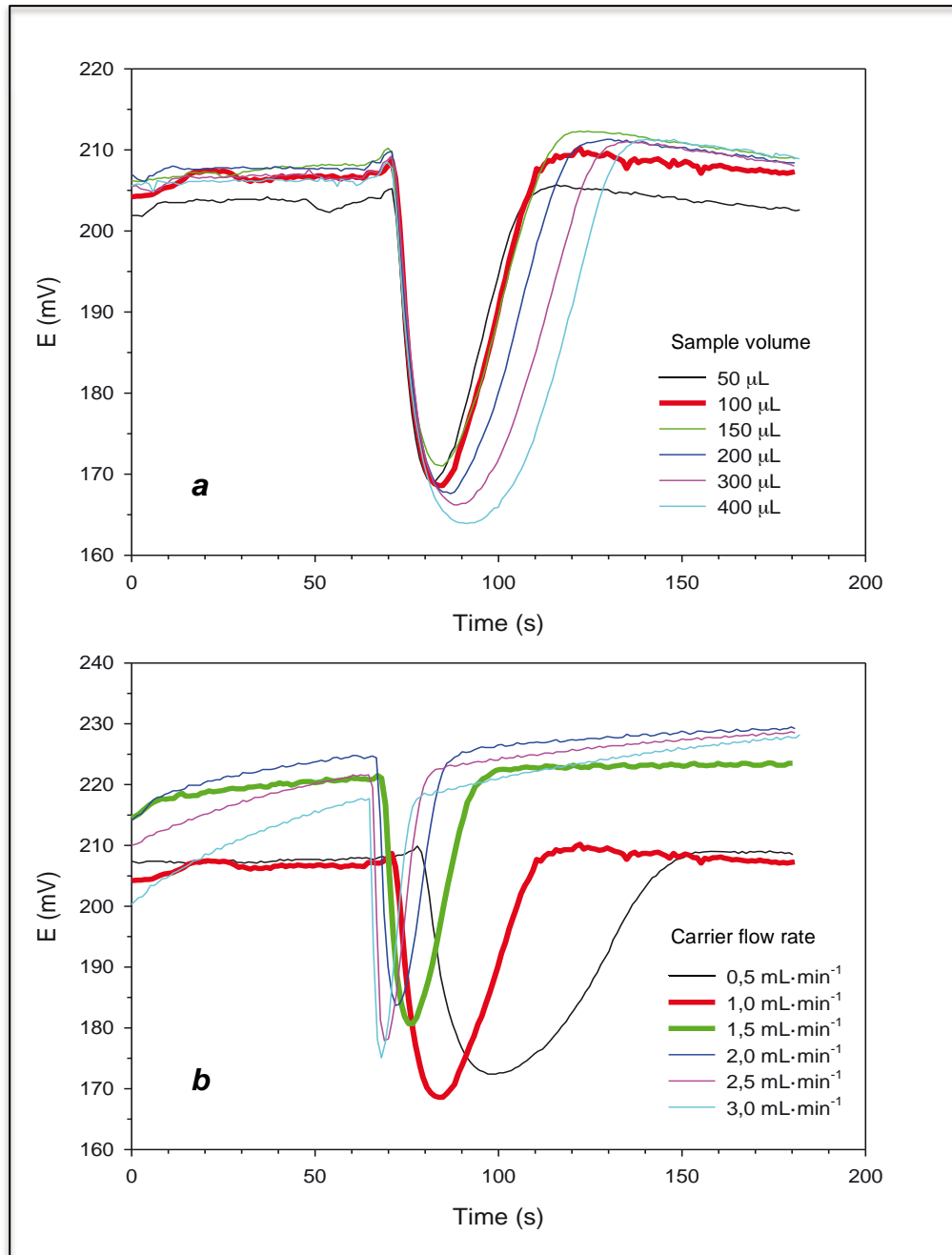
Figure 6.2 Optimization of (**a**) sample volume and (**b**) carrier flow rate of the FIA system for preliminary interference evaluation

The preliminary interference evaluation with the FIA system pointed to an important interfering effect of NO_3^-, NO_2^- and Cl^-, as the potential interfering anions encountered in the real samples from the BTF. Results of a dynamic study, performed by the sequential injection of the main analyte (SO_4^{2-}) at different concentrations, followed by the injection of the potential interfering anions is presented in **Figure 6.3**. No significant analytical response was

obtained by the injection of HEPES and bicarbonate. However, a markedly strong response to NO_3^- and Cl^- suggested that electrodes selectivity should be further investigated for both anions in order to evaluate the feasibility of the constructed electrodes for real analytical applications. The interfering effect of NO_2^- was not further investigated because the concentration of this compound was negligible in comparison with the others interfering anions in the liquid phase of the BTF.
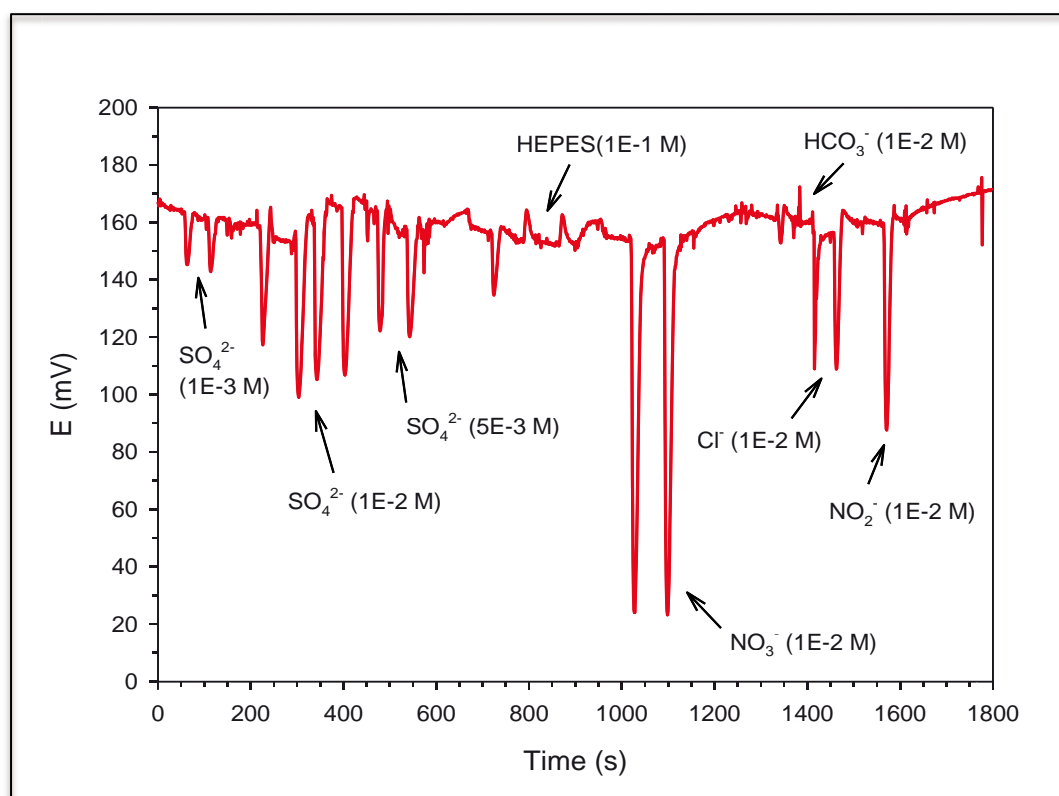
Figure 6.3 Preliminary verification of interfering anions with a FIA system, evaluated at optimal operational conditions

The calculation of the potentiometric selectivity coefficients (Kpot) was performed according to **Equation 33**, following the methodology described by Umezawa *et al.* (1995). Results are presented in **Table 6.5**, with the expression of the common logarithm of Kpot [*log(*Kpot)] for analysis simplification. The theoretical selectivity coefficients reported by Nishizawa *et al.* (1998) are also presented. Interferences were studied for a fixed interfering ion concentration and variable SO_4^{2-} concentration, covering a concentration range from 5.0×10^{-5} to 1.0×10^{-1} mol $S\text{-}SO_4^{2-} \cdot L^{-1}$ (4.8 to

9,606.3 mg S-$SO_4^{2-} \cdot L^{-1}$), as defined by the MPM calculation method. The interferences study during this work was performed by serial 12 calibrations for each condition, with n=7 points for the FIA system and n=24 points for the batch mode system, using HEPES (1×10^{-2} mol$\cdot L^{-1}$) as carrier/buffer solution with pH adjusted to 7.08. Nitrate interference was investigated at concentrations normally found during BTF operation, specifically at 4.0×10^{-4} and 8.0×10^{-4} mol N-$NO_3^- \cdot L^{-1}$ (24.8 and 49.6 mg N-$NO_3^- \cdot L^{-1}$), as encountered under neutral pH operation and at 8.0×10^{-5} mol N-$NO_3^- \cdot L^{-1}$ (5.0 mg N-$NO_3^- \cdot L^{-1}$), as found under acidic pH operation. As chloride concentration remained stable during both pH conditions, Cl^- was otherwise investigated at 1.0×10^{-2} and 1.7×10^{-2} mol Cl-$Cl^- \cdot L^{-1}$ (354.3 and 602.7 mg Cl-$Cl^- \cdot L^{-1}$), representing the lower and higher concentration during total BTF operation.

Table 6.5   Interference study in flow and batch modes (n=12)

Interfering anion	Interference concentration (mol$\cdot L^{-1}$)	log(Kpot) (this study)	log(Kpot) (Nishizawa *et al.*, 1998)
Nitrate	4.0×10^{-4} (FIA)	3.3 ± 0.2	
	8.0×10^{-4} (FIA)	3.9 ± 0.4	1.6
	8.0×10^{-5} (batch)	5.9 ± 0.3	
Chloride	1.0×10^{-2} (batch)	1.4 ± 0.1	0.1
	1.7×10^{-2} (batch)	1.4 ± 0.2	

Since the calculation of the selectivity coefficients depends in a great extent on the operational conditions applied during its determination, results obtained in the work presented in this Chapter are not directly comparable to those reported by Nishizawa *et al.* (1998). The interfering effect of NO_3^- was proportional to the concentration evaluated with the FIA system, while a significant increment in the selectivity for nitrate was observed during the study performed in batch mode, at neutral pH, probably because of the membrane saturation commonly found in batch systems. Surprisingly, the obtained values of logKpot for chloride as interfering ion showed to be independent to the ion concentration. In general, the poor selectivity results

obtained for the determination of SO_4^{2-} in the presence of interfering anions was considered as a limiting condition for the utilization of the constructed electrodes in real systems. Further investigation is required in other to elucidate the origin of the obtained results, which are not in agreement with the reported performance for the same active ionophore (Nishizawa *et al.*, 1998). Likewise, the application of polymeric matrix ISEs for the direct determination of SO_4^{2-}, as investigated during this work, is not recommended because of the significant unfavorable effect of interferences. Research recommendations are given in **Chapter 10** in order to overcome the main difficulties faced during this study.

6.5 Conclusions

The proposed analytical system for sulfate determination, based on an ISE of polymeric liquid membrane was found not applicable for real monitoring tasks, since the high level of interfering anions encountered in the liquid phase of the studied BTF resulted in low selectivity for SO_4^{2-}. In general, constructed electrodes were characterized by direct potentiometry in both batch and flow systems. Electrodes shown a sub-Nernstian behavior, with sensitivity lower than -29.5 mV·dec^{-1}. The best sensitivity obtained in all studied cases was -27.70 mV·dec^{-1}, with an average value around -23 mV·dec^{-1}. The linear range and limit of detection were found at normal values for this kind of analytical systems. On the other hand, electrodes response indicated that the studied analytical system could be suitable for on-line monitoring of processes without interferences.

Regarding to the composition of the liquid sensing cocktail, the use of lipophilic additives was proven to be essential for the correct functioning of the electrode. The presence of lipophilic additives in the composition of the membrane turns out to be indispensable for neutral ionophores, allowing the exchange of ions throughout the membrane. Also, the presence of the active ionophore was found crucial for the electrode response. The nature of the plasticizer compound was considered as less influencing in the

overall analytical response, even when best results were obtained for o-NPOE, a commonly used plasticizing compound. The best membrane composition was found for 1% (wt) of ionophore, 66% (wt) of plasticizer and 100% (molar) of lipophilic additive, a formulation slightly different from the reported results for the same commercially available ionophore. For overcoming the limitations encountered during this word, further investigation is suggested on the development of a microanalyzer based on low temperature cofired ceramics (LTCC) device and non-potentiometric detection strategy.

※

7

neutral H$_2$S biotrickling filtration

and transition to acidic pH

❧

"I agree with no one's opinion.
I have some of my own."

Ivan S. Turgenev
(Oryol, 1818 – Bougival, 1883)

7 Neutral H$_2$S biotrickling filtration and transition to acidic pH

7.1 Summary and scope

A research conducted previously at the Gas Research Group (UAB) by Dr. Marc Fortuny resulted in the construction of the initial configuration of the BTF system herein studied. During that operation, neutral pH was maintained and a structured plastic packing material was used. Before of the long-term operation reported in this thesis, a refurbishment was performed in the BTF in collaboration with Dr. Roger Rovira, for improving biomass sampling procedures and for the integration of the H$_2$S/TDS flow analyzer described in **Chapter 5**. The selection of the new random packing material, the decision of performing the transition to acidic pH and operating under acidic pH conditions (**Chapter 9**) were done at comparable circumstances as in the case of a real-scale biotrickling filter (Rodriguez *et al.*, 2012; 2013).

In comparison with previous studies with PU foam and a plastic structured packing material obtained by others (Fortuny *et al.*, 2008; 2010), the studied random packing material showed similar performance results, in terms of H$_2$S removal capacity under reference conditions, indicating that under both neutral (6.0 to 6.50) and acidic (2.50 to 2.75) pH conditions, the studied BTF is able to treat synthetic biogas containing 2,000 ppm$_v$ of H$_2$S (51.48 g S-H$_2$S·m^{-3}·h^{-1}), with RE values above 99% at EBRT of 131 s. However, the study of the EC under performed experiments revealed values slightly lower of critical EC (100 g S-H$_2$S·m^{-3}·h^{-1}) and maximum EC (135 g S-H$_2$S·m^{-3}·h^{-1}), when compared with previous studies at similar conditions. In spite of no significant differences being found in terms of H$_2$S removal performance, a persistent accumulation of elemental sulfur was verified (8.49% of the total oxidized sulfide) during acidic pH operation.

The aim of the work presented in this Chapter was to study the effect of the used random packing material in a BTF during the desulfurization of high H_2S-loaded biogas. Start-up period and operational optimization were studied at neutral pH. Controlled and gradual transition to acidic pH was performed, fulfilling a total uninterrupted 600-days operation period. During the optimization period, operational parameters such as aeration rate, TLV and HRT were optimized, in order to minimize the production of elemental sulfur. During the neutral steady-state operation, the performance of the reactor was studied as a function of the gas contact time. During the pH transition period and during the operation at acid pH (until day 600 of operation), the reactor performance was assessed in terms of elemental sulfur production. Moreover, the effect of the simultaneous removal of methylmercaptan and H_2S was investigated during the neutral pH steady-state operation, as reported in **Chapter 8**. Also, on-line and off-line samples from the studied BTF were employed for sensing and monitoring studies, according to results presented in **Chapter 5** and **Chapter 6**, for H_2S/TDS and sulfate, respectively. Results obtained at acidic pH condition until the end of the operation (990 days) are reported later in **Chapter 9**.

✿

7.2 Introduction

The use of structured packing material has been previously proven to be effective in the desulfurization of high loads of H$_2$S (Fortuny *et al.*, 2008; Montebello *et al.*, 2010; Fortuny *et al.*, 2011). Maximum ECs of 210 – 280 g S-H$_2$S·m^{-3}·h^{-1}, with a RE of 80 – 90% were encountered for PU foam and HD-QPac, a structured plastic packing material in Fortuny *et al.* (2008), treating H$_2$S concentrations up to 12,000 ppm$_v$ of H$_2$S. Air was directly supplied to the biogas flow in both reported operations with the different packing material (PU and HD-QPac). Maximum ECs of 201 g S-H$_2$S·m^{-3}·h^{-1} at a RE of around 90% was found by Montebello *et al.* (2010), treating H$_2$S concentrations up to 8,000 ppm$_v$ of H$_2$S, with the same structured packing material previously studied by Fortuny *et al.* (2008). In this case (Montebello *et al.*, 2010), air was supplied both to the biogas flow and to the liquid phase through an auxiliary aeration unit. Moreover, mass transfer limitations are commonly reported during the treatment of high loads of H$_2$S caused by reduced gas contact times (Dorado *et al.*, 2009). Also with the same structured packing material and with the same aeration system as reported by Montebello et al. (2010), maximum ECs of 130 – 145 g S-H$_2$S·m^{-3}·h^{-1} were found by Fortuny *et al.* (2011) by decreasing the gas contact time down to 30 seconds.

Although random packing material is frequently used in industrial applications involving packed bed towers, some problems has been reported in industrial scale, by the excessive accumulation of elemental sulfur (Tomas *et al.*, 2009). Even so, the use of random packing material in this kind of reactors is recommended for maintenance activities, since the reposition of a portion of the packed bed can be easily performed with random packing material, during a quick, non-disturbing procedure that must not affect the overall performance of the system. Contrarily, when structured rigid elements are applied, the complete stop-operation of the reactor is required and the replacement of packing material elements requires a time consuming actuation.

7.3 Materials and methods

7.3.1 Inoculation and operational conditions

Aerobic sludge from a local municipal wastewater treatment plant (Manresa, Barcelona) was used for the unspecific inoculation of the reactor. Fresh sludge was diluted 1:1 with mineral medium, thus having a final volatile suspended solids concentration of 2.4 $g \cdot L^{-1}$. The inoculum was recirculated along the packing material for 24 hours without gas feeding or liquid renewing. Next, the inlet H_2S concentration was set to 1,500 ppm_v of H_2S (38 g S-$H_2S \cdot m^{-3} \cdot h^{-1}$) during 20 hours and was adjusted after that to 2,000 ppm_v of H_2S (51.48 g S-$H_2S \cdot m^{-3} \cdot h^{-1}$) as the reference value. The pH control was set at the original inoculum pH value (6.0 – 6.5). During start-up period, the flow air supplied ensured an O_2/H_2S ratio of 23.60 ($v \cdot v^{-1}$), which is the optimal value found by Fortuny *et al.*, (2010) for the complete oxidation of H_2S to sulfate, in the same experimental setup but with a structured packing material. Also, the HRT was kept at 70 ± 7 h and the TLV was of 3.8 $m \cdot h^{-1}$ (255 $mL \cdot min^{-1}$).

Three main operational periods are differenced:
   I.   Start-up and optimization (from day 1 to 140),
  II.   Steady neutral pH operation (from day 140 to 440) and
 III.   Acidic pH transition and operation (from day 440 to 600).

Start-up period, covering the first 15 to 21 operation days is followed by a 4-months-period of operational optimization which refers to the adjustment of some operation parameters, in order to minimize the accumulation of extra-cellular elemental sulfur, improving this way the results of biomass sampling and processing for biological characterization. Optimization period extends up to day 140 of operation. The supplied O_2/H_2S ratio was tested at the following values ($v \cdot v^{-1}$): 23.60; 29.50 and 49.17, with the strategy showed in **Table 7.1**, concomitantly with the adjustment of the TLV and HRT values.

Table 7.1 Operational parameters during optimization period

Time (days)	O$_2$/H$_2$S (v·v^{-1})	Qair $_{in}$ (mL·min^{-1})	TLV (m·h^{-1})	HRT (h)
0 – 15	23.60 – 29.50	150.0 – 187.5	4 – 6	70 – 87
15 – 25	49.17 – 59.01	312.5 – 375.0		
25 – 38	29.50	187.5	4	45 – 60
38 – 60				
60 – 111			12	
111 – 131	49.17	312.5		18 – 21
131 – 140			6	33 – 34

The second period, a steady state operation at neutral pH (6.0 – 6.5), extends from day 140 to 440. During this period, experiments on the reduction of the gas contact time were performed, as described later on **Section 7.3.2**. The third and last studied period begins at day 440 of operation and comprises the gradual and controlled pH transition until reaching the working pH of 2.50 – 2.75. Values of pH during the BTF operation and during the transition to acidic pH are shown in **Table 7.2**.

Table 7.2 pH setup during reactor operation

Operation days	*pH*
0 – 440	6.00 – 6.50
440 – 442	5.00 – 5.50
442 – 446	4.00 – 4.50
446 – 600	2.50 – 2.75

Total acidic pH operation extended for 550 days, totalizing the uninterrupted operation of the reactor for 990 days. In this Chapter, results are shown until day 600 of operation. Results obtained during the steady-state operation at acidic pH conditions (from days 600 to 990) are shown and discussed later in **Chapter 9**.

7.3.2 Experimental conditions

During the steady neutral pH operation period, after 430 days of neutral pH operation, two experiments were performed to investigate the effect of the gas contact time reduction on the performance of the reactor, at constant and at variable increasing LR of H_2S. Detailed experimental conditions adopted during experiments **E1** and **E2** are given in **Table 7.3**. The duration of each EBRT value step was of 1.5 h in both experiments.

Table 7.3 Experimental conditions at neutral pH

Experiment	$[H_2S]_{biogas}$ (ppm$_v$)	H_2S LR ($gS \cdot m^{-3} \cdot h^{-1}$)	O_2/H_2S ($v \cdot v^{-1}$)	EBRT (s)
E1	2,002.59			131
	1,002.30			76
	666.49	51.48	39.49	53
	501.40			41
	342.51			29
E2	2,002.65 ± 0.29	51.48	39.49	131
		102.98	19.74	76
		154.92	13.12	53
		203.95	9.97	42
		301.12	8.44	29

Firstly, during experiment **E1**, the EBRT was stepwise decreased from the reference operation value of 131 s until a minimum value of 29 s, keeping constant the load of H_2S entering the BTF (51.48 g S-$H_2S \cdot m^{-3} \cdot h^{-1}$). Finally, during experiment **E2**, the EBRT was also stepwise decreased, at identical hydraulic conditions as for **E1** experiment, but at increasing H_2S inlet load, as a consequence of keeping constant the H_2S concentration of the synthetic biogas (around 2,000 ppm$_v$ of H_2S). As the air inlet flow to the aeration unit was kept constant during experiments (250 mL·min^{-1}), except for the last step in experiment **E2** (312.50 mL·min^{-1}), the ratio O_2/H_2S ($v \cdot v^{-1}$)

entering the reactor was kept constant during experiment **E1** at 39.49 while decreases from 39.49 to 8.44 at the end of experiment **E2**. During experiments, a TLV of 7 m·h^{-1} and a HRT of 9 h were maintained, in order to assure the representativeness of liquid phase samples in front of the short time experimental changes performed. Liquid and gas samples were analysed at the end of each experimental change to assess the EC and the RE, as well as the sulfur mass balance.

7.4 Results and discussion

7.4.1 Start-up and operational optimization

After the inoculation of the reactor, the H$_2$S inlet concentration was established at 1,500 ppm$_v$ of H$_2$S. Rapidly, within one hour of operation, H$_2$S was already detected in the outlet gas stream from the biofilter. This illustrates the low sorption capacity of the system, even working at controlled pH between 6.0 – 6.5. The RE evolution during the start-up period is shown in **Figure 7.1**.
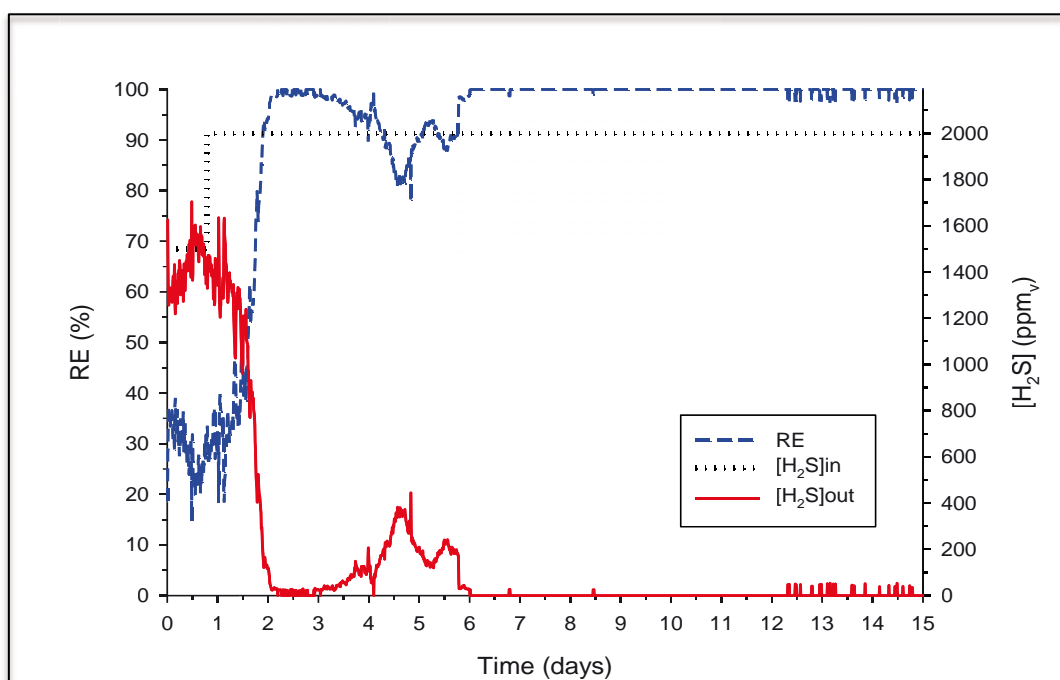
Figure 7.1 RE evolution during the start-up period

Even at the beginning of the operation, incipient biological activity coupled to absorption of H_2S into fresh mineral medium and $NaHCO_3$ solution allowed obtaining RE values of 20 − 40% during the first day of operation. Subsequently, the H_2S inlet concentration was rose to 2,000 ppm_v of H_2S and, after 50 hours of operation, RE values higher than 90% were achieved (**Figure 7.1**), resulting in an apparent fast start-up of the system. However from the third day of operation, H_2S outlet concentration increased up to 400 ppm_v of H_2S, denoting a longer start-up phase in comparison with previous operations (Fortuny *et al.*, 2008; 2011).

The RE fluctuations and system instability during start-up period are usual in this kind of bioprocess (Gabriel and Deshusses, 2003b), basically due to the lack of stable microbial populations in the bioreactor. Also, the increase in the aeration ratio performed on day 4, as showed in detail in **Figure 7.2** and discussed later on, not only did not result in the expected diminution of the produced S^0 but instead resulted in the observed lost of performance, probably because of a negative effect produced by the extra stripping phenomena when the microbial activity was not yet stable. In spite of the RE oscillation during this period, the BTF performance evolved until the sixth day of operation achieving a RE value higher than 95%. The significance of the consolidation of the microbial community can be inferred by the performance stability observed on day 12 and following, when once again the aeration ratio was increased, but not negative effect related to a stripping increment was observed. The developed set of operational parameters optimization is shown in detail in **Figure 7.2**, along with the accumulative mass balance of sulfur species calculated from the oxidation of H_2S (Janssen *et al.*, 1997).

Starting with the BTF inoculation and during the first 4 days of operation, TDS was on-line monitored in the BTF liquid recirculation phase by the FIA/GD-CFA configuration system described in **Chapter 5** (Montebello *et al.*, 2010) under continuous operation, to assess the performance of the BTF during the start-up period.
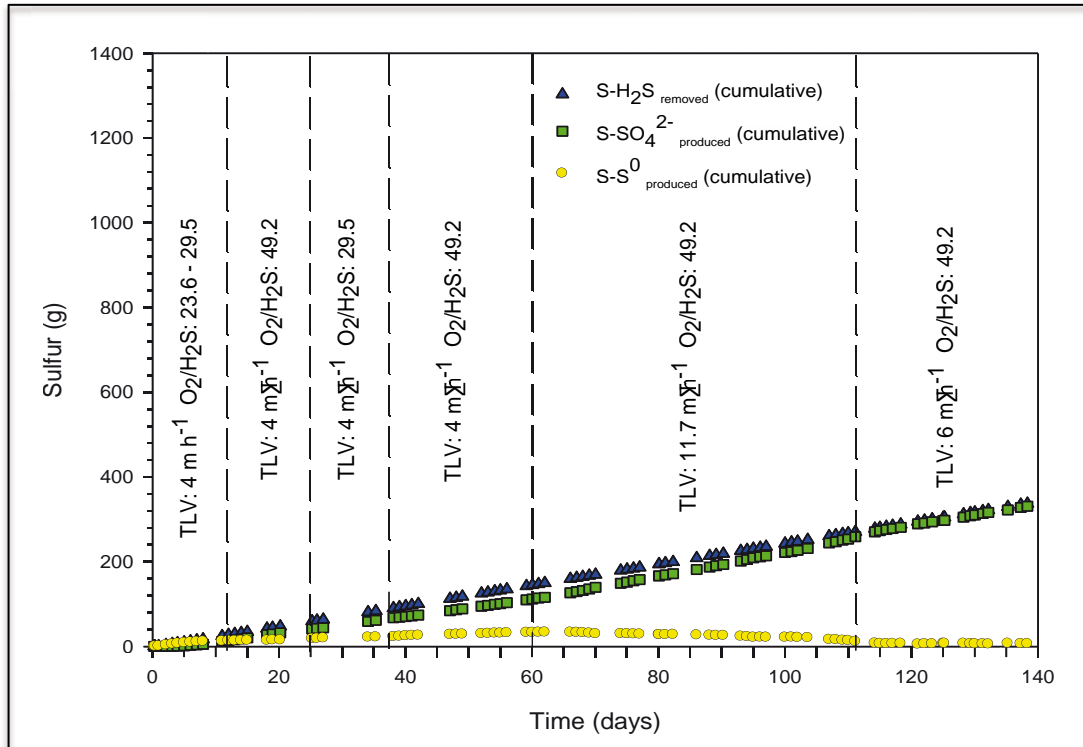
Figure 7.2 Sulfur mass balance during optimization period. Vertical dashed lines indicate operational changes

TDS monitoring data demonstrated a slight accumulation of TDS in the liquid phase during the first 40 hours of operation, when values of TDS were close to the limit of detection of the analyzer ($1.5 \times 10^{-5} \pm 0.9 \times 10^{-5}$ mol S-S^{2-} ; 0.48 ± 0.29 mg S-S^{2-}·L^{-1}). From that point on, no TDS accumulation was detected. Thereafter ORP values monitored ranged from -90 mV to 100 mV, being these values relatable to sulfate production situations, without sulfur accumulation in the liquid phase (Fortuny *et al.*, 2011) at neutral pH.

Despite achieving a RE of H₂S above 95% in less than a week, a significant production of S^0 was promptly observed, easily noticeable along the reactor bed. The S^0 production rate (pS-S^0) was calculated according to **Equation 22**. During the first 4 days of operation, the calculated pS-S^0 was 40.4 g S-S^0·m^{-3}·h^{-1}, totalizing 7.76 g of biologically produced elemental sulfur (biosulfur), which corresponded to approximately 77% of the total removed sulfur. In order to minimize the S^0 production and to lead the operation to the complete oxidation to SO₄$^{2-}$, a set of actions based on the experimentation of the load of oxygen (LO₂) supplied to the system was

performed. LO_2 was calculated according to **Equation 19**. Specifically, experiencing different TLV and O_2/H_2S ratios during the biofilter optimization period enabled to drive the bioprocess to new stationary conditions with minimal S^0 production.

A constant TLV of 4 $m\cdot h^{-1}$ was kept over the first 60 days of operation. Oppositely, during the same period, several changes in the air inlet flow were performed resulting in different O_2/H_2S $_{supplied}$ ratios. After 4 days of operation, the air inlet flow was increased in 25%, from 150.00 to 187.50 $mL\cdot min^{-1}$, in an attempt to minimize the excessive observed biosulfur production. This air inlet flow (187.50 $mL\cdot min^{-1}$) corresponded to a LO_2 of 0.95 mg $O_2\cdot min^{-1}$, which resulted in a $pS-S^0$ of 17.4 g $S-S^0\cdot m^{-3}\cdot h^{-1}$. However, a noteworthy decrease on the production of biosulfur only occurred after day 12 of operation, when the air inlet flow was increased to 312.5 $mL\cdot min^{-1}$ (49.17 O_2/H_2S $v\cdot v^{-1}$), which corresponded to a LO_2 of 1.51 mg $O_2\cdot min^{-1}$, resulting in a $pS-S^0$ of 6.6 g $S-S^0\cdot m^{-3}\cdot h^{-1}$. The LO_2 was maintained unaltered between days 12 to 25 of operation. Then, from days 25 to 38, the air inlet flow was reduced back to 187.5 $mL\cdot min^{-1}$ (29.5 O_2/H_2S $v\cdot v^{-1}$) with the intention to confirm the biofilter response and discard possible causes related to start-up and adaptation phenomena. This latest change corresponded to a LO_2 of 1.33 mg $O_2\cdot min^{-1}$, which produced an increment on the $pS-S^0$ resulting in 10.3 g $S-S^0\cdot m^{-3}\cdot h^{-1}$. In order to allow the biofilter to operates at minimum S^0 accumulation conditions and to warrant the quality of biomass samples for further microbiological analysis procedures, at day 38 the air inlet flow was increased once again back to 312.5 $mL\cdot min^{-1}$ (49.17 O_2/H_2S $v\cdot v^{-1}$), corresponding to an LO_2 of 1.27 mg $O_2\cdot min^{-1}$. This configuration was kept until day 60 of operation and the air inlet flow was maintained as the reference value.

Even with this last increment in the aeration rate of the system, the biosulfur production rate was only slightly reduced, resulting in $pS-S^0$ of 9.8 g $S-S^0\cdot m^{-3}\cdot h^{-1}$ during this period (days 38 to 60), a value significantly higher than the expected from the previous tested condition between days 12 to 25 of operation ($pS-S^0$ of 6.6 g $S-S^0\cdot m^{-3}\cdot h^{-1}$). Taking into account the obtained

data up to this point, the accumulation of biosulfur as well as biomass massive colonization of the packing material were appointed as an impairment for the effective penetration of oxygen into the biofilm. In this way, at day 60, the TLV was significantly incremented (11.7 m·h^{-1}), in order to spread the penetration of O$_2$ along the filter bed. This high TLV, maintained up to day 111 of operation, resulted in an LO$_2$ of 2.83 mg O$_2$·min^{-1}, stimulating from day 65 and on a clear change on the behavior of the BTF. Not only the increase on the value of SO$_4^{2-}$ produced was observed, but also a dramatically decline of the S^0 accumulated was corroborated, due to the activity of certain bacteria, which have the capacity of biologically oxidizes S^0 to SO$_4^{2-}$, according to **Equation 10**. This condition led to a negative value of the biosulfur production rate during this period, indicating that biosulfur was been consumed instead of produced. The biosulfur consumption rate (-pS-S^0) was calculated according to **Equation 23**. Consequently, the calculated -pS-S^0 was -9.2 g S-S^0·m^{-3}·h^{-1}, which was in good agreement with the visual verification of the consumption of the accumulated biosulfur inside the filter bed.

Thus, after approximately 115 days after the inoculation, the S^0 accumulated had been minimized and the biofilter was operating primarily producing SO$_4^{2-}$. At this point, the TLV was reduced back to 6 m·h^{-1} in order to assimilate to the typical values encountered for this kind of bioprocess (Fortuny *et al.*, 2010), resulting in a LO$_2$ of 1.48 mg O$_2$·min^{-1} and a -pS-S^0 of -2.4 g S-S^0·m^{-3}·h^{-1}. Therefore it can be stated that the different configuration changes of TLV and air inlet flow carried out over the first 140 days of operation allowed consolidating a stable operation with the characteristics pursued of minimum S^0 production and maximum SO$_4^{2-}$ production from overall performance. Moreover, produced biosulfur accumulated inside the filter bed was effectively oxidized to SO$_4^{2-}$.

The performance of the reactor was satisfactorily supported during the operation at neutral pH, until day 440 of operation, with minimum S^0 production, as confirmed by the sulfur mass balance calculation. Once the pH transition was implemented and during the total acidic operation period

reported in this Chapter (days 440 to 600), a noticeable S^0 production and accumulation was observed, as discussed later on **Section 7.4.3**.

According to the LO_2 supplied to the BTF, different stages of operation can be distinguished. **Figure 7.3** shows the effect of the oxygen load on the behavior of the BTF in terms of SO_4^{2-} production, expressed as the sulfate selectivity ($S-SO_4^{2-}/S-H_2S_{removed}$), calculated according **Equation 25**.
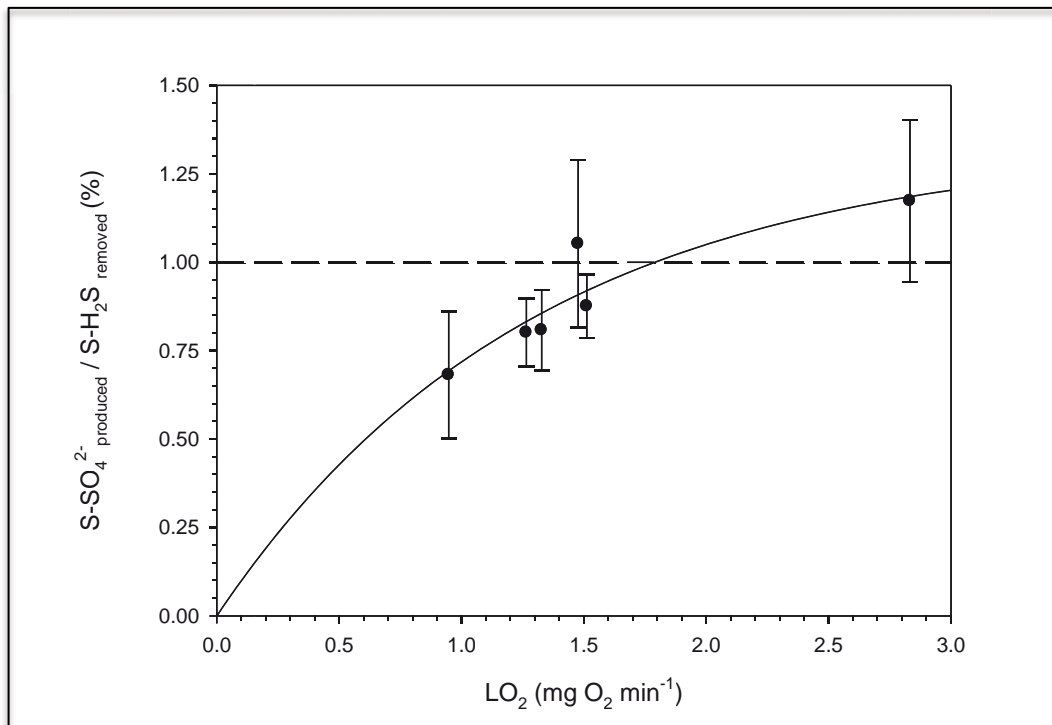
Figure 7.3 SO_4^{2-} selectivity *versus* LO_2 during optimization period. Dashed line indicates 100% of SO_4^{2-} production

It is worth noticing that, due to the experimental setup, the auxiliary aeration unit presents a direct gas-phase by-pass of air to the gas inlet section of the reactor, obtaining an extra O_2 supply in the gas phase, besides the dissolved O_2 supplied in the liquid recirculation line, after the auxiliary aeration unit. Values of the first 6 days of operation were not considered in the calculation of the SO_4^{2-} selectivity and LO_2 presented in **Figure 7.3**, because of the possible non-representative data variability produced by the characteristically unconsolidated start-up of the reactor.

From the SO_4^{2-} production yields based on the LO_2 provided, it was possible to delimit the optimum BTF operation with Pall rings as packing material to avoid S^0 generation. The appropriate LO_2 that lead to complete SO_4^{2-} production corresponded to around 1.7 mg $O_2 \cdot min^{-1}$ (**Figure 7.3**). Underneath this LO_2 value, even with H₂S RE above 98%, only part of the H₂S removed was completely oxidized to SO_4^{2-}. Interestingly, this optimal LO_2 supplied through the liquid phase corresponded to a molar ratio of 0.83 mol of O_2 supplied per mol of H₂S removed, which is lower than 2, the stoichiometric ratio according to **Equation 9**. Although such molar ratio is reduced to 1.6 when a typical biomass growth stoichiometry is considered (Gabriel *et al.*, 2013), we can infer that the apparently insufficient O_2 supply was complemented by the extra O_2 obtained by the direct gas by-pass from the auxiliary aeration unit to the BTF. However, further research is needed with proper O_2 mass balances calculations to precisely elucidate the contribution of excess air by-pass through the BTF to H₂S removal.

7.4.2 Effect of the gas contact time

The effect of EBRT was studied at constant (**E1**) and variable (**E2**) H₂S LRs, by gradually decreasing the EBRT from the reference value of 131 s down to 29 s. Data of monitored DO and ORP during experiment E1 are shown in **Figure 7.4**, alongside with the calculated RE for each applied EBRT. ORP kept at a stable range between 0 and 40 mV, considered as a normal value under the studied conditions, for the production of SO_4^{2-} (Montebello *et al.*, 2010). However, since ORP monitoring is performed in the liquid phase, no direct correlation with the gas phase dynamics can be established in this kind of reactors, because of the difference between the gas and liquid residence time in the system. Also, because of the relative short duration of the performed experiments (90 minutes for each experimental change) in front of the applied HRT (9 hours), no steady state is reached after each experimental change, even when stable values of RE were obtained at the gas phase.
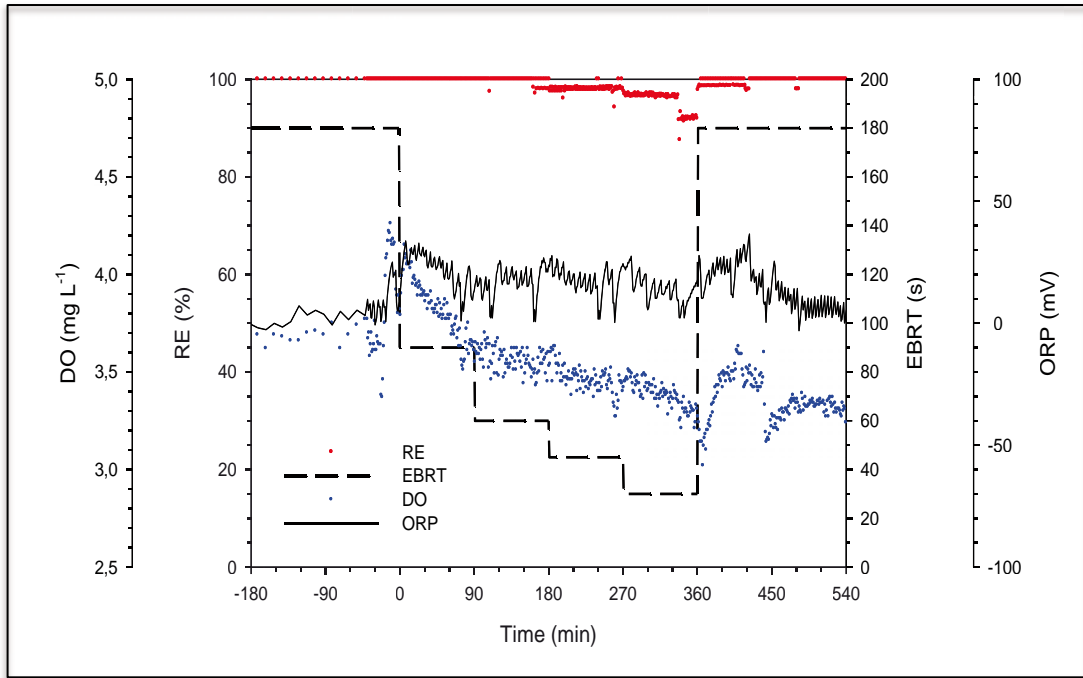
Figure 7.4 DO, RE, EBRT and ORP during E1

The calculated EC and RE during **E1** in front of the applied EBRT are shown in **Figure 7.5**. A slight reduction in the RE during experiment **E1** was noticeable only at an EBRT shorter than 53 seconds.
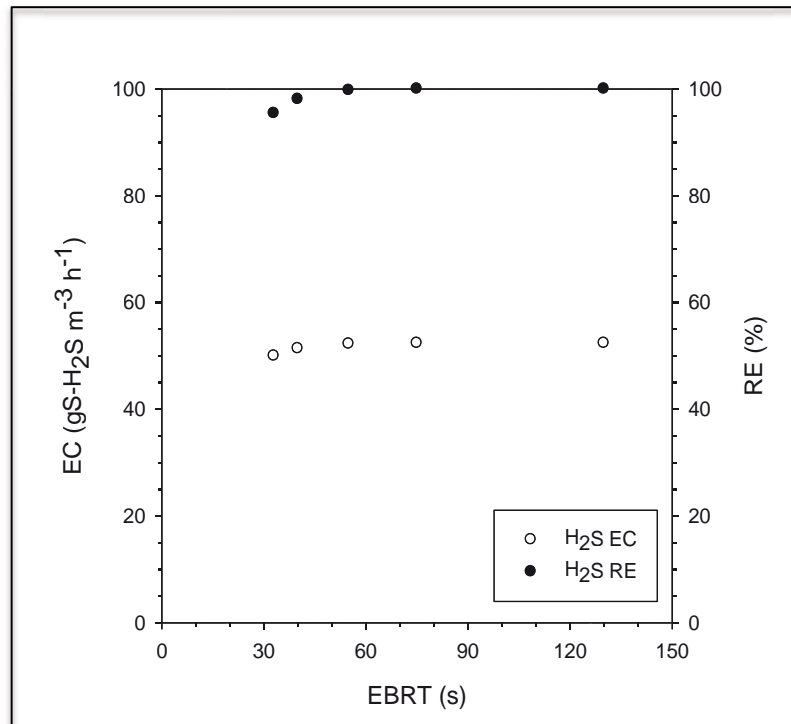
Figure 7.5 EC and RE *versus* EBRT during E1

Results obtained during experiment **E1** indicated a high performance in H$_2$S removal even at the most restrictive gas contact time studied (29 s), presenting a slight reduction in RE values from 100% to 95%. Critical EBRT was found around 55 s (**Figure 7.5**), considered as an ordinary value for biotrickling filtration at high H$_2$S loads (Sercu *et al.*, 2005; Datta *et al.*, 2007; Fortuny *et al.*, 2008; Montebello *et al.*, 2010; Fortuny *et al.*, 2011; Chaiprapat *et al.*, 2011). Moreover, the possibility of treating biologically almost 700 ppm$_v$ of H$_2$S, keeping and RE around 99% for a gas contact time as low as 55 s, suggests a wide applicability potential for energetically rich gas desulfurization processes.

As expected, it was verified that the effect of the EBRT reduction on the H$_2$S RE was significantly higher under variable H$_2$S LR (**E2**). Monitoring data of during **E2** are shown in **Figure 7.6**, alongside with calculated RE for each experimental step. Once more, it is worth noticing that parameters calculated from liquid phase are not directly relatable to the gas phase behavior, because of the dissimilar residence time for each phase. However, the integrated assessment of monitored parameter aids in the understanding of the biological desulfurization process.
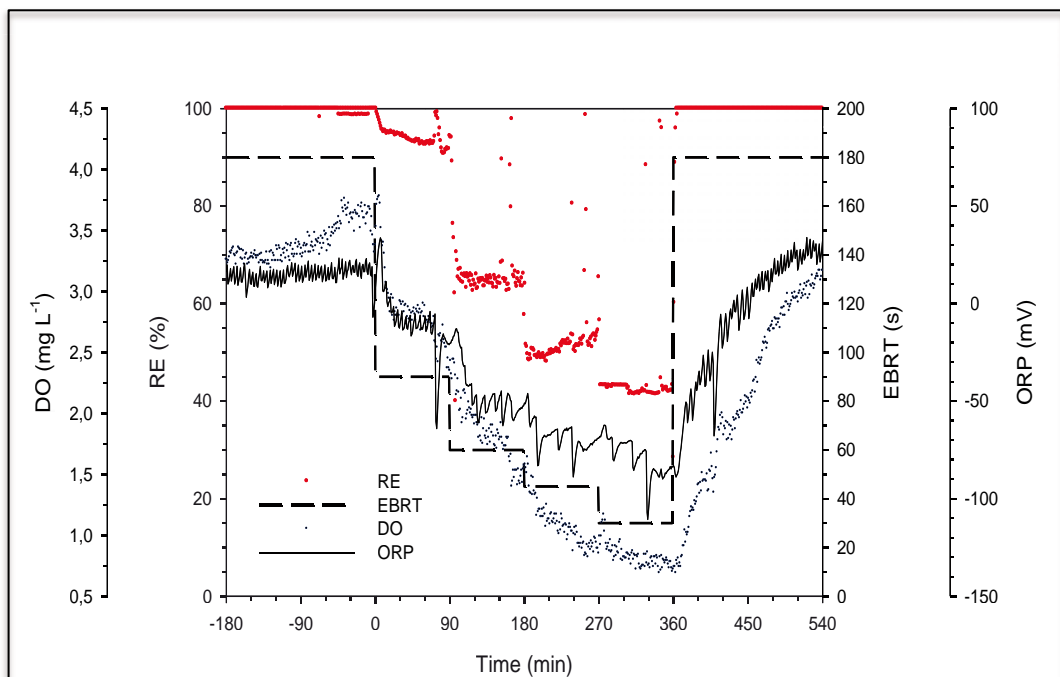
Figure 7.6 DO, RE, EBRT and ORP during experiment E2

During experiment **E2**, the RE suffered a significant diminution when the EBRT was reduced to 53 s, which corresponds to a H_2S LR of 154.92 g S-$H_2S \cdot m^{-3} \cdot h^{-1}$ and kept decreasing until reaching a minimum value of around 45% at 29 s of EBRT (301.12 g $S-H_2S \cdot m^{-3} \cdot h^{-1}$). Data of DO monitoring indicated a drop in the O_2 available in the liquid phase from the normal value of 3.5 mg $O_2 \cdot L^{-1}$ to less than 1.0 mg $O_2 \cdot L^{-1}$ at EBRT of 29 s, even with the increment in the aeration performed at this last operational step, from 250 mL air$\cdot min^{-1}$ to 312.50 mL air$\cdot min^{-1}$. Data obtained from ORP monitoring indicated a significant reduction in ORP values, from 30 mV (at 131 s) to -80 mV (at 29 s). Yet, monitoring of TDS indicated values below the detection limit ($1.5 \times 10^{-5} \pm 0.9 \times 10^{-5}$ M S^{2-} / 0.48 $\pm$ 0.29 mg $S^{2-} \cdot L^{-1}$), suggesting that no significant TDS accumulation in the liquid was occurring (Montebello *et al.*, 2010), thus indicating that the main limiting process is due to the mass transfer limitation of H_2S at reduced gas contact times, which is in accordance with Montebello *et al.* (2012) and Fortuny *et al.* (2011). The H_2S RE sharply decreased from the initial value of 100% down to 45% at the end of the experiment **E2** (**Figure 7.7**).
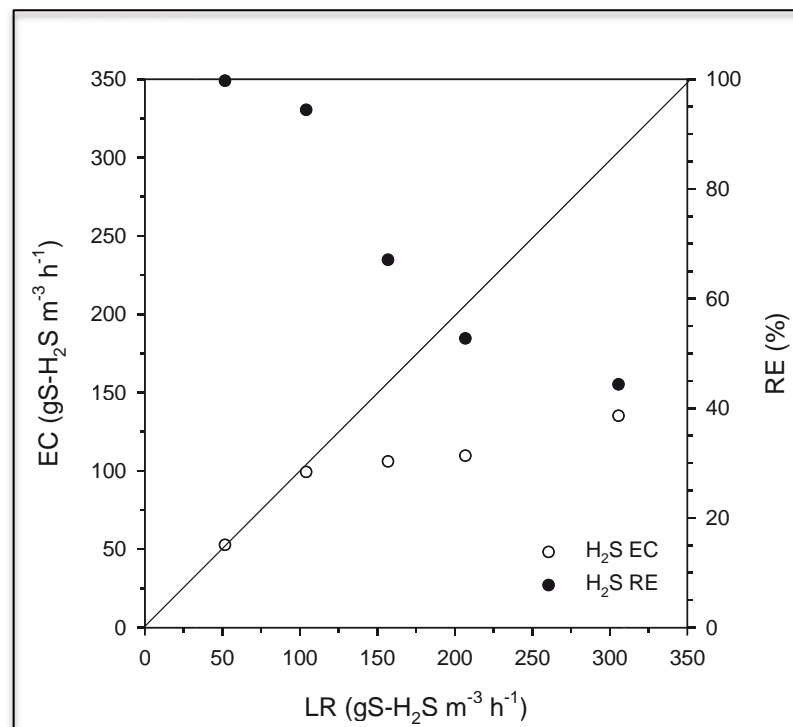
Figure 7.7 EC and RE *versus* LR during E2

The critical EBRT for the removal of H_2S during experiment **E2** was found around 75 s, a value higher than that obtained during E1 experiment, due to the considerably higher H_2S LR applied during experiment **E2**. Critical and maximum ECs were found at 100 and 135 g $S\text{-}H_2S\cdot m^{-3}\cdot h^{-1}$, respectively, comparable to the results obtained previously by Fortuny *et al.* (2011), under similar experimental conditions but with a different packing material. It can be supposed that the extent of mass transfer limitation was comparable for the two different packing because of the similarity between specific surface values for each material: 433 $m^2\cdot m^{-3}$ in the case of the HDQPac elements (Fortuny et al., 2008) and 515 $m^2\cdot m^{-3}$ for the Pall rings applied in this study. Once the experimental period was concluded, reference operation conditions were resumed and RE of H_2S fast recovered to around 99%, confirming the high recovery capacity of the system. It is worth noticing that at the last EBRT period studied (29 s), data obtained from the on-line monitoring of DO (data not shown) indicated that the system was at limiting oxygen conditions, so the air supply was increased from 250.00 $mL\cdot min^{-1}$ to 312.50 $mL\cdot min^{-1}$, as an attempt to improve the H_2S removal, as showed by the increment in the observed EC and RE values at the lowest EBRT (29 s). However, no significant changes were observed in terms of RE, probably because of the difference between gas and liquid residence time in the system, e.g. EBRT of 131 – 29 s and HRT of 9 h.

7.4.3 Transition to acidic pH conditions

After 440 days of neutral pH conditions operation (6.0 < pH < 6.5), the transition to acidic pH was performed, applying the pH set-up control values shown in **Table 7.2**, up to the final value of 2.50 < pH < 2.75. Surprisingly, after the six-days period that lasted the gradual pH transition, the system was efficiently performing on the desulfurization of 2,000 ppm_v of H_2S at acidic pH conditions, after more than one year under neutral pH operation and without any re-inoculation of the reactor. In spite of the sustained removal of H_2S, it is worth noticing that a meaningful quantity of S^0

accumulated during the six first days of the pH transition (6.67 gS-S^0), accounting for the 42% of the total oxidized sulfide during this period.

The calculated biosulfur production rate during the same period (days 440 to 446 of operation) was 23.1 g S-S^0·m^{-3}·h^{-1}, which represented a value lower than the obtained during the first 4 days of operation at the start-up at neutral pH (pS-S^0 = 40.4 g S-S^0·m^{-3}·h^{-1}), but yet higher than the value obtained during days 4 to 12 of neutral pH operation (pS-S^0 = 17.4 g S-S^0·m^{-3}·h^{-1}), when the system was still achieving the sulfide oxidizing capacity. The production of biosulfur was found to be persistent during the acidic operation, as shown in **Figure 7.8**, and more significant at the long-term acidic operation up top day 990, as discussed later on **Chapter 9**.
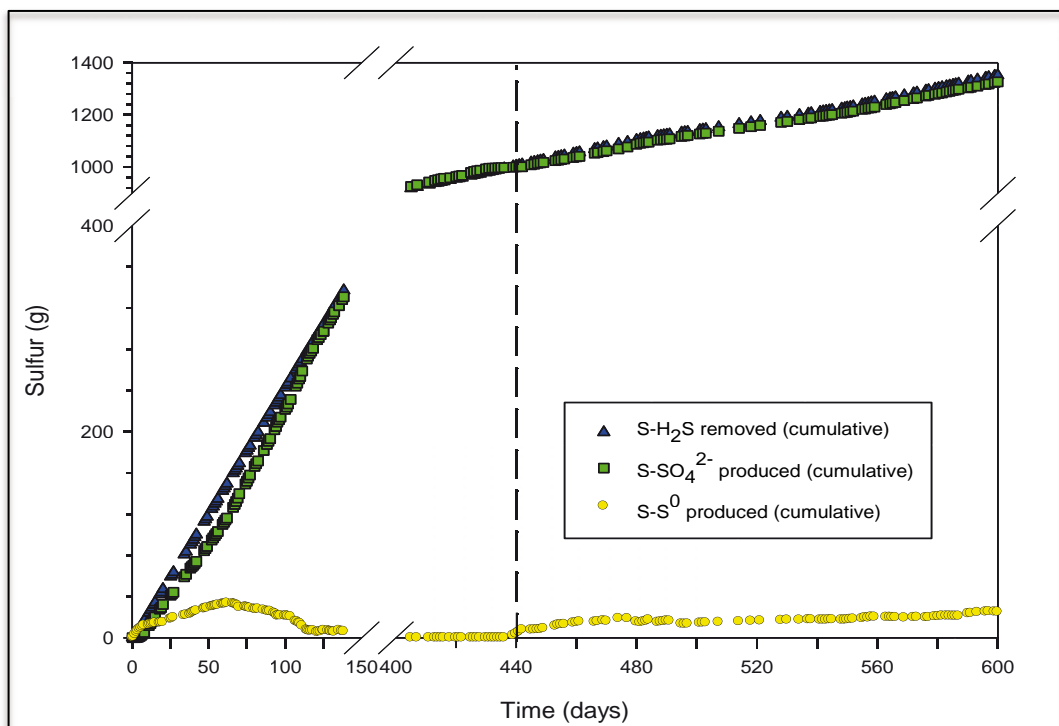
Figure 7.8 Sulfur mass balance up to day 600 of operation. Vertical dashed line indicates pH transition to acidic conditions

However, without any operational modification, the biosulfur production rate was significantly reduced to 3.8 g S-S^0·m^{-3}·h^{-1} after the initial 6-day period of pH transition up to the end of the monitored period reported in this Chapter (day 600 of operation), obtaining a total of 7.35% of biosulfur accumulated, considering the total sulfide removed over the same period.

These results revealed an exceptional biological desulfurization capacity and suggested that the microbial consortium already present in the filter bed rapidly evolved to a community able to subsist at acidic pH conditions, without any re-inoculation procedure. Dynamics of the microbial community diversity of the BTF was studied by others, before and after the performed pH transition from neutral to acidic conditions (Bezerra *et al.*, 2013). The obtained data of relative abundance denoted a large complexity of the bacterial community under neutral pH. Most abundant families found at neutral pH were Xanthomonadaceae (γ-Proteobacteria), with 35% of abundance and Nitrosomonadaceae (β-Proteobacteria), with 22.5% of abundance. However, a dramatic diversity reduction occurred at acidic pH, even when the desulfurizing capacity of the reactor remained unaffected. Results of relative abundance indicated the complete disappearance of the phylum β-Proteobacteria at acidic pH, while phyla γ-Proteobacteria (86%) and α-Proteobacteria (12%) prevailed. At acidic pH, the most abundant species were *Acidithiobacillus thiooxidans* (47%), *Acidiphillum sp.* (12%) and *Acidithiobacillus sp.* (10%) (Bezerra *et al.*, 2013).

Overall, since no reduction on the H$_2$S removal capacity was observed after pH transition, no substantial differences were found, at macroscopic level, in the performance of the BTF at neutral and acidic pH conditions. Differently, Kim and Deshusses (2005) have found that the biodegradation activity was significantly increased when the operational pH rose from 2 to near neutral, which in turn was in disagreement with the results obtained by Gabriel and Deshusses (2003b), who reported better activity at low pH. Furthermore, it is not possible to elucidate the reason of so conflictive results since different operational conditions and acclimatization strategies have been applied in each study.

The effect of short-term pH variations on the overall reactor performance has been already studied in comparable conditions with the present study, but with a rigid, structured packing material at near neutral pH values (Fortuny *et al.*, 2011). In that study, they found that the overall system

response was quite insensitive to a pH drop from 6 − 6.5 to 2.5, but was markedly affected by a pH increase from 6 − 6.5 to 9.5. To the author's knowledge, no literature is available regarding to the effect of a permanent pH change over the biogas biological desulfurization. In the treatment of VOCs and H_2S at odor level by biotrickling filtration with PU foam, Gabriel and Deshusses (2003b) reported a severe lost of performance when the operational pH was instantly changed from acidic to neutral condition, attributed to the possible culture inhibition during pH transition; the effect of extra chlorine supply was also appointed as a possible explanation. Probably, a similar behavior would be obtained with the BTF studied in this thesis if the pH transition were suddenly performed; contrary, the gradual pH transition executed apparently helped in the adaptation of the indigenous microbial consortium, as inferred by the obtained results.

Moreover, the applied packing material shown to be effective at both pH conditions studied, for the period of operation reported. Also, the adopted gradual pH transition strategy showed appropriate to ensure the continuous BTF operation without the necessity of re-inoculating the reactor. However, further investigation is required in order to compare the overall reactor performance under neutral and acidic pH condition operation, when a steady-state acidic operation has been achieved (**Chapter 9**).

7.5 Conclusions

Highly H_2S-loaded (51.48 g S-H_2S·m^{-3}·h^{-1}) biogas desulfurization in the studied aerobic biotrickling filter was proven to be effective for both neutral and acidic pH operation with an inert random packing material. The performed unspecific inoculation was considered acceptable, resulting in high H_2S removal after a short start-up period.

The optimization of operational parameters, such as the aeration rate, the liquid trickling velocity and the hydraulic residence time resulted in an optimal O_2/H_2S $_{supplied}$ ratio for the achievement of the minimum elemental

sulfur production, defined as the targeted reactor performance for the parallel study (by others) of the microbiological community developed in the filter bed. The oxygen load was enhanced by the concomitant optimization of the aeration rate and the liquid recirculation rate, resulting in the maximum sulfate selectivity under the investigated conditions. Oxygen load was confirmed as a key driven parameter of the H$_2$S oxidation products control. The study of the hydrodynamic characteristics of the system, as well as the investigation on the reactor performance in front of the pollutant load and the gas contact time confirmed that, under the studied conditions, mass transfer was the main limiting process.

The operational pH transition of the BTF was successfully executed by gradually reducing the pH down to 2.50 – 2.75. This strategy shown effective and sufficient for the adaptation of the microbial community to perform at such acidic environment, even with no re-inoculation of the filter bed. An important simplification was encountered in the microbiological ecology of the reactor, indicating than the selective pressure imposed by th operational pH resulted in a fast, dynamic microbiological adaptation, with outstanding H$_2$S removal capacitiy. Results obtained confirmed the high adaptability capacity and the robustness of this kind of reactors. Moreover, the packing material employed, AISI 304 Pall rings, shown suitable for operation under neutral operation and acidic condition for the studied period reported in this Chapter (600 days), even when deterioration of packing elements was verified over the long-term acidic operation (**Chapter 9**).

❋

8

---

simultaneous removal of

methylmercaptan and H$_2$S

"What for centuries raised man above the beast is not the cudgel
but the irresistible power of unarmed truth."

Boris L. Pasternak
(Moscow, 1890 –Peredelkino, 1960)

8   Simultaneous removal of methylmercaptan and H$_2$S

8.1 Summary and scope

During the stable long-term operation of the reactor at neutral pH conditions, different experiments were conducted in order to study the effect of the presence of CH$_3$SH in the inlet biogas stream over the desulfurizing capacity of the reactor. Experiments were conducted, at comparable technical conditions, jointly with the Biological and Enzymatic Reactors Group, from the University of Cadiz, responsible for the operation of a BTF under anoxic conditions. However, only results obtained from the aerobic BTF studied in this thesis are presented in this Chapter. Further information about the performance of the anoxic reactor can be found elsewhere (Montebello *et al.*, 2012).

The studied BTF was run for more than one year treating H$_2$S as the unique S-contaminant, at a concentration of 2,000 ppm$_v$ of H$_2$S. Then, without any re-inoculation of the reactor, the effect of the presence of CH$_3$SH on the H$_2$S and CH$_3$SH removal capacity of the system was investigated maintaining a constant load of H$_2$S (52 g S-H$_2$S·m^{-3}·h^{-1}). Initially, CH$_3$SH concentration was stepwise increased from 0 to 75 ppm$_v$ of CH$_3$SH. Maximum EC of around 1.8 g S-CH$_3$SH·m^{-3}·h^{-1} was found. After that, CH$_3$SH LR was indirectly increased by testing different EBRTs between 180 and 30 seconds. Significantly lower ECs were found at short EBRTs, indicating that the system was mostly mass transfer limited.

Finally, EBRT was reduced from 180 to 30 seconds at variable CH$_3$SH and H$_2$S loads. Maximum H$_2$S EC found was 100 gS-H$_2$S·m^{-3}·h^{-1}. A negative influence was found on the removal of CH$_3$SH by the presence of high H$_2$S loads. However, sulfur mass balance and batch tests showed that CH$_3$SH chemically reacts with S^0 at neutral pH, enhancing the overall reactors performance, by reducing the impact of sulfur accumulation inside

the packed bed. Also, the reactor was able to treat CH_3SH without prior inoculation because of the already existing SOB consortium grown during H_2S treatment exhibited a high CH_3SH elimination capacity. Co-treatment of H_2S and CH_3SH under aerobic conditions was considered as a feasible operation for concentrations commonly found in biogas (2,000 ppm_v of H_2S and below 20 ppm_v of CH_3SH).

The aim of the work presented in this Chapter was to investigate the impact of the presence of CH_3SH and H_2S and the effect of the gas contact time reduction on the overall desulfurizing performance of a well-established BTF operated under aerobic condition during the co-treatment of typical loads of H_2S and CH_3SH in biogas.

<div align="center">✿</div>

8.2 Introduction

In terms of process performance impact, van den Bosch *et al*. (2009) reported that CH_3SH severely inhibits biological sulfide oxidation (50% reduction of the biological oxidation rate) at concentrations above 0.05 mM of CH_3SH under natron-alkaline-aerobic conditions. Complete inhibition was found at concentrations of 0.65 mM of CH_3SH. However, no previous studies of simultaneous H_2S and CH_3SH are available at high H_2S loading rates in bioreactors operating at neutral pH, neither under aerobic nor anoxic conditions. Thus, potential accumulation of CH_3SH in BTFs may hinder H_2S removal to a certain extent.

The biological oxidation of CH_3SH under aerobic conditions produces as intermediary products formaldehyde and H_2S (Bentley and Chasteen, 2004). The overall reaction can be expressed according to **Equation 34** (Sipma *et al*., 2004):

$$\textbf{2 CH}_3\textbf{SH + 7 O}_2 \rightarrow \textbf{2 CO}_2 \textbf{ + 2 H}_2\textbf{SO}_4 \textbf{ + 2 H}_2\textbf{O} \hspace{2cm} \textbf{[34]}$$
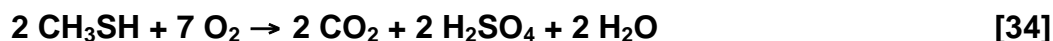
Even if the oxidation of CH_3SH with molecular oxygen have also been described to happen in strongly alkaline solutions in presence of metal ion catalysts while the oxidation rates in the absence of catalytic materials are extremely low (Harkness and Murray, 1970). Also chemical oxidation of CH_3SH to DMDS in an aerobic reactor has been reported to occur according to **Equation 5** (van Leerdam *et al*., 2008). Recently, van Leerdam *et al*. (2011) have found that CH_3SH also reacts chemically with biosulfur particles at pH 8.7 to form DMDS and other polysulfides according to **Equation 35** and **Equation 36**:

$$\textbf{2 CH}_3\textbf{S}^- \textbf{ + H}^+ \textbf{ + 1/8 S}_8 \leftrightarrow \textbf{HS}^- \textbf{ + CH}_3\textbf{SSCH}_3 \hspace{2cm} \textbf{[35]}$$

$$\textbf{2 CH}_3\textbf{S}^- \textbf{ + S}_8 \leftrightarrow \textbf{S}_y^{2-} \textbf{ + CH}_3\textbf{S}_x\textbf{CH}_3 \text{ (with x + y = 10)} \hspace{1.5cm} \textbf{[36]}$$

These reactions depend on the CH_3SH and biosulfur concentration, temperature and nature of biosulfur particles (van Leerdam *et al.*, 2011). Main products are dimethyl disulfide (DMDS), and dimethyl trisulfide (DMTS) and some longer-chain dimethyl polysulfides $((CH_3)_2S_{4-7})$. DMDS and DMTS are less inhibitory than CH_3SH on biological (poly)sulfide oxidation (van den Bosch *et al.*, 2009). However, further research is needed in order to elucidate the complex chemical and biological CH_3SH reaction mechanisms under neutral pH conditions.

8.3 Materials and methods

8.3.1 Experimental conditions

Three different experiments were performed to face potential crossed effects during CH_3SH and H_2S simultaneous treatment, under the conditions detailed in **Table 8.1**.

Table 8.1 Experimental conditions for CH_3SH and H_2S co-treatment

Experiment	$[H_2S]_{in}$ (ppm$_v$)	H_2S LR (gS-$H_2S \cdot m^{-3} \cdot h^{-1}$)	$[CH_3SH]_{in}$ (ppm$_v$)	CH_3SH LR (gS-$CH_3SH \cdot m^{-3} \cdot h^{-1}$)	EBRT (s)
E1	2,000	52.5	10	0.26	180
			20	0.53	
			40	1.05	
			60	1.58	
			75	2.00	
E2	2,000	52.4	13	0.34	180
	1,001			0.68	90
	666			1.02	60
	501			1.36	45
	342			1.99	30
E3	2,000	52	13	0.34	180
		105		0.68	90
		158		1.02	60
		207		1.36	45
		306		1.99	30

First, a CH_3SH inlet concentration increase experiment (**E1**) was performed at constant H_2S LR, in order to verify the possible effect of CH_3SH over the already existing H_2S desulfurization capacity of the reactor. Secondly, an EBRT decreasing experiment at constant H_2S LR (**E2**) was performed and, finally, an EBRT decreasing experiment at variable H_2S LR (**E3**) was executed. Experiments **E2** and **E3** were designed to investigate the operational limit and potential mass transfer limitation effects for both investigated pollutant.

In **E1**, the H_2S inlet concentration was kept constant at around 2,000 ppm_v while the CH_3SH concentration was stepwise increased from 10 to 75 ppm_v of CH_3SH. Concentration steps were kept constant during 24 h, that corresponded to almost three liquid residence times, if compared to the HRT of 9 h of the liquid phase during experimental period. Then, a pseudo-steady-state condition after each concentration step was considered to be reached. The EBRT was kept unaltered at 180 s during **E1**.

In **E2**, a constant H_2S LR was maintained to verify the single effect of the increasing CH_3SH LR produced by the reduction in the gas contact time down to 30 seconds. The EBRT was stepwise decreased, being each EBRT step kept for 1.5 h.

In **E3**, both H_2S and CH_3SH concentrations were kept constant, leading to an indirect increase in both pollutants LRs, due to the reduction of the gas contact time. Similarly to **E2**, the EBRT was stepwise decreased in **E3**, being each EBRT step kept for 1.5 h. In all cases, liquid and gas samples were analyzed at the end of each step to assess the EC and RE of each pollutant as well as the sulfur mass balance. The oxygen supplied to the aeration unit and the inlet H_2S ratio (O_2/H_2S $_{supplied}$), calculated according to **Equation 18**, corresponded to a molar ratio of 43 mol $O_2 \cdot$(mol S-H_2S)$^{-1}$ during experiments **E1** and **E2**, and from 43 to 7.4 mol $O_2 \cdot$(mol S-H_2S)$^{-1}$ during experiment **E3**.

8.4 Results and discussion

8.4.1 Effect of CH$_3$SH in biogas desulfurization

The calculation of the EC at the end of each pseudo steady-state period (**Figure 8.1**) during stepwise concentration increases along **E1** showed that the critical CH$_3$SH EC was 0.51 g S-CH$_3$SH·m^{-3}·h^{-1}. Maximum EC of 1.68 g S-CH$_3$SH·m^{-3}·h^{-1} was reached. Maximum ECs in the range of 3 to 25.6 g S-CH$_3$SH·m^{-3}·h^{-1} previously reported (Ruokojarvi *et al.*, 2001; Hartikainen *et al.*, 2002; Caceres *et al.*, 2010), indicated that a larger microbiological activity could be still developed, with greater adaptation to CH$_3$SH removal.
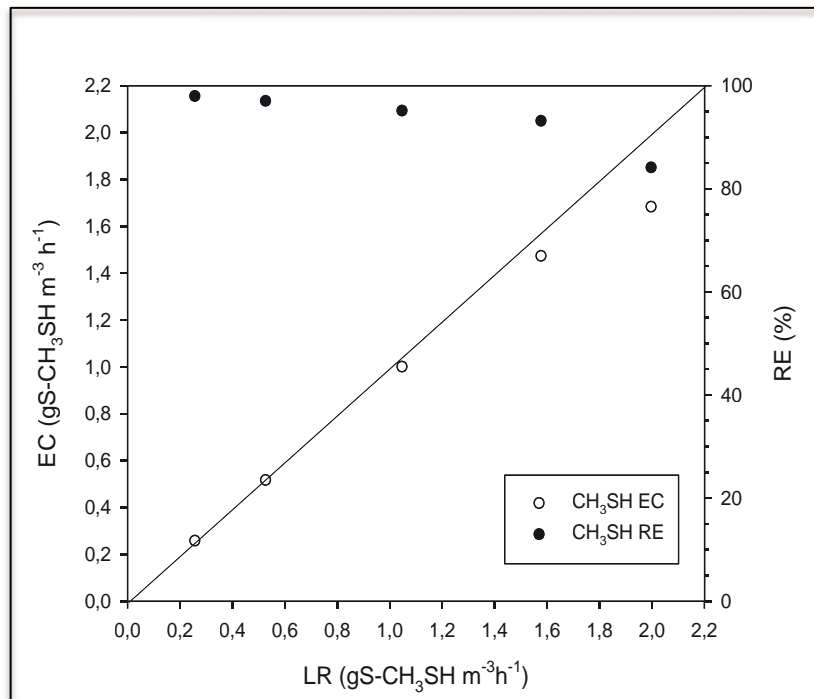
Figure 8.1 EC and RE *versus* CH$_3$SH LR during E1

No detrimental effect over the desulfurization of H$_2$S was observed by the presence of CH$_3$SH since the H$_2$S RE was kept around 99% during the complete **E1** experiment. Furthermore, a beneficial effect on H$_2$S desulfurization was found by the presence of CH$_3$SH at the studied concentration range that led to a clear reduction on the accumulated biosulfur inside the reactor bed, as discussed later on **Section 8.4.3**.

8.4.2 Effect of the gas contact time

The effect of EBRT was studied at constant (**E2**) and variable (**E3**) H_2S LR. Results of both experiments showed a larger impact in the RE of CH_3SH in comparison with **E1** results. During **E2**, the RE of CH_3SH gradually decreased from 100% to 47% (**Figure 8.2**). Maximum EC of 1.0 g $S\text{-}CH_3SH\cdot m^{-3}\cdot h^{-1}$ was obtained. In comparison to **E1**, results obtained during **E2** indicated that the significant reduction in the RE and EC of CH_3SH was probably caused by mass transfer limitation under the experimental conditions tested, mainly at lower EBRTs.
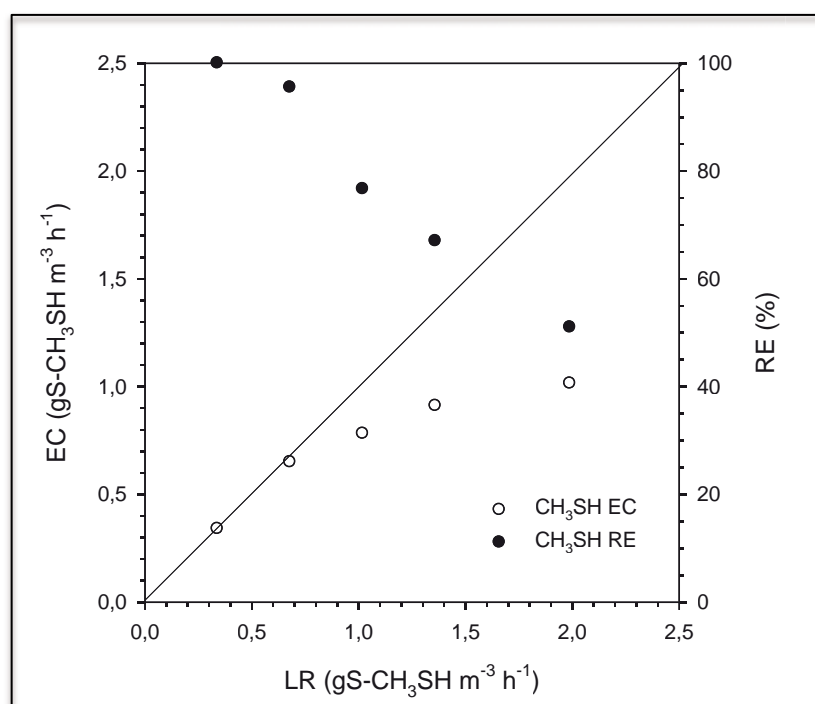
Figure 8.2 EC and RE versus CH_3SH LR during E2

Results herein presented are compared to the results obtained by an anoxic BTF (not shown), under similar conditions, but packed with PU foam cubes (Montebello *et al.*, 2012). Although PU foam is a well-known packing material in biofiltration, with large surface areas that may help reducing mass transfer limitations (Gabriel and Deshusses, 2003b), clogging problems have been also reported to occur due to biosulfur build-up and accumulation into the packed bed (Fortuny *et al.*, 2008). In addition, high

gas velocities of around 6,000 m·h^{-1} were found to contribute to reducing H$_2$S mass transfer limitations (Gabriel and Deshusses, 2003). In this sense, Kim and Deshusses, (2005) studied, among other parameters, the TLV in a BTF packed with PU foam and concluded that under low gas flow rates (under 4,000 m·h^{-1}), mass transfer from the gas phase to the liquid phase was the limiting factor and the recirculation rate had no effect on H$_2$S EC.

Thus, results obtained during **E2** indicated that no special advantage was found for PU foam in the anoxic reactor (Montebello *et al.*, 2012) in front of Pall rings, used in the aerobic BTF described in this thesis, in terms of mass transfer improvement for CH$_3$SH removal, confirming that the specific surface area of the packing material is not that important in terms of mass transfer in desulfurizing BTFs because they are commonly operated at much larger EBRTs if compared to BTFs for odor removal. During **E2**, the H$_2$S EC was less affected than the CH$_3$SH EC by the reduction of EBRT (**Figure 8.3**), because of the progressive decrease of the H$_2$S inlet concentration and the reduced solubility reported for CH$_3$SH in comparison to H$_2$S (Sander, 1999). RE of H$_2$S decreased from 100% to 95% during **E2**.
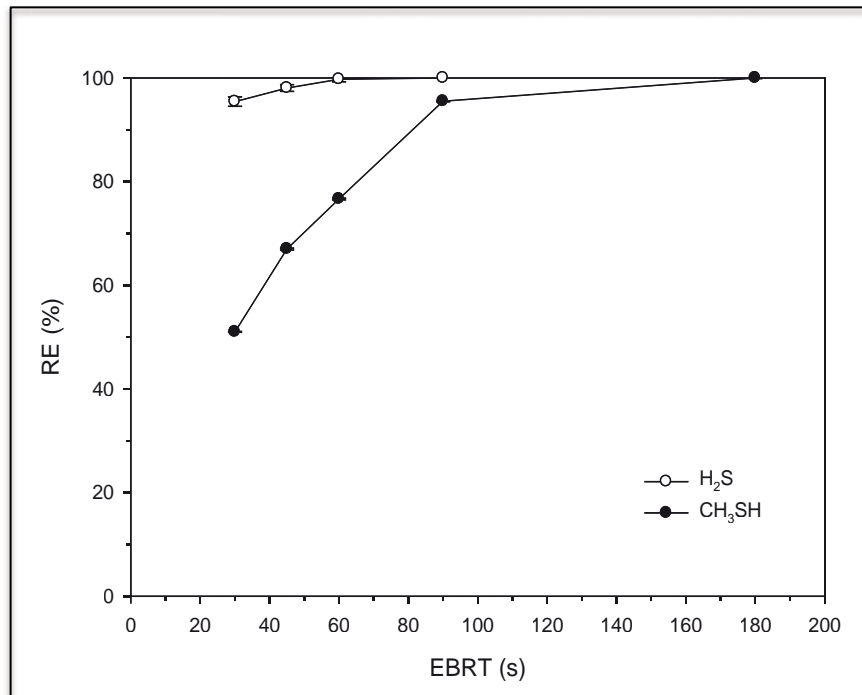
Figure 8.3 EC of H$_2$S and CH$_3$SH *versus* EBRT during E2

It is interesting to notice that such H_2S RE above 95% achieved at the lowest EBRT studied (30 s) corresponded to the inlet H_2S concentration of 342 ppm_v of H_2S, a commonly found H_2S concentration in some reported biogas streams (**Table 2.5**). In addition, critical EBRT was found at 60 s. Therefore, almost 700 ppm_v of H_2S can be treated efficiently (RE > 98%) under the studied conditions at 60 s of gas contact time.

Few references exist on the co-treatment of H_2S and CH_3SH in BTFs. Co-treatment of these compounds has been carried out for odor treatment (65 – 220 ppm_v of H_2S and 26 – 47 ppm_v of CH_3SH) in two-stage BTFs connected in series (Ruokojarvi *et al.*, 2001; Ramirez *et al.*, 2011). Generally, the first stage at acidic pH removes most of the H_2S, small amounts of CH_3SH and other VOSCs. The second step, at neutral pH, removes the rest of VOSCs. Maximum ECs of 47.9 g $S\text{-}H_2S \cdot m^{-3} \cdot h^{-1}$ and 2.75 g $S\text{-}CH_3SH \cdot m^{-3} \cdot h^{-1}$ were reported by Ruokojarvi *et al.* (2001) at EBRTs of 61 and 118 s per stage. Ramírez *et al.* (2011) obtained maximum ECs of 70.6 g $S\text{-}H_2S \cdot m^{-3} \cdot h^{-1}$ and 9.8 g $S\text{-}CH_3SH \cdot m^{-3} \cdot h^{-1}$ at EBRT of 60 s. Same authors (Ramírez *et al.*, 2011) also tested the co-treatment of H_2S, CH_3SH and other VOSC at neutral pH and found a decrease in the RE of CH_3SH from 83 to 33% when the H_2S inlet concentration was increased from 23 to 376 ppm_v of H_2S, for a CH_3SH inlet load of 2.4 g $S\text{-}CH_3SH \cdot m^{-3} \cdot h^{-1}$. It is known that H_2S is removed preferentially than other RSCs under aerobic conditions (Wani *et al.*, 1999).

During **E3**, the effect of a variable H_2S LR due to the decrease of the EBRT was clearly noticed by the impact on the EC of CH_3SH encountered, if compared to **E2** , as shown in **Figure 8.4**. The RE of CH_3SH was reduced from 100% to 16%. Interestingly, the EC-LR profile did not follow the profile typically reported in which the EC reaches a *plateau* at high pollutant loads (Devinny *et al.*, 1999). Instead, a maximum is observed close to the critical EC value. Later, a progressive decrease of the EC was found as the LRs of both pollutants increased. A similar behaviour was observed by Ramírez *et al.* (2011), with a decreasing in the RE of CH_3SH from 83% to 33% when

the H_2S concentration was increased from 23 to 376 ppm_v of H_2S. Thus, the high H_2S LR produced a crossed, negative effect in the removal of CH_3SH.
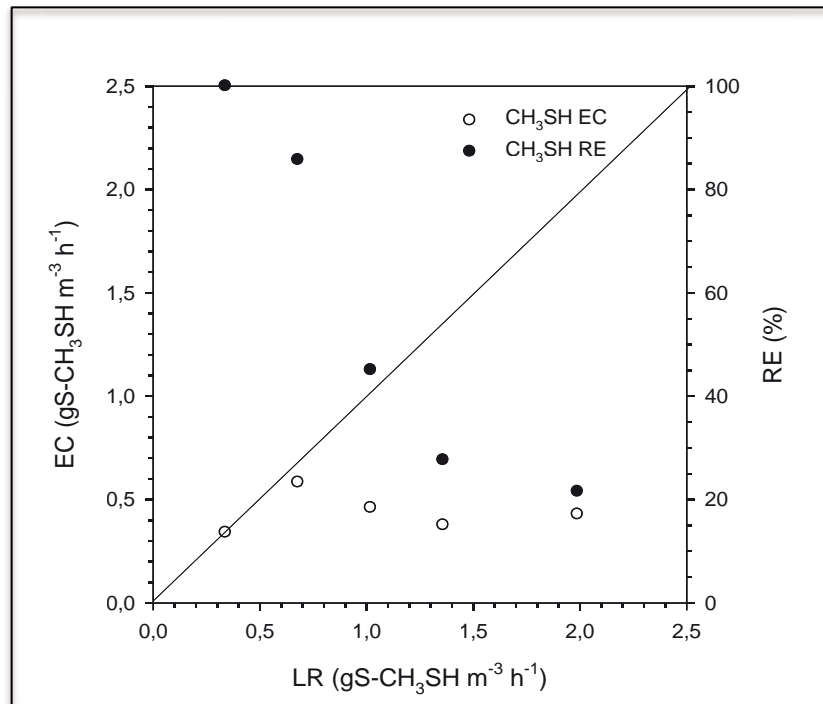
Figure 8.4 EC and RE versus CH_3SH LR during E3

It is worth observing that during the last EBRT period (30 s) in **E3**, the DO concentration measured dropped down to values close to zero, thus indicating that the system was under O_2 limiting conditions for the complete H_2S oxidation to SO_4^{2-}. Instead, partial oxidation to S^0 occurred, which cannot be verified through mass balances because of the insufficient duration of the experiment (total 7.5 h) when compared to the HRT (9 h). At this point, the air supply was increased from 250 mL·min^{-1} to 313 mL·min^{-1} in an attempt to improve the H_2S removal efficiency, but no significant changes were observed, probably because of the mismatched dynamics between the gas (EBRT = 180 – 30 s) and the liquid phase (HRT = 9 h).

As expected, the effect of the EBRT reduction during **E3** on the removal of H_2S was considerably significant, as shown in **Figure 8.5**. The RE of H_2S was sharply reduced from 100% to 31%.
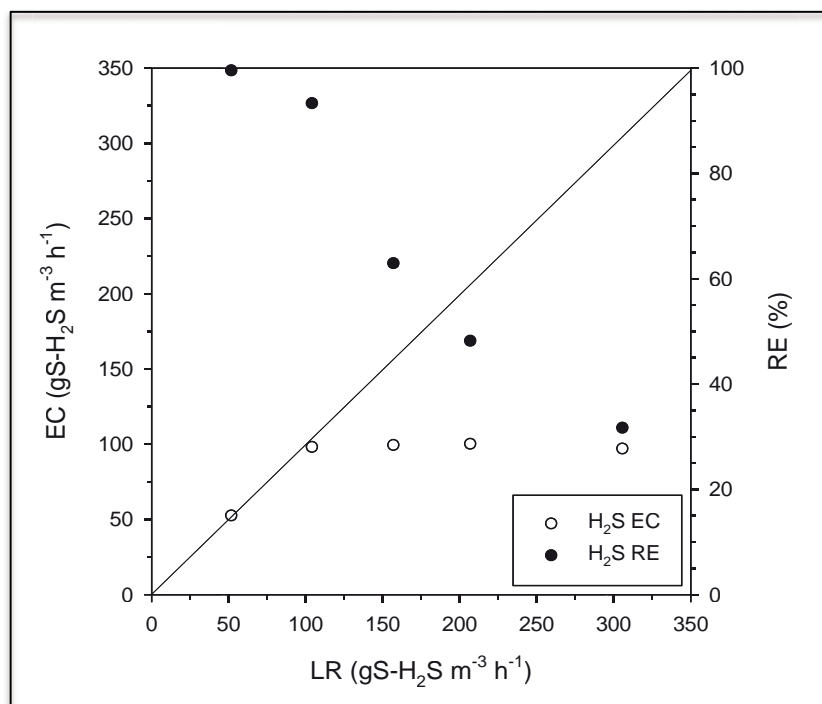
Figure 8.5 EC and RE *versus* H_2S LR during E3

Despite of the differences between the HRT and the duration of the experiment, data obtained from ORP monitoring indicated a reduction in ORP from 30 mV (at 180 s, LR of 53 g S-H_2S·m^{-3}·h^{-1}) to -80 mV (at 30 s, LR of 306 g S-H_2S·m^{-3}·h^{-1}). According to Montebello at al. (2010) and Fortuny *et al.* (2011), such final ORP value suggests almost no TDS accumulation in the liquid phase and, thus, that mass transfer was the main limiting process.

Monitoring of TDS indicated concentrations below the limit of detection ($1.5 \times 10^{-5} \pm 0.9 \times 10^{-5}$ mol S-S^{2-}·L^{-1} ; 0.48 ± 0.29 mg S-S^{2-}·L^{-1}). The critical and maximum EC of H_2S during **E3** was found around 100 g S-H_2S·m^{-3}·h^{-1}. The EC and RE of H_2S are comparable to the results obtained previously by Fortuny *et al.* (2011) under similar experimental conditions with a different packing material, confirming that CH_3SH did not have any detrimental effect on the removal of H_2S under the range of conditions tested. After the experimental period, normal operating conditions were resumed and the RE of H_2S quickly recovered normal values (around 99%), confirming the high recovery capacity of the BTF (Fortuny *et al.*, 2008; Montebello *et al.*, 2010).

At this point, it is difficult to confirm the cause of such negative effect in the EC of CH_3SH due to the H_2S LR increase. Since H_2S is an intermediate product of the biological CH_3SH oxidation (Smet *et al.*, 1998; Bentley and Chasteen, 2004), the biological oxidation of H_2S is preferred by microorganisms over CH_3SH. However, the higher O_2 requirements for the biological oxidation of CH_3SH (**Equation 34**) in comparison with the O_2 requirement for H_2S biological aerobic oxidation (**Equation 9**) may have also influenced the results under aerobic conditions and, probably, also under anoxic conditions (Montebello *et al.*, 2012). Since microorganisms involved in CH_3SH and H_2S removal are not totally identical, further research is needed to identify the microbial populations in the reactor as well as their degradation activities, to understand the underlying mechanisms observed. The reactor was at some point limited by the electron acceptor availability to end up with SO_4^{2-} as the final product of H_2S oxidation. Thus, improving the electron acceptor supply is warranted to reduce biosulfur accumulation in the packed bed (Rodriguez *et al.*, 2013).

Critical EBRT for the removal of H_2S during **E3** was found around 120 s, as shown in **Figure 8.6**, which is significantly higher than during **E2**.
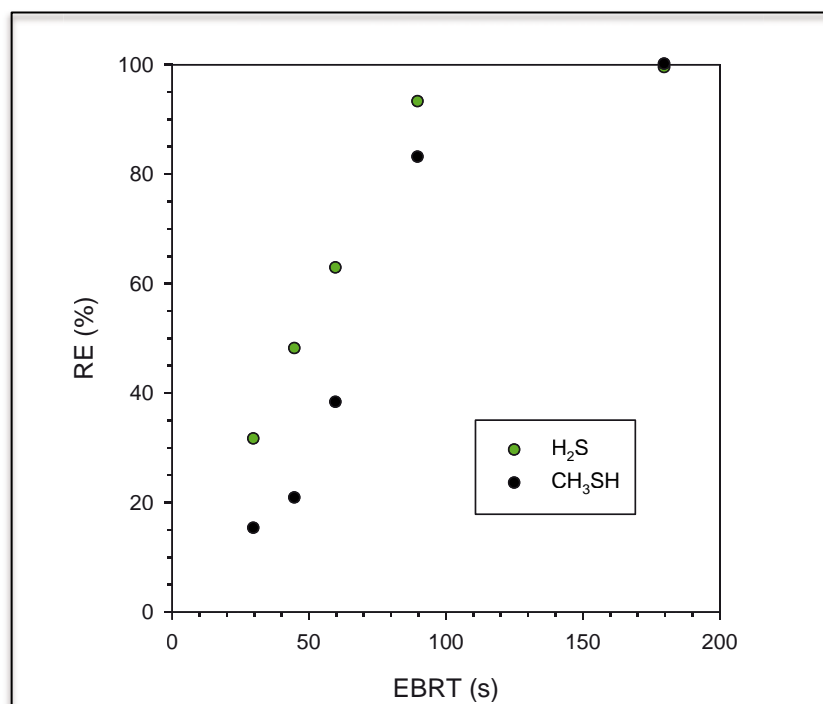
Figure 8.6 RE of H_2S and CH_3SH versus EBRT during E3

Overall, results obtained during EBRT reduction experiments indicated that the reactor was capable of treating H$_2$S at a LR as high as 100 g S-H$_2$S·m^{-3}·h^{-1} at a gas contact time of around 120 s. The obtained EC of around 100 g S-H$_2$S·m^{-3}·h^{-1} at EBRT of 90 s corresponded to a slight reduction in the RE of H$_2$S to approximately 95%, suggesting that for EBRT values lower than 90 s, mass transfer limitation is the main restriction for the simultaneous removal of CH$_3$SH and H$_2$S at the tested conditions. However, such high H$_2$S LR had a detrimental effect over CH$_3$SH removal.

8.4.3 Sulfur mass balance

A sulfur mass balance was performed by substraction (Janssen *et al.*, 1997), allowing estimating the quantity of biosulfur produced. Sulfur mass balance during **E1** is shown in **Figure 8.7**. For mass balances calculation, it was assumed that the only final products were S^0 and SO$_4^{2-}$, since DMDS, the sole by-product formed by the chemical reaction between CH$_3$SH and biosulfur particles at neutral pH, is further biologically oxidized to SO$_4^{2-}$.
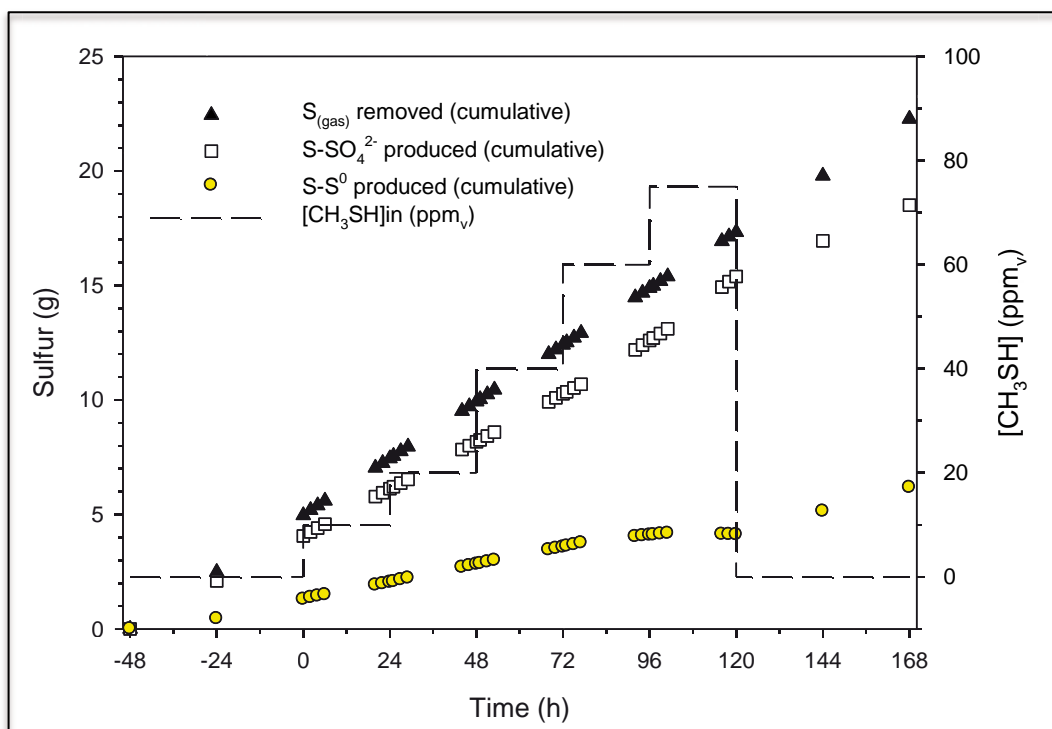
Figure 8.7 Sulfur mass balance during E1

Sulfur mass balance calculation was performed as described by **Equation 21**. Results during **E1** shown that the pS-S^0 was kept almost stable during the first three CH$_3$SH concentration steps (around 1.86 g S-S^0·m^{-3}·h^{-1}), resulting in a SO$_4^{2-}$ selectivity of around 80% (**Figure 8.7**). Interestingly, the pS-S^0 was reduced to 1.55 g S-S^0·m^{-3}·h^{-1} during the last steps, leading to an increase in the SO$_4^{2-}$ selectivity up to 90%. Such results indicated that during the higher CH$_3$SH LR periods the consumption of biosulfur by chemical reaction with CH$_3$SH probably occurred according to the batch tests performed under neutral pH (6.8 – 7.0) (Montebello *et al.*, 2012). It can be deduced that the biological oxidation of DMDS, produced by the chemical reaction between CH$_3$SH and biosulfur (**Equation 35**) was the reason for the increase on the SO$_4^{2-}$ production observed at the end of experiment **E1**. After the experimental period, the production rate of biosulfur was restored to the initial values.

Also, the visual evidence of the reduction of accumulated biosulfur inside the reactor confirmed the consumption of biosulfur by chemical reaction with CH$_3$SH. Such observations indicated that the presence of CH$_3$SH favours the reduction of the amount of biosulfur that generally accumulates in highly-loaded H$_2$S desulfurizing systems, even if artificial feeding of CH$_3$SH cannot be considered as an economically viable alternative to prevent clogging of the filter bed. Results from a full-scale BTF (Tomas *et al.*, 2009) treating a biogas flowrate of around 80 m^3·h^{-1} under the same conditions studied herein, indicated that the annual cost of externally added CH$_3$SH is as high as three times the initial investment cost of the BTF. Nonetheless, the natural presence of CH$_3$SH in biogas could be considered as a technical advantage during the biogas desulfurization in BTFs. Finally, it is worth noticing that no CH$_3$SH or other mercaptans and polysulfides were fed to the reactor prior to the experiment, which confirms that SOB developed in the studied BTF were capable of degrading CH$_3$SH or any of the chemical reaction by-products and that no further inoculation of the system was needed.

8.5 Conclusions

Overall, results showed that the co-treatment of H_2S and CH_3SH is feasible in aerobic biotrickling filters, with no detrimental effects in H_2S removal under the typical concentrations of CH_3SH found in biogas. Oppositely, a beneficial effect was found on the performance of the reactor due to the chemical reaction of CH_3SH with elemental sulfur, enhancing the overall reactor performance, by minimization of the effects of sulfur accumulation inside the filter bed.

The reactor was able to treat CH_3SH without prior inoculation because of the already existing sulfide-oxidizing microorganisms grown during H_2S treatment. However, H_2S LR above 100 g $S\text{-}H_2S \cdot m^{-3} \cdot h^{-1}$ has a negative impact in the CH_3SH treatment capacity mainly caused by substrate competition. The EBRT was parameterized either for H_2S and CH_3SH as main pollutants in biogas desulfurization. According to the results, the EBRT at which the H_2S-desulfurizing aerobic BTF was sized (180 s) provided adequate results in terms of CH_3SH and H_2S treatment. Moreover, results obtained during the experiments presented in this Chapter were compared to an anoxic biotrickling filter, similarly operated by others (results not shown), according to Montebello *et al.* (2012), indicating that also under anoxic conditions, BTFs are capable to cope with the desulfurization of biogas. Overall, no significant differences were found in terms of global desulfurizing capacity between the two systems (aerobic and anoxic BTFs) because of the different applied packing material – PU foam in the case of the anoxic BTF.

※

9

acidic H$_2$S biotrickling filtration

"It's the most righteous, which of course
is not the same thing as the most profitable."

Nikolai V. Gogol
(Sorochyntsi, 1809 – Moscow, 1852)

9 Acidic H$_2$S biotrickling filtration

9.1 Summary and scope

The complete long-term operation of the studied BTF under acidic pH conditions (2.50 < pH < 2.75), from day 600 to 990 of operation is presented in this Chapter. Previous operation at acidic pH, from day 440 to 600 of operation was reported in **Chapter 7**, as well as the initial 440-days period at neutral pH conditions (6.0 < pH < 6.5) and the performed gradual, uninterrupted transition to acidic pH. The effect of the EBRT reduction and the effect of the increase of the H$_2$S LR were investigated under steady-state at acidic pH conditions.

The EBRT was gradually reduced down to 33 s. The critical EBRT was found at 75 s, corresponding to a critical EC of 100 g S-H$_2$S·m^{-3}·h^{-1}. The maximum EC, obtained during the LR increasing experiment, was 220 g S-H$_2$S·m^{-3}·h^{-1}. Additionally, the oxidation rate of biologically produced elemental sulfur (biosulfur) accumulated inside the filter bed was assessed by discontinuing the H$_2$S gas feeding, during periodical H$_2$S starvation episodes. Moreover, the H$_2$S removal profile along the filter bed was also assessed at 1/3, 2/3 and 3/3 of the filter bed height. Results indicated that the first third of the filter bed (bottom section) was responsible for 70 to 80% of the total H$_2$S removal. Biosulfur oxidation to sulfate was suggested as interesting sulfur clogging control strategy under acidic operating conditions. Overall, biotrickling filter performance under acidic pH conditions was comparable to that under neutral pH conditions, in terms of overall desulfurizing capacity of the system, even if a significant quantity of biosulfur was produced under acidic pH.

The aim of the work presented in this Chapter was to investigate the impact of the H$_2$S load and the gas contact time in the performance of a well-established aerobic biotrickling filter, operated at long-term under acidic

pH conditions, during the desulfurization of synthetic biogas. The effect of H$_2$S periodical starvation was also investigated as a simulated real-operation episode and as possible sulfur clogging control strategy. Also, the H$_2$S removal profile along the filter bed height was studied. Results were compared to previously reported studies under neutral pH conditions.

❦

9.2 Introduction

Acidic pH conditions have been successfully employed in the treatment of low and high H_2S loading rates (LR) in BTFs, applying mainly SOB from the genus *Acidithiobacillus*, with pH values between 1 and 4 (Sercu *et al.*, 2005; Lee *et al.*, 2006; Aroca *et al.*, 2007; Chaiprapat *et al.*, 2011; Manucci *et al.*, 2012). Several studies indicate that *Thiobacillus* sp. and *Acidithiobacillus* sp. are the most frequently applied SOB in H_2S biofiltration at neutral and acidic pH conditions, respectively (Robertson and Kuenen, 2006). According to **Equation 8**, **Equation 9** and **Equation 10**, the production of SO_4^{2-} or S^0 is directly related to the DO availability. Different DO limiting conditions have been reported to occur in a highly loaded BTF operating under neutrophilic conditions (Fortuny *et al.*, 2010). Recently, 5% of biologically produced elemental sulfur (biosulfur) was reported to be produced during acidic biotrickling filtration of up to 100 ppm_v of H_2S (Mannucci *et al.*, 2012). Higher amounts of biosulfur have been found (34%) during the treatment of 2,000 to 12,000 ppm_v of H_2S under acidic pH (Aroca *et al.*, 2007).

At laboratory scale, the system performance is normally assessed under steady-state conditions and neither interruptions nor significant alterations on the operating conditions are studied, limiting thus the applicability of the obtained results when facing real industrial operational fluctuations. In the removal of H_2S, a few studies have been reported investigating the effect of transient-state conditions, such as H_2S starvation episodes in biofilters (Wani *et al.*, 1998; Romero *et al.*, 2013) and BTFs at odor levels (Zhang *et al.*, 2009; Namini *et al.*, 2012).

Consumption of the biosulfur accumulated inside the filter bed during H_2S starvation period has been already proposed by Fortuny *et al.* (2010) as sulfur clogging control strategy under neutrophilic conditions. However, no literature was found regarding biosulfur consumption at acidic pH for high-loaded H_2S gas streams. Under acidic pH conditions, the stratification of the

filter bed has been studied during H_2S removal at odor level (Lafita *et al.*, 2012). Moreover, the H_2S removal profile along the filter bed was studied by Ramirez *et al.* (2009b) for low to moderate H_2S LRs. However, no literature is available regarding the removal profile of H_2S at high H_2S LR, as in the present study.

9.3 Materials and methods

9.3.1 Operational and experimental conditions

Reference operating conditions in the long-run operation were adopted according to Table 4.1, which corresponded to an EBRT of 130 s and H_2S LR of 52.28 g S-$H_2S\cdot m^{-3}\cdot h^{-1}$, at 2,000 ppm$_v$ of H_2S in the inlet synthetic biogas. The pH was controlled in the range of 2.50 to 2.75. After 249 days of steady operation under acidic pH, corresponding to 689 days of the total reactor operation, three experiments were performed (**E1**, **E2** and **E3**), as shown in **Table 9.1**. During the experiments herein reported, a TLV of 7 m·h^{-1} and a HRT of 9 h were applied.

During experiment **E1**, the EBRT was stepwise decreased from 130 to 33 s, keeping each EBRT value for 1 h, while the inlet H_2S concentration in the synthetic biogas was kept unaltered (2,000 ppm$_v$ of H_2S). Thus, the H_2S LR indirectly increased from 52.28 up to 262.54 g S-$H_2S\cdot m^{-3}\cdot h^{-1}$ as a consequence of the EBRT reduction. During experiment **E2**, at a constant EBRT of 130 s, the inlet H_2S concentration in the biogas was stepwise increased from 2,000 to 10,000 ppm$_v$ of H_2S, resulting in H_2S LRs from 52.28 to 262.54 g S-$H_2S\cdot m^{-3}\cdot h^{-1}$. Each concentration step was kept for 24 h. Besides the normal continuous outlet H_2S monitoring at the G 3/3 gas outlet port (top section), periodic determination of H_2S at G 1/3 (bottom section) and G 2/3 (middle section) of the filter bed height was also performed to assess the EC and RE as well as the sulfur mass balance in the reactor during each experiment, to discern the H_2S removal profile along the filter bed height.

Table 9.1 Experimental conditions at acidic pH

Exp	[H$_2$S]$_{biogas}$ (ppm$_v$)	H$_2$S LR (gS·m^{-3}·h^{-1})	O$_2$/H$_2$S [a] (v·v^{-1})	EBRT (s)	Duration (h)	Previous operation [b] (day)
E1	1,999.99 ± 0.31	52.28	41.20	130	1	249
		104.44	20.62	76	1	
		155.39	13.86	54	1	
		206.39	10.44	42	1	
		263.09	8.19	33	1	
E2	1,999.53	52.28	41.20		24	250
	4,000.44	104.80	20.55		24	
	6,000.34	157.51	13.67	130	24	
	7,999.91	209.93	10.26		24	
	10,000.02	262.54	8.20		24	
E3-1	0	–	–	–	168	256
E3-2	0	–	–	–	192	385
E3-3	0	–	–	–	336	453
E3-4	0	–	–	–	192	491
E3-5	6,000.34	157.51	13.67	130	168	521
	10,000.02	262.54	8.20	130	96	529
E3-6	0	–	–	–	408	533

[a] Aeration flow was kept unaltered during H$_2$S starvation experiments (312.50 mL·min^{-1}).

[b] Days from the beginning of the operation at acidic pH (after 440 days at neutral pH).

Experiment **E3** was subdivided into 6 different experiments. **E3-1**, initiated immediately after the end of **E2**, consisted in the interruption of the H$_2$S feeding during 7 days, while keeping other operational conditions unaltered. Similar experimental conditions were applied during **E3-2**, **E3-3**, **E3-4** and **E3-6**, with duration of 8, 14, 8 and 17 days, respectively. Differently, **E3-5** consisted in the simulation of a sudden increase in the inlet biogas concentration from 2,000 to 6,000 and 10,000 ppm$_v$ of H$_2$S during a total 10-days period. Applied H$_2$S LR was 157.51 g S-H$_2$S·m^{-3}·h^{-1} during 6

days (6,000 ppm$_v$ of H$_2$S) followed by 262.54 g S-H$_2$S$\cdot$m$^{-3}\cdot$h^{-1} during the next 4 days (10,000 ppm$_v$ of H$_2$S). Experiment **E3-6**, the last starvation period studied, was initiated immediately after **E3-5**. The frequency of starvation experiments, which represents the time period between experiments, varied from 23 to 122 days, as can be deduced from the diverse previous operation period detailed in **Table 9.1** for each experiment.

9.4 Results and discussion

9.4.1 Effect of the gas contact time

The effect of the EBRT reduction over the reactor performance is commonly studied in BTFs (Sercu *et al.*, 2005; Lee *et al.*, 2006; Ramirez *et al.*, 2009; Chaiprapat *et al.*, 2011; Fortuny *et al.*, 2011; Montebello *et al.*, 2012). In this study, the EBRT was gradually reduced from the reference value of 130 s down to 33 s during **E1**.

Data of on-line monitoring of DO and ORP during **E1** are shown in **Figure 9.1**, alongside with the calculated H$_2$S RE. Also, a discontinuous DO measure was performed in the liquid purge line of the main reactor. The comparison between available DO at the recirculation line (DO$_{in}$) and the DO present at the purge line (DO$_{out}$) allowed estimating the consumed DO as a consequence of the microbial activity inside the filter bed. However, the observed consumed DO must be considered as a qualitative figure, because steady state is not reached after each operational alteration. The estimated consumption of O$_2$ during experiment **E1** was found to be around 3 mg O$_2\cdot$L^{-1}, (0.15 mg O$_2\cdot$L$^{-1}\cdot$min^{-1}) for each experimental step, suggesting that microbial activity was not a limiting process. Instead, O$_2$ transfer was found to be the main limiting process, which is in agreement with other reported studies at comparable experimental conditions (Montebello *et al.*, 2010; Fortuny *et al.*, 2011).
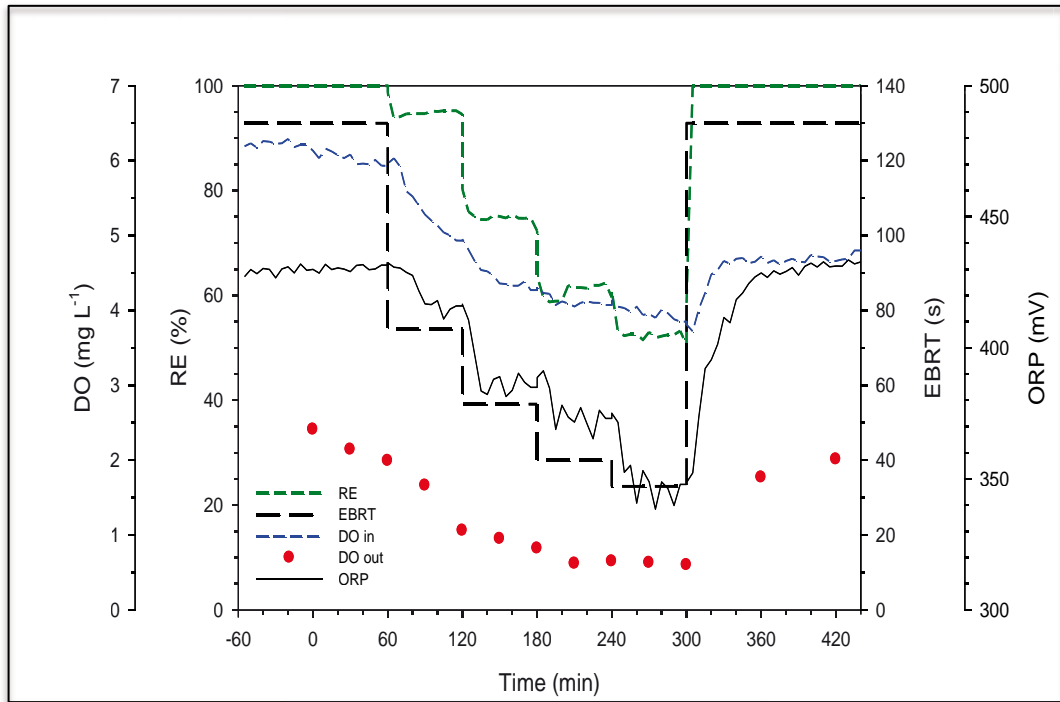
Figure 9.1 DO, RE, EBRT and ORP during E1

The monitored ORP profile during **E1** shown a gradual decline from the reference value of 430 mV (at EBRT of 130 s) down to 350 mV (at EBRT of 33 s). Once the reference conditions were resumed, after **E1**, values of ORP monitoring rapidly recovered the normal reference operating value. The H$_2$S RE during **E1** gradually dropped from 100%, at the reference EBRT of 130 s, to 55% at 33 s.

The assessment of the maximum EC as well as the critical EBRT provides interesting data for bioreactor design, operation and modeling. Both parameters were assessed during experiments **E1** and **E2**. Results indicated that during **E1**, critical and maximum ECs were around 100 and 140 g S-H$_2$S·m^{-3}·h^{-1}, respectively, as shown in **Figure 9.2**. The critical EBRT, at which the critical EC is found, was around 75 s. Recently, Chaiprapat *et al.* (2011) reported a reduction of the H$_2$S RE from 80 – 90% to 30 – 40% when the EBRT was reduced from 313 to 78 s in a full-scale biotrickling filter at acidic pH (1 < pH < 4.5) treating biogas containing around 2,000 ppm$_v$ of H$_2$S. The negative effect of the reduction of EBRT was related to the low solubility of both H$_2$S and specially O$_2$ under the studied conditions.
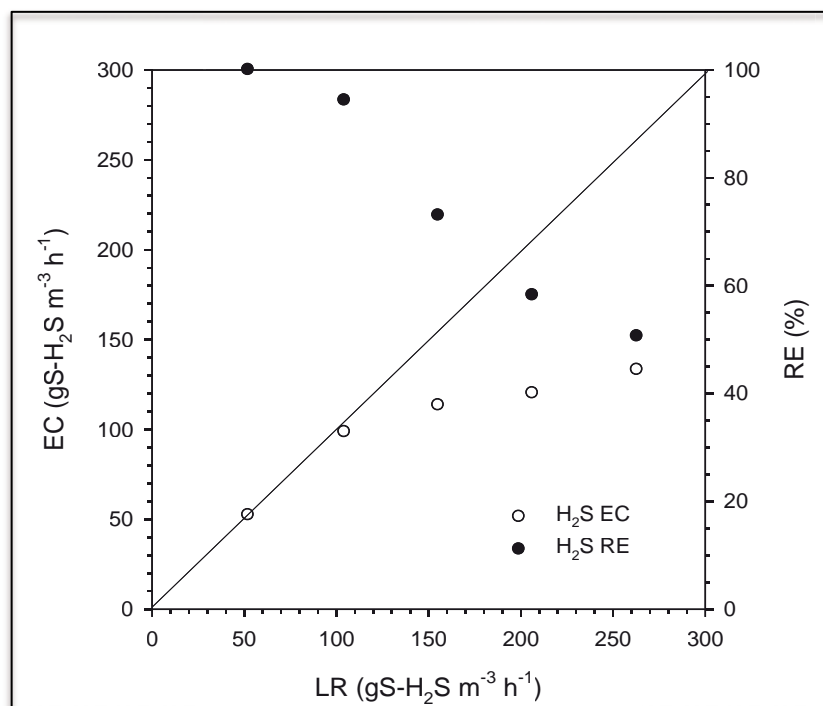
Figure 9.2 EC and RE versus LR during E1

The average SO_4^{2-} selectivity, calculated according to **Equation 25**, was found to be around 92% (for H_2S LR = 52.28 g S-$H_2S \cdot m^{-3} \cdot h^{-1}$) during the steady-state operation at acidic pH, before the experiments herein reported (from day 440 to 689 of operation). Under neutral pH operation (**Chapter 5**), a higher SO_4^{2-} selectivity (100% for H_2S LR = 51.08 g S-$H_2S \cdot m^{-3} \cdot h^{-1}$) was found by Montebello *et al.* (2010), using a structured rigid packing material under equivalent operating conditions. Same authors obtained a SO_4^{2-} selectivity of 55 – 59% at a LR of 215.30 g S-$H_2S \cdot m^{-3} \cdot h^{-1}$. In both experiments herein reported (**E1** and **E2**), mass balance results indicated that at the higher H_2S LR (around 263 g S-$H_2S \cdot m^{-3} \cdot h^{-1}$), the production of biosulfur was approximately as high as the production of SO_4^{2-}, resulting in a SO_4^{2-} selectivity of around 50%, as shown in **Figure 9.3** for **E2**.

Thus, despite no loss in the RE was found at acidic pH, a larger biosulfur production was found at acidic pH compared to that at neutral pH using the same packing material (**Chapter 7**). In addition, results from the total acidic operation period (550 days) showed an important gradual loss in the SO_4^{2-} production, even if the H_2S RE remained at 100%. At reference conditions

under acidic pH, the average SO$_4^{2-}$ selectivity ranged from 84 to 55% during the long-term operation. Reasons behind such loss of SO$_4^{2-}$ production capacity remained unknown and need of further research. Probably one of the reasons for such high biosulfur production found at acidic pH is the deterioration of the packing material elements, as visually verified during biomass sampling procedures, as commented later on Section **9.4.4**. Also, it must be considered that the SO$_4^{2-}$ selectivity calculation, according to **Equation 25**, does not take into account the presence of biomass and other solids than S^0, such as metallic salts formed by leached minerals from oxidized packing elements, which certainly incremented the observed biosulfur accumulated inside the reactor bed.

9.4.2 Effect of the H$_2$S loading rate

The RE during experiment **E2** dropped from 100% at the reference LR (52.28 g S-H$_2$S·m^{-3}·h^{-1}) to 85% at the highest LR experimented (262.54 g S-H$_2$S·m^{-3}·h^{-1}) as shown in **Figure 9.3**.
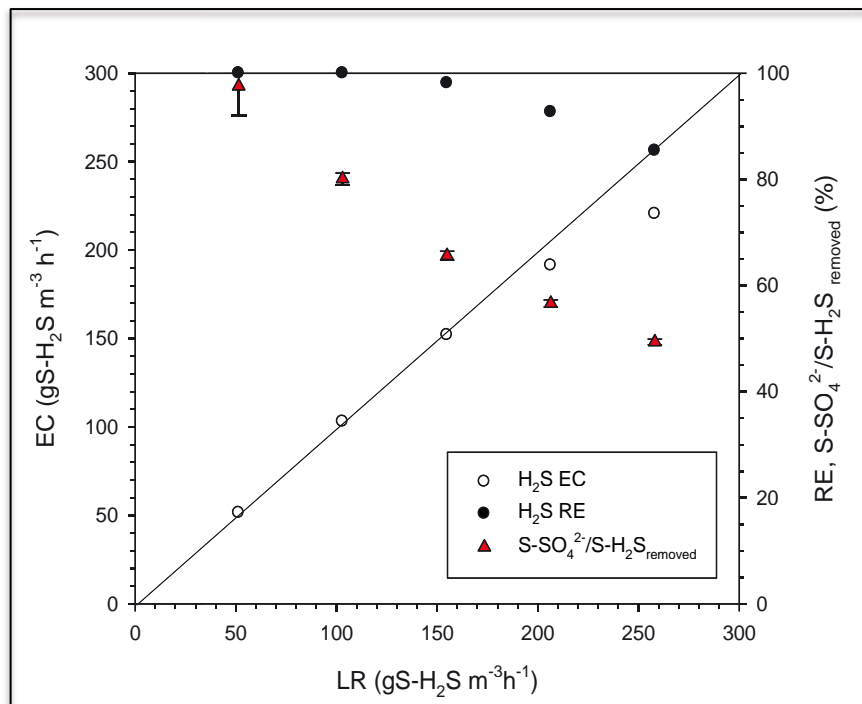
Figure 9.3 EC, RE and SO$_4^{2-}$ selectivity *versus* LR during E2

During **E2**, critical and maximum ECs were around 160 and 220 g S-$H_2S \cdot m^{-3} \cdot h^{-1}$, respectively. EC is considerably higher than the obtained in experiment **E1**, probably because of the mass transfer limitation at reduced EBRTs. SO_4^{2-} selectivity was of around 95% at the beginning of the **E2** and was gradually decreased down to around 50% at the end of the experiment.

The maximum EC obtained in the present study (220 g S-$H_2S \cdot m^{-3} \cdot h^{-1}$) is comparable to that reported by Chaiprapat *et al.* (2011), who obtained a maximum EC of 256 g S-$H_2S \cdot m^{-3} \cdot h^{-1}$, using coconut fiber as packing material. Comparable results were also published by Tomás *et al.* (2009), who obtained a maximum EC of 170 g S-$H_2S \cdot m^{-3} \cdot h^{-1}$, using plastic Pall rings as packing material in a full-scale biotrickling filter under comparable operational conditions. The highest value of maximum EC reported for acidic biotrickling filtration of high loads of H_2S is 370 g S-$H_2S \cdot m^{-3} \cdot h^{-1}$ (Aroca *et al.*, 2007) treating inlet H_2S concentrations ranging from 2,000 to 12,000 ppm_v of H_2S at an EBRT of 45 s, with a pH from 1.8 to 2.5 and using polyethylene rings as packing material.

Critical ECs as obtained in the present study (160 g S-$H_2S \cdot m^{-3} \cdot h^{-1}$) have been previously reported by others (Lee *et al.*, 2006) in a BTF inoculated with *Acidithiobacillus thiooxidans* over a porous ceramic packing material. Desulfurization of 200 to 2,200 ppm_v of H_2S at 18 to 6 s of EBRT indicated that the gas contact time is more influential than the inlet concentration. Also, O_2 transport from gas to liquid phase was considered the main limiting process.

Overall results obtained during the long-term operation at acidic pH and herein presented were comparable to those obtained during the previous operation of the same reactor at neutral pH conditions (**Chapter 7**), as reported by Fortuny *et al.* (2011) and Montebello *et al.* (2012). No significant differences were found in terms of desulfurizing capacity of high loads of H_2S (2,000 to 10,000 ppm_v of H_2S / 50 to 260 g S-$H_2S \cdot m^{-3} \cdot h^{-1}$) at neutral and acidic pH under the studied conditions.

9.4.3 H₂S removal profile throughout the bed

The H$_2$S elimination profile along the filter bed height during **E1** is shown in **Figure 9.4**. The RE was calculated at three filter bed heights (gas ports G1/3, G2/3 and G3/3), corresponding to the bottom, middle and top sections of the filter bed. During **E1**, the RE was suddenly reduced at EBRTs lower than 70 s, which corresponded to a H$_2$S loading rate of 100 g S-H$_2$S$\cdot$m$^{-3}\cdot$h^{-1}. As expected, results indicated that the most significant elimination of H$_2$S was obtained at the bottom section of the reactor (G 1/3), close to the gas inlet section, where a higher H$_2$S/O$_2$ gradient probably exists due to the counter-current flow mode of the liquid and the gas phases. However, the feeding of exhaust air from the aeration unit directly to the gas inlet section of the BTF certainly played an important role in the dynamic of SO$_4^{2-}$ production along the BTF bed height, enhancing the SO$_4^{2-}$ selectivity at the bottom of the reactor by the extra O$_2$ supply. Further research focused on the oxygen balance along the filter bed is suggested as a tool to elucidate the mechanism of the observed H$_2$S removal stratification.
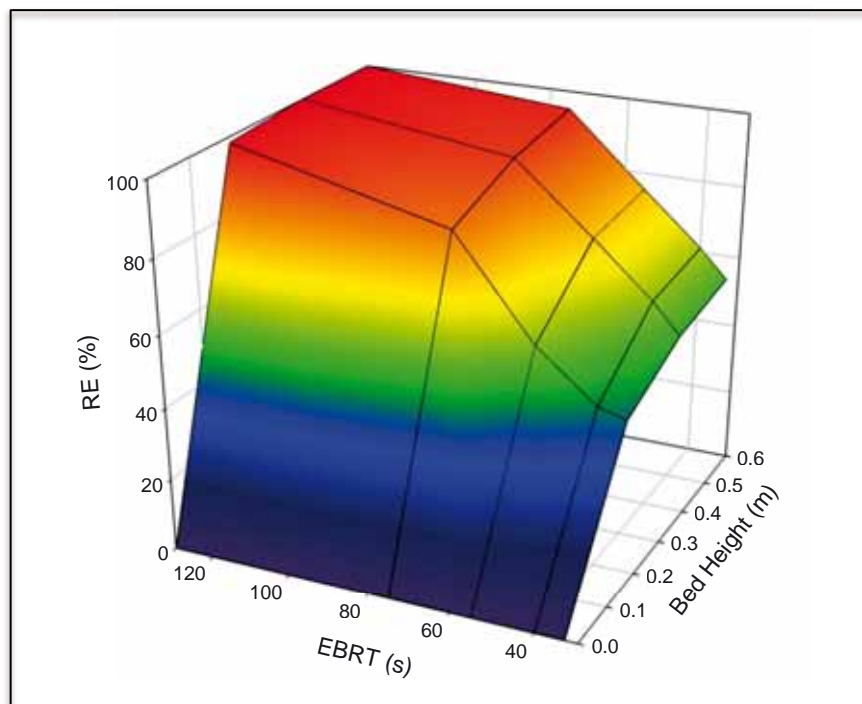
Figure 9.4 RE as a function of the filter bed height during E1

The H_2S elimination profile along the filter bed height during experiment **E2** is shown in **Figure 9.5**. Around 90% of RE at H_2S LR as high as 120 g $S-H_2S \cdot m^{-3} \cdot h^{-1}$ was obtained at the bottom section of the reactor.
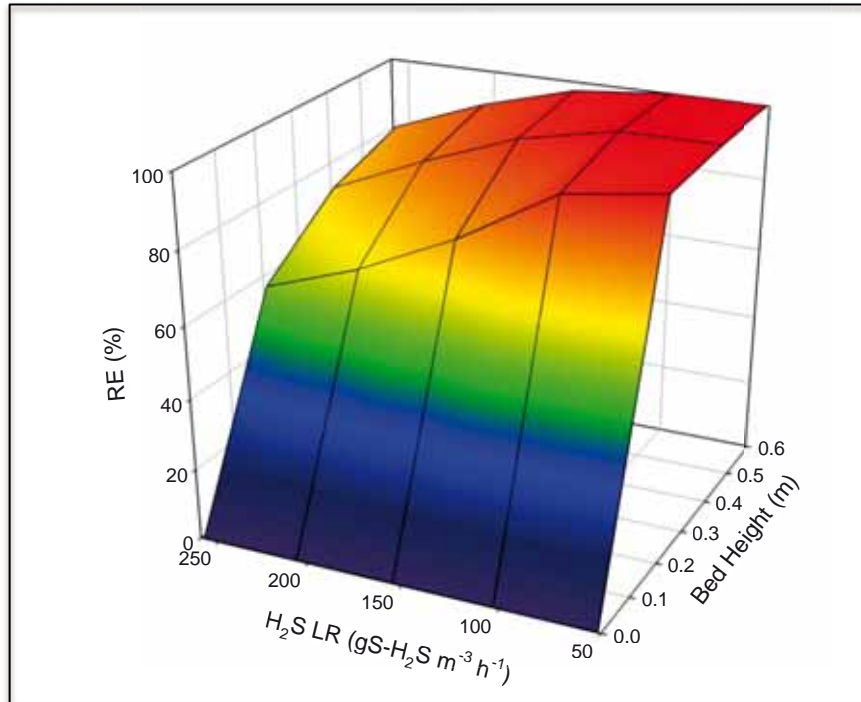
Figure 9.5 RE as a function of the filter bed height during E2

Such high performance was attributed to the extra aeration obtained by described the aeration system. Ramirez *et al.* (2009b) also reported a similar behavior for H_2S LR ranging from 4 to 59 g $S-H_2S \cdot m^{-3} \cdot h^{-1}$. Thus, assessment of the SO_4^{2-} and/or DO concentrations along the BTF bed height is necessary in future research on this topic.

9.4.4 Biosulfur to sulfate oxidation

Results from experiment **E3-1** showed that the biosulfur previously accumulated inside the filter bed during experiments **E1** and **E2** (approximately 23 g $S-S^0$) was effectively oxidized, resulting in the continuous production of SO_4^{2-}, in agreement with the **Equation 10**, even under H_2S starvation, as shown in **Figure 9.6**.
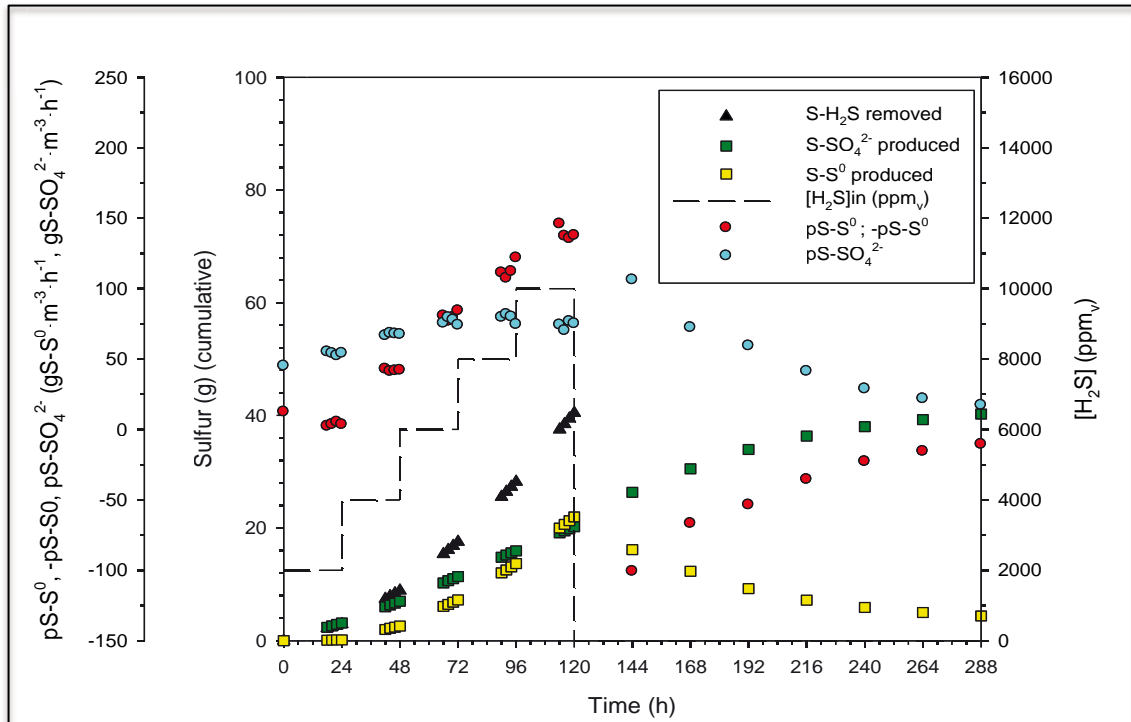
Figure 9.6 Sulfur mass balance during E2 and E3

After 7 days of H$_2$S starvation (**E3-1**), almost 80% of all accumulated S^0 was consumed (18 g S-S^0), indicating that the microbial consortium was able to utilize biosulfur as the only substrate under aerobic conditions. Values of the initial and the average -pS-S^0 were -100.6 g S-S^0·m^{-3}·h^{-1} and -43.6 g S-S^0·m^{-3}·h^{-1} during **E3-1**. Fortuny *et al.* (2010) reported the oxidation of 57% of the accumulated biosulfur after 6 days of H$_2$S starvation at neutral pH conditions. However, experimental conditions were not totally comparable to the present study and differences are not conclusive. To the author knowledge, no literature is available on the S^0 oxidation at acidic pH.

Results from sulfur mass balances during **E3-1** to **E3-6** are shown in **Figure 9.7**. Biosulfur production was notably increased after 840 days of total operation (400 days at acidic pH), which occurs after experiment **E3-2**. Probably, sulfur clogging started at some point inside the filter bed, even when pressure drop monitoring showed no significant pressure drop increases. Also, accumulation of biomass and biosulfur hindered the O$_2$ availability through the inner layers of the biofilm, producing the observed increment in the production of S^0.
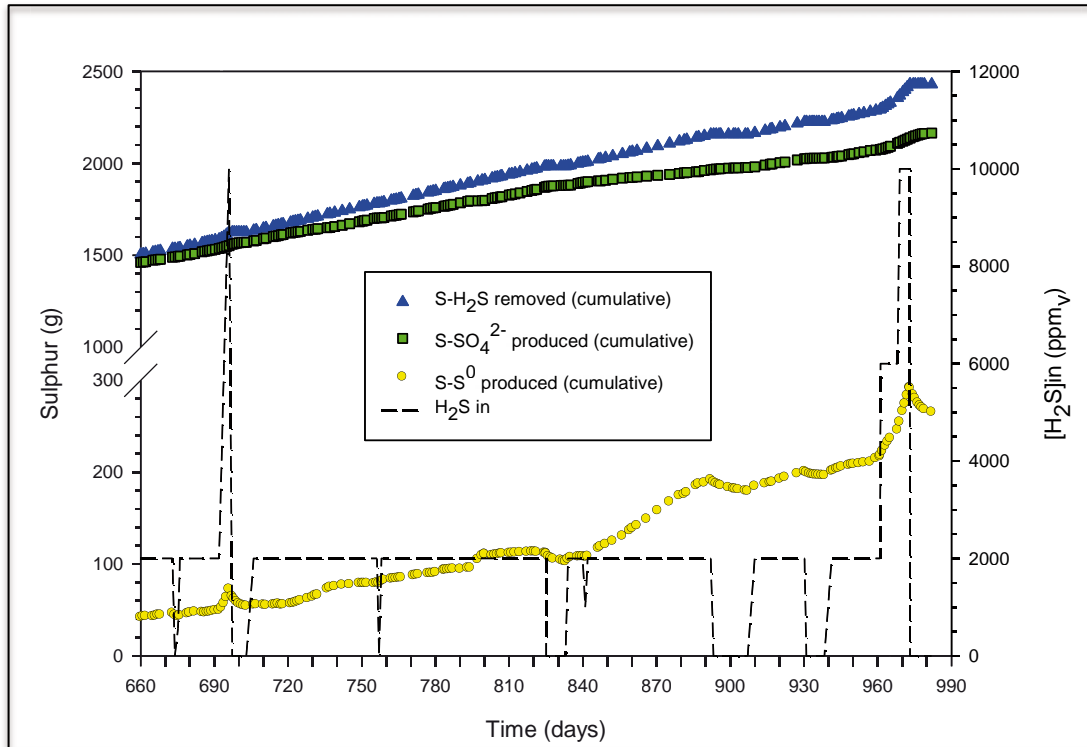
Figure 9.7 Sulfur mass balance from days 660 to 990 of operation.

Results obtained during starvation experiments (**E3-1** to **E3-4** and **E3-6**) are detailed in **Table 9.2**. The average and the initial value of the biosulfur consumption rate (-pS-S^0) were calculated for each experiment according to **Equation 23**.

Table 9.2 Biosulfur consumption during starvation experiments

EXP	Days of operation (*)	-pS-S^0 average (g S-S$^0 \cdot$m$^{-3} \cdot$h^{-1})	-pS-S^0 initial (g S-S$^0 \cdot$m$^{-3} \cdot$h^{-1})	S^0 consumed (g S-S^0)
C1	256 – 263	-43.6	-100.6	17.58
C2	385 – 393	-22.2	-192.9	10.22
C3	453 – 467	-13.3	-36.35	10.72
C4	491 – 498	-7.5	-27.9	2.59
C6	533 – 550	-66.0	-99.6	30.41

* at acidic pH (after 440 days at neutral pH operation).

Results of experiment **E3-5** are not shown because no starvation regime was performed during this experiment. Instead, a sudden increase in the biogas inlet H_2S concentration was performed, as indicated in **Table 9.1**. A total production of 69 g S-S^0 was obtained during the complete experiment **E3-5**, with average pS-S^0 of 82.1 g S-S$^0 \cdot$m$^{-3} \cdot$h^{-1} for 6,000 ppm$_v$ of H_2S (157.51 g S-H$_2$S$\cdot$m$^{-3} \cdot$h^{-1}) and 160.1 g S-S$^0 \cdot$m$^{-3} \cdot$h^{-1} for 10,000 ppm$_v$ of H_2S (262.54 g S-H$_2$S$\cdot$m$^{-3} \cdot$h^{-1}).

Looking at the starvation experiments results (**E3-1** to **E3-4**), it can be inferred that the capacity of oxidation of the accumulated biosulfur inside the bed decreased during the long-term operation, as a consequence of the effect of the sulfur accumulation inside the bed, as shown in **Figure 9.8**.
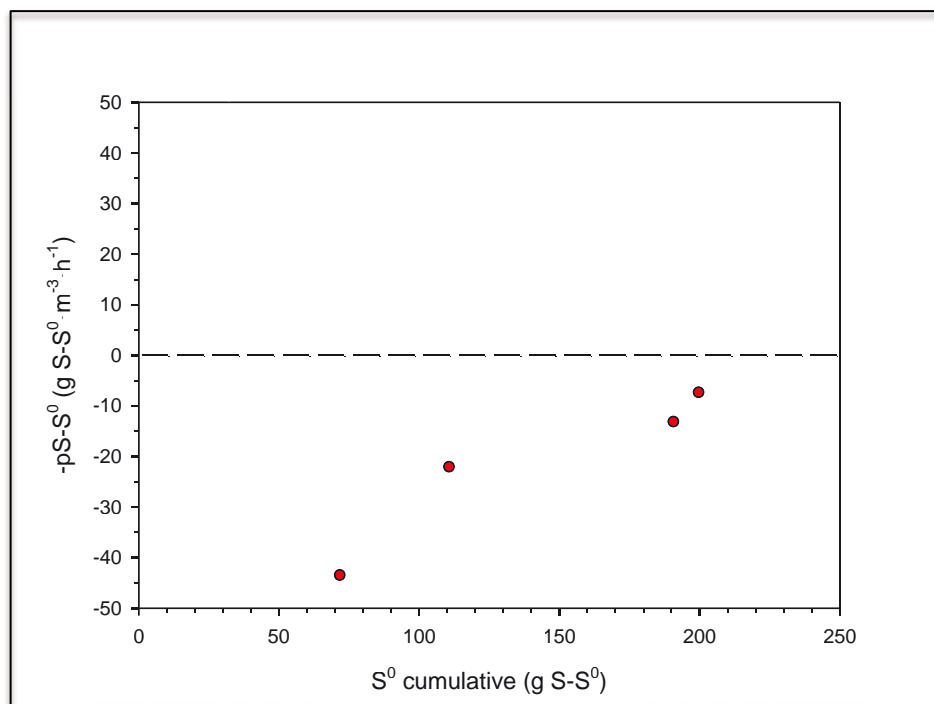
Figure 9.8 Biosulfur consumption rate during starvation experiments

It has been reported that the accumulation of biomass inside biofilters and BTFs leads to a lost in performance because the related undesired effects produced mainly by the porosity and tortuosity changes inside the packed bed (Dorado *et al*., 2009; Dumont *et al*., 2012). Also, biomass and solids accumulation are related to the increase of the pressure drop and to the diminishing of the O_2 spread inside the biofilm (Dorado *et al*, 2010;

Mannuci *et al.*, 2012; Andreasen *et al.*, 2012). Except for the high initial velocity of S^0 consumption obtained during **E3-2**, this parameter also tends to decrease along the reactor operation. High values of initial and average biosulfur consumption rate were obtained during experiment **E3-6** because of the increment in the bacterial community produced by the high loads of H_2S treated. In this way, the biosulfur oxidation capacity of the reactor was improved, reaching values comparable to those obtained during experiment **E3-1**, performed more than 9 months before. Visual verification of biosulfur accumulation inside the filter bed was obtained during biomass sampling procedures, as shown in **Figure 9.9**.
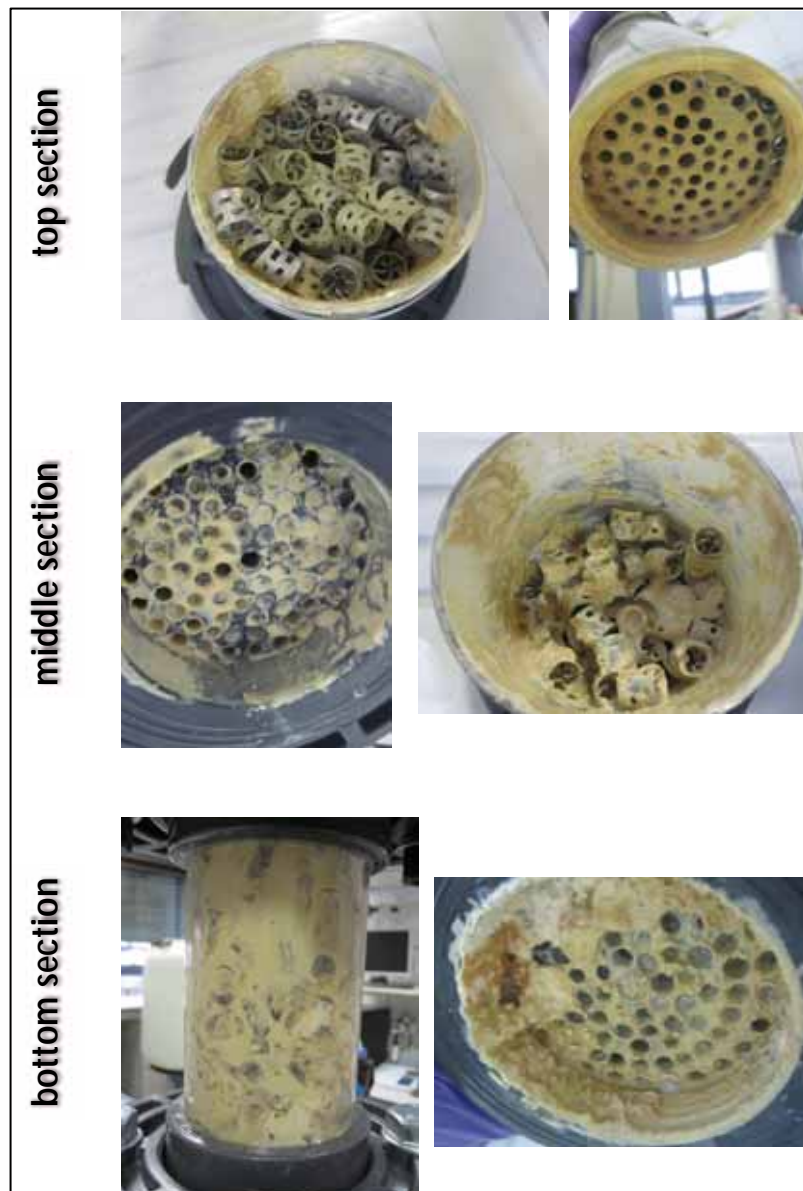
Figure 9.9 Images of biomass and solids sampling after 317 days at acidic pH

Also, evidence of corrosion of the packing material was observed during biomass sampling procedures (**Figure 9.10**), since 317 days after the transition to acidic pH (757 days of total operation).
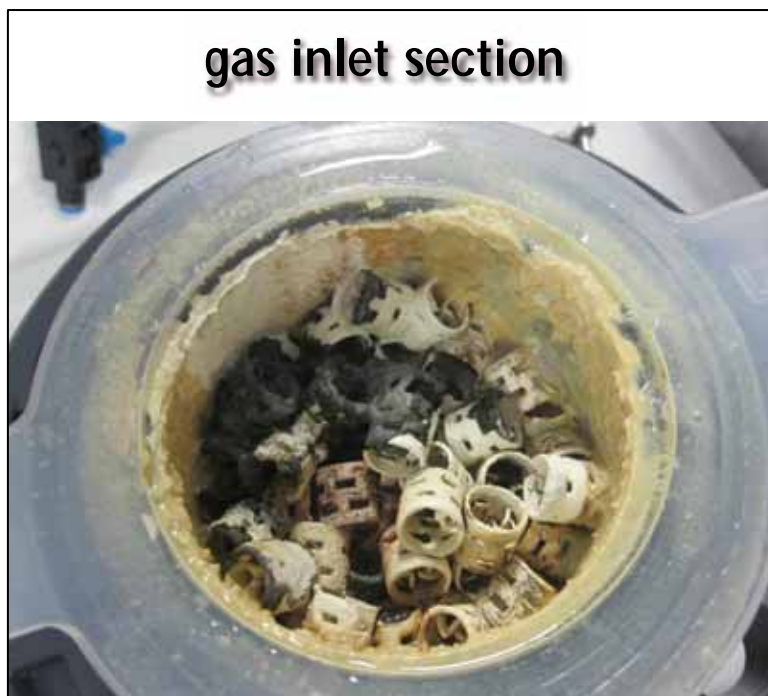
Figure 9.10 Image of packing material after 317 days at acidic pH

The applied metallic packing material (AISI 304) is not recommended for acidic operation in corrosive environments as in the case of the studied operation, even when RE values during the long-term performance kept at values higher than 99% for the reference conditions. Instead, plastic material is supposed to avoid all corrosion problems inside the filter bed, even when biomass sampling procedure must be improved for recovering viable samples from the plastic surface. Overall, obtained results from starvation experiments indicated that real-operation situations like biogas feeding interruption can be beneficial for the system operation because of the consumption of the accumulated biosulfur, as suggested previously for neutrophilic pH conditions for comparable conditions as in this study (Fortuny *et al*., 2010). However further research is needed to asses the system behavior under starvation periods considering also the interruption of the aeration supply system.

Adittionaly, the study of the solids sample obtained at the end of the BTF operation is being performed by X-ray diffraction analysis, in order to identify the composition of the solid phase accumulated inside the filter bed.

9.5 Conclusions

Overall, results showed that the desulfurization of high loaded H_2S biogas under acidic pH conditions is feasible in aerobic biotrickling filters and its performance comparable to that at neutral pH. The reactor performance was successfully sustained after the pH transition reported in **Chapter 7**. Moreover, the study of the H_2S elimination profile along the filter bed indicated that the elimination of H_2S was done mostly at the first third of the filter bed, close to the gas inlet, even when the counter-current operation mode of the studied BTF suggested an unfavorable O_2/H_2S ratio at this point. The aeration system characteristic of the experimental setup herein studied was suggested as the probable reason for such high desulfurizing capacity at the bottom part of the filter bed.

Also, H_2S starvation periodical regime was showed as an interesting S^0 clogging control strategy. Further research is recommended in order to establish a relationship between total accumulated elemental sulfur inside the filter bed and the elemental sulfur oxidation to sulfate under H_2S restriction in gas feeding. Moreover, the studied metallic (AISI 304) Pall rings is not recommended for acidic H_2S biotrickling filtration at long-term operation under high loads of H_2S, because of the deterioration of the packing elements after corrosion. Instead, plastic random packing material is recommended for further applications.

※

10

conclusions and future work

"When everything is easy, one quickly gets stupid."

Maxim Gorky
(Nizhny Novgorod, 1868 – Gorki-Leninskiye, 1936)

10 Conclusions and future work

10.1 General conclusions

An analytical system based on a flow injection analysis technique, was successfully validated for the on-line monitoring of the studied BTF, by the real-time determination of total dissolved sulfide (in liquid phase) and H_2S (in gas phase). The analytical system, based on an ISE of Ag_2S sensible to sulfide, exhibited the advantages of flow-based analyzers, such as reliability, repetitivity and stability of the analytical response, high analytical frequency with low sampling requirements, wide analytical range and overall low cost for the long-run operation. The lifetime of the constructed tubular electrodes showed exceptionally high and, together with the robustness of the tubular-type electrodes, represents a significant competitive advantage when facing the application of chemical sensors in real monitoring systems. Moreover, the pre-treatment steps proposed for sulfide monitoring, comprising an in-line filtration system and a pH adjustment system ensured the operation of the analyzer for continuous, non-stop operation, during the on-line monitoring of diverse experimental conditions, simulating in a good extent the real necessities of such kind of systems at industrial scale. Regarding the on-line determination of $H_2S_{(g)}$, the proposed analytical system showed suitable for systems operating at high H_2S concentrations, such as biogas desulfurization, with the advantage of presenting a wide operating range of analysis ($\approx$200 to 10,000 ppm_v of H_2S). Also, the control system developed for this application resulted in a convenient, user-friendly interface that offered the possibility of the unattended operation of the analytical system, a highly valuable feature for the use of the analyzer in real monitoring applications. Moreover, the proposed analytical system for H_2S/sulfide determination was consistently applied during real monitoring episodes during the execution of the experiments at both neutral and acidic pH operation of the studied BTF.

The preliminary study on the on-line determination of SO_4^{2-} shown that the proposed analytical system was not suitable for real samples monitoring, because of the extremely high response to interfering anions, specifically for the species encountered in the liquid phase of the BTF, mainly nitrate and chloride. However, developed electrodes were considered applicable for synthetic samples containing sulfate as the only analyte. Overall, conventional and tubular electrodes of polymeric liquid membrane were constructed and characterized by direct potentiometry, resulting in a simple, economic and fast analytical approach to the preliminary study performed in this research. Different liquid sensing cocktail formulations were studied, resulting in the best response for a membrane composition slightly different to that recommended in literature. Lipophilic additive was found to be crucial to electrode response, as well as the presence of an active ionophore. The used ionophore (Sulfate-Ionophore I – Selectophore™) is not recommended for the application proposed, because of the mentioned low selectivity to the main analyte. Instead, an alternative analytical method is proposed as future research line, consisting in the optical detection of the precipitate formed by the reaction of SO_4^{2-} and $BaCl_2$, based on the standard analytical procedure for sulfate determination, implemented into a microfluidic platform.

Several important findings must be highlighted concerning the long-term operation of the studied BTF. Overall, the selected random packing material was found applicable for the desulfurization of synthetic high-loaded biogas for both neutral and acidic pH, in terms of desulfurizing capacity of the system. However, the metallic nature of the packing elements represented a drawback, especially under acidic pH conditions, because of the related negative effects of the packing material corrosion and the possible detrimental effects of iron lixiviation over the biological activity. The start-up of the system with unspecific inoculation was successfully conducted at neutral pH (6.0 < pH < 6.50), applying a high H_2S loading rate (51.48 g S-$H_2S \cdot m^{-3} \cdot h^{-1}$), at a reference gas contact time of around 130 s. Furthermore, the manipulation of crucial operational parameters allowed the optimization of the sulfate-producing capacity of the system, resulting in minimum

elemental sulfur production, as required for the studies on the microbial ecology of the system, performed concomitantly by others (Rovira *et al.*, 2010; Bezerra *et al.*, 2013). Also, the oxygen load, representing the biologically available oxygen, was confirmed as a key parameter for the control of the sulfate/elemental sulfur production in this kind of reactors. The neutral pH operation was successfully conducted up to 440 days of operation, with H_2S removal capacity close to 100% for the reference conditions. Also, experiments performed to investigate the system behavior in front of the H_2S load and the gas contact time confirmed that the main limiting proces in this kind of systems is related to mass transfer limitations.

During the steady-state operation at neutral pH, the execution of experiments on the co-treatment of H_2S and CH_3SH shown that the simultaneous removal of both pollutants was feasible in aerobic BTFs, with no detrimental effects in the removal of H_2S by the presence of CH_3SH at concentrations normally found in biogas. In contrary, an interesting beneficial effect of filter bed unclogging was found by the chemical reaction of CH_3SH with elemental sulfur accumulated inside the reactor. Results suggested a wider application field for this kind of systems performing in real biogas treatment plants in which the natural presence of CH_3SH could represent an operational advantage.

The gradual, uninterrupted operational transition to acidic pH (2.50 < pH < 2.75) was performed after 440 days of operation at neutral pH. Overall results demonstrated a high adaptation of the system, with almost no reduction on the desulfurizing capacity of the BTF under reference conditions. The robustness of the BTF system was also verified by the high recovery capacity after transitory changes on the load and gas contact time. Overall, results showed that the desulfurization of high loaded H_2S biogas under acidic pH conditions is feasible in aerobic biotrickling filters, with a global performance comparable to that previously obtained at neutral pH. The H_2S elimination profile investigation along the filter bed height indicated that almost 70 – 80% of the H_2S removal took place at the first third of the filter bed, close to the gas inlet. Also, during the steady-state operation at

acidic pH, the execution of periodical H_2S starvation experiments over an extended period, suggested that the consumption of the accumulated biosulfur inside the filter bed should be considered as a control strategy against sulfur-clogging episodes, by the biological S^0 oxidation. Finally, even when no desulfurizing capacity loss was verified over the extended 990-days operation of the BTF, the applied metallic (AISI 304) Pall rings is not recommended for acidic H_2S biotrickling filtration at long-term operation, especially under high loads of H_2S, because of the deterioration of the packing elements after corrosion. Instead, plastic random packing material is recommended for further applications.

10.2   Future research recommendations

After the execution of the experiments reported in this work and after the assessment of the long-term operation of the studied BTF, some future research recommendations are suggested, dividing the proposed actions in two main categories: Monitoring and Performance, in accordance with the main objectives of this work.

Monitoring

The improvement of the proposed monitoring systems, for H_2S/sulfide on-line determination and for sulfate determination, should focus on the following issues:

- Improvement of the pre-treatment filtration step used for the continuous operation of the FIA/GD-CFA system, in order to facilitate the integration of the analytical system to different BTFs configurations. A self-cleaning filtration device should be applied, including a preventive trap for solids separation before entering the filtration device itself.
- Optimization of the gas diffusion cell is suggested for diminishing the analytical frequency of the CFA system. Also, other diffusion membrane

composition and configuration should be experimented for stabilizing the required conditioning time before analysis.

- Enhancement of the gas-phase automatic sampling procedure under continuous operation by the inclusion of an automated valve. This feature offers an extended unattended period operation, besides representing a safer operation.

- Further research oriented to the miniaturization of the analytical system for H_2S/TDS determination is highly recommended, including the possibility of developing a commercial prototype of the complete analytical system. Interest on the modularization of the proposed system has been already showed by few technical consults coming from real industrial applications.

- For overcoming the significant drawbacks faced during the development of the proposed analytical system for sulfate determination, a low temperature cofired ceramics (LTCC) miniaturized device is suggested as an alternative analytical system. This strategy is based on the optical determination of $BaSO_4$ obtained by the standard analytical procedure based on SO_4^{2-} precipitation by reaction with $BaCl_2$.

- The preliminary study on the application of the LTCC device was already started during this research, in collaboration with the Sensors and Biosensors Research Group (Department of Chemistry of this University), including the design of a first prototype. Further research is needed for the optimization of the optical detection system and the operational conditions of such analyzer.

Performance

The amelioration of the BTF performance as well as the better understanding of the biological aerobic desulfurization process should be obtained from the research intensification on the following proposed topics:

- Optimization of the oxygen supply to the system, including the betterment of the O_2 transfer device. Also, for overcoming the

limitations faced during this study, the measurement of O_2 concentration in gas phase is suggested as an improvement, which could allow the precise calculation of mass balances.

- Intensification on the study of the biological desulfurization process, performed with reliable mass balance calculations, with the objective of implementing an automated O_2/H_2S control system.

- Upgrading of the preliminary study on the calculation of the proton production rate (HPR), initiated during this research (results not shown). The implementation of automated HPR calculations should be possible once O_2 and CO_2 mass balance were accurately performed.

- Further investigation is suggested on the effect of the gas/liquid circulation mode inside the BTF. In this sense, the operation of the BTF in co-current mode (both gas and liquid phase in down-flow mode) could help understanding the mass transfer limitation effect identified under counter-current operation.

- Continuation of the initiated studies on the effect of the long-term pH changes is required to establishing the microbial community sensitivity to such operational conditions. Also, the effect of short-term pH variation is suggested to investigate the operational limits of the system.

- Further research focused on the oxygen balance along the filter bed height is suggested as a tool to elucidate the mechanism of the observed H_2S removal stratification.

- The application of a random packing material is highly recommended to overcoming the problems found with metallic material related to corrosion and trace metal lixiviation. Plastic PP 5/8" Pall rings were selected at the end of this research as the suggested alternative packing material for future operation.

- Intensification on the study of the effect of starvation regimes is recommended under different conditions, to elucidate the biosulfur consumption mechanism and to promote the optimal conditions for obtaining the filter bed unclogging.

<div align="center">※</div>

11

references

"I think like a genius, I write like a
distinguished author and I speak like a child."

Vladimir V. Nabokov
(Saint Petersburg, 1899 – Montreux, 1977)

11 References

Abatzoglou N, Boivin S (**2009**) A review of biogas purification processes. *Biofuels, Bioproducts and Biorefining*, 3, 42-71.

ACGIH – American Conference of Governmental Industrial Hygienists. (**1996**) TLV® / BEI® Introduction – Last updated 21.Aug.2012.
(http://www.acgih.org/Products/tlv_bei_intro.htm, 19.Dec.2012).

Alegret S, Alonso J, Bartroli J, Lima JLFC, Machado AASC, Paulis JM (**1985**) Flow-through sandwich PVC matrix membrane electrode for flow injection analysis. *Analytical Letters*, 18, 2291-2303.

Andreasen RR, Nicolai RE, Poulsen TG (**2012**) Pressure drop in biofilters as related to dust and biomass accumulation. *Journal of Chemical Technology and Biotechnology*, 87, 806-816.

APHA – American Public Health Association (**1980**) Standard methods for the examination of water and wastewater, 15th Ed. Method 426C – Sulfate. Washington, DC, USA.

APHA (**2006a**) Standard methods for the examination of water and wastewater, 21st Ed. Method 4500-S^{2-} – Sulfide. Washington, DC, USA.

APHA (**2006b**) Standard methods for the examination of water and wastewater, 21st Ed. Method 2540 - Solids. Washington, DC, USA.

Arellano-Garcia L, Gonzalez-Sanchez A, Baquerizo G, Hernandez-Jimenez S, Revah S (**2009**) Treatment of carbon disulfide and ethanethiol vapors in alkaline biotrickling filters using an alkaliphilic sulfo-oxidizing bacterial consortium. *Journal of Chemical Technology and Biotechnology*, 85, 328-335.

Aroca G, Urrutia H, Nuñez D, Oyarzun P, Arancibia A, Guerrero K (**2007**) Comparison on the removal of hydrogen sulfide in biotrickling filters inoculated with *Thiobacillus thioparus* and *Acidithiobacillus thiooxidans*. *Electronic Journal of Biotechnology*, 10(4), 514-520.

ATSDR – Agency for Toxic Substances and Disease Registry (**1992**) Toxicological Profile for Methyl Mercaptan. US Department of Health and Human Services, Atlanta, USA.
(http://www.atsdr.cdc.gov/toxprofiles/tp139.pdf, 18.Jan.2013).

ATSDR (**2006**) Toxicological Profile for H_2S. US Department of Health and Human Services, Atlanta, USA.
(http://www.atsdr.cdc.gov/toxprofiles/tp114.pdf, 18.Jan.2013).

Baeza M (**2004**) Novel approach for automated flow analyzers applied to environmental analysis. *PhD Thesis*, UAB, Spain.
(available at: http://hdl.handle.net/10803/3284).

Bailon LA (**2007**) An innovative biotrickling filter for H_2S removal from biogas. In Proceedings of the II International Congress on Biotechniques for Air Pollution Control, A Coruña, Spain, 215-224.

Bakker E, Buhlmann P, Pretsch E (**1999**) Polymer membrane ion-selective electrodes – What are the limits? *Electroanalysis*, 11(13), 915-933.

Barbosa V, Hobbs P, Sneath R, Burgess J, Callan J, Stuetz R (**2006**) Investigating the capacity of an activated sludge process to reduce volatile organic compounds and odor emissions. *Water Environment Research*, 78(8), 842-851.

Barquero EJ (**2001**) Design, construction and evaluation of analyzers for environmental monitoring. *PhD Thesis*, UAB, Spain.
(available at: http://hdl.handle.net/10803/3179).

Benschop A, Ghonim Z, Wolschlag L, van Heeringen G (**2004**) Biological process removes sulfur from three refinery streams. Proceedings of the ERTC 9th Annual Meeting. Prague, Czech Republic, 1-17.

Bentley R, Chasteen TG (**2004**) Environmental VOSCs – formation and degradation of dimethyl sulfide, methanethiol and related materials. *Chemosphere*, 55, 291-317.

Berrocal MJ, Cruz A, Badr IHA, Bachas LG (**2000**) Tripodal ionophore with sulfate recognition properties for anion-selective electrodes. *Analytical Chemistry*, 72, 5295-5299.

Bezerra T, Rovira R, Montebello AM, Llagostera M, Lafuente J, Campoy S, Gabriel D (**2013**) Metagenomics and metatranscriptomics of a H_2S desulfurizing biotrickling filter. Proceedings of the 5th IWA Conference on Odours and Air Emissions, March 4-7, San Francisco, California, USA.

Bruser T, Lens PNL, Truper HG (**2004**) The biological sulfur cycle. In: Environmental technologies to treat sulfur pollution. Principles and engineering. Lens P, Hulshoff Pol L, Eds. IWA Publishing, London, UK.

Buhlmann P, Nishizawa S, Xiao KP, Umezawa Y (**1997**) Strong hydrogen bond-mediated complexation of H2PO4- by neutral bis-thiourea hosts. *Tetrahedron*, 53(5) 1647-1654.

Buhlmann P, Umezawa Y, Rondinini S, Vertova A, Pigliucci A, Bertesago L (**2000**) Lifetime of ion-selective electrodes based on charged ionophores. *Analyticial Chemistry*, 72, 1843-1852.

Burgess JE, Parsons SA, Stuetz RM (**2001**) Developments in odour control and waste gas treatment biotechnology: a review. *Biotechnology Advances*, 19, 35-63.

Busca G, Pistarino C (**2003**) Technologies for the abatement of sulfide compounds from gaseous streams: a comparative overview. *Journal of Loss Prevention in the Process Industries*, 16, 363-371.

Caceres M, Morales M, Martin RS, Urrutia H, Aroca G (**2010**) Oxidation of volatile reduced sulfur compounds in biotrickling filter inoculated with *Thiobacillus thioparus*. *Electronic Journal of Biotechnology*, 13, 5, DOI: 10.2225/vol13-issue5-fulltext-9.

Card T (**2001**) Chemical odour scrubbing systems. In: Odours in wastewater treatment: measurement, modeling and control. Stuetz R and Frechen FB (Editors) – 1st Edition, IWA Publishing, London, UK.

Catalan LJJ, Liang V, Jia CQ (**2006**) Comparison of various detection limit estimates for volatile sulfur compounds by gas chromatography with pulsed flame photometric detection. *Journal of Chromatography A*, 1136, 89-98.

Cerda V, Estela JM, Forteza R, Cladera A, Becerra E, Altimira P, Sitjar P (**1999**) Flow techniques in water analysis. *Talanta*, 50, 695-705.

Cesario MT, Beverloo WA, Tramper J, Beeftink HH (**1997**) Enhancement of gas-liquid mass transfer rate of apolar pollutants in the biological waste gas treatment by a dispersed organic solvent. *Enzyme and Microbial Technology*, 21, 578-588.

Chaiprapat S, Mardthing R, Kantachote D, Karnchanawong S (**2011**) Removal of hydrogen sulfide by complete aerobic oxidation in acidic biofiltration. *Process Biochemistry*, 46, 344-352.

Cho KS, Ryu HW, Lee NY (**2000**) Biological deodorization of hydrogen sulfide using porous lava as a carrier of *Thiobacillus thiooxidans. Journal of Bioscience and Bioengineering*, 90(1), 25-31.

Ciccoli R, Cigolotti V, Lo Presti R, Massi E, McPhail SJ, Monteleone G, Moreno A, Naticchioni V, Paoletti C, Simonetti E, Zaza F (**2010**) Molten carbonate fuel cells fed with biogas: combating H_2S. *Waste Management*, 30, 1018-1024.

Coll C, Labrador RH, Martinez-Mañez R, Soto J, Sancenon F, Segui MJ, Sanchez E (**2005**) Ionic liquids promote selective responses towards the highly hydrophilic anion sulfate in PVC membrane ion-selective electrodes. *Chemical Communications*, 24, 3033-3035.

Cox HHJ, Deshusses MA (**2002**) Co-treatment of H_2S and toluene in a biotrickling filter. *Chemical Engineering Journal*, 87, 101-110.

Coyne L, Kuhlman C, Zovack N (**2011**) The stability of sulfur compounds, low molecular weight gases and VOCs in five air sample bag materials. SKC Inc., Publication 1805REV1208.
(www.skcinc.com/instructions/1805.pdf, 16.Apr.2013).

Datta I, Fulthorpe RR, Sharma S, Allen DG (**2007**) High-temperature biotrickling filtration of hydrogen sulfide. *Applied Microbiology and Biotechnology*, 74, 708-716.

de Angelis A (**2012**) Natural gas removal of hydrogen sulfide and mercaptans. *Applied Catalysis B: Environmental*, 113-114, 37-42.

de Bo I, van Langenhove H, Heyman J (**2002**) Removal of dimethyl sulfide from waste air in a membrane bioreactor. *Desalination*, 148, 281-287.

de Marco R, Clarke G, Pejcic B (**2007**) Ion-selective electrode potentiometry in environmental analysis. *Electroanalysis*, 19(19-20), 1987-2001.

Dehouk E, Chevrier V, Gaudin A, Mangold N, Mathe PE, Rochette P (**2012**) Evaluating the role of sulfide-weathering in the formation of sulfates or carbonates on Mars. *Geochimica et Cosmochimica Acta*, 90, 47-63.

Delgado L, Masana M, Baeza M, Gabriel D, Alonso J (**2006**) New approach for on-line simultaneous monitoring of hydrogen sulfide and sulfide in gas-phase bioreactors for biogas treatment. In: Proceedings of the Flow Analysis 10th International Conference, Porto, Portugal, p.148.

Detchanamurthy S, Gostomski PA (**2012**) Biofiltration for treating VOCs: an overview. *Reviews in Environmental Science and Biotechnology*, 11, 231-241.

Deublein D, Steinhauser A (**2008**) Biogas from waste and renewable resources, Wiley-VCH Verlag GmbH & Co. KGaA, Weinheim, Germany.

Devinny JS, Deshusses MA, Webster TS (**1999**) Biofiltration for air pollution control. CRC-Lewis Publishers, Boca Raton, Florida, USA.

Devinny JS, Ramesh J (**2005**) A phenomenological review of biofilter models. *Chemical Engineering Journal*, 113, 187-196.

Dilgin Y, Canarslan S, Ayyildiz O, Ertek B, Nisli G (**2012**) Flow injection analysis of sulfide based on its photoelectrocatalytic oxidation at poly-methylene blue modified glassy carbon electrode. *Electrochimica Acta*, 66, 173-179.

Dorado AD, Rodriguez G, Ribera G, Bonsfills A, Gabriel D, Lafuente J, Gamisans X (**2009**) Evaluation of mass transfer coefficients in biotrickling filters: experimental determination and comparison to correlations. *Chemical Engineering and Technology*, 32(12), 1941-1950.

Dorado AD, Lafuente J, Gabriel D, Gamisans X (**2010**) The role of water in the performance of biofilters: Parameterization of pressure drop and sorption capacities for common packing materials. *Journal of Hazardous Materials*, 180, 693-702.

Duan HQ, Yan R, Koe LCC (**2005**) Investigation on the mechanism of H_2S removal by biological activated carbon in a horizontal biotrickling filter. *Applied Microbiology and Biotechnology*, 69 (3), 350-357.

Duic N, Guzovic Z, Kafarov V, Klemes JJ, van Mathiessen B (**2013**) Sustainable development of energy, water and environment systems. *Applied Energy*, 101, 3-5.

Dumont E, Andres Y (**2010**) Evaluation of innovative packing materials for the biodegradation of H_2S: a comparative study. *Journal of Chemical Technology and Biotechnology*, 85, 429-434.

Dumont E, Ayala-Guzman LM, Rodriguez-Susa MS, Andres Y (**2012a**) H_2S biofiltration using expanded schist as packing material: performance evaluation and packed-bed tortuosity assessment. *Journal of Chemical Technology and Biotechnology*, 87, 725-731.

Dumont D, Darracq G, Couvert A, Couriol C, Amrane A, Thomas D, Andres Y, Le Cloirec P (**2012b**) Hydrophobic VOC absorption in two-phase partitioning bioreactors; influence of silicone oil volume fraction on absorber diameter. *Chemical Engineering Science*, 71, 146-152.

Egorov V, Rakhman'ko E, Okaev E, Nazarov V, Pomelyenok E, Pavlova T (**2004**) Novel anion exchangers for electrodes with improved selectivity to divalent anions. *Electroanalysis*, 16(17), 1459-1461.

Egorov VV, Nazarov VA, Okaev EB, Pavlova TE (**2006**) A new sulfate-selective electrode and its use in analysis. *Journal of Analytical Chemistry*, 61(4), 382-388.

Elias A, Barona A, Arreguy A, Rios J, Aranguiz I, Peñas J (**2002**) Evaluation of a packing material for the biodegradation of H_2S and product analysis. *Process Biochemistry*, 37, 813-820.

Epelman S, Tang WHW (**2012**) H_2S – The newest gaseous messenger on the block. *Journal of Cardiac Failure*, 18(8), 597-599.

Ertek B, Vu DL, Cervenka L, Dilgin Y (**2012**) Flow injection amperometric detection of sulfide using a prussian blue modified glassy carbon electrode. *Analytical Sciences*, 28, 1075-1080.

Estrada JM, Kraakman NJR, Lebrero R, Muñoz R (**2012**) A sensitivity analysis of process design parameters, commodity prices and robustness on the economics of odour abatement technologies. *Biotechnology Advances*, 30, 1354-1363.

European Commission (**2011**) Communication from the Commission to the European Parliament, the Council, the European Economic and Social Committee and the Committee of the Regions. Energy Roadmap 2050. Brussels, 15.12.2011. COM(2011) 885 final. (http://ec.europa.eu/energy/energy2020/roadmap/index_en.htm, 6.Jan.2013).

Evgenev MI, Garmonov SY, Shakirova LS (**2001**) Flow-Injection analysis of pharmaceuticals. *Journal of Analytical Chemistry*, 56(4), 313-323.

Faridbod F, Ganjali MR, Dinarvand R, Norouzi P (**2008**) Developments in the field of conducting and non-conducting polymer based potentiometric membrane sensors for ions over the past decade. *Sensors*, 8, 2331-2412.

Felix FS, Angnes L (**2010**) Fast and accurate analysis of drugs using amperometry associated with flow injection analysis – Review. *Journal of Pharmaceutical Sciences*, 99(12), 4784-4804.

Ferrer L, Miro M, Estela JM, Cerda V (**2007**) Analytical methodologies for reliable sulfide determinations in aqueous matrices exploiting flow-based approaches. *Trends in Analytical Chemistry*, 26(5), 413-422.

Fibbioli M, Berger M, Schmidtchen FP, Pretsch E (**2000**) Polymeric membrane electrodes for monohydrogen phosphate and sulfate. *Analytical Chemistry,* 72, 156-160.

Fine GF, Cavanagh LM, Afonja A, Binions R (**2010**) Metal oxide semi-conductor gas sensors in environmental monitoring. *Sensors*, 10, 5469-5502.

Firouzabadi S, Razavipanah I, Zhiani R, Ghanei-Motlagh M, Reza-Salavati M (**2013**) Sulfate-selective electrode based on a bis-thiourea ionophore. *Monatshefte für Chemie – Chemical Monthly*, 144, 113-120.

Fortuny M, Baeza JA, Gamisans X, Casas C, Lafuente J, Deshusses MA, Gabriel D (**2008**) Biological sweetening of energy gases mimics in biotrickling filters. *Chemosphere*, 71, 10-17.

Fortuny M, Guisasola A, Casas C, Gamisans X, Lafuente J, Gabriel D (**2010**) Oxidation of biologically produced elemental sulfur under neutrophilic conditions. *Journal of Chemical Technology and Biotechnology*, 85, 378-386.

Fortuny, M, Gamisans X, Deshusses MA, Lafuente J, Casas C, Gabriel D (**2011**) Operational aspects of the desulfurization process of energy gases mimics in biotrickling filters. *Water Research*, 45, 5665-5674.

Gabriel D, Baeza J, Valero F, Lafuente J (**1998**) A novel FIA configuration for the simultaneous determination of nitrate and nitrite and its use for monitoring an urban waste water treatment plant based on N/D criteria. *Analytica Chimica Acta*, 359, 173-183.

Gabriel D, Deshusses MA (**2003a**) Performance of a full-scale biotrickling filter treating H$_2$S at a gas contact time of 1.6 to 2.2 seconds. *Environmental Progress*, 22, 111-118.

Gabriel D, Deshusses MA (**2003b**) Retrofitting existing chemical scrubbers to biotrickling filters for H$_2$S emission control, *Proceedings of the National Academy of Sciences USA*, 100, 6308-6312.

Gabriel D, Deshusses MA (**2004**) Technical and economical analysis of the conversion of a full-scale scrubber to a biotrickling filter for odor control. *Water Science and Technology*, 50(4), 309-318.

Gabriel D, Deshusses MA, Gamisans X (**2013**) Desulfurization of biogas in biotrickling filters. In: Air Pollution Prevention and Control: Bioreactors and Bioenergy, John Wiley and Sons Ltd., 513-523.

Gadzekpo VPY, Christian GD (**1984**) Determination of selectivity coefficients of ion-selective electrodes by a matched-potential method. *Analytical Chimica Acta*, 164, 279-282.

Ganjali MR, Naji L, Poursaberi T, Taghizadeh M, Pirelahi H, Yousefi M, Yeganeh-Faal A, Shamsipur M (**2002**) Novel sulfate ion-selective polymeric membrane electrode based on a derivative of pyrilium perchlorate. *Talanta*, 58, 359-366.

Ganjali MR, Pourjavid MR, Shamsipur M, Poursaeri T, Rezapour M, Javanbakht M, Sharghi H (**2003**) Novel membrane potentiometric sulfate ion sensor based on zinc-phthalocyanine for the quick determination of trace amounts of sulfate. *Analytical Sciences*, 19, 995-999.

Garcia-Calzada M, Marban G, Fuertes AB (**1999**) Potentiometric determination of sulfur in solid samples. *Analytica Chimica Acta*, 380, 39-45.

Gonzalez-Sanchez A, Revah S, Deshusses MA (**2008**) Alkaline biofiltration of H_2S odors. *Environmental Science and Technology*, 42, 7398-7404.

Gracia A, Barreiro-Hurle J, Perez y Perez L (**2012**) Can renewable energy by financed with higher electricity prices? Evidence from a Spanish region. *Energy Policy*, 50, 784-794.

Hansen EH (**1996**) Principles and applications of flow injection analysis in biosensors – Critical review. *Journal of Molecular Recognition*, 9, 316-325.

Hara H, Takahashi K, Ohkubo H (**1994**) Nitrate ion-selective field effect transistor based on bis(bathocuproin)-copper(I) nitrate dissolved in solid solvents. *Analytical Chimica Acta*, 290(3), 329-333.

Harkness AC, Murray FE (**1970**) Oxidation of methylmercaptan with molecular oxygen in aqueous solution. *Atmospheric Environment*, 4(4), 417-424.

Hartikainen T, Martikainen PJ, Olkkonen M, Ruuskanen J (**2002**) Peat biofilters in long-term experiments for removing odorous sulfur compounds. *Water, Air and Soil Pollution*, 133(1-4), 335-348.

Hennig C, Gawor M (**2012**) Bioenergy production and use: Comparative analysis of the economic and environmental effects. *Energy Conversion and Management*, 63, 130-137.

Hernandez J (**2012**) Study on bioreactors configurations and packing materials for the treatment of complex mixtures of organic and inorganic volatile compounds. *PhD Thesis*, UAB, Spain.
(available at: http://hdl.handle.net/10803/42292).

Hernandez SC, Kakoullis JJ, Lim JH, Mubeen S, Hangarter CM, Mulchandani A, Myung NV (**2012**) Hybrid ZnO/SWNT nanostructures based gas sensor. *Electroanalysis*, 24(7), 1613-1620.

Hirai M, Ohtake M, Shoda M (**1990**) Removal kinetics of hydrogen sulfide, methanethiol and dimethyl sulfide by peat biofilters. *Journal of Fermentation and Bioengineering*, 70(5), 334-339.

Horikawa MS, Rossi F, Gimenes ML, Costa CMM, da Silva MGC (**2004**) Chemical absorption of H_2S for biogas purification. *Brazilian Journal of Chemical Engineering*, 21(3), 415-422.

HSDB – Hazardous Substances Databank, Methyl Mercaptan (**2003**) National Library of Medicine, Bethesda, MD, USA. (http://toxnet.nlm.nih.gov/cgibin/sis/search/hsdb:term+DOCNO+813, 18.Jan.2013).

HSDB, Hydrogen sulfide (**2012**) National Library of Medicine, Bethesda, MD, USA. (http://toxnet.nlm.nih.gov/cgi-bin/sis/search/f?./temp/SGTglh:1, 18.Jan.2013).

NSHT – Instituto Nacional de Seguridad e Higiene en el Trabajo (**2012**) Límites de Exposición Profesional para Agentes Químicos en España. Ministerio de Empleo y Seguridad Social, Madrid, España.

Iranpour R, Cox HHJ, Deshusses MA, Schroeder ED (**2005**) Literature review of air pollution control biofilters and biotrickling filters for odor and volatile organic compound removal. *Environmental Progress*, 24(3), 254-267.

Islander RL, Devinny JS, Mansfeld F, Postyn A, Hong S (**1991**) Microbial ecology of crown corrosion in sewers. *Journal of Environmental Engineering*, 117, 751-771.

Janssen AJH, Sleyster R, van der Kaa C, Jochemsen A, Bontsema J, Lettinga G (**1995**) Biological sulphide oxidation in a fed-batch reactor. *Biotechnology and Bioengineering*, 47, 327-333.

Janssen AJH, Ma SC, Lens P, Lettinga G (**1997**) Performance of a sulfide-oxidizing expanded-bed reactor supplied with dissolved oxygen. *Biotechnology and Bioengineering*, 53, 32-40.

Janssen AJH, Lens PNL, Stams AJM, Plugge CM, Sorokin DY, Muyzer G, Dijkman H, van Zessen E, Luimes P, Buisman CJN (**2008**) Application of bacteria involved in the biological sulfur cycle for paper mill effluent purification. *Science of the Total Environment*, 407, 1333-1343.

Jensen HS, Lens PNL, Nielsen JL, Bester K, Nielsen AH, Hvitved-Jacobsen T, Vollertsen J (**2011**) Growth kinetics of hydrogen sulfide oxidizing bacteria in corroded concrete from sewers. *Journal of Hazardous Materials*, 189, 685-691.

Jia C, Wu B, Li S, Huang X, Yang XJ (**2010**) Tetraureas versus triureas in sulfate binding. *Organic Letters*, 12(24), 5612-5615.

Jin Y, Veiga MC, Kennes C (**2007**) Co-treatment of hydrogen sulfide and methanol in a single-stage biotrickling filter under acidic conditions. *Chemosphere*, 68, 1186-1193.

Johnston DT (**2011**) Multiple sulfur isotopes and the evolution of Earth's surface sulfur cycle. *Earth-Science Reviews*, 106, 161-183.

Kelly DP (**1999**) Thermodynamic aspects of energy conservation by chemolithotrophic sulfur bacteria in relation to the sulfur oxidation pathways. *Archives Microbiology*, 171, 219-229.

Kennes C, Veiga MC (**2004**) Fungal biocatalysts in the biofiltration of VOC-polluted air. *Journal of Biotechnology*, 113, 305-319.

Kennes C, Rene ER, Veiga MC (**2009**) Bioprocesses for air pollution control. *Journal of Chemical Technology and Biotechnology*, 84, 1419-1436.

Khalid A, Arshad M, Anjum M, Mahmood T, Dawson L (**2011**) The anaerobic digestion of solid organic waste. *Waste Management*, 31, 1737-1744.

Kim S, Deshusses MA (**2005**) Understanding the limits of H₂S degrading biotrickling filters using a differential biotrickling filter. *Chemical Engineering Journal*, 113, 119-126.

Kim S, Deshusses MA (**2008a**) Determination of mass transfer coefficients for packing materials used in biofilters and biotrickling filters for air pollution control. 1. Experimental results. *Chemical Engineering Science*, 63, 841-855.

Kim S, Deshusses MA (**2008b**) Determination of mass transfer coefficients for packing materials used in biofilters and biotrickling filters for air pollution control. 2. Development of mass transfer coefficients correlations. *Chemical Engineering Science*, 63, 856-861.

King PL, McLennan SM (**2010**) Sulfur on Mars. *Elements*, 6, 107-112.

Kolthoff IM, Sandell EB, Meehan EJ, Bruckenstein S (**1969**) Quantitative chemical analysis, 4th Ed. Macmillan, New York, USA, p. 857.

Koseoglu S, Lai C, Ferguson C, Buhlmann P (**2008**) Response mechanism of ion-selective electrodes based on a guanidine ionophore: an apparently "two-thirds Nernstian" response slope. *Electroanalysis*, 20(3), 331-339.

Kuenen JG (**1975**) Colourless sulphur bacteria and their role in the sulfur cycle. *Plant and Soil,* 43, 49-76.

Kumar A, Dewulf J, van Langenhove H (**2008**) Membrane-based biological waste gas treatment. *Chemical Engineering Journal*, 136, 82-91.

Kymalainen M, Lahde K, Arnold M, Kurola JM, Romantschuk M, Kautola H (**2012**) Biogasification of biowaste and sewage sludge – Measurement of biogas quality. *Journal of Environmental Management*, 95, 5122-5127.

Lafita C, Penya-Roja JM, Sempere F, Waalkens A, Gabaldon C (**2012**) Hydrogen sulfide and odor removal by field-scale biotrickling filters: Influence of seasonal variations of load and temperature. *Journal of Environmental Science and Health, Part A*, 47, 970-978.

Lastella G, Testa C, Cornacchia G, Notornicola M, Voltasio F, Sharma VK (**2002**) Anaerobic digestion of semi-solid organic waste: biogas production and its purification. *Energy Conversion and Management*, 43, 63-75.

Lebrero R, Rodriguez E, Garcia-Encina PA, Muñoz R (**2011**) A comparative assessment of biofiltration and activated sludge diffusion for odour abatement. *Journal of Hazardous Materials*, 190, 622-630.

Lee EY, Lee NY, Cho KS, Ryu HW (**2006**) Removal of hydrogen sulfide by sulfate-resistant *Acidithiobacillus thiooxidans* AZ11. *Journal of Bioscience and Bioengineering*, 101(4), 309-314.

Li ZQ, Liu GD, Duan LM, Shen GL, Yub RQ (**1999**) Sulfate-selective PVC membrane electrodes based on a derivative of imidazole as a neutral carrier. *Analytical Chimica Acta*, 382, 165-170.

Liu C, Hayashi K, Toko K (**2012**) Au nanoparticles decorated polyaniline nanofiber sensor for detecting volatile sulfur compounds in expired breath. *Sensors and Actuators B: Chemical*, 161, 504-509.

Liu D, Feilberg A, Nielsen AM, Adamsen APS (**2013**) PTR-MS measurement of partition coefficients of reduced volatile sulfur compounds in liquids from biotrickling filters. *Chemosphere*, 90, 1396-1403.

Lomako SV, Astapovich RI, Nozdrin-Plotniskaya OV, Pavlova TE, Lei S, Nazarov VA, Okaev EB, Rakhman'ko EM, Egorov VV (**2006**) Sulfate-selective

electrode and its application for sulfate determination in aqueous solutions. *Analytical Chimica Acta*, 562, 216-222.

Mackowiak J (**2011**) Model for the prediction of liquid phase mass transfer of random packed columns for gas-liquid systems. *Chemical Engineering Research and Design*, 89, 1308-1320.

Maestre JP, Rovira R, Alvarez-Hornos FJ, Fortuny M, Lafuente J, Gamisans X, Gabriel D (**2010**) Bacterial community analysis of a gas-phase biotrickling filter for biogas mimics desulfurization through the rRNA approach. *Chemosphere*, 80, 872-880.

Malhautier L, Gracian C, Roux JC, Fanlo JL, Le Cloirec P (**2003**) Biological treatment process of air loaded with an ammonia and hydrogen sulfide mixture. *Chemosphere*, 50, 145-153.

Manconi I, Carucci A, Lens P, Rossetti S (**2006**) Simultaneous biological removal of sulfide and nitrate by autotrophic denitrification in an activated sludge system. *Water Science and Technology*, 53, 91-99.

Mannucci A, Munz G, Mori G, Lubello C (**2012**) Biomass accumulation modelling in a highly loaded biotrickling filter for hydrogen sulphide removal. *Chemosphere*, 88, 712-717.

Martelli A, Testai L, Breschi MC, Blandizzi C, Virdis A, Taddei S, Calderone V (**2012**) Hydrogen sulfide: novel opportunity for drug discovery. *Medicinal Research Reviews*, 32(6), 1093-1130.

Martinez-Barrachina S, Alonso J, Matia Ll, Prats R, del Valle M (**1999**) Determination of trace levels of anionic surfactants in river wáter and wastewater by a flow injection analysis system with on-line preconcentration and potentiometric detection. *Analytical Chemistry*, 71, 3684-3691.

Mazloum-Ardakani M, Akrami Z, Mansournia M, Zare H (**2006**) Sulfate-selective electrode based on a complex of copper. *Analytical Science*, 22, 673-678.

Mazloum-Ardakani M, Dehghan-Manshadi A, Bagherzadeh M, Kargar H (**2012**) Impedimetric and potentiometric investigation of a sulfate anion-selective electrode: experiment and simulation. *Analytical Chemistry*, 84, 2614-2621.

Melchert WR, Reis BF, Rocha FRP (**2012**) Green chemistry and the evolution of flow analysis. A review. *Analytica Cimica Acta*, 714, 8-19.

Migdisov AA, Williams-Jones AE, Lakshtanov LZ, Alekhin YV (**2002**) Estimates of the second dissociation constant of H_2S from the surface sulfidation of crystalline sulfur. *Geochimica et Cosmochimica Acta*, 66(10), 1713-1725.

Miro M, Frenzel W (**2004**) Automated membrane-based sampling and sample preparation exploiting flow-injection analysis, *TrAC, Trends in Analytical Chemistry*, 23, 624-636.

Miro M, Estela JM, Cerda V (**2004**) Application of flowing-stream techniques to water analysis. Part II. General quality parameters and anionic compounds: halogenated, sulfur and metalloid species. *Talanta*, 62, 1-15.

Miro M, Hansen EH (**2012**) Recent advances and future prospects of mesofluidic Lab-on-a-Valve platforms in analytical sciences – A critical review. *Analytica Chimica Acta*, 750, 3-15.

Mohammadzadeh F, Jahanshahi M, Rashidi AM (**2012**) Preparation of nanosensors based on organic functionalized MWCNT for H_2S detection. *Applied Surface Science*, 259, 159-165.

Montebello AM, Baeza M, Lafuente J, Gabriel D (**2010**) Monitoring and performance of a desulfurizing biotrickling filter with an integrated continuous gas/liquid flow analyzer. *Chemical Engineering Journal*, 165, 500-507.

Montebello AM, Fernandez M, Almenglo F, Ramirez M, Cantero D, Baeza M, Gabriel D (**2012**) Simultaneous methylmercaptan and hydrogen sulfide removal in the desulfurization of biogas in aerobic and anoxic biotrickling filters. *Chemical Engineering Journal*, 200-202, 237-246.

Morigi M, Scavetta E, Berrettoni M, Giorgetti M, Tonelli . (**2001**) Sulfate-selective electrodes based on hydrotalcites. *Analytical Chimica Acta*, 439, 265-272.

Muñoz R, Daugulis AJ, Hernandez M, Quijano G (**2012**) Recent advances in two-phase partitioning bioreactors for the treatment of volatile organic compounds. *Biotechnology Advances*, 30, 1707-1720.

Namini MT, Abdegagh N, Heydarian SM, Bonakdarpour B, Davood-Zare BK (**2012**) Hydrogen sulfide removal performance of a bio-trickling filter employing Thiobacillus thiparus immobilized on polyurethane foam under various starvation regimes. *Biotechnology and Bioprocess Engineering*, 17, 1278-1283.

National Academy of Science (**2010**) Acute Exposure Guideline Levels for Selected Airborne Chemicals, Volume 9 – Last updated on 1 February 2012. The National Academies Press, Washington, DC, USA.
(http://www.nap.edu/catalog/12978.html, 1.Feb.2013).

Nikeima J, Bibeua L, Lavoie J, Brzezinski R, Vigneux J, Heitz M (**2005**) Biofitration of methane: an experimental study. *Chemical Engineering Journal*, 113, 111-117.

NIOSH – National Institute for Occupational Safety and Health (**1994**) Manual of analytical methods (NMAM) – Mercaptans, Method 2542.
(http://www.cdc.gov/niosh/docs/2003-154/pdfs/2542.pdf, 1.Feb.2013).

NIOSH (**2011a**) Pocket Guide to Chemical Hazards, Hydrogen sulfide.
(http://www.cdc.gov/niosh/npg/npgd0337.html, 1.Feb.2013).

NIOSH (**2011b**) Pocket Guide to Chemical Hazards, Methyl mercaptan.
(http://www.cdc.gov/niosh/npg/npgd0425.html, 1.Feb.2013).

Nishizawa S, Buhlmann P, Xiao KP, Umezawa Y (**1998**) Application of a bis-thiourea ionophore for an anion selective electrode with a remarkable sulfate selectivity. *Analytica Chimica Acta*, 358, 35-44.

Olenic L, Hopirtean E, Olenic L (**1997**) Potentiometric differential microdetector with interchange solid membranes used in flow injection analysis. *Analyst*, 122, 107-109.

OSHA – Occupational Safety and Health Administration (**1981**) Methyl mercaptan analytical method – Method no. 26.
(http://www.osha.gov/dts/sltc/methods/organic/org026/org026.html, 1.Feb.2013).

OSHA (**2005**) Fact sheet of Hydrogen sulfide (H_2S), DSG 10/2005.
(http://www.osha.gov/OshDoc//hydrogen_sulfide_fact.pdf, 1.Feb.2013).

OSHA (**2006**) Hydrogen sulfide analytical method – T-1008-FV-01-0609-M.
(http://www.osha.gov/dts/sltc/methods/validated/1008/1008.pdf, 1.Feb.2013).

Pantoja-Filho JL, Sader LT, Damianovic MHRZ, Foresti E, Silva EL (**2010**) Performance evaluation of packing materials in the removal of hydrogen sulphide in gas-phase biofilters: Polyurethane foam, sugarcane bagasse and coconut fibre. *Chemical Engineering Journal*, 158, 441-450.

Parker T, Dottridge J, Kelly S (**2002**) Investigation of the composition and emissions of trace components in landfill gas. R&D Technical Report P1-438/TR Environment Agency, Bristol, UK.

Peng B, Zhu J, Liu X, Qin Y (**2008**) Potentiometric response of ion-selective membranes with ionic liquids as ion-exchanger and plasticizer. *Sensors and Actuators B: Chemical*, 133, 308-314.

Pfenning N, Widdel F, Truper HG (**1981**) The dissimilatory sulfate-reducing bacteria. In: Starr MP, Stolp H, Truper HG, Balows A, Schlegel HG (Eds), The Prokaryotes, Vol. 1. Springer Verlag, NY, USA, 926-940.

Phillips KN, Lantz C, Buhlmann P (**2005**) Visible and FTIR microscopic observation of bisthiourea ionophore aggregates in ion-selective electrode membranes. *Electroanalysis*, 17(22), 2019-2025.

Piano M, Serban S, Biddle N, Pittson R, Drago GA, Hart JP (**2010**) A flow injection system, comprising a biosensor based on a screen-printed carbon electrode containing Meldola's Blue-Reinecke salt coated with glucose dehydrogenase, for the measurement of glucose. *Analytical Biochemistry*, 396, 269-274.

Pinjing H, Liming S, Zhiwen Y, Guojian L (**2001**) Removal of hydrogen sulfide and methylmercaptan by a packed tower with immobilized micro-organism beads. *Water Science and Technology*, 44(9), 327-333.

Prado OJ, Gabriel D, Lafuente J (**2009**) Economical assessment of the design, construction and operation of open-bed biofilters for waste gas treatment. *Journal of Environmental Management*, 90, 2515-2523.

Predmore BL, Lefer DJ, Gojon G (**2012**) Hydrogen sulfide in biochemistry and medicine. *Antioxidants and Redox Signaling*, 17(1), 119-140.

Pretsch E (**2007**) The new wave of ion-selective electrodes, *Trends in Analytical Chemistry*, 26 (1), 46-51.

Ramirez M, Gomez JM, Aroca G, Cantero D (**2009a**) Removal of hydrogen sulfide by immobilized *Thiobacillus thioparus* in a biotrickling filter packed with polyurethane foam. *Bioresource Technology*, 100, 4989-4995.

Ramirez M, Gomez JM, Cantero D, Paca J, Halecky M, Kozliak EI, Sobotka M (**2009b**) Hydrogen sulfide removal from air by *Acidithiobacillus thiooxidans* in a trickle bed reactor. *Folia Microbiologica*, 54(5), 409-414.

Ramirez M, Fernandez M, Granada C, Le Borgne S, Gomez JM, Cantero D (**2011**) Biofiltration of reduced sulfur compounds and community analysis of sulfur-oxidizing bacteria. *Bioresource Technology*, 102(5), 4047-4053.

Rasi S, Veijanen J, Rintala J (**2007**) Trace compounds of biogas from different biogas production plants. *Energy*, 32, 8, 1375-1380.

Rasi S, Lantela J, Rintala J (**2011**) Trace compounds affecting biogas energy utilization – A review. *Energy Conversion and Management*, 52, 3369-3375.

Redondo R, Cunha-Machado V, Baeza M, Lafuente J, Gabriel D (**2008**) On-line monitoring of gas-phase bioreactors for biogas treatment: hydrogen sulfide and sulfide analysis by automated flow systems. *Analytical and Bioanalytical Chemistry*, 391, 789-798.

Reij MW, Keurentjies JTF, Hartmans S (**1998**) Membrane bioreactors for waste gas treatment. *Journal of Biotechnology*, 59, 155-167.

Rene ER, Veiga MC, Kennes C (**2012**) Combined biological and physicochemical waste-gas cleaning techniques. *Journal of Environmental Science and Health, Part A*, 47, 920-939.

Robertson LA, Kuenen JG (**2006**) The colorless sulfur bacteria. In: The Prokaryotes – A Handbook on the Biology of Bacteria. Dworkin M, Falkow S, Rosenberg E, Schleifer KH and Stackebrandt E (Editors) – Third Edition, Springer Science+Business Media, Inc., New York, USA.

Rocha-Rios J, Quijano G, Thalasso F, Revah S, Muñoz R (**2011**) Methane biodegradation in a two-phase partition internal loop airlift reactor with gas recirculation. *Journal of Chemical Technology and Biotechnology*, 86, 353-360.

Rodriguez G, Dorado AD, Bonsfills A, Sanahuja R, Gabriel D, Gamisans X (**2012**) Optimization of oxygen transfer through venturi-based systems applied to the biological sweetening of biogas. *Journal of Chemical Technology and Biotechnology*, 87, 854–860.

Rodriguez G, Dorado AD, Bonsfills A, Gabriel D, Gamisans X (**2013**) Optimization of oxygen transfer through membrane diffusers for biological sweetening of biogas. *Chemical Engineering and Technology*, 36(3), 513-518.

Rojo N, Muñoz R, Gallastegui G, Barona A, Gurtubay L, Prenafeta-Boldu FX, Elias A (**2012**) Carbon disulfide biofiltration: Influence of the accumulation of biodegradation products on biomass development. *Journal of Chemical Technology and Biotechnology*, 87, 764-771.

Romero-Hernandez AC, Rodriguez-Susa MS, Andres Y, Dumont E (**2013**) Steady- and transient-state H_2S biofiltration using expanded schist as packing material. New Biotechnology, 30(2), 210-218.

Rovira R, Montebello AM, Valle A, Gómez JM, Langostera M, Lafuente J, Campoy S, Gabriel D (**2010**) Advanced tools in microbial characterization and gene expression of a biotrickling filter treating high loads of H_2S. In: Proceedings of the 2010 Duke-UAM Conference on Biofiltration. Washington, DC, USA.

Rovira R (**2012**) Characterization of the operation and metatranscriptomic study of a bioreactor for desulfurization of high loads of H_2S. *PhD Thesis*, UAB, Spain. (available at: http://hdl.handle.net/10803/96713).

Ruiz-Romero S, Colmenar-Santos A, Castro-Gil MA (**2012**) EU plans for renewable energy. An application to the Spanish case. *Renewable Energy*, 43, 322-330.

Ruokojarvi A, Aatamila M, Hartikainen T, Olkkonen M, Salmi J, Ruuskanen J, Martikainen PJ (**2000**) Removal of dimethyl sulfide from off-gas mixtures containing hydrogen sulfide and methanethiol by a biotrickling filter. *Environmental Technology*, 21(10), 1173-1180.

Ruokojarvi A, Ruuskanen J, Martikainen PJ, Olkkonen M (**2001**) Oxidation of gas mixtures containing dimethyl sulfide, hydrogen sulfide and methanethiol using a two-stage biotrickling filter. *Journal of the Air and Waste Management Association*, 51(1), 11-16.

Ruzicka J, Lamm CG (**1971**) Selectrode TM – universal ion-selective solid-state electrode. 1. Halides. *Analytica Chimica Acta*, 54(1), 1-12.

Ruzicka J, Hansen EH (**1975**) Flow injection analysis. 1. New concept of fast continuous-flow analysis. *Analytica Chimica Acta*, 78(1), 145-157.

Ruzicka J (**1994**) Discovering Flow Injection: journey from sample to a live cell and from solution to suspension. *Analyst*, 119, 1925-1934.

San Miguel G, Servert J, Canoira L (**2010**) Analysis of the evolution in biomass to energy strategies and regulation in Spain. *Global Nest Journal*, 12(4), 374-383.

Sander R (**1999**) Compilation of Henry's Law Constants for Inorganic and Organic Species of Potential Importance in Environmental Chemistry, Version 3 (http://www.mpch-mainz.mpg.de/~sander/res/henry.html, 8 April 1999).

Santos JCC, Korn M (**2006**) Exploiting sulphide generation and gas diffusion separation in a flow system for indirect sulphite determination in wines and fruit juices. *Microchimica Acta*, 153, 87-94.

Sarma TVS, Tao S (**2007**) An active core fiber optic sensor for detecting trace H_2S at high temperature using cadmium oxide doped porous silica optical fiber as a transducer. *Sensors and Actuators B*, 127, 471-479.

Sathyapalan A, Zhou A, Kar T, Zhou F, Su H (**2009**) A novel approach for the design of a highly selective sulfate-ion-selective electrode. *Chemical Communications*, 3, 325-327.

Schieder D, Quicker P, Scheneider R, Winter H, Prechtl S, Faulstich M (**2003**) Microbiological removal of hydrogen sulfide from biogas by means of a separate biofilter system: experience with technical operation. *Water Science and Technology*, 48(4), 209-212.

Schlegelmilch M, Streese J, Stegmann R (**2005**) Odour management and treatment technologies: An overview. *Waste Management*, 25, 928-939.

Sekerka I, Lechner JF (**1977**) New zero-current chronopotentiometric technique with ion-selective electrode. *Analytica Chimica Acta*, 93, 129-137.

Sercu B, Nuñez D, van Langenhove H, Aroca G, Verstraete W (**2005**) Operational and microbiological aspects of a bioaugmented two-stage biotrickling filter removing hydrogen sulfide and dimethyl sulfide. *Biotechnology and Bioengineering*, 90(2), 259-269.

Sercu B, Boon N, Vander Beken S, Verstraete W, van Langenhove H (**2007**) Performance and microbial analysis of defined and non-defined inocula for the removal of dimethyl sulfide in a biotrickling filter. *Biotechnology and Bioengineering*, 96(4), 661-672.

Shamsipur M, Yousefi M, Ganjali MR, Poursaberi T, Faal-Rastgar M (**2002**) Highly selective sulfate PVC-membrane electrode based on 2,5-diphenyl-1,2,4,5-tetraaza-bicyclo[2.2.1]heptane as a neutral carrier. *Sensors and Actuators B*, 82, 105-110

Shareefdeen Z (**2012**) A biofilter design tool for hydrogen sulfide removal calculations. Clean *Technologies and Environmental Policy*, 14, 543-549.

Shishkanova TV, Sykora D, Vinsova H, Kral V, Mihai I, Gospodinova NP (**2009**) A novel way to improve sulfate recognition. *Electroanalysis*, 21(17-18), 2010-2013.

Sigma Aldrich (**2012**) Sigma-Aldrich Quimica, S.L., Spain. Safety Data Sheet – Sulfate-ionophore I. Version 5.0 Revision Date 24.07.2012. (http://www.sigmaaldrich.com/catalog/product/fluka/17892, 28.Mar.2013).

Sipma J, Svitelskaya A, van der Mark B, Hulstoff Pol LW, Lettinga G, Buisman CJN, Janssen AJH (**2004**) Potentials of biological oxidation processes for the treatment of spent sulfidic caustics containing thiols, *Water Research*, 38, 4331-4340.

Smet E, Lens P, van Langenhove H (**1998a**) Treatment of waste gases contaminated with odorous sulfur compounds. *Critical Reviews in Environmental Science and Technology*, 28(1), 89-117.

Smet E, van Langenhove H (**1998b**) Abatement of volatile organic sulfur compounds in odorous emissions from the bio-industry. *Biodegradation*, 9, 273-284.

Soleymanpour A, Hamidi-Asl E, Nasserib MA (**2006**) Chemically modified carbon paste electrode for determination of sulfate ion by potentiometric method. *Electroanalysis*, 18(16), 1598-1604.

Soreanu G, Beland M, Falletta P, Edmonson K, Seto P (**2008**) Laboratory pilot scale study for H2S removal from biogas in an anoxic biotrickling filter. *Water Science and Technology*, 57(2), 201-207.

Steudel R (**2004**). The chemical sulfur cycle. In: Environmental technologies to treat sulfur pollution. Principles and engineering, Lens,PNL, Hulshoff Pol L, Eds. IWA Publishing, London, UK, 1-31.

Sublette KL, Kolhatkar R, Raterman K (**1998**) Technological aspects of the microbial treatment of sulfide-rich wastewaters: A case study. *Biodegradation*, 9, 259-271.

Syed M, Soreanu G, Falletta P, Beland M (**2006**) Removal of hydrogen sulfide from gas streams using biological processes – A review. *Canadian Biosystems Engineering*, 48, 2.1-2.14.

Tang K, Baskaran V, Nemati M (**2009**) Bacteria of the sulfur cycle: An overview of microbiology, biokinetics and theis role in petroleum and mining industries. *Biochemical Engineering Journal*, 44, 73-94.

Tangerman A (**2009**) Measurement and biological significance of the volatile sulfur compounds hydrogen sulfide, methanethiol and dimethyl sulfide in various biological matrices. *Journal of Chromatography B*, 877, 3366-3377.

Tomas M, Fortuny M, Lao C, Gabriel D, Lafuente D, Gamisans X (**2009**) Technical and economical study of a full-scale biotrickling filter for H_2S removal from biogas. *Water Practice and Technology*, 4(2), doi:10.2166/WPT.2009.026.

Trojanowicz M (**2009**) Recent developments in electrochemical flow detections – A review. Part I. Flow analysis and capillary electrophoresis. *Analytica Chimica Acta*, 653, 36-58.

Tyurina LA, Tsodikov MV, Tarkhanova IG (**2011**) Field technology for desulfurization of associated petroleum gas. *Russian Journal of General Chemistry*, 81(12), 2611-2618.

Umezawa Y, Umezawa K, Sato H (**1995**) Selectivity coefficients for ion-selective electrodes: recommended methods for reporting Kpot A,B values (Technical Report). *Pure and Applied Chemistry*, 67(3), 507-518.

Umezawa Y, Buhlmann P, Umezawa P, Tohda K, Amemiya S (**2000**) Potentiometric selectivity coefficients of ion-selective electrodes. Part I.

Inorganic cations (Technichal Report). *Pure and Applied Chemistry*, 72(10), 1851-2082.

US EPA – US Environmental Protection Agency (**2003**) Toxicological Review of Hydrogen Sulfide, EPA/635/R-03/005, Washington, USA. (http://www.epa.gov/iris/toxreviews/0061tr.pdf, 1.Feb.2013).

Van den Bosch PLF, van Beusekom OC, Buisman CJS, Janssen AJH (**2007**) Sulfide oxidation at halo-alkaline conditions in a fed batch bioreactor. *Biotechnology and Bioengineering*, 97(5), 1053-1063.

van den Bosch PLF, de Graaf M, Fortuny-Picornell M, van Leerdam RC, Janssen AJH (**2009**) Inhibition of microbiological sulfide oxidation by methanethiol and dimethyl polysulfides at natron-alkaline conditions. *Applied Microbiology and Biotechnology*, 83, 579-587.

van Groenestijn JW, Hesselink PGM (**1993**) Biotechniques for air pollution control. *Biodegradation*, 4(4), 283-301.

van Groenestijn JW, van Heiningen WNM, Kraakman NJR (**2001**) Biofilters based on the action of fungi. *Water Science and Technology*, 44(9), 227-232.

van Groenestijn JW, Kraakman NJR (**2005**) Recent developments in biological waste gas purification in Europe. *Chemical Engineering Journal*, 113, 85-91.

van Langenhove H, De Heyder B (**2001**) Biotechnological treatment of sewage odours. In: Stuetz R, Frechen FB (Eds.), Odours in Wastewater Treatment: measurement, modelling and control, Int. Water Assoc. Publishing, London, UK, 396-414.

van Leerdam RC, Bonilla-Salinas M, de Bok FAM, Bruning H, Lens PNL, Stams AJM, Janssen AJH (**2008**) Anaerobic methanethiol degradation and methanogenic community analysis in an alkaline (pH 10) biological process for liquefied petroleum gas desulfurization, *Biotechnology and Bioengineering*, 101(4), 691-701.

van Leerdam RC, van den Bosch PLF, Lens PNL, Janssen AJH (**2011**) Reactions between methanethiol and biologically produced sulfur particles. *Environmental Science and Technology*, 45, 1320-1326.

Vandiver MS, Snyder SH (**2012**) Hydrogen sulfide: a gasotransmitter of clinical relevance. *Journal of Molecular Medicine*, 90, 255-263.

Vergara-Fernandez A, Hernandez S, Muñoz R, Revah S (**2012**) Influence of the inlet load, EBRT and mineral medium addition on spore emission by Fusarium solani in the fungal biofiltration of hydrophobic VOCs. *Journal of Chemical Technology and Biotechnology*, 87, 778-784.

Vitenberg AG, Kovalenko OG, Toma VI, Dobryakov YG (**2007**) Gas-Chromatographic determination of volatile sulfur-containing impurities in industrial emissions and aqueous solutions. *Journal of Analytical Chemistry*, 62(9). 857-867.

Vlasov YG, Ermolenko YE, Legin AV, Rudnitskaya AM, Kolodinov VV (**2010**) Chemical sensors and their systems. *Journal of Analytical Chemistry*, 65(9), 880-898.

Wani AH, Branion RMR, Lau AK (**1998**) Effects of periods of starvation and fluctuating hydrogen sulfide concentration on biofilter dynamics and performance. *Journal of Hazardous Materials*, 60, 287-303.

Wani AH, Lau AK, Branion MR (**1999**) Biofiltration control of pulping odors – hydrogen sulphide: Performance, microkinetics and coexistence effects of organo-sulfur species. *Journal of Chemical Technology and Biotechnology*, 74, 9-16.

Woodcock KE, Gottlieb M (**2004**) Natural gas. In: Kirk-Othmer Encyclopedia of Chemical Technology, Wiley, 12, 377- 386.

Wojciechowski K, Kucharek M, Wroblewski W, Warszynski P (**2010**) On the origin of the Hofmeister effect in anion-selective potentiometric electrodes with tetraalkylammonium salts. *Journal of Electroanalytical Chemistry*, 638, 204-211.

Yamasaki Y, Kanno M, Suzuki Y, Kaneko S (**2013**) Development of an engine control system using city gas and biogas fuel mixture. *Applied Energy*, 101, 465-474.

Yang Y, Allen ER (**1994**) Biofiltration control of hydrogen sulfide. 1. Design and operational parameters. *Journal of the Air and Waste Management Association*, 44, 863-868.

Young PG, Jolliffe KA (**2012**) Selective recognition of sulfate by tripodal cyclic peptides functionalized with (thio)urea binding sites. *Organic and Biomolecular Chemistry*, 10, 2664-2672.

Yuan YJ, Kuriyama H (**2000**) Determination of hydrogen sulfide in a yeast culture solution by flow analysis utilizing methylene blue spectrophotometric detection. *Biotechnology Letters*, 22, 795-799.

Zayed SIM Issa YM (**2010**) Sibutramine selective electrodes for batch and flow injection determinations in pharmaceutical preparations. *Analytical Sciences*, 26, 45-49.

Zhang L, Meng X, Wang Y, Liu L (**2009**) Performance of biotrickling filters for hydrogen sulfide removal under starvation and shock loads conditions. *Journal of Zhejiang University Science B*, 10(8), 595-601.

Zuliani C, Diamond D (**2012**) Opportunities and challenges of using ion-selective electrodes in environmental monitoring and wearable sensor. Electrochimica Acta, 84, 29-34.
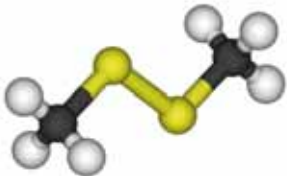
※

annexes
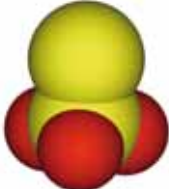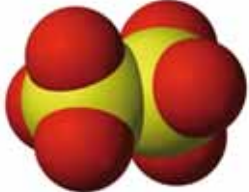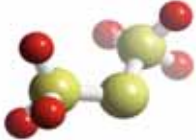
"An unusual beginning must have an unusual end."

Mikhail Y. Lermontov
(Moscow, 1814 – Pyatigorsk, 1841)

⭐

Molecular representation of some sulfur compounds *

COS Carbonyl sulfide	**DMDS (CH_3SSCH_3)** Dimethyl disulfide	**DMS (CH_3SCH_3)** Dimethyl sulfide
DMTS (CH_3SSSCH_3) Dimethyl trisulfide	**ET (CH_3CH_2SH)** Ethylmercaptan	**H_2S** Hydrogen sulfide
CH_3SH Methylmercaptan	**S_8^0** Elemental sulfur (ortomolecular S_8)	**$S_2O_3^{2-}$** Thiosulfate
$S_2O_6^{2-}$ Dithionate	**$S_3O_6^{2-}$** Trithionate	**$S_4O_6^{2-}$** Tetrathionate
SO_2 Sulfur dioxide	**SO_3^{2-}** Sulfite	**SO_4^{2-}** Sulfate

* Images free of copyright

❄

Video "990 days in 3 minutes" – Description and comments

The file entitled ***990 days in 3 minutes*** is a video file (*990 days in 3 minutes.mov*, 29.4 MB) edited using the software QuickTime (Apple Inc., USA). It can be played using any software for movies watching. This document was prepared and edited by Andrea M. Montebello, 2013. All information and pictures showed are property of the author. A CD containing the video file ***990 days in 3 minutes*** is included in the hard copy version of this Thesis, in the internal back cover.

The author acknowledge the collaboration of all colleagues from Gas Treatment Group - UAB, specially: Dr. Roger Rovira, during the operation and biomass sampling under neutral pH; Luis Rafael López and Mabel Mora, during acidic pH operation; Tércia Bezerra, during biomass sampling under acidic pH; Margot Clariana for lab support during neutral pH operation and Lorena Ferrer for lab support during the complete operation.

The video was conceived as a supporting tool for being played during internal project meetings. The intention was to show the evolution of the physical appearance of the reactor during the total operating time of 990 days. Selected pictures of the reactor are shown, with special attention to the visual aspect of the biofilm attached to packing material and to the quantity of elemental sulfur accumulated inside the filter bed during the acidic pH operation. Also some details of biomass sampling procedures are shown, including the evidence of corrosion of packing material at the gas inlet section. The total duration of the video is 3 minutes. Detailed information of the video content is presented in **Table A.1**, including legend of each picture and the duration of each image animation, as played.

Table A.1   Video "990 days in 3 minutes" – Detailed content

#	Title / Legend	Time (mm:ss)
1	990 days in 3 minutes aerobic biotrickling filtration for biogas desulfurization	00.00 – 00:10
2	START UP @ neutral pH / 11 march 2010	00:10 – 00:15
3	6 days @ neutral pH / 17 march 2010	00:15 – 00:20
4	15 days @ neutral pH / 26 march 2010	00:20 – 00:25
5	26 days @ neutral pH / 7 april 2010	00:25 – 00:29
6	26 days @ neutral pH / 7 april 2010	00.29 – 00:34
7	75 days @ neutral pH / 26 may 2010	00:34 – 00:39
8	416 days @ neutral pH / 7 may 2011 (EXPs H_2S + CH_3SH)	00:39 – 00:45
9	440 days @ neutral pH / 1 june 2011 – acidic pH transition	00:45 – 00:52
10	5 days @ acidic pH / 6 june 2011	00:52 – 00:58
11	8 days @ acidic pH / 9 june 2011	00:58 – 01:03
12	13 days @ acidic pH / 14 june 2011	01:03 – 01:07
13	16 days @ acidic pH / 17 june 2011	01:08 – 01:12
14	26 days @ acidic pH / 27 june 2011	01:12 – 01:17
15	177 days @ acidic pH / 28 november 2011 – EXPs (2,000 ppm$_v$ H_2S)	01:17 – 01:22
16	178 days @ acidic pH / 29 november 2011 – EXPs (4,000 ppm$_v$ H_2S)	01:22 – 01:27
17	179 days @ acidic pH / 30 november 2011 – EXPs (6,000 ppm$_v$ H_2S)	01:27 – 01:32
18	254 days @ acidic pH / 16 february 2012 – EXPs (10,000 ppm$_v$ H_2S)	01:32 – 01:37
19	256 days @ acidic pH / 18 february 2012 – EXPs (0 ppm$_v$ H_2S)	01:37 – 01:42
20	266 days @ acidic pH / 27 february 2012 – EXPs (2,000 ppm$_v$ H_2S)	01:42 – 01:47
21	317 days @ acidic pH / 18 april 2012	01:47 – 01:52
22	317 days @ acidic pH / 18 april 2012	01:52 – 01:56
23	317 days @ acidic pH / 18 april 2012	01:57 – 02:02
24	317 days @ acidic pH / 18 april 2012	02:02 – 02:06
25	317 days @ acidic pH / 18 april 2012	02:06 – 02:11
26	401 days @ acidic pH / 12 july 2012	02:12 – 02:16
27	401 days @ acidic pH / 12 july 2012	02:16 – 02:21
28	401 days @ acidic pH / 12 july 2012	02:21 – 02:26
29	401 days @ acidic pH / 12 july 2012	02:26 – 02:31
30	401 days @ acidic pH / 12 july 2012	02:31 – 02:36
31	550 days @ acidic pH / 10 december 2012	02:36 – 02:41
32	550 days @ acidic pH / 10 december 2012	02:41 – 02:45
33	550 days @ acidic pH / 10 december 2012	02:46 – 02:50
34	550 days @ acidic pH / 10 december 2012	02:51 – 02:55
35	990 days in 3 minutes aerobic biotrickling filtration for biogas desulfurization	02:56 – 03:01

Curriculum Vitae Académico

Andrea M. Montebello
Barcelona, Mayo 2013

Apellidos:	**MONZÓN MONTEBELLO**	Nombre:	**ANDREA**
D.N.I.:	**X8614988-Q**	Fecha de nacimiento:	**16/04/1971**

Situación profesional actual

Organismo:	**UNIVERSIDAD AUTÓNOMA DE BARCELONA**
Facultad, Escuela o Instituto:	**ESCUELA DE INGENIERÍA (EE)**
Depto./Secc./Unidad estr.:	**DEPARTAMENTO DE INGENIERÍA QUÍMICA**
Dirección postal:	Campus de Bellaterra, 08193 Bellaterra (Barcelona)
Teléfono:	+ 34 935814792 Fax: + 34 935812013
Correo electrónico:	andrea.monzon@uab.es

Especialización (Códigos UNESCO): 330801, 330804, 330810, 330530
Categoría profesional: BECARIA DOCTORAL (BECA PIF)   Fecha inicio: 21/10/2009
Dedicación: A tiempo completo

Líneas de investigación

Tratamiento de efluentes gaseosos, tratamiento de aguas residuales, monitorización

Formación académica

Titulación Superior	Centro	Fecha
Doctorado en Ciencia y Tecnología Ambientales	Universidad Autónoma de Barcelona	2013 (en curso)
Máster en Estudios Ambientales	Universidad Autónoma de Barcelona	2008
Especialización en Ingeniería de Saneamiento Básico	Universidade de São Paulo, Brasil	2000
Ingeniería Química	Fundação Armando Alvares Penteado, Brasil	1999

Actividades anteriores de carácter científico profesional

Puesto	Institución	Fechas
Ingeniero Comercial	Montebello Engenharia Ltda., São Paulo, Brasil	01/2007–08/2007
Ingeniero Comercial (Negocios)	Degrémont Trat. Aguas Ltda., São Paulo, Brasil	11/2003–12/2006
Ingeniero Comercial (Productos)	Pieralisi do Brasil Ltda., São Paulo, Brasil	08/2000–08/2003
Ingeniero Trainee	Degrémont Trat. Aguas Ltda., São Paulo, Brasil	04/2000–08/2000

Idiomas
(R = regular, B = bien, C = correctamente)

Idioma	Habla	Lee	Escribe
Inglés	B	C	C
Castellano	C	C	C
Portugués	C	C	C
Catalán	B	C	B

Participación en proyectos de I+D financiados en convocatorias públicas
(nacionales y/o internacionales)

Título del proyecto: **Grupo de investigación de calidad. Pla de Recerca de Catalunya.**
Entidad financiadora: CIRIT. Generalitat de Catalunya. 2009 SGR 815
Entidades participantes: Grupo de tratamiento biológico de efluentes líquidos y gaseosos. Eliminación de Nutrientes, Olores y Compuestos Orgánicos Volátiles (Departamento de Ingeniería Química – UAB)
Duración   desde: Julio 2009   hasta: Julio 2014
Investigador principal: Javier Lafuente Sancho
Número de investigadores participantes: 13

Título del proyecto: **Desulfuración de gases ricos energéticamente mediante biofiltros percoladores: desarrollo y optimización del proceso en condiciones anóxicas y aerobias.**
Entidad financiadora: CICYT nº CTM2009-14338-C03-01
Entidades participantes: Dpt. d'Enginyeria Química (UAB) , Dpt. Enginyeria Minera Recursos Naturals (UPC), Universidad de Cádiz (UCA)
Duración   desde: 1-1-2010   hasta: 31-12-2012
Investigador responsable: David Gabriel Buguña (UAB)
Número de investigadores participantes: 13

Título del proyecto: **Desulfuración sostenible de biogás mediante biorreactores para su aprovechamiento como fuente de energía alternativa.**
Entidad financiadora: Ministerio de Asuntos Exteriores y cooperación – AECID ref: A2/037075/11
Entidades participantes: Dpt. d'Enginyeria Química (UAB) , Dpt. Enginyeria Minera Recursos Naturals (UPC), Universidad Autónoma Metropolitana - Iztapalapa(UAMI), Universidad Autónoma Metropolitana - Cuajimalpa(UAMC)
Duración   desde: 1-1-2012   hasta: 31-12-2012
Investigador responsable: David Gabriel Buguña (UAB)
Número de investigadores participantes: 17

Publicaciones o Documentos Científico-Técnicos
(CLAVE: L = libro completo, CL = capítulo de libro, A = artículo, R = "review", E = editor,
S = Documento Científico-Técnico restringido)

Autores: Montebello AM, Gamisans X, Lafuente J, Baeza M, Gabriel D
Título: **Aerobic desulfurization of biogas by acidic biotrickling filtration**
Ref. Revista: *Accepted – Environmental Technology*
Clave: A   Volumen: Páginas: Fecha: 2013

Autores: Montebello AM, Gamisans X, Lafuente J, Baeza M, Gabriel D
Título: **Desulfurization of biogas by acidic biotrickling filtration**
Ref. Revista: *Proceedings of the 5th IWA Conference on Odours and Air Emissions, San Francisco, California, USA. Paper # 47*
Clave: A   Volumen: Páginas: 1-8   Fecha: 2013

Autores:	Bezerra T, Rovira R, Montebello AM, Llagostera M, Lafuente J, Campoy S, Gabriel D
Título:	**Metagenomics and metatranscriptomics of a H$_2$S desulfurizing biotrickling filter**
Ref. Revista:	*Proceedings of the 5th IWA Conference on Odours and Air Emissions, San Francisco, California, USA. Paper # 48*
Clave:	A Volumen: Páginas: 1-8 Fecha: 2013

Autores:	Montebello AM, Fernandez M, Almenglo F, Ramirez M, Cantero D, Baeza M, Gabriel D
Título:	**Simultaneous methylmercaptan and hydrogen sulfide removal in the desulfurization of biogas in aerobic and anoxic biotrickling filters**
Ref. Revista:	*Chemical Engineering Journal*
Clave:	A Volumen: 200-202 Páginas: 237-246 Fecha: 2012

Autores:	Montebello AM, Fernandez M, Almenglo F, Ramirez M, Cantero D, Baeza M, Gabriel D
Título:	**Simultaneous methylmercaptan and hydrogen sulfide removal in the desulfurization of biogas in aerobic and anoxic biotrickling filters**
Ref. Revista:	*Proceedings of the Congress on Biotechniques for Air Pollution Control. Biotechniques 2011*
Clave:	A Volumen: Páginas: 1-8 Fecha: 2011

Autores:	Montebello AM, Baeza M, Lafuente J, Gabriel D
Título:	**Monitoring and performance of a desulfurizing biotrickling filter with an integrated continuous gas/liquid flow analyser**
Ref. Revista:	*Chemical Engineering Journal*
Clave:	A Volumen: 165 Páginas: 500-507 Fecha: 2010

Autores:	Rovira R, Montebello AM, Valle A, Gomez JM, Llagostera M, Lafuente J, Campoy S, Gabriel D
Título:	**Advanced tools in microbial characterization and gene expression of a biotrickling filter treating high loads of H$_2$S**
Ref. Revista:	*Proceedings of the 2010 Duke – UAM Conference on Biofiltration for Air Pollution Control, Washington, DC, USA.*
Clave:	A Volumen: Páginas: 155-162 Fecha: 2010

Contribuciones a Congresos

Autores:	Montebello AM, Gamisans X, Lafuente J, Baeza M, Gabriel D
Título:	**Desulfurization of biogas by acidic biotrickling filtration**
Participación:	Presentación oral
Congreso:	2013 5th IWA Conference on Odours and Air Emissions
Lugar de celebración:	San Francisco, Estados Unidos Fecha: Marzo 2013

Autores:	Montebello AM, Fernandez M, Almenglo F, Ramirez M, Cantero D, Baeza M, Gabriel D
Título:	**Simultaneous methylmercaptan and hydrogen sulphide removal in the desulphurization of biogas in aerobic and anoxic biotrickling filters**
Tipo de participación:	Presentación oral
Congreso:	Congress on Biotechniques for Air Pollution Control. Biotechniques 2011
Lugar de celebración:	A Coruña, España Fecha: octubre 2011

Autores:	Rovira R, Montebello AM, Valle A, Gomez JM, Llagostera M, Lafuente J, Campoy S, Gabriel D
Título:	**Advanced tools in microbial characterization and gene expression of a biotrickling filter treating high loads of H_2S**
Participación:	Presentación oral
Congreso:	2010 Duke-UAM Conference on Biofiltration for Air Pollution Control
Lugar de celebración:	Washington, Estados Unidos Fecha: octubre 2010